USE OF ISOTOPE HYDROLOGY TO CHARACTERIZE GROUNDWATER SYSTEMS IN THE VICINITY OF NUCLEAR POWER PLANTS

Results of a Coordinated Research Project (CRP) F33022, 2016–2020

National Academy of Sciences of Ukraine
Institute for Safety Problems of Nuclear Power Plants

USE OF ISOTOPE HYDROLOGY TO CHARACTERIZE GROUNDWATER SYSTEMS IN THE VICINITY OF NUCLEAR POWER PLANTS

Results of a Coordinated Research Project (CRP) F33022, 2016–2020

Monograph

Kyiv 2022

UDC 621.311.25:556.3](02)=111
U88

Reviewers:

Dr. S. Chidambaram, Research Scientist Water Research Centre, Kuwait Institute for Scientific Research, Kuwait; *Mohammad Arzoo Ansari*, Isotope and Radiation Application Division, Bhabha Atomic Research Centre, Mumbai, India; *Tomas Vitvar*, Facultad de Ingeniería en Ciencias de la Tierra (FICT), ESPOL Polytechnic University, Guayaquil, Ecuador

Recommended for publication by the Academic Council
Institute for Safety Problems of Nuclear Power Plants National Academy of Sciences of Ukraine
(protocol no 12 dated 25.11.2021)

The monograph was created in the framework of cooperation with the International Atomic Energy Agency

U88 **Use** of isotope hydrology to characterize groundwater systems in the vicinity of nuclear power plants. Results of a Coordinated Research Project (CRP) F33022, 2016–2020 : monograph / Institute for Safety Problems of Nuclear Power Plants of National Academy of Sciences of Ukraine ; International Atomic Energy Agency. Chornobyl ; Kyiv: ISP NPP NAS of Ukraine, 2022. – 150 p.

ISBN 978-966-02-9876-7

The monograph contains results of the coordinated research project conducted by the International Atomic Energy Agency with the purpose to explore the use of new isotope techniques together with conventional ones to better assess the hydrogeological conditions in the geological settings of nuclear power plant sites and to provide basic information that may be used for predicting the fate of radioactive contaminants, such as tritium, released into groundwater in case of a radiological accident and/or during normal operations. To this end, research projects were conducted in ten countries to characterize the groundwater system in the vicinity of NPPs which are at different stages of development. The monograph contains the reports of these ten research projects and a summary of the achievements of the individual projects. The results of the determination of isotopes ^{18}O, ^{2}H, ^{13}C, ^{14}C, ^{3}H, ^{3}He, ^{4}He and noble gases in water were used. The results of traditional hydrochemical analyzes and distributions of ^{90}Sr, uranium, and transuranic elements in groundwater were also used. This CRP aims to develop guidelines for studying the hydrogeological characteristics of groundwater in local and regional groundwater systems in the vicinity of nuclear power plants using environmental isotopes and conventional techniques.

For scientists and engineers working in the field of hydrogeology, radioecology, and safety in nuclear energy, as well as for students and graduate students of geological and physical faculties of universities.

UDC 621.311.25:556.3](02)=111

ISBN 978-966-02-9876-7

CONTENTS

FOREWORD

A coordinated research project (CRP) was conducted by the International Atomic Energy Agency (IAEA) with the purpose to explore the use of new isotope techniques together with conventional ones to better assess the hydrogeological conditions in the geological settings of nuclear power plant (NPP) sites and to provide basic information that may be used for predicting the fate of radioactive contaminants, such as tritium, released into groundwater in case of a radiological accident and/or during normal operations. Defining groundwater flow patterns, flow rates (velocity) and direction of groundwater movement near the NPP can be used to help in the NPP site selection procedure. Though, the common isotope techniques are already used in such investigations but the newly developed isotope tools like noble gases isotopes can provide better information on the dynamics of very fast and/or very slow-moving groundwater. Testing of such techniques will help produce the guidelines on application of suitable methodologies for better hydrogeological characterization near NPPs. This will also help promote confidence in the continued safety of the site during the operational and post operation periods and assist in controlling contamination of water resources in case of unforeseen incidents.

It should be noted here that serving the purpose of an integrated safety assessment of NPPs requires different types of studies, e.g., behavior of NPP-produced radionuclides in soil, assessment of probabilistic doses etc., but these do not fall within the scope of the proposed CRP.

To this end, research projects were conducted in ten countries to characterize the groundwater system in the vicinity of NPPs which are at different stages of development. In Lithuania and Italy, the studied NPPs are in a decommission phase; Brazil, there are two in operation and one under construction; in Pakistan, there are 7 sites (3 in operation and 4 under construction); in Morocco, China and Vietnam, there is one planned; Argentina, one under construction; Japan and Ukraine after the accidents in the stage of decommissioning.

This monograph contains the reports of these ten research projects and a summary of the achievements of the individual projects. The final report of this CRP reviews the usefulness and current status of the combined application of isotope hydrology and other hydrogeochemical tools to develop guidelines for better hydrogeological characterization of groundwater systems in the vicinity of NPPs.

The IAEA officers in charge of designing and coordinating all of the related works in this CRP were Mr. UMAYADOSS Saravana Kumar, Mr. CHOUDHRY Manzoor Ahmad and Mr MATIATOS Ioannis of the Isotope Hydrology Section, Division of Physical and Chemical Sciences/ Department of Nuclear Sciences and Applications/IAEA.

ACKNOWLEDGMENTS

We wish to extend our warm thanks and our deepest gratitude to IAEA for its efforts to encourage nuclear applications throughout the world and especially for the resources provided during this research coordinated project. We would also like to thank the national and international experts as well as all participants for their contribution to the success of this Research Coordinated Project (CRP 33.0.22).

ABSTRACT

The monograph is an outcome of the Coordinated Research Project (CRP) F33022 conducted by the IAEA to investigate the use of the latest isotope technologies in conjunction with traditional ones to better assess the hydrogeological conditions in the geological settings of nuclear power plant (NPP) sites and also provide critical information that could be used to estimate the fate of radioactive materials discharged into groundwater in the event of a radiological accident or during normal operations. The study was conducted from 2016 to 2020, in 10 countries Argentina, Brazil, China, Italy, Japan, Lithuania, Morocco, Pakistan, Ukraine and Vietnam. The studied countries are represented by different stages of NPP, namely planning, under construction, decommission phase and decommissioning after accidents.

Monograph reports the study's key findings under different geological conditions, aquifer properties, climatic conditions, and relative geographical positions of the NPPs to adjacent surface water bodies. The meteorological variables like temperature, humidity, rainfall; hydrological variables like water level and hydraulic conductivity were studied. Samples were collected from groundwater, surface water and rainwater. Environmental samples like air, tree leaf, aquatic plants etc., were also collected in a few studies. The collected samples were analyzed for major and minor ions, stable and radioactive isotopes, noble gases to determine the background values of these parameters and to understand the level of contamination in the aquatic environment. A part from these observations, groundwater age, geochemical process, rate of movement, and groundwater source were also addressed in these findings. The standard geochemical plots, statistical analysis and few bivariate plots were adopted to achieve the objectives of the study. The monograph has also attempted to understand the fate of contaminant migration by adopting groundwater modelling techniques.

The results and findings of these studies compiled in the monograph would serve as a basic understanding of the aquatic environment around the NPPs on a global scale. The coordinated research project has also provided a platform to share the experience of experts from different countries, fellowships, and training for young staff members. Furthermore, since the investigations have been attempted in regions with different stages of NPPs, it would provide an idea for deriving the administrative policies. These would define site selection criteria, parameters to be monitored, the time interval of monitoring, and to revisit the precaution to be adhered to in case of failure due to unforeseen events. Finally, I would like to record my appreciation to the team and the agency for having conceived a novel and a basic requisite concerning the aquatic environments adjacent to the NPPs.

Finally, this monograph is conceived as a novel and a basic requisite concerning the aquatic environments adjacent to the NPPs.

1. INTRODUCTION

Every country in the world dealing with sitting, constructing, operating and decommissioning nuclear power plants has developed and/or adapted a framework of norms and regulations to assure that the power plant will achieve the designed degree of operation in safe and economic conditions, causing as low impact as possible to the public and to the environment.

Such norms and regulations are based upon national laws and criteria and are expected to be frequently updated, taking into account new technological improvements and new environmental demands from the public in general. Less developed countries usually follow the legislations of the developed countries. Much of these regulations are also elaborated by the International Atomic Energy Agency (IAEA) and issued as recommendations/guidelines for the authorities of the countries under consideration (Member States).

One of the most detailed and widespread set of norms, regulations and criteria concerning the power reactors siting is that prescribed by the Code of Federal Regulations (CFR) of the United States, available on the following website: https://www.ecfr.gov/cgi-bin/text-idx?SID=5e72713084a99117-835b0439039ab3c6&c=ecfr&tpl=/ecfrbrowse/Title10/10cfrv2_02.tpl).

As a matter of fact, in its Chapter I, Title 10, Section 100.10, **Factors to be considered before January 1997**, the Appendix A, "Seismic and Geologic Siting Criteria for Nuclear Power Plants", in its item (1) describes "the nature of investigations required to obtain the geologic and seismic data

necessary to determine site suitability and to provide reasonable assurance that a nuclear power plant can be constructed and operated at a proposed site without undue risk to the health and safety of the public. It describes procedures for determining the quantitative vibratory ground motion design basis at a site due to earthquakes and describes information needed to determine whether and to what extent a nuclear power plant need be designed to withstand the effects of surface faulting". Item (2) mentions what meteorological conditions should be considered and investigated at the site and in the surrounding area. Item (3) mentions that "geological and hydrological characteristics of the proposed site may have a bearing on the consequences of an escape of radioactive material from the facility. Special precautions should be planned if a reactor is to be located at a site where a significant quantity of radioactive effluent might accidentally flow into nearby streams or rivers or might find ready access to underground water tables".

A review was made considering the scenario for factors introduced after January 1997, but taking into account the same physical characteristics of the site, including seismology, meteorology, geology and hydrology. The revised section, now named Section 100.23, "Geologic and seismic siting factors" describes (1) "the criteria and nature of investigations required to obtain the geologic and seismic data necessary to determine the suitability of the proposed site and the plant design bases". Item (2) prescribes what meteorological characteristics of the site that are necessary for safety analysis or that may have an impact upon plant design (such as maximum probable wind speed and precipitation) must be identified and characterized. Item (3) mentions that factors important to hydrological radionuclide transport, such as soil, sediment, and rock characteristics, adsorption and retention coefficients, groundwater velocity, and distances to the nearest surface body of water, must be obtained from on-site measurements. The maximum probable flood along with the potential for seismically induced floods discussed in §100.23 (d) (3) must be estimated using historical data.

For the purpose of this Code, groundwater means water below the land surface in a zone of saturation. More specifically, for purposes of this appendix, groundwater is the water contained within an aquifer as defined above. [61 FR 65176, Dec. 11, 1996, as amended at 78 FR 34250, June 7, 2013].

But, unfortunately, although the NPP´s site selection and operation follow very strict safety guidelines, there is always the chance of unforeseen accidents, with very low probability, given that the nuclear industry is considered one of the safest human high technology activities.

Some examples can be cited, in a very brief resume: Windscale, United Kingdom, October, 1957; Three Mile Island, US, March, 1979; Chornobyl, Ukraine, April, 1986; Goiânia, Brazil, September, 1987 and Fukushima, Japan, March, 2011.

For more information, please visit the following website: (List of nuclear power accidents by country): https://en.wikipedia.org/wiki/List_of_nuclear_power_accidents_by_country

Nuclear energy remains the largest source of low-carbon electricity and the second largest source of energy in the world. Both developed and developing countries continue to express interest in nuclear energy and many have announced plans to acquire it. Several existing nuclear energy states, notably in Asia, are already building new NPPs, while others are studying the possibilities.

1.1. Background situation analysis

The demand for energy is continually growing both in the developed and the developing countries. There are over 435 commercial NPPs operating in 31 countries, with over 375,000 MW(e) of total capacity. They provide over 11% of the world's electricity as continuous, reliable base-load power, without carbon dioxide emissions. About 70 more power reactors are under construction. Fifty-six countries operate a total of about 240 research reactors and a further total of 180 nuclear reactors power some 140 ships and submarines (WNA, 2015). One of the key messages that emerged from the IAEA Ministerial Conference on Nuclear Power in the 21st Century, which took place in St. Petersburg in June 2013, was that for many States, nuclear power would play an important role in achieving energy security and sustainable development goals, (https://www.iaea.org/newscenter/news/iaea-releases-2019-data-on-nuclear-power-plants-operating-experience).

NPPs are usually built either in the coastal areas near sea or near big rivers and lakes. Although multiple safety measures are used to handle radioactive materials in an NPP, yet they are subject to leakages due to any abnormal incident which often results in the direct contamination of groundwater. The Fukushima NPP accident occurred in 2011 in Japan has been proved to be an eye opener in this

direction. Groundwater can also be contaminated indirectly by accidental release of radioactive material into the atmosphere or into the surface water, from either of which it can enter the groundwater. In such cases the radioactive contamination may reach points where water is extracted for use, and so results in exposure for the public. Although in most of the cases, these contamination incidents have an insignificant radiation dose consequence, it is important to determine in detail the groundwater circulation in the vicinity of the NPPs, in order to assure local stakeholders that the public health and safety are being taken care of.

Groundwater is the critical dissolving, mobilizing and transport medium of radionuclides. It is therefore important that mechanisms leading to the inflow of water into the NPPs as well as the outflow of contaminated water from the facility are well understood. A good knowledge of the behavior of water in and out of the NPPs is a prerequisite for facility design and an essential input for performance and safety assessment. In order to understand the groundwater (flow) processes/behaviour in the vicinity of an NPP and to evaluate potential pathways for radionuclide migration, hydrogeological aspects, such as recharge and discharge areas and rates, interactions between surface and/or groundwater bodies, infiltration or leakages of water, either from reservoirs constructed for the needs of the NPP, or due to natural recharge by precipitation, groundwater flow paths and residence time, must be evaluated (Mazeika et al., 2013; Singh et al., 2013; Stadler et al., 2010). A fully understood conceptual model is highly important in the implementation of a mathematical simulation model, where the fate of radioactive contaminants can be predicted. A general requirement for the evaluation of a hydrogeological setting is that all the relevant parameters shall be studied in detail to help predicting the consequences of a contamination release at the points of water use.

During the IAEA/UNESCO Technical Meeting on Groundwater Contamination following the Fukushima Nuclear Accident, IAEA Headquarters, Vienna, September 8–10, 2014, the characterization of groundwater in the vicinity of NPPs was addressed by the participants a one of the most serious challenges, because the NPPs are established in specific hydrogeological settings and because the radionuclides released in surface water and groundwater could reach the water-use points where they could pose radiological hazards.

IAEA safety standards already exist and are available in form of safety guides/requirements for hydrogeological investigations (IAEA 1984, 2002, 2003 and 2011). However, guidelines are available in these documents on techniques for proper characterization of groundwater in the vicinity of NPPs and generation of reliable information to plan countermeasures for protection of public and the environment in case of accidental release of radioactive materials.

Environmental isotope techniques can be applied for better characterization of the hydrogeology in the vicinity of NPPs and for the assessment of groundwater dynamics in order to control the pollution from spreading into the system in case of accidental release. Stable- and radio-isotopes have been widely applied in hydrogeological studies for their ability to provide a sharper focus on some of the underlying processes that control chemical and physical behavior of elements and compounds in the natural environment (Aggarwal et al., 2000; Blasch and Bryson, 2007; Clark and Fritz, 1997; Gat and Gonfiantini, 1981; Gat, 1996; Hameed et al., 2015; Solomon et al., 1995).

This was the main motivation for the proposal of a new Coordinated Research Project, (CRP F33022 – ***Use of Isotope Hydrology to Characterize Groundwater Systems in the Vicinity of Nuclear Power Plants***) focused in the comprehensive characterization of groundwater systems in the vicinity of NPP´s in order to better assess the groundwater dynamics and define the pathways by which radionuclides released, in case of accident, can migrate to open environment and locations where water may be used by or for the population in the region. By using environmental isotopes in water (e.g., ^{18}O, ^{2}H, ^{13}C, ^{14}C, ^{3}H, noble gas isotopes etc.), together with conventional hydrochemical analyses, this CRP aims to develop guidelines for better hydrogeological characterization of local and regional groundwater systems in the vicinity of nuclear power plants using environmental isotopes and conventional techniques.

The CRP also seeks to improve expertise among participating Member States in the implementation of isotopes for the assessment of groundwater protection near NPP´s, providing an important asset in safety regulations for NPP´s site selection and operation. It should be noted here that serving the purpose of an integrated safety assessment of NPPs requires different types of studies,

e.g., behavior of NPP-produced radionuclides in soil, assessment of probabilistic doses etc., but these do not fall within the scope of the proposed CRP.

Ten Member States have joined the Project, namely: Argentina, Brazil, China, Italy, Japan, Lithuania, Morocco, Pakistan, Ukraine and Vietnam. During the period covered by this project, three Research Coordination Meetings (RCM´s) have been held: 1st RCM from 4–7 October 2016, Vienna (IAEA- Austria); 2nd RCM from 18–22 June 2018, Vienna (IAEA- Austria) and 3rd RCM from 11–15 November 2019, Belo Horizonte (CDTN- Brazil). Every country holding a Research Contract or having stipulated with IAEA a Research Agreement has prepared three Annual Progress Reports, covering the years 2016 to 2019. The final report of this CRP is submitted to IAEA in November 2020.

1.2. Methodological and technical approaches

The ten projects in this CRP cover a wide range of research approaches based on the available isotopic and conventional techniques in order to develop guidelines for comprehensive characterization of local and regional groundwater pathways in the vicinity of NPPs sites.

In particular, it has been recognized that each geological and hydrogeological setting needs a special approach, according to the vicinity of the NPP to rivers or the sea. To accurately characterize groundwater systems in the vicinity of NPPs, Table 1.1 summarizes a list of the specific scientific issues that were addressed by different and integrated approaches.

Moreover, the newly developed isotopic tools, like noble gas isotopes, were used to provide better information on the dynamics of very fast and/or very slow-moving groundwater in the vicinity of NPP's.

The use of Tritium as groundwater dating tool in the vicinity of NPP sites could be based from the controlled liquid releases from the NPP and for this reason the group recommends using different dating tools, such as $^{3}H/^{3}He$ isotopic ratio or CFCs.

Table 1.1. Spectrum of suitable isotope techniques for groundwater (GW) and surface water (SW) studies in the vicinity of NPPs

Scientific issue	Hydrogeological context	Samples Typology	Isotopic tools	Other tools
Recharge areas	Shallow/deep aquifers	Meteoric water, GW, SW	$\delta^{18}O$, δD, ^{3}H, $^{3}H/^{3}He$, ^{85}Kr (shallow), ^{4}He (deep)	Meteorologic and hydrometric records, physical parameters, major ions
Residence times/ GW age	Shallow/ deep aquifers	Meteoric water, GW	Young waters: ^{3}H, $^{3}H/^{3}He$, ^{85}Kr, CFCs Old waters: ^{14}C-DIC, ^{4}He	Hydrometric records, physical parameters, major ions
SW–GW interactions, Subsurface GW Discharge	Shallow aquifers	Meteoric water, GW, SW	$\delta^{18}O$, δD, ^{3}H, ^{222}Rn, ^{226}Ra, ^{228}Ra, $^{87}Sr/^{86}Sr$, $\delta^{11}B$	Hydrometric records, physical parameters, major ions (e.g., Cl^{-}, SO_4^{-2}), trace compounds (e.g. Br), geophysics is recommended for SGD and seawater intrusion studies
GW flow paths and velocity	Shallow/ deep aquifers	Meteoric water, GW, SW	$\delta^{18}O$, ^{3}H, ^{14}C-DIC, $^{3}H/^{3}He$, $^{236}U/^{238}U$, $^{240}Pu/^{239}Pu$, ^{85}Kr, ^{4}He	Hydrometric records, physical parameters, major ions, artificial tracer tests
Mass transport in porous and fractured aquifers	Shallow/ deep aquifers	GW, SW	Regional: $\delta^{18}O$ Local: $\delta^{18}O$, ^{3}H, ^{14}C-DIC	Chloride (regional and local), flow and mass transport modeling codes
Interactions between aquifers via aquitards	Shallow/ deep aquifers	Meteoric water, SW, GW in shallow and deep wells	Regional: $\delta^{18}O$ Local: ^{3}H, ^{14}C-DIC, ^{4}He	Hydrometric records, physical parameters, major ions, chloride (regional and local), bromide (local), flow and mass transport modeling codes

Thereby, the methodological highlights in processing and data interpretation techniques undertaken during this CRP can be stated as follows, depending on the MS's.

Lithuania used MODPATH software for particle tracking modelling and INGEM-1 device for dissolved in the groundwater helium measurements. The helium age was calculated by average uranium and thorium contents in the crystalline rocks. Morocco and Argentina used QGIS software for mapping geo-referential information system. Brazil and Ukraine used ArcGIS software and geo-referred tools to produce an initial set of maps depicting geologic features of the region in the vicinity of NPPs. Morocco, Pakistan and Argentina used Software Quality Hydrochemistry DIAGRAMS (Piper, Stiff, Schoeller-Berkalov, Korzhinsky, Riverside and Wilcox, Stabler, ternary diagram; Statistics "frequencies, correlation matrix", calculation of ionic balance and conductivity; Simulation of neutralization, ^{14}C dating, ^{18}O relationship and deuterium). Pakistan used point dilution technique for filtration velocity and multiwell technique for groundwater flow direction. Combination of these two techniques provided an estimate on in situ porosity and permeability. Brazil pointed the importance to have a preliminary conceptual model before designing the monitoring network. Brazil used Rockwork software for processing drilling information for the geology. Morocco and Pakistan used Tracer LPM software for modelling groundwater ages. Pakistan used EOC technique for estimation of recharge sources. This technique is useful to distinguish between sources or recharges where stable isotopes signatures of possible sources are similar (e.g., river and canal originating locally or from distant upstream) and the same has been successfully applied in alluvial formation.

These guidelines can be used for characterizing the groundwater systems at both operating and new proposed NPP sites.

1.3. Short description of the studied NPPs sites

The 10 Member States (MSs) participating in this CRP have NPPs which are at different stages of development (Fig. 1.1). In Brazil there are two NPPs in operation and one in construction; in Italy and Lithuania the NPPs are in a decommissioning phase; in Pakistan there are four NPPs in operation, three in construction and two planned; in Morocco, in Vietnam and in China there is one planned NPP; in Argentina there is one NPP in construction; in Japan and in Ukraine the NPPs object of study were closed after the accidents.

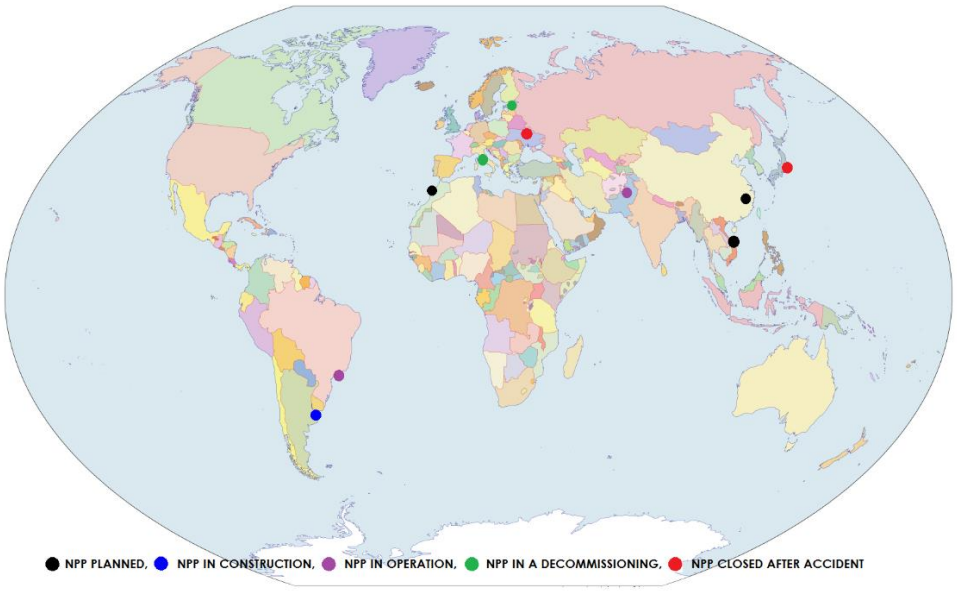

Fig. 1.1. Map of the NPPs studying during the CRP, which are at different stages of development

1.3.1. Argentina

The Ezeiza Atomic Centre is located in Buenos Aires province, which is far 33 km from Buenos Aires city. It covers an area of 840 hectares and is limited to the northwest by Matanza River and in the east by the Ezeiza International Airport. The Centre is located in the alluvial Matanza River basin.

This basin is considered the largest water system of regional relevance in the metropolitan area of Buenos Aires, covering an area of 2,240 km and traveling about 70 km before draining into the River Plate. The basin is characterized by an upper aquifer (Pampeano) and a lower aquifer (Puelche). Extraction for drinking water supply in urban areas is done from the Puelche aquifer and in suburban and rural areas from the Pampeano aquifer.

1.3.2. Brazil

The Centrais Nucleares Almirante Álvaro Alberto Nuclear Power Facilities – CNAAA I, II and III (under construction) are sited in the South Atlantic coastline, near the borders of the states of São Paulo and Rio de Janeiro, the two largest Brazilian states in economy and population. The distance of the power plants site to the nearest town, Angra dos Reis (169,330 inhabitants in 2010) is of 20 km. Angra lies some 100 km west of Rio de Janeiro. The site also lies some 220 km east-northeast of São Paulo city. This happens to be right at the epicenter of one of the most active tourism places in Brazil. BR-101 highway traverses the region at an average distance of 200 m north of the power plant site limits. The field investigation was confined to an area of about 5 km^2, including the CNAAA's premises and its immediate surroundings. It is well known that a thorough study of a candidate site for a NPP, including the aquatic environment, should be carried out during the siting process. Brazil has plans to build five additional NPPs, three of them in the southeast part of the country, where CNAAA is located. These plans have been postponed due to several reasons but they will hardly be dropped, in as much as the hydraulic potential for electricity generation in this region is nearly exhausted.

1.3.3. China

HK NPP, a planned NPP engineering in Jiangxi province, eastern China, is chosen as the research area in this project to study the migration of radionuclides in groundwater system in the vicinity of this inland NPP, using geochemical methods and isotopic techniques, in order to assist in controlling the pollution of water resources if unforeseen incidents happen. Isotopic compositions of hydrogen-2 and oxygen-18 in groundwater was applied in this project, combined with hydrochemical data, to decipher groundwater recharge resources and water-rock reactions in groundwater system of the vicinity of HK NPP.

1.3.4. Italy

The Garigliano NPP is situated in an inlet of the course of the Garigliano river, about 7 km away from the Tyrrenian sea between Rome and Naples.

In Italy, the nuclear technology to produce electric power has been abandoned since 1987, one year after the Chornobyl nuclear accident. Since then, the four Italian NPPs are in the decommission phase. During the decommission phase, environmental monitoring plans are carried out according to prescriptions of the Ministry of Environment and in agreement with the Ministry of Cultural Heritage and Tourism. In particular, for the Garigliano NPP of Sessa Aurunca, a semiannual environmental impact assessment is needed in order to monitor the atmosphere, water bodies (river and groundwater), soil, ecosystems (vegetation, flora and fauna) and ionizing radiations.

1.3.5. Japan

The Fukushima Daiichi NPP site lies approximately 220 km north of Tokyo at almost the midpoint of the Pacific coast of Fukushima Prefecture (North latitude: 37°25', East longitude: 141°00'). It straddles Okuma and Futaba townships of Futaba County in the Fukushima Prefecture. Its area is approximately 3.5 km^2. The region has an oceanic climate influenced by the warm waters of the Japan Current, which makes summers cooler and winters warmer than in inland areas. There is groundwater in the 20–30 m thick layer of sand and clay immediately below the site's thin layer of topsoil. Underneath the layer of sand and clay is an impermeable Neogene mudstone layer; groundwater flows through the layer of sand and clay towards the coast at approximately 10 cm/d.

1.3.6. Lithuania

The Ignalina NPP is located in the north-eastern part of Lithuania, near the borders with Belarus and Latvia. Previous investigations of NPP followed safety relevant external factors such as seismic activities, near surface geotechnical conditions, meteorological conditions, possibility of flooding in the area, external risks caused by human activity. The Strategy on Radioactive Waste Management was approved by the Government of Lithuania in 2008. Its objective is to define a radioactive waste management policy. This strategy is approved to implement the provisions of the Law of the Republic of Lithuania for Radioactive Waste Management, which establishes basic principles of Radioactive Waste Management. New management facilities, which are or will be built under the Decommissioning Programme, such as solid radioactive waste management and storage facility, spent nuclear fuel storage, landfill and near surface disposal facilities and others, are being financed by the Ignalina International Decommissioning Support Fund, Ignalina Programme and co-financed by the National Ignalina NPP Decommissioning Fund.

1.3.7. Morocco

Sidi Boulbra site selected to host the 1st Moroccan NPP, is located on the Moroccan Atlantic coast and presents all the physical characteristics necessary for the safe and economic construction and operation of the NPP. Sidi Boulbra site is a part of Akermoud plain that extends between the Atlantic Sea and Jbel Kourati and Jbel Hadid Mountains. Its northern boundary width of a dozen kilometres is marked by the outlet of Tensift River towards the Atlantic Ocean. Sidi Boulbra area contains a multilayered coastal aquifer flowing in Quaternary sandstones and Cretaceous limestone. It extends along the coast of width 15 km and length 45 km. The thickness of the layer varies from a few meters at Quaternary to more than 80 m in the Cretaceous aquifer. The groundwater flow direction: is SW to NE. The groundwater recharge occurs mainly from direct infiltration by rain and drainage from the underlying aquifers.

1.3.8. Pakistan

Chashma Nuclear Power Plant Complex is a commercial NPP consisting of four operating units (CHASHNUPPI-IV). It is located on the left bank of the river Indus about 10 km downstream of Chashma Barrage at an altitude of 200 m above mean sea level. The river Indus flows along the western boundary of the project area. The major hydrological features in the vicinity are the Indus River, Chashma Lake, Thal Canal and CJL canal Aeolian deposits overlie the Alluvium having thickness more than 400 in the form of Sand dunes. The climate is semi-arid and hot with average annual precipitation of 325 mm. The purpose of study is to know any change in the groundwater parameters due to NPPs operation, characterization of groundwater, dating of groundwater using modern techniques of noble gases and to develop a conceptual groundwater flow and contaminant transport model of the NPP site.

1.3.9. Ukraine

The Chornobyl Power Complex, lying about 130 km north of Kyiv, Ukraine, and 20 km south of the border with Belarus, consisted of four nuclear reactors of the RBMK-1000 design. On April 26, 1986, a sudden surge of power during a reactor systems test destroyed Unit 4 of the nuclear power station in Chornobyl. The accident and the fire that followed released massive amounts of radioactive material into the environment. The objective of this work is to develop methods to estimate hydrogeological parameters of aquifers according to observation results of the indicators distribution in the geological environment.

1.3.10. Vietnam

The Ninh Thuận 1 is the first NPP of Vietnam, planned at Phước Dinh in Thuận Nam District, which is a coastal province in the south of Central region of Vietnam. Although the NPPs design and

operation follows very strict safety guidelines, there is a possibility of unforeseen accidents, which may result in the release of radioactive materials into the environment or cause contamination of groundwater. This study was focused on characterizing hydrogeological conditions in the Ninh Thuan province using isotope hydrology tools and radioactive tracer isotopes.

1.4. Brief description on the use of isotope hydrology in solving hydrological problems

One of the prerequisites for efficient management of a water resource is reliable information about the quantity, flow and circulation of water within the resource that is being exploited. During the past six decades, isotope techniques have come to play a major role in the qualitative and quantitative assessment of water resources.

Isotope techniques can be used to solve such problems as: identification of the origin of groundwater, determination of its age, flow velocity and direction, interrelations between surface waters and groundwaters, possible connections between different aquifers, local porosity, transmissivity and dispersivity of an aquifer. The cost of such investigations is often small in comparison to the cost of classical hydrological techniques, and in addition they are able to provide information which sometimes cannot be obtained by other techniques.

With the evaluation of isotope data, many conclusions can be drawn, some of them unobtainable or difficult to ascertain by other methods. However, it should be emphasized that the use of these methods requires close collaboration with hydrologists in order to ensure a proper use and maximum interpretation of the isotope data. Probably the most important initial step is a clear definition of the problem, which, on the basis of the common hydrogeological investigational methods, may be expressed as which of a number of hypotheses is the most probable. The isotope method may then be used to indicate the hypothesis which is tenable or at least to eliminate some of the hypothesis made.

1.5. Summary, lessons learnt and recommendations

The present CRP was undertaken to develop guidelines for better hydrogeological characterization of local and regional groundwater systems in the vicinity of NPPs using environmental isotopes and conventional techniques. It also aimed to explore the use of new isotope techniques together with conventional ones to better assess the hydrogeological conditions in the geological settings of NPP sites and to provide basic information that may be used for predicting the fate of radioactive contaminants, such as tritium, released into groundwater in case of a radiological accident and/or during normal operations.

Defining groundwater flow patterns, flow rates (velocity) and direction of groundwater movement near the NPP can be used to help in the NPP site selection procedure.

The NPP's sites studied in this CRP are at different stages of development, as demonstrated in Fig. 1.1 and covered a wide variety of the hydrogeological settings including: fractured rock, metamorphic rock, crystalline rock, sedimentary rock.

Argentina. The hydrogeological system consists of an integrated multi-aquifer: a phreatic aquifer (free), a semi-free aquifer (Pampeano) that is associated to the phreatic building up a hydrogeological unit denominated Freático/Pampeano Aquifer, both contained in the geological formation Pampeano; and a deeper semi-confined aquifer called Puelche that corresponds to Arenas Puelches. The free and Pampeano aquifers consist of brown silt, clayey silt, and silty clay sediments; the Puelche Aquifer is situated on sand and gravel. Within this hydrogeological system, there is an internal transfer of groundwater between the Freático/Pampeano and the Puelche aquifers through the interposed aquitard.

Brazil. The lithological units of the areas of influence, both direct or indirect, are mainly formed by crystalline and sedimentary rocks. The crystalline rocks are mainly located at the hillside, while the sedimentary rocks are found mainly at beaches and rivers throughout the area.

China. The strata is mainly divided into two layers; the overburden layer is Quaternary unconsolidated sediment and the underlying bedrock is Triassic granite. There are four aquifer units – a loosely porous aquifer group, a clastic pore fissure aquifer group, a magmatic pore fissure aquifer group, and a metamorphic aquifer group.

Italia. The Garigliano River plain is a NE-SW oriented graben filled with upper Miocene-Quaternary infra-littoral, deltaic and continental clastic deposits, containing in the uppermost part volcanoclastic sediments from nearby Roccamonfina. The aquifer consists of marine and alluvial deposits, often with peat levels. In the NE sector these deposits overlap (or are interbedded with) pyroclastic layers of the Roccamonfina complex. Depending on the stratigraphy and granulometry of the deposits, the aquifer is confined or semi-confined.

Japan. The site is made up of the Tomioka Formation, which is approximately 200–400 m thick and consists of sandstone and mudstone at the bottom and a lenticular sand layer sandwiched by tuffaceous fine grain sandstone and mudstone at the top. This is covered by coastal terrace sediments approximately 5–10 m thick and made up of pebbles, sand, silt and clay. In order to build the plant on an acceptable bedrock foundation, the site was excavated, and the main plant and buildings of Units 1–4 were built at an elevation of approximately 10 m. The thick sediment of sandstone and mudstone was sufficient for bedrock supporting nuclear reactor buildings, so the primary structures were constructed directly on this mudstone.

Lithuania. The Baltic Artesian Basin (BAB) is contained mainly within the Neoproterozoic-Paleozoic and Meso-Cenozoic parts of the sedimentary bedrock of the Baltic region. BAB is a multistoried basin fulfilled with series aquifer systems and aquitards.

Morocco. Two main aquifers constitute the system of Sidi Boulbra NPP site: The Mio-Plio-Quaternary upper aquifer, represents an unconfined aquifer which is mainly composed of sand, sandstone and conglomerates, and The Cenomanian-Turonian lower aquifer is mainly calco-dolomitic. This carbonate formation represents a confined and discontinuous aquifer at a depth of more than 80 m.

Pakistan. A part of the upper Thal Doab, an interfluve between rivers Indus and Jhelum. It is underlain by unconsolidated Aeolian and alluvial deposits of quaternary age. The Aeolian deposits are mainly composed of fine sands. The Aeolian deposits overlie the alluvial sediments in the form of sand dunes.

Ukraine. In tectonic respect, it is located within the North-western slope of the Ukrainian Shield. The crystalline basement occurs at 20 to 80 m a.s.l., and the thickness of the sedimentary cover varies from 130 to 190 m. The sedimentary cover consists of marine and continental rocks of Mesozoic and Cenozoic erathems. The Chornobyl NPP site occupies a part of the first terrace above the floodplain at the right bank of the Pripyat River.

Vietnam. The groundwater flows in Holocene and Pleistocene aquifers, with the depths of 10 m and 16–21 m, respectively and the dominant flow is from southwest to northeast, corresponding to the river flow direction in this area. There seems to be an interaction of surface water and groundwater in this region. Streams and wells near the shoreline are affected by brackish water with high Na-Cl. The lithological composition of the Holocene and Pleistocene aquifers is mainly sand from coarse to fine, while the Upper Pliocene aquifer is formed mainly by powder and very fine sand. As being unconfined or partly unconfined aquifer, the source of water in aquifers could be rainwater which infiltrates into aquifers through aquifer's outcrop and/or from shallower aquifer.

The diversity of these sites resulted in use of a wide range of approaches in this CRP to resolve movement of water in the vicinity of NPP's (see paragraph 3).

The research conducted during this CRP has produced significant findings. The following lessons were learnt from this project:

✓ NPPs staff could have an opportunity to work with different concepts and methods that could be useful for their new developments on addressing environmental aspects. On the scientific staff point of view, there was the opportunity of getting more practical, on the job, perspectives of the usefulness of the methods applied to the area of study;

✓ understanding of hydrogeological and hydrogeochemical conditions is very important for siting of new nuclear facilities (repositories, NPPs);

✓ preparation of a baseline hydrogeological database to study the impact of NPPs operation on the environment.

The MSs involved in the CRP have different stages of development in nuclear industry; so, a closer cooperation among them is recommended, with the Agency's supervision to enhance MSs working groups collaboration on NPPs sites hydrological and environmental investigations.

Implement a Technical Cooperation Project on this topic for routine use in the MSs. Hydrogeological and environmental studies related to other nuclear facilities like repositories in addition to NPPs may be included in a future research project. The likely addition of tritium and other radionuclides in the atmosphere due to NPPs operation could disturb the natural isotopic signatures in the environment and for this situation; strategies or tools should be developed to account for these releases.

Continue sharing and transferring of isotope hydrology knowledge and technical experiences through training courses and academic researches.

References

Aggarwal, P.K., Basu, A.R., Poreda, R.J., Kulkarni, K.M., Froehlich, K., Tarafdar, S.A., Ali, M., Ahmed, N., Hussain, A., Rahman, M., Ahmed, S.R. (2000) A report on isotope hydrology of groundwater in Bangladesh: implications for characterization and mitigation of arsenic in groundwater. International Atomic Energy Agency-TC Project BGD/8/016, 64p.

Blasch, K.W. and Bryson, J.R. (2007) Distinguishing sources of ground water recharge by using δ^2H and $\delta^{18}O$. Ground Water, 45, 294–308.

Clark, I.D. and Fritz, P. (1997) Environmental Isotopes in Hydrogeology. Lewis Publishers, Boca Raton, New York.

Gat J.R. and Gonfiantini, R. (Eds) (1981) Stable Isotope Hydrology: Deuterium and Oxygen18 in the Water Cycle. IAEA Technical Report Series No. 210. IAEA: Vienna.

Gat JR. (1996) Oxygen and hydrogen isotopes in the hydrological cycle. Annual Review of Earth and Planetary Science 24: 225–262.

Hameed, A.S. et al. (2015) Isotopic characterization and mass balance reveals groundwater recharge pattern in Chaliyar river basin, Kerala, India. Journal of Hydrology: Regional Studies, doi: 10.1016/j.ejrh.2015.01.003.

International Atomic Energy Agency (1984) Nuclear Power Plant Siting: Hydrogeologic Aspects, Safety Series No. 50-SG-S7, IAEA, Vienna.

International Atomic Energy Agency (2002) Dispersion of Radioactive Material in Air and Water and Consideration of Population Distribution in Site Evaluation for Nuclear Power Plants, IAEA Safety Standards Series, safety Guide No. NS-G-3.2, IAEA, Vienna.

International Atomic Energy Agency (2003) Site Evaluation for Nuclear Installations, IAEA Safety Standards Series, Safety Requirements, No. NS-R-3, IAEA, Vienna.

International Atomic Energy Agency (2011) Meteorological and Hydrological Hazards in Site Evaluation for Nuclear Installations, IAEA Safety Standards for protecting people and environment, Specific Safety Guide No. SSG-18, http://wwwpub.iaea.org/MTCD/publications /PDF/ Pub1506_web.pdf.

Mazeika, J. et al. (2013) Radiocarbon and other environmental isotopes in the groundwater sites dor a planned new nuclear power plant in Lithuania. Proceedings of the 21st International Radiocarbon Conference edited by A J T Jull & C Hatté RADIOCARBON, Vol 55, Nr 2–3, 2013, p 951–962.

Singh, M.; Kumar, S.; Kumar, B.; Singh, S.; Singh, I.B. (2013) Investigation on the hydrodynamics of Ganga Alluvial Plain using environmental isotopes: A case study of the Gomati River Basin, northern India. Hydrogeol. J., 21, 687–700.

Solomon, D.K., Poreda, R.J., Cook, P.G., and Hunt, A., (1995) Site characterization using 3H/3He groundwater ages, Cape Cod, MA. Groundwater, V33 (6), 988-996.

Stadler, S., et al. (2010) Groundwater flow regime, recharge and regional-scale solute transport in the semi-arid Kalahari of Botswana derived from isotope hydrology and hydrochemistry. Journal of Hydrology, V388, 3-4, 291-303.

WNA (World Nuclear Association) (2015) Nuclear Power in the World Today, 2015, http://www.world-nuclear.org/info/Current-and-Future-Generation/Nuclear-Power-in-theWorld-Today/

ARGENTINA

Construction site of the RA10 reactor in the Ezeiza Atomic Center
https://www.argentina.gob.ar/cnea/ra10/en-imagenes.

2. CHARACTERIZATION OF GROUNDWATER SYSTEM IN EZEIZA ATOMIC CENTRE USING ENVIRONMENTAL ISOTOPES

P. SANCHEZ PROAÑO, L. FOLGUERA, G. NADER, V. SOLANES

Comisión Nacional de Energía Atómica. Buenos Aires, ARGENTINA

Abstract

The study area of this research is the Ezeiza Atomic Centre (CAE), in Buenos Aires province, Argentina, where the National Atomic Energy Commission is building a research reactor. The main objective of this work is to develop a hydrogeological conceptual model of the groundwater system using stable isotopes, noble gases and chemistry parameters. To achieve this goal, two sampling campaigns were carried out in March (rainy season) and August (dry season) 2018. In each one, groundwater and surface water samples were collected for physicochemical, stable isotopes and tritium determinations. In addition, three sampling campaigns of ^{222}Rn, electrical conductivity, temperature, and flow, and one campaign of noble gas and tritium were carried out. Based on the results, a preliminary hydrogeological conceptual model was developed: the groundwater system consists of two aquifers separated by an aquitard. The upper aquifer is recharged by local rainwater infiltration, and the ion concentration increases gradually through different hydrogeochemical processes. The flow path is influenced by the topography and the main creek that receives an inlet of groundwater. The bottom aquifer is recharged by the upper aquifer through the aquitard, therefore both aquifers have similar isotopic and chemical composition.

2.1. Introduction

In the Ezeiza Atomic Centre, the National Atomic Energy Commission (CNEA) is running a project for a new multipurpose research reactor: the RA-10. This new reactor will provide a replacement for the RA-3 reactor with greater capabilities for radioisotopes production in order to support local and regional future demand, it will allow to increase the production of molybdenum-99, lutetium-177 and iridium-192 and attempt the generation of new radioisotopes such as bismuth-213. Moreover, in this atomic centre there are other facilities related to the reactor applications, like a spent fuel assembly storage facility, hot cells, a fission plant, a solid waste storage facility and a liquid effluent treatment plant.

The CAE is located in the Buenos Aires Metropolitan Area (AMBA) which has been widely studied due to its socio-environmental complexity. For this reason, at regional level there is information on hydrogeology (Auge, 1986; Auge, 2004; INA, 2010; Vives, Mancino, and Scioli, 2012), surface and underground hydrodynamics (Auge, 1986; Auge, 2004; UNLP, 2008; INA, 2010; Vives, et. al., 2012; Armengol, Manzano, Bea, Pelizardi, Ormaechea and Martínez, 2016; Armengol, Manzano, Bea, and Martínez, 2017) and groundwater hydrochemistry (Auge, 1986; Auge, 2004; Zabala, Martinez, Manzano and Vives, 2016; Armengol, et. al., 2016 and Armengol, et. al., 2017). At the local level, Romanazzi, Hernandez and Augheben, 2016, propose a hydrogeological conceptual model that coincides in many ways with the regional model. However, despite the study system relevance, the information available is not enough to develop a conceptual model that allows describing the most important hydrogeochemical processes, estimating the residence times of groundwater and identifying the interconnection between surface water and groundwater.

Knowledge of the groundwater system in the Ezeiza Atomic Centre and its possible connections to the Matanza River are of fundamental importance for generation of reliable information to plan countermeasures of protection in case of accidental release of radioactive materials. For this achievement, the specific objectives of this work are: (1) the study of groundwater flow pathways and residence times, (2) the characterization of recharge areas, (3) the assessment of surface and groundwater connections nearby the Ezeiza Atomic Centre and (4) the development of a hydrogeological conceptual model.

2.2. Description of the study area

2.2.1. General features

The site under study belongs to the Chaco-Pampeana plain, which has a low topographic slope. The hydrological behavior in this region is characterized by diffuse basins where most of the rivers, lagoons and marshes are effluents. Recharge sites coincide with the upper parts (interfluves or watersheds) where, in general, water has better quality, increasing its saline content in the flow direction. The climatic characteristic results in hydraulic surplus because precipitation exceeds evapotranspiration.

The CAE is located in Buenos Aires province, 33 km far from Buenos Aires city. It covers an area of 840 hectares and is limited to the northwest by the Matanza River and in the east by the Ezeiza International Airport (Fig. 2.1). The Centre is in the Matanza River basin, which is considered the largest water system of regional relevance in the AMBA, covering 2,240 km^2. The basin is characterized by an upper aquifer (Pampeano) and a lower aquifer (Puelche). Extraction for drinking water supply in urban areas is done from the Puelche Aquifer and in suburban and rural areas from the Pampeano Aquifer.

Fig. 2.1. Ezeiza Atomic Centre location. Pink line marks CAE limits (source: Google Earth 2021)

In the area under study, the mean annual rainfall is 1,008 mm/y and the mean annual evapotranspiration is 812 mm. The distribution of rainfall along the year defines a rainier period from October to April that concentrates approximately 70% of the total rainfall, being the least rainy period from June to September. The water budget for the period 1951–2014 (Romanazzi, Hernandez and Augheben, 2016) shows that water excess occurs during the months of May to November (196 mm/y), while water deficit occurs from December to February with only 9 mm/y, coinciding with a higher evapotranspiration (Fig. 2.2).

The thermal regime has an annual variation between average minimum temperatures of 9.6 °C in July and average maximum temperatures of 23.6°C in January, for an annual modular temperature of 16.4 °C.

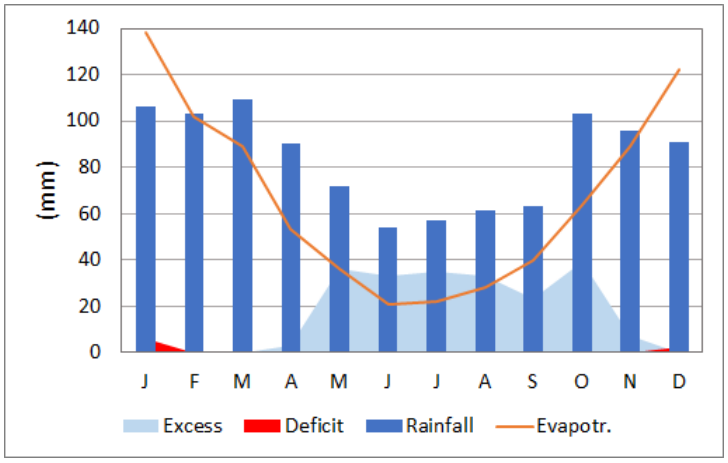

Fig. 2.2. Water budget. Modified from Romanazzi et al., 2016

2.2.2. Surface hydrology

The CAE is located in the sub-basin of the Aguirre Creek, which is a tributary on the right bank of the main collector of the basin, the Matanza River. The Aguirre Creek is the main water course inside the CAE, crossing it from SW to NE. Previous studies suggest that, within the bounds of the CAE, the Aguirre is an influent water course (Romanazzi et. al, 2016). This creek has two tributaries: El Palo Creek and the called "wetland", because in the area where the sample is collected the watercourse takes the form of a wetland. The preferential water recharge to the system is carried out in the interfluvial areas, adjacent to the watershed of the Aguirre Creek. These interfluves are located between the Matanza River and the Aguirre Creek and between the latter and the Ortega Creek (Fig. 2.3).

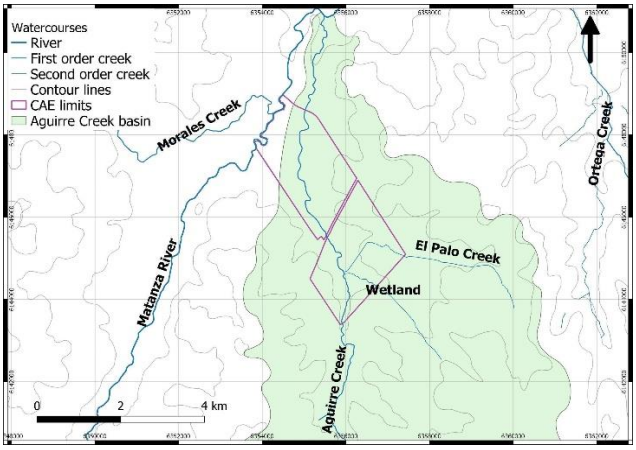

Fig. 2.3. Surface hydrology of Aguirre Creek basin

2.2.3. Geology and hydrogeology

From the bottom to the top, four sedimentary units can be identified: Olivos formation, an Eocene to early Miocene continental unit, Paraná formation from marine origin, Arenas Puelches formation, an early Pliocene and Pampeano and Post Pampeano sediments, the youngest geological units from Pleistocene-Holocene and Holocene respectively (Auge, 1986, 2004).

The hydrogeological system consists of an integrated multi-aquifer: a phreatic aquifer (free), a semi-free aquifer (Pampeano) that is associated to the phreatic building up a hydrogeological unit denominated Freático/Pampeano Aquifer, both contained in the geological formation Pampeano; and a deeper semi-confined aquifer called Puelche that corresponds to Arenas Puelches. The free and Pampeano aquifers go through brown silt, clayey silt, and silty clay sediments; the Puelche Aquifer is situated on sand and gravel (Fig. 2.4). Within this hydrogeological system, there is an internal transfer of groundwater between the Freático/Pampeano and the Puelche aquifers through the interposed aquitard.

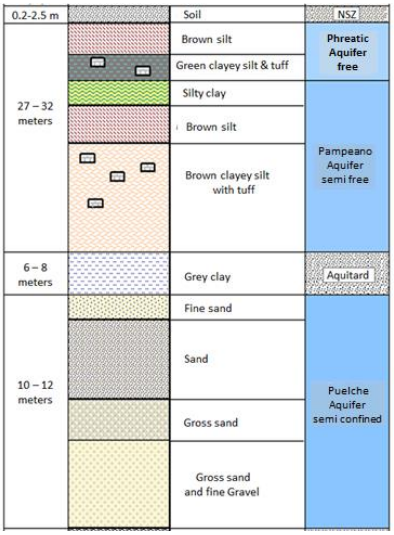

Fig. 2.4. A general hydrolithological profile of the study area
(Modified from Tangir, 2017)

2.3. Methodology

2.3.1. Sampling Network

The sampling network was designed based on the objectives set out in this project, criteria of representativeness and easy access. This network consists of 8 surface water points: 2 in the Matanza River, 3 in the Aguirre Creek and 3 in the tributaries (Fig. 2.5, a); and 27 wells located inside and outside the CAE, 16 of them from the Freático/Pampeano Aquifer and 11 from the Puelche Aquifer (Fig. 2.5, b). The characteristics of each sampling point are listed in Table 2.1.

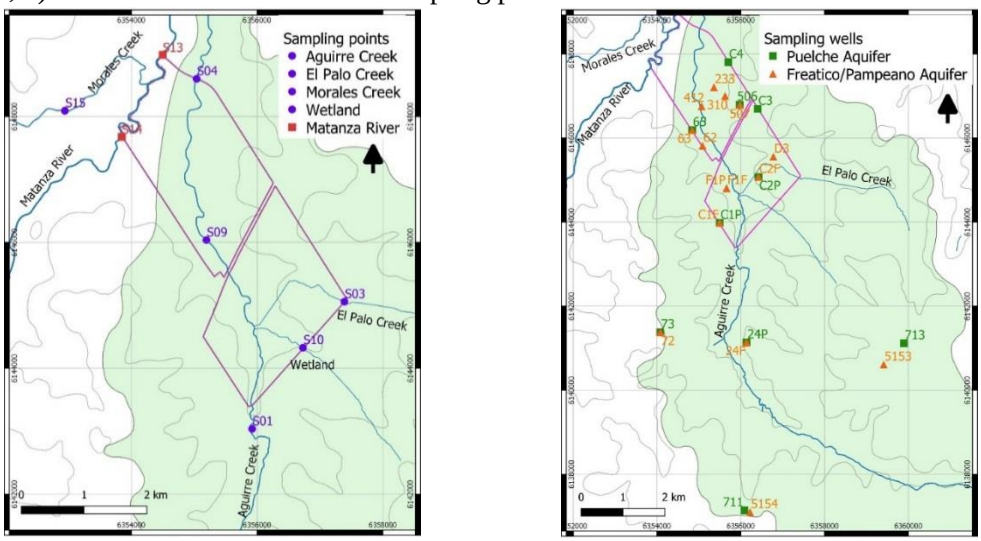

(a) (b)

Fig. 2.5. Sampling network: (a) surface water; (b) groundwater

A totalizer type rain collector was installed in the CAE in May 2018. Rainwater samples are being collected at the beginning of each month from that time to the present.

2.3.2. Piezometry

Water levels and electrical conductivity have been measured from 2016 to the present every three months on 17 wells; from October 2019 the measurements are carried out monthly on 7 wells. The piezometric levels were analyzed temporally and spatially.

2.3.3. Physicochemical parameters and stable isotopes

Two sampling campaigns were carried out, one of them in the rainy season: March 2018 and the other in dry season: August 2018. In each campaign 51 surface and groundwater samples were collected for physicochemical and stable isotopes determination. Water temperature, electrical conductivity (EC) and pH were measured in the field using an EC/pH meter. Alkalinity was determined by titration with 0.05N sulfuric acid. The major cations (calcium, magnesium, potassium, and sodium) and anions (chloride, sulphate, and nitrate) concentrations were determined by Atomic Absorption Spectrometry and Ion Chromatography, respectively. Stable isotopes samples were measured by DLT-100 liquid water isotope analyzer in "Laboratorio de hidroquímica e hidrología isotópica" of Mar del Plata National University, Argentina. The quality of the chemical analysis was evaluated with ion balance error $\leq 10\%$ criteria.

The hydrochemical data were analyzed by statistical analysis, temporal and spatial analysis of EC, Stiff and Piper diagrams, Principal Component Analysis (PCA) and comparison of major ions with EC. The obtained data for stable isotopes were analyzed by classical δ^2H vs $\delta^{18}O$ graphics and the comparison of stable isotope values with chloride concentration. As regards rainfall isotopic data, the

currently available results correspond to the series May 2018 to December 2019, upon the basis of these a Local Meteoric Water Line (LMWL) for the CAE is being constructed to compare to the Buenos Aires Meteoric Water Line that was made with historical $\delta^{18}O$ and $\delta^{2}H$ rainfall values (1979–2002) of Buenos Aires city (Dapeña and Panarello, 2004).

Table 2.1. Description of the sampling points

Site	Label	Source	Aquifer	Depth (m)	Latitude S	Longitude O
CAE 1 F	C1F	Groundwater	Freático/Pampeano	28,2	34°50'24,10"	58°34'47,20"
CAE 1 PU	C1P	Groundwater	Puelche	59,0	34°50'24,10"	58°34'47,20"
CAE 2 F	C2F	Groundwater	Freático/Pampeano	38,7	34°49'49,20"	58°34'10,20"
CAE 2 PU	C2P	Groundwater	Puelche	55,7	34°49'49,20"	58°34'10,20"
CAE 3	C3	Groundwater	Puelche	46,5	34°48'56,60"	58°34'10,00"
CAE 4	C4	Groundwater	Puelche	52,9	34°48'20,20"	58°34'36,80"
DAP 3	D3	Groundwater	Freático/Pampeano	12,2	34°49'33,74"	58°33'55,91"
FACIRI 1P	F1P	Groundwater	Freático/Pampeano	9,8	34°49'57,5''	58°34'40,4''
FACIRI 1F	F1F	Groundwater	Freático/Pampeano	8,7	34°49'57,4''	58°34'40,3''
62	62	Groundwater	Freático/Pampeano	11,2	34°49'24,4''	58°35'2,2''
63	63	Groundwater	Freático/Pampeano	35,0	34°49'12,2''	58°35'11,8''
65	65	Groundwater	Puelche	38,9	34°49'12,2''	58°35'11,8''
72	72	Groundwater	Freático/Pampeano	15,6	34°51'47,90"	58°35'44,60"
73	73	Groundwater	Puelche	37,3	34°51'47,80"	58°35'44,80"
233	233	Groundwater	Freático/Pampeano	7,5	34°48'9,41''	58°34'50,67''
310	310	Groundwater	Freático/Pampeano	11,0	34°48'46,28''	58°34'40,37''
412	412	Groundwater	Freático/Pampeano	27,9	34°48'54,0''	58°35'2,5''
506	506	Groundwater	Puelche	35,7	34°48'53,3''	58°34'26,7''
507	507	Groundwater	Freático/Pampeano	12,7	34°48'53,4''	58°34'26,6''
ACUMAR 24 F	24F	Groundwater	Freático/Pampeano	13,7	34°51'56,74"	58°34'23,85"
ACUMAR 24 P	24P	Groundwater	Puelche	38,2	34°51'56,74"	58°34'23,85"
ACUMAR 15 F	15F	Groundwater	Freático/Pampeano	11,5	34°49'24,30"	58°30'40,10"
ACUMAR 15 P	15P	Groundwater	Puelche	39,7	34°49'24,30"	58°30'40,10"
AySA-EZ5153	5153	Groundwater	Freático/Pampeano	20,2	34°52'15,51"	58°32'15,31"
AySA-EE713	713	Groundwater	Puelche	47,2	34°51'59,32"	58°31'56,06"
AySA-EZ5154	5154	Groundwater	Freático/Pampeano	20,0	34°54'7,81"	58°34'23,04"
AySA-EE711	711	Groundwater	Puelche	--	34°54'6,36"	58°34'28,37"
1	S01	Surface water	N/A	N/A	34°50'55"	58°34'31,2"
3	S03	Surface water	N/A	N/A	34°49'50,2"	58°33'32,2"
4	S04	Surface water	N/A	N/A	34°47'54,1"	58°35'02,5"
9	S09	Surface water	N/A	N/A	34°49'17,32"	58°34'57,97"
10	S10	Surface water	N/A	N/A	34°50'13,6"	58°33'58,6"
13	S13	Surface water	N/A	N/A	34°47'41,49"	58°35'23,44"
14	S14	Surface water	N/A	N/A	34°48'23,33"	58°35'49,86"
15	S15	Surface water	N/A	N/A	34°48'9,47"	58°36'25,27"

2.3.4. Tritium

To characterize the tritium content of surface and groundwater, in March 2018, 10 samples were collected: 1 in surface water (Aguirre Creek), 4 in the Freático/Pampeano Aquifer and 5 in the Puelche Aquifer. In August 2018, 15 samples were collected: 3 in surface water, 6 in the Freático/Pampeano Aquifer and 6 in the Puelche Aquifer. In February 2020, 11 samples were collected: 5 from the Freático/Pampeano Aquifer and 6 from the Puelche Aquifer. Samples were sent to: "Laboratoire d'Analyses Structurales et Isotopiques de Centre National de l`Energie des Sciences et des Techniques Nucléaires", Morocco (1st campaign); "Laboratorio de Tritio Ambiental, Centro de Desenvolvimento da Tecnologia Nuclear", Brazil (2nd campaign) and Isotope Hydrology Laboratory (IHL), IAEA, Vienna (3rd campaign). Tritium content values of rain, surface and groundwater were analyzed.

2.3.5. Groundwater dating

The apparent age of groundwater samples was determined using the tritium-helium 3 methodology (T-^{3}He), for which, in February 2020, a campaign was carried out, 12 groundwater samples (C1F, C1P, C2F, C2P, 507, 506, 72, 73, 5153, 711, 5154 and 713) were taken using an adequate methodology for sampling noble gases dissolved in water (Aeschbach-Herting and Solomon, 2013; IAEA, 2007). Measurements on the samples were performed by the IHL of the IAEA. Before calculating the apparent ages, two analyzes were carried out. First, the neon concentration (Ne) was

analyzed as a function of the xenon concentration (Xe) in order to visualize those samples that are degasified and therefore not datable. Then an analysis of the $^{3}He/^{4}He$ ratio vs the Ne/He ratio was carried out with the aim of identifying those samples containing helium generated in the crust and therefore with very old apparent ages. After these analyzes, the apparent ages were calculated for the corresponding samples, using the T-^{3}He method (Schlosser, 1992).

The mean residence time was determined in those samples with apparent ages less than 60 years. It was calculated using a lumped parameter model (LPM) and tritium (measured in the campaigns explained before) as a tracer for fit. The partial exponential model (PEM) was selected because it is the one that best adjusts to the characteristics of the Freático/Pampeano Aquifer. To build the input function, the data of the tritium content in rainwater measured in Ciudad Universitaria (33 km from the CAE) and in the town of Ezeiza (5 km from the CAE) were used. These data are available in the databases of the Global Network on Isotopes in Precipitation of the IAEA (IAEA 2020). Mean residence time calculations were performed using TracerLPM, a free software developed by the United States Geological Survey (Jurgens, Böhlke, and Eberts, 2012).

2.3.6. ^{222}Radon

The determination of the ^{222}Rn activity in water, together with the knowledge of the flow rates of the receiving rivers and other physicochemical parameters, such as electrical conductivity, allows an approximate characterization of the discharge (Pritchard, Herczeg and Lamontagne, 2003). This tool was used to identify possible stretches of the Aguirre Creek with groundwater inflows.

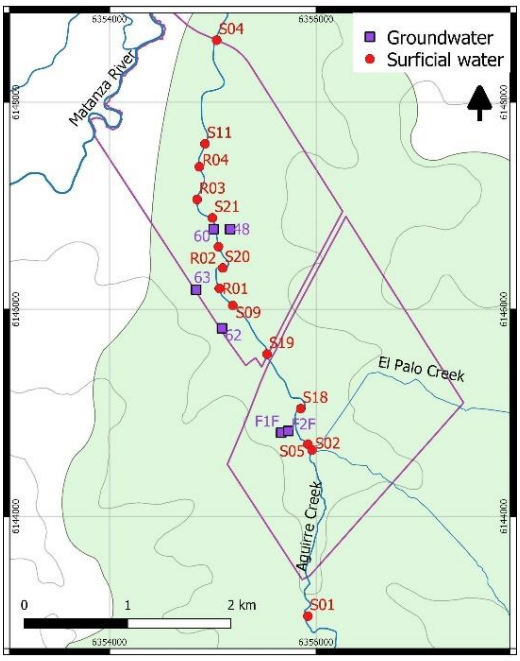

Fig. 2.6. ^{222}Rn sampling points

The activity of ^{222}Rn was measured along the Aguirre Creek in a section between its entrance (S01) and its exit (S04) from the CAE and on selected piezometers closest to the watercourse (Fig. 2.6). Three field campaigns were conducted where EC, ^{222}Rn activity and flow were measured. ^{222}Rn activity determination was performed in the laboratory by means of the Sarad RTM 1688 portable spectrometer. Duplicate Rn measurements from each sample were carried out. The first field campaign took place in January 2019. Its objective was to do a preliminary survey to verify that quantifiable ^{222}Rn values could be obtained and to corroborate significant differences between Rn activity values in surface and groundwater. This campaign included 5 surface water and 6 groundwater sampling points. Surface water was sampled by means of a bucket, while a pump was used for groundwater sampling. The second field campaign was carried out in August 2019. A longer section of the stream was covered during this campaign, between its entrance (S01) and its exit (S04) from the

CAE. The objective of this sampling was to detect significant variations in ^{222}Rn activity along the Aguirre Creek that could be indicative of groundwater inflow. Surface water samples were obtained using a submerged pump at the closest point to the stream bed, avoiding sediment resuspension. The third field campaign took place in September 2019. Based on the previous results (second campaign), a special emphasis was placed on the section between S09 and S011 sampling points because it was expected to detect an underground water ingress based on ^{222}Rn and EC measurements. Surface water samples were taken by means of a submerged pump, as in the second campaign.

2.4. Results and discussions

2.4.1. Piezometry

2.4.1.1. Temporal analysis

The temporal analysis of the water level shows that the behavior is similar in almost all the wells: it rises after a rainy period and goes down after a dry period (Fig. 2.7). In the sampling points where there are wells to both aquifers, the water levels of the Freático/Pampeano Aquifer (upper aquifer) are always higher than those of the Puelche Aquifer (lower aquifer) (see Fig. 2.7), confirming the downward flow between them (Vives, Mancino and Scioli, 2012). The Puelche Aquifer response is almost identical to that of the Freático/Pampeano Aquifer. This could be due to the pressure generated by the upper aquifer which is transmitted through the aquitard (plastic medium) to the lower aquifer, increasing the level in it.

2.4.1.2. Spatial analysis

The piezometric maps of the three campaigns are very similar in both aquifers. The flow paths in the Freático/Pampeano Aquifer seem to be conditioned by surface morphology; they follow the same direction as the Aguirre Creek. In the Puelche Aquifer the flow lines follow a southwest-northeast direction (Fig. 2.8). These behaviors, in both aquifers, were described by UNLP (2008) at regional level.

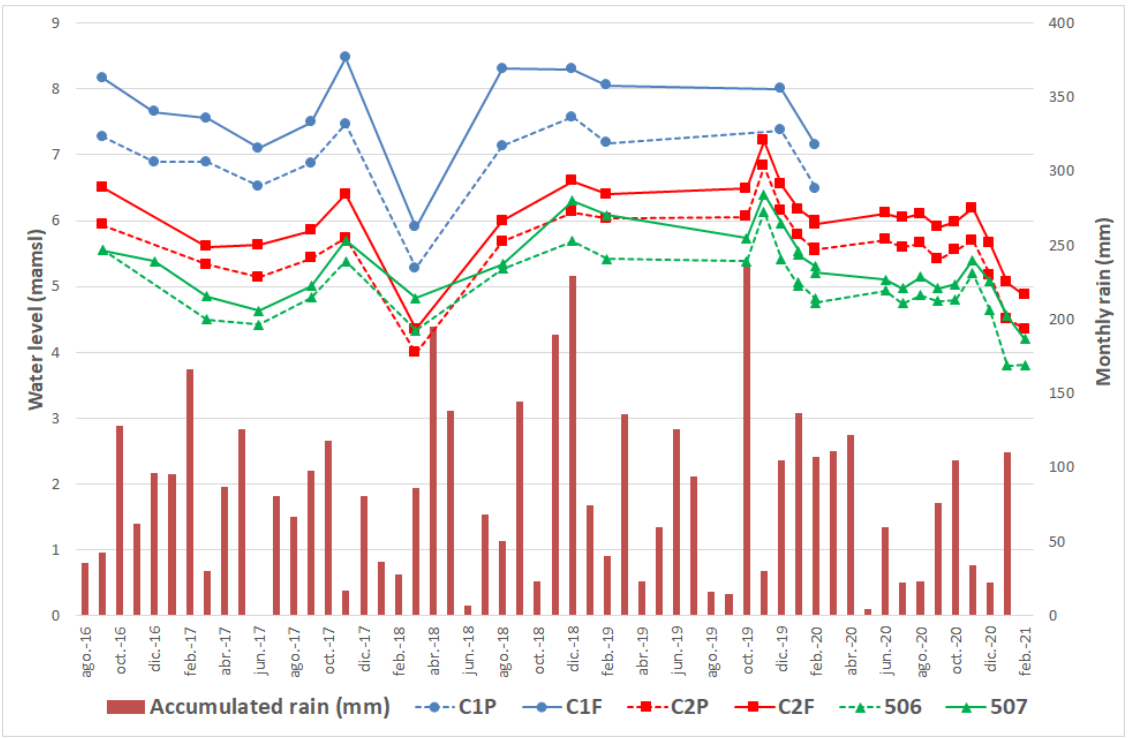

Fig. 2.7. Water level temporal variation in wells: 507, C1F and C2F (Freático/Pampeano Aquifer), and 506, C1P and C2P Puelche Aquifer)

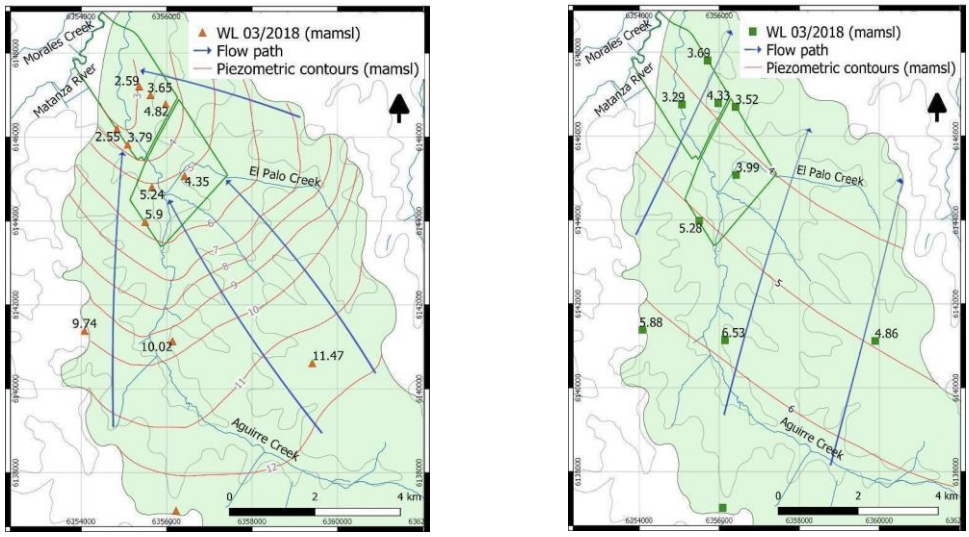

(a) (b)

Fig. 2.8. Piezometric map: (a) Freático/Pampeano Aquifer; (b) Puelche Aquifer. March 2018

2.4.2. Hydrochemistry

Physicochemical analysis results of March and August 2018 campaigns are shown in Tables 2.2 and 2.3, where the values of number of samples (n), means, standard deviation (SD), minimum (Min.) and maximum (Max.) of the parameters measured are indicated. Most of the chemical analysis (90%) showed ionic balance errors smaller than 10%, whereas the remaining showed errors slightly higher.

Table 2.2. Physicochemical parameters values of surface water in March and August 2018 campaigns

Surface water - March 2018						
	Units	**n**	**Mean**	**Min.**	**Max.**	**SD**
pH		8	6.8	4.7	8.4	1.6
EC	µS/cm	8	1029	400	1898	499
Total alkalinity	mg CaCO3/l	8	320	165	542	113
Na	mg/l	8	157	69	286	75
K		8	17	9	26	5
Mg		8	13	7	16	3
Ca		8	28	22	31	3
NH_4^+		8	14	1	30	13
F^-		8	0.8	0.3	1.3	0.4
Cl^-		8	79	18	233	75
NO_3^-		8	25	8	61	20
SO_4^{-2}		8	73	23	225	75
PO_4^{-3}		8	3	0	9	3

Surface water - August 2018						
	Units	**n**	**Mean**	**Min.**	**Max.**	**SD**
pH		8	8.0	7.6	8.4	0.3
EC	µS/cm	8	1400	1050	1965	326
Total alkalinity	mg CaCO3/l	8	494	449	532	31
Na	mg/l	8	216	153	309	53
K		8	16	13	19	2
Mg		8	18	13	23	4
Ca		8	35	27	42	5
NH_4^+		8	7	3	21	6
F^-		8	0.9	0.6	1.1	0.2
Cl^-		8	87	38	190	51
NO_3^-		8	28	21	43	8
SO_4^{-2}		8	112	19	310	105
PO_4^{-3}		8	2	1	3	1

Table 2.3. Physicochemical parameters values of groundwater in March and August 2018 campaigns

FREÁTICO/PAMPEANO AQUIFER						
	Units	**n**	**Mean**	**Min.**	**Max.**	**SD**
pH		32	7.7	6.5	8.6	0.5
EC	µS/cm	32	1220	398	3900	649
Total alkalinity	mg CaCO3/l	31	462	154	669	107
Na	mg/l	32	216	17	483	115
K		32	13	7	22	4
Mg		32	25	5	54	14
Ca		32	42	9	152	36
F^-		32	3	1	6	1
Cl^-		32	57	1	208	57
NO_3^-		32	29	1	101	31
SO_4^{-2}		32	64	8	189	55
B	µg/l	32	419	101	840	213
Ba		32	130	20	378	96
Sr		32	512	50	1700	441
U		32	31	5	101	30

PUELCHE AQUIFER						
	Units	**n**	**Mean**	**Min.**	**Max.**	**SD**
pH		18	7.9	7.4	8.6	0.3
EC	µS/cm	18	933	423	1770	340
Total alkalinity	mg CaCO3/l	17	397	141	613	98
Na	mg/l	18	178	32	425	92
K		18	12	7	33	6
Mg		18	13	4	30	8
Ca		18	21	7	46	11
F^-		18	3	1	5	1.2
Cl^-		18	24	4	118	35
NO_3^-		18	46	1	101	35
SO_4^{-2}		18	28	11	111	30
B	µg/l	18	368	101	670	184
Ba		18	68	5	240	53
Sr		18	308	50	780	216
U		18	33	7	102	35

Analysis by PCA on groundwater based on both major and minor ion concentrations (Fig. 2.9), differentiates two groups of samples along PC2, that would correspond to each aquifer. PC2 shows high positive loadings for pH, fluoride and sodium, and high negative loadings for calcium, potassium, and magnesium. Consistently, the Tukey test (p=0.05) revealed that EC, total alkalinity, calcium, magnesium, barium, strontium, chloride, and sulfate concentrations are significantly higher in the Freático/Pampeano Aquifer than the Puelche Aquifer. These results suggest that the Freático/Pampeano Aquifer has, in general, a higher EC and calcium/sodium ratio. Subsequent analysis carried out in this work will try to find an explanation for these observations.

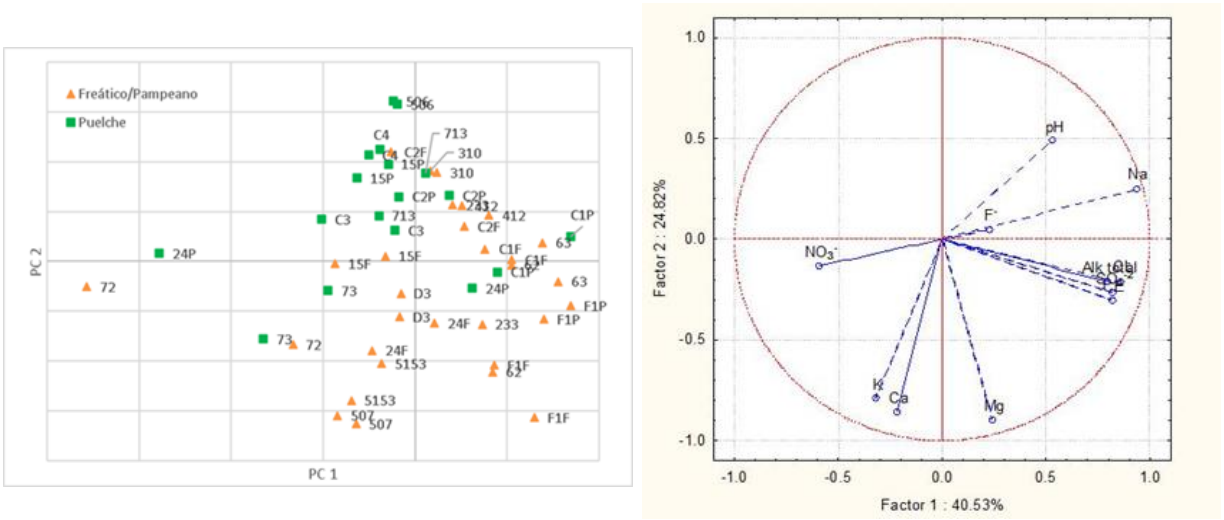

(a) (b)

Fig. 2.9. PCA of groundwater physicochemical data, March and August 2018; (a) water samples in PC1 vs PC2, orange marks: Freático/Pampeano Aquifer, green marks: Puelche Aquifer; (b) weights of the physicochemical variables on the first two PCs

In the case of surface water, cation and anion concentrations in the March 2018 campaign are, in general, lower than those of the August 2018 campaign (Table 2.2); this is probably due to the dilution effect caused by rains. In the same way, PCA analysis differentiates the two sampling campaigns along PC2 (Fig. 2.10, a). This differentiation is determined by the variables EC, alkalinity (bicarbonate), Ca, Mg and Na (Fig. 2.10, b), which are higher in August 2018 than March 2018 when the water would be diluted. However, statistically significant differences were detected only for calcium, magnesium, and total alkalinity (Tukey test, p=0.05). It is likely that, as more data will be gathered in future campaigns, clearer differences in other parameters will be spotted.

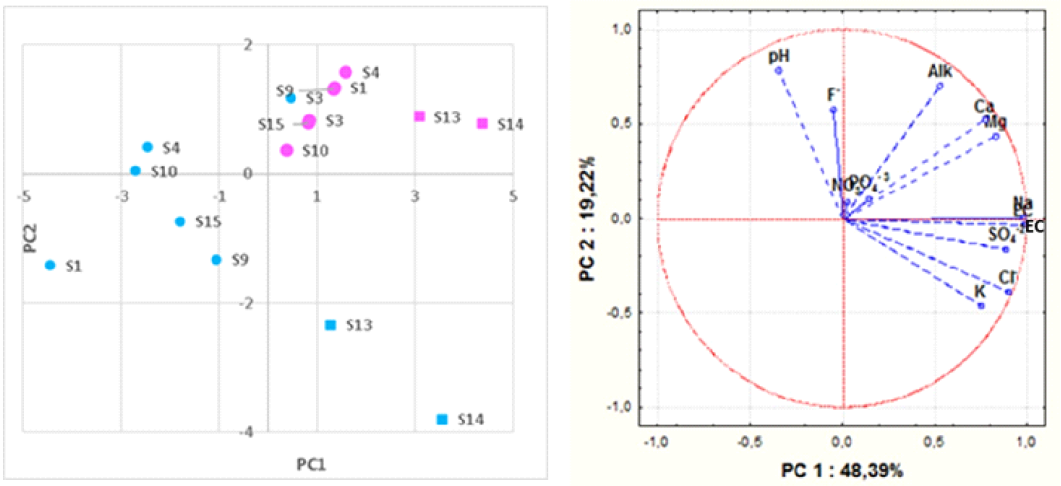

(a) (b)

Fig. 2.10. PCA of groundwater physicochemical data, March and August 2018: (a) water samples in PC1 vs PC2, light blue marks: March 2018, pink marks: August 2018; (b) weights of the physicochemical variables on the first two PCs (right)

2.4.2.1. Electrical Conductivity

Electrical conductivity analysis of the total data set (surface and groundwater) shows that the mean is 1,162 µS/cm with a standard deviation of 503 µS/cm. The maximum value is 3,760 µS/cm and the minimum value is 445 µS/cm. Statistical values indicate a significant variability of the total data set. The average EC for the surface water points is 1,086 µS/cm and 1,106 µS/cm for groundwater points. This indicates that there are no significant EC differences between both types of water bodies. Groundwater presents an average conductivity of 1220 µS/cm for the Freático/Pampeano Aquifer and 933 µS/cm for the Puelche Aquifer. Very high EC values were observed in well 65 (3,760 µS/cm and 3,690 µS/cm, in March and August 2018, respectively). This might indicate the presence of another process in addition to those already existing in the groundwater study area. Therefore, this sampling point was not included in this analysis.

2.4.2.1.1. Spatial variability analysis as a function of depth

Two different groups can be observed in the graph of EC as a function of depth (Fig. 2.11): one group marked with an arrow corresponds to the wells of the Freático/Pampeano Aquifer and another marked with an oval to the wells of the Puelche Aquifer. In most cases, in the first group, the EC increases as the depth of the well increases. As the recharge water flows downward, its dissolved ions concentration increases. In the second group where the wells collect water from the Puelche Aquifer, EC does not vary with depth. This is consistent with the fact that the Puelche Aquifer is a semi-confined aquifer without significant vertical flow.

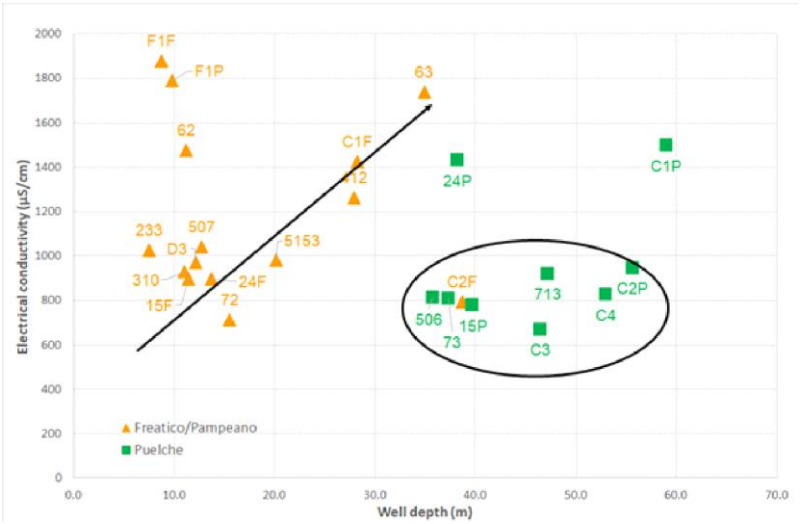

Fig. 2.11. EC as a function of depth, March 2018.
Orange marks: Freático/Pampeano Aquifer; green marks: Puelche Aquifer

2.4.2.1.2. Spatial variability analysis as a function of location

A map with the EC values measured in the Freático/Pampeano Aquifer is presented in the Fig. 2.12, a. Some wells with low EC values are in the upper part of the basin and some wells with higher EC values are in the lower part of the basin. This could be related to the flow direction described in the piezometric analysis. It can also be noticed that in the wells C1F, F1F, F1P, 62, 63 and 412, the EC values are higher than the average EC in the aquifer; this indicates a local affectation. These points have the singularity of being located near the stream bed of the Aguirre Creek. Fig. 2.12, b shows the map with the EC values measured in the Puelche Aquifer. The EC values do not suggest an evolution as a space function (within the analyzed scale). In the three campaigns, in the wells 24P and C1P, the EC values are above the average which could be due, as in the Freátco/Pampeano Aquifer, to local EC impact (natural or anthropogenic).

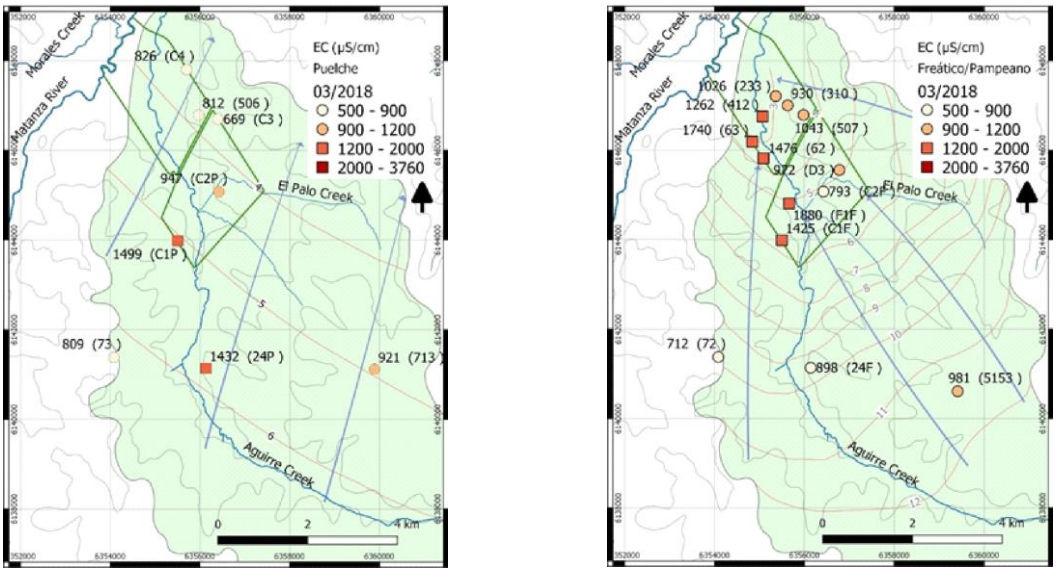

(a) (b)

Fig. 2.12. Map of EC variability in: (a) Freático/Pampeano Aquifer (March 2018),
(b) Puelche Aquifer (August 2018)

2.4.2.2. Water typologies and hydrological processes

2.4.2.2.1. Surface water

Stiff and Piper diagrams analysis, in both campaigns (March and August 2018), showed that surface water is sodium bicarbonate type in the creeks inside CAE and sodium sulphate in the Matanza River (Figs. 2.13 and 2.14). This differentiation could be attributed to a greater anthropogenic impact suffered by this river.

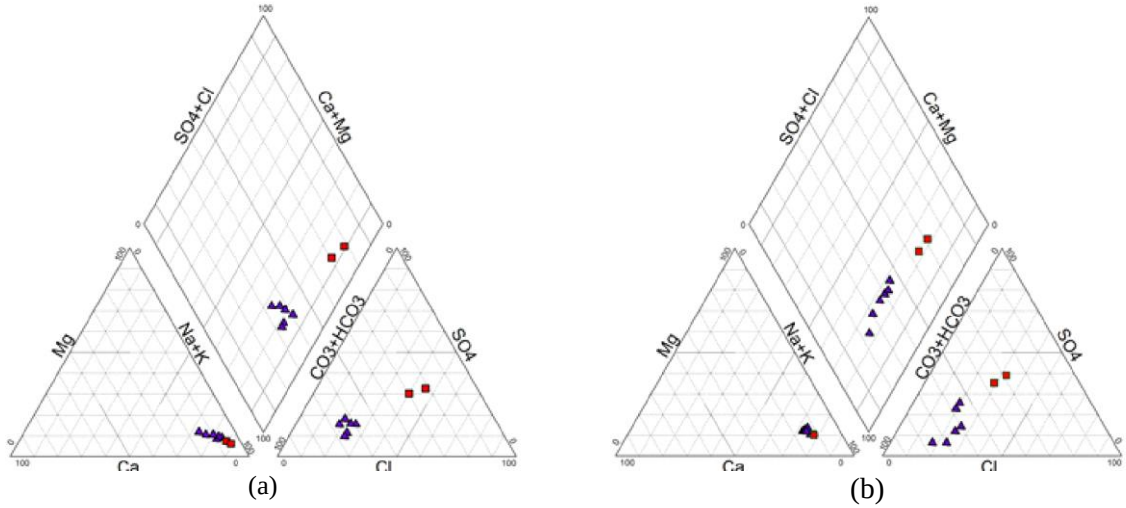

Fig. 2.13. Piper diagrams of surface water: (a) March 2018; (b) August 2018.
Red marks: Matanza River, purple marks: Aguirre Creek and tributaries

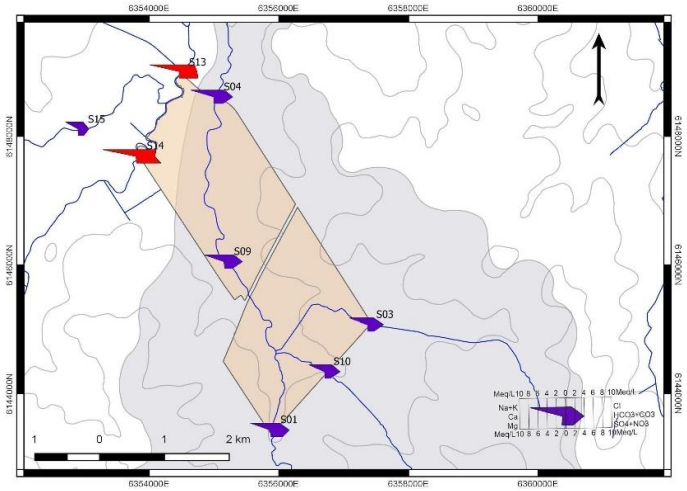

Fig. 2.14. Spatial distribution of surface water typologies; August 2018.
Red marks: Matanza River, purple marks: Aguirre Creek and tributaries

2.4.2.2.2. Groundwater

Major ion analysis (Fig. 2.15) allows the classification of the groundwater into sodium bicarbonate type and in a few samples as calcium bicarbonate. No differences between campaigns and aquifers as regards water type was evident. This description coincides with the historical data corresponding to previous sampling campaigns, studies carried out previously in the Ezeiza Atomic Center and in the Matanza Riachuelo basin, which indicates that the chemical composition is stable over the time (UNLP, 2008; Manzano, Zabala and Martinez, 2013; Zabala, Martinez, Manzano and Vives, 2016).

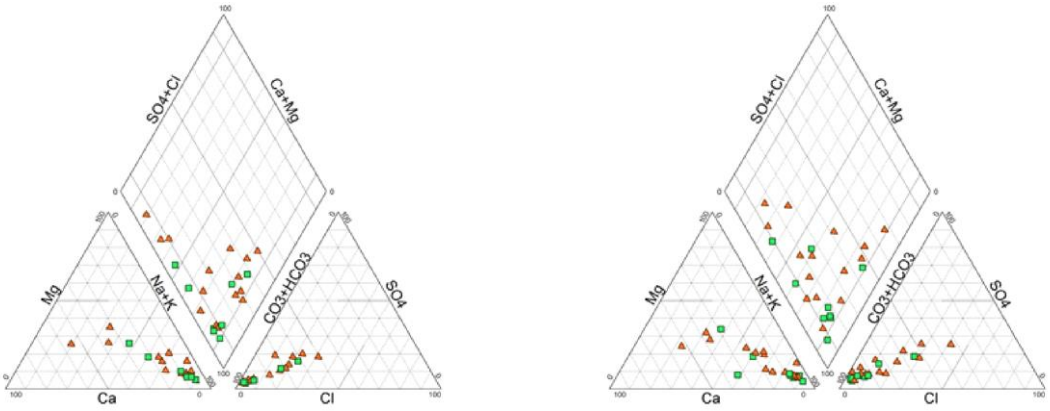

(a) (b)

Fig. 2.15. Piper diagrams of groundwater: (a) March 2018; (b) August 2018.
Orange marks: Freático/Pampeano Aquifer, green marks: Puelche Aquifer

The spatial distribution of the Stiff diagrams in both aquifers show that spatial evolution of water typology has no variation in flow direction (Figs. 2.16 and 2.17).

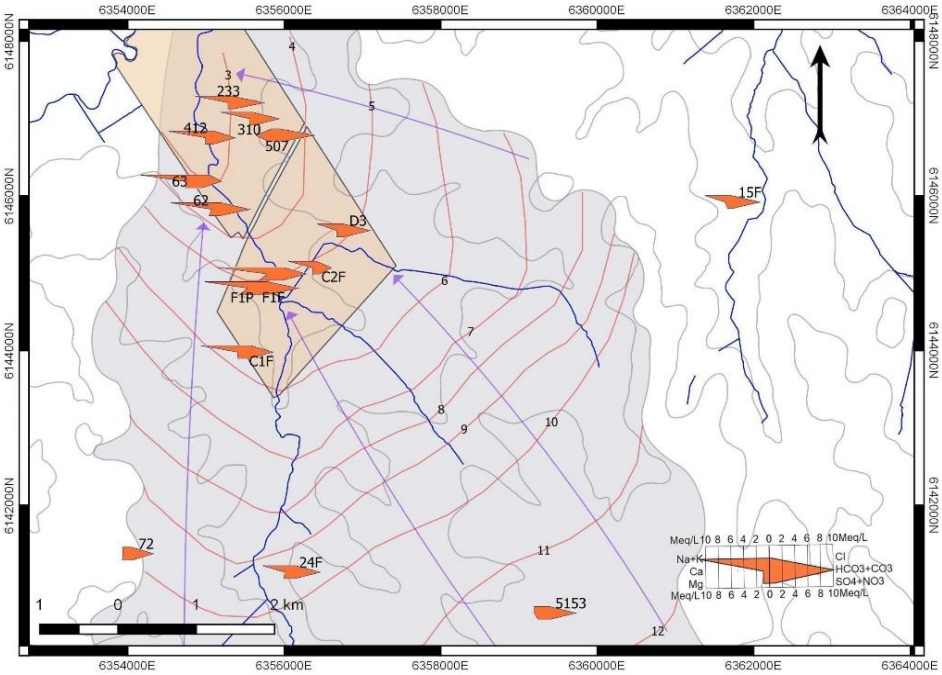

Fig. 2.16. Spatial distribution of the Freático/Pampeano
Aquifer typologies; March 2018

Piper diagrams in both campaigns (see Fig. 2.15) show that there is an evolution from calcium bicarbonate water into sodium bicarbonate water, which suggests a cation exchange process with sodium release and calcium adsorption. Bicarbonate abundance could be explained by edaphic CO_2, carbonates, albite and anorthite dissolution process. In certain samples, an increase in the sulphate and chloride content with respect to the mean is observed. That could be caused by sulphate and chloride high concentrations in the water mix process (contamination). A rich chloride sodium mix (sea water) is not observed as in other points of the Matanza River basin (Armengol, Manzano, Bea and Martinez, 2017).

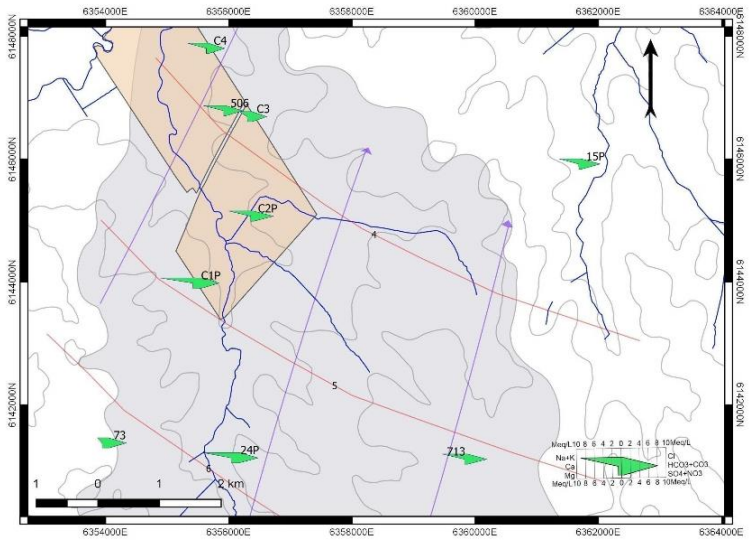

Fig. 2.17. Spatial distribution of the Puelche Aquifer typologies; March 2018

In cation triangle detailed analysis of both campaigns (Fig. 2.18), it can be observed that samples with highest calcium content are 507, 72 and 5,153, all of them from the Freático/Pampeano Aquifer. It could be assumed that these samples correspond to recently recharged water which has not gonethrough a cation exchange process. A set of samples with an intermediate calcium content is observed (partial cation exchange process). Some of them correspond to the Freático/Pampeano Aquifer (24F, D3, F1F and 15F) and others to the Puelche Aquifer (73, C3 and 24P).

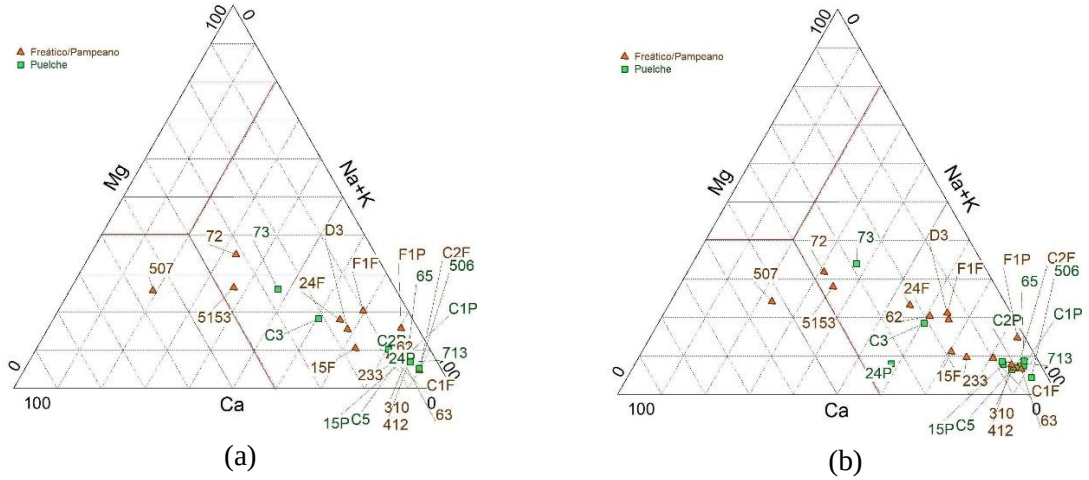

Fig. 2.18. Cations: (a) March 2018; (b) August 2018.
Orange marks: Freático/Pampeano Aquifer, green marks: Puelche Aquifer

The cation exchange process can be verified by analyzing the excess of sodium and potassium content with respect to chloride content as a function of the excess of calcium and magnesium content with respect to bicarbonate and sulfate content (Fig. 2.19). All the samples present an excess of sodium and potassium that is balanced by a deficit of calcium and magnesium with a trend line of slope approximately –1.

The analysis of the relationship of major ions with EC allowed us to determine that there is no pattern that relates calcium concentration to EC in any campaigns. This could be due to, in addition to the cation exchange process, a carbonate dissolution occurs at the same time. In particular, there are two points (calcium bicarbonate water type) in the Freático/Pampeano Aquifer with calcium values above the average and low EC values (< 1,200 µS/cm), which suggests that the calcium incorporation occurs very close to the moment of recharge, probably due to the dissolution of edaphic CO_2 and carbonates in the unsaturated zone (Armengol, 2017).

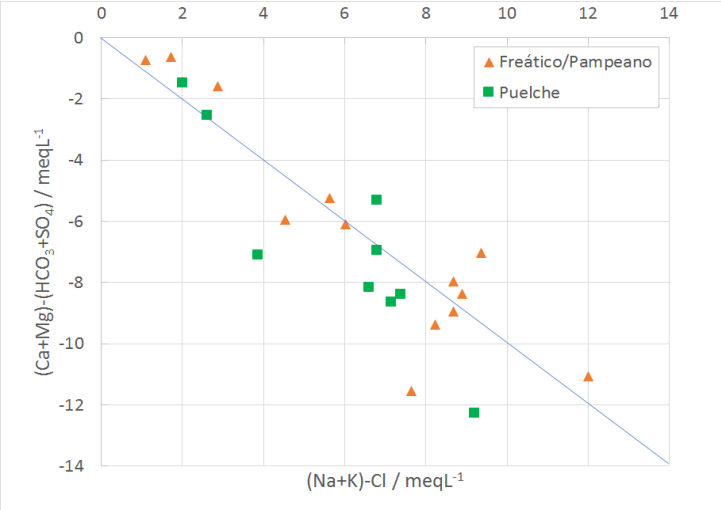

Fig. 2.19. Excess sodium and potassium compared to chloride vs deficit of calcium and magnesium compared to bicarbonate and sulfate, August 2018

On the contrary, a linear relationship between magnesium concentration and EC is observed (Fig. 2.20, a), but it differs according to the EC values. In samples with low EC values (< 1,200 µS/cm), the magnesium concentration increases with a greater slope than in the case of samples with high EC values (> 1,200 µS/cm). This would indicate that in samples with low EC values, magnesium does not disappear due to the cation exchange process and its concentration increases due to carbonate dissolution processes. In samples with high EC values the increase in magnesium is less significant, probably due to the mixing with polluted waters. Also, a linear correlation between sodium concentration and EC can be observed at all points except those considered to be the calcium bicarbonate type (507, 5153, 72 and 73) (Fig. 2.20, b). This agrees with the cation exchange hypothesis for samples with low EC values and the assumption of mixing with contaminated waters for samples with high EC values.

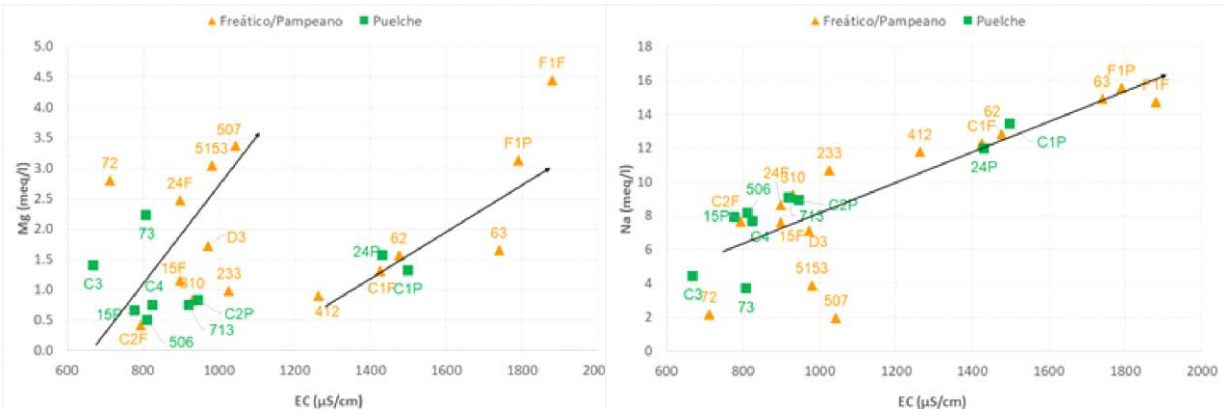

(a) (b)

Fig. 2.20. Magnesium concentration vs EC (a), sodium concentration vs EC (b). March 2018

In the March 2018 campaign, a linear relationship between bicarbonate concentration and EC is observed and two types of correlation can be differentiated. In samples with low EC values, the bicarbonate concentration increases linearly with the EC and the slope is lower in the other samples (Fig. 2.21, a). However, in the August 2018 campaign this pattern is not observed. Once again, this situation could be explained with the hypothesis of edaphic CO_2 and carbonates dissolution (for low EC samples) and mixing with polluted waters (for high EC samples).

Chloride and sulfate concentration increase linearly with EC in both campaigns (Fig. 2.21, b shows the pattern of chloride concentration). In low EC samples the slope is much lower than in high EC samples. This situation is consistent with the hypothesis of a possible mixing process with contaminated waters.

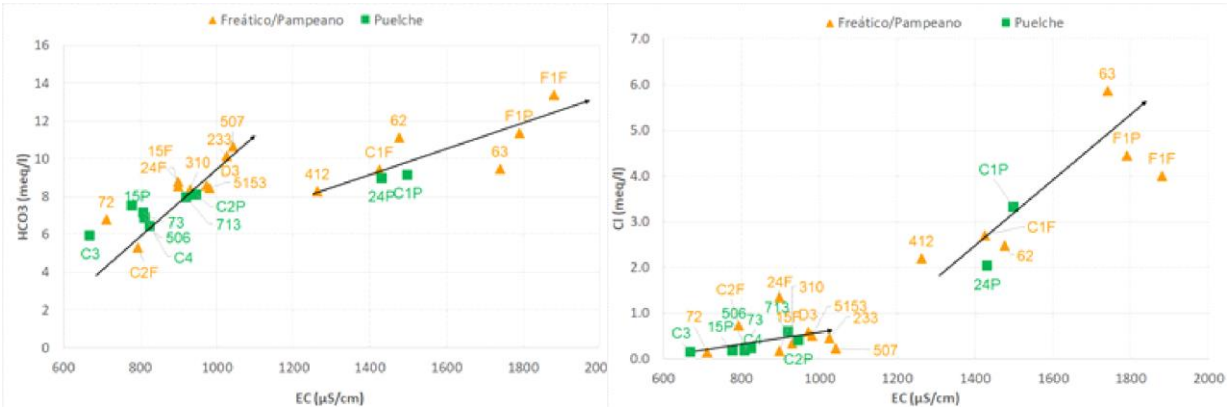

(a) (b)

Fig. 2.21. Bicarbonate concentration vs EC (a). Chloride concentration vs EC (b). March 2018

Based on this analysis, two main groups of groundwater samples with different relationships between EC and major ions concentrations can be defined: the mineralized samples with EC > 1,200 µS/cm (value close to the average) and the non-mineralized samples (EC < 1,200 µS/cm).

2.4.3. Stable isotopes

The analysis of the stable isotope concentrations shows that δ^2H and $\delta^{18}O$ in rainfall are statistically lower (p=0.05) than in the Freático/Pampeano Aquifer (Fig. 2.22 and Table 2.4). No statistical difference could be stated between both aquifers, which coincides with the findings in physicochemical parameters (Section 4.2). Surface water is expected to be more evaporated than groundwater, and in fact, lower average δ^2H and $\delta^{18}O$ values are seen in both aquifers compared to surface water. The fact that this difference could not be detected using the Anova technique is because, up to now, the available data corresponds to a short time series (less than two years) so it might not be representative of the complete universe of isotopic concentrations, for which more data compiling is needed.

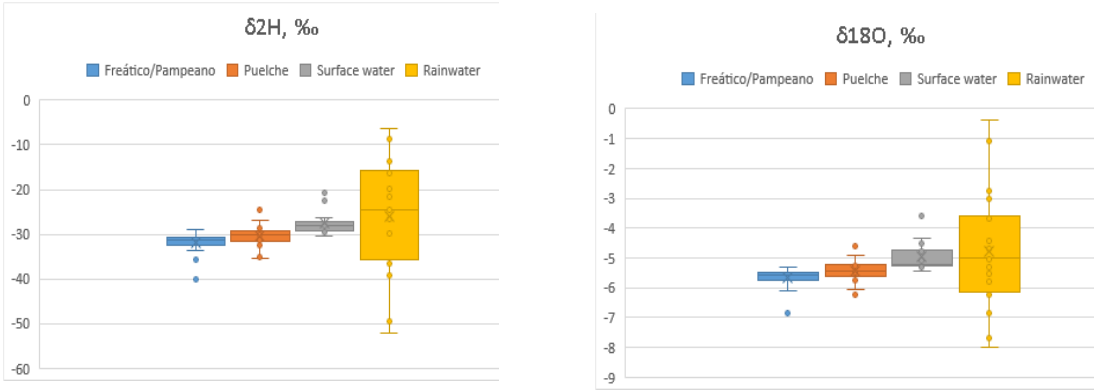

Fig. 2.22. Distribution of δ^2H and $\delta^{18}O$ in surface and groundwater (March and August 2018) and in rainwater (May 2018 through December 2019)

Fig. 2.23 shows stable isotopes data of rainfall samples collected at the CAE. The preliminary local meteoric water line for the system under study (May 2018 – December 2019 series) follows the equation $\delta^2H = 8{,}7*\delta^{18}O + 20$ while the Ciudad de Buenos Aires meteoric water line follows the equation $\delta^2H = 8*\delta^{18}O + 13$ (Dapeña and Panarello, 2004). Once again, given the shortness of the available data series, we cannot ensure the representativeness of this local meteorological line, and the records need to be expanded to improve the model. For this reason, in this work the LMWL of Ciudad Universitaria is used.

Table 2.4. Statistic parameters of δ^2H and $\delta^{18}O$ in surface and groundwater (March and August 2018) and in rainwater (May 2018 through December 2019)

	δ^2H(‰) Mean	δ^2H(‰) SD	$\delta^{18}O$(‰) Mean	$\delta^{18}O$(‰) SD	n
Rainwater	-25.96	12.84	-4.76	1.97	28
Freático/Pampeano	-31.82	2.16	-5.66	0.30	20
Puelche	-30.47	2.40	-5.45	0.35	21
Surface water	-27.54	2.54	-4.97	0.49	16

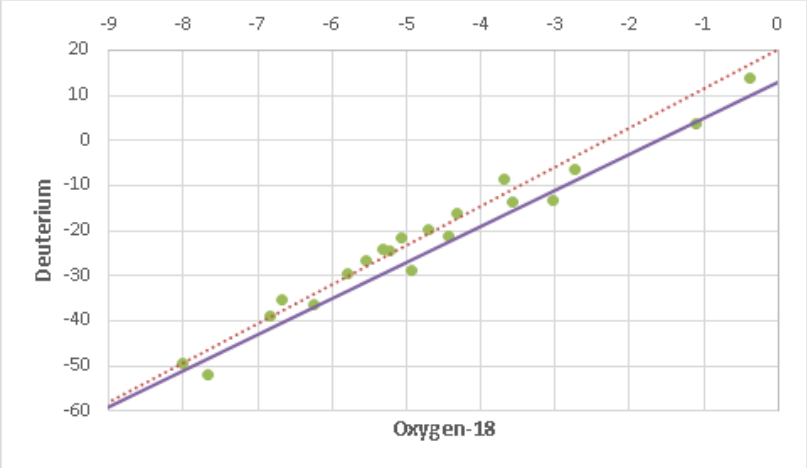

Fig. 2.23. Stable isotopes deviations ($\delta^{18}O$ and $\delta^{2}H$ VSMOW) of rainwater sampled at the CAE, May 2018 – December 2019 series. Dashed line: preliminary weighted local meteoric water line; solid line: Ciudad de Buenos Aires local meteoric water line

As regards hydrogeochemical processes, stable isotopes in surface water sampled in March 2018 suggest that evaporation is a clearly relevant process affecting the wetland and the Matanza River. But this is not the case in the Aguirre Creek, which has lower residence time (Fig. 2.24). This is consistent with the fact that in the wet season evapotranspiration is greater than precipitation. However, in August 2018, the results are different because there are no samples that line up following an evaporation line.

The ranges of $\delta^{18}O$ and $\delta^{2}H$ in both groundwater campaigns suggest that rainwater recharges the system locally, since they coincide with the range observed for local precipitation.

From the analysis of the relation between $\delta^{18}O$ and chloride, it could be determined that there is no mixture of seawater with groundwater, as was observed in the Piper diagrams, and that evapotranspiration is not a relevant process in the groundwater system under study.

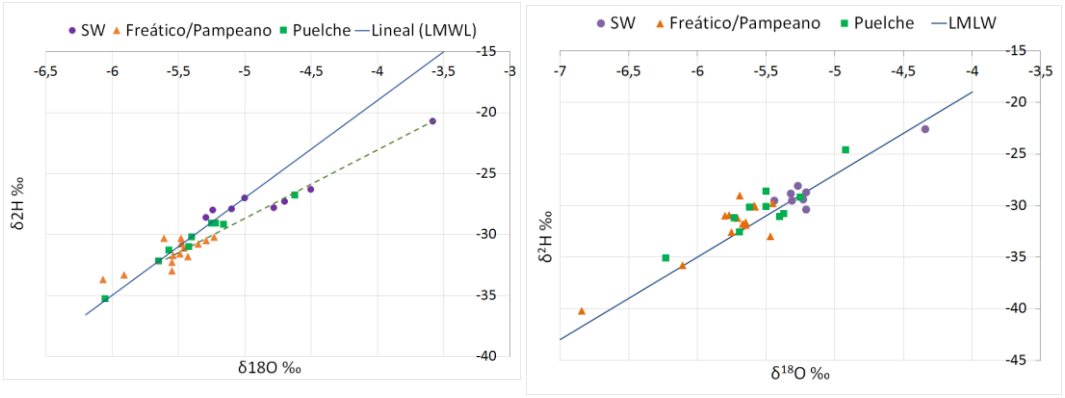

(a) (b)

Fig. 2.24. $\delta^{2}H$ vs $\delta^{18}O$ for surface waters (purple markings), Freático/Pampeano Aquifer (orange marks) and Puelche Aquifer (green marks). (a) Rainy season (March 2018); (b) Dry season (August 2018)

2.4.4. Tritium

To characterize the tritium content of rainwater, a one-point database of the GNIP was used. This point (Ciudad Universitaria) is 33 km from the CAE and has 199 tritium data measured between 1978–2002. The mean of this data series is 9.2 TU with a standard deviation of 3.5 TU.

Fig. 2.25 shows the tritium values in each sampled well for the three campaigns. The differences in the tritium values in surface water samples could be explained by the fact that a long-lasting rain event for 5 days (≈57 mm) occurred eight days before the August sampling campaign. The sampling point S14 is in the Matanza River approximately in the middle of their basin (with an area of 2,240 km^2), thus the river was probably still discharging much of the rainwater when the sample was collected. Therefore, the tritium content (3.42 TU) was influenced by the rainwater ($\bar{x}$=9.20 TU). The sampling points S01 and S03 are in the Aguirre Creek sub-basin (90 km^2) and the El Palo Creek sub-basin (10 km^2) respectively which are much smaller than the Matanza River basin. Thereby the amount of runoff water that was draining from these basins was less and the tritium content in the samples were mainly influenced by the contribution of groundwater more than the rainwater.

In samples from the Freático/Pampeano Aquifer (507, C1F, 5153, C2F and 72), the tritium values were similar in all campaigns. Samples 507, 5153 and 72 presented values above 1.5 TU, which would indicate young waters. In samples C1F and C2F the tritium values were always below 0.6 TU, which would indicate older waters.

In all the campaigns, samples from the Puelche Aquifer were taken from the same 5 wells. In 4 of them (C1P, 506, C2P, and 713) the tritium values were similar and less than 0.5 TU, which would indicate an older water age (with respect to the Freático/Pampeano Aquifer). The tritium values in wells C1F/C1P and C2F/C2P were very similar and always below 0.6 TU; this is consistent with the hydrochemical analysis results. In well 73, tritium values show great variability between campaigns (1.06 TU, 2.50 TU and 0.2 TU).

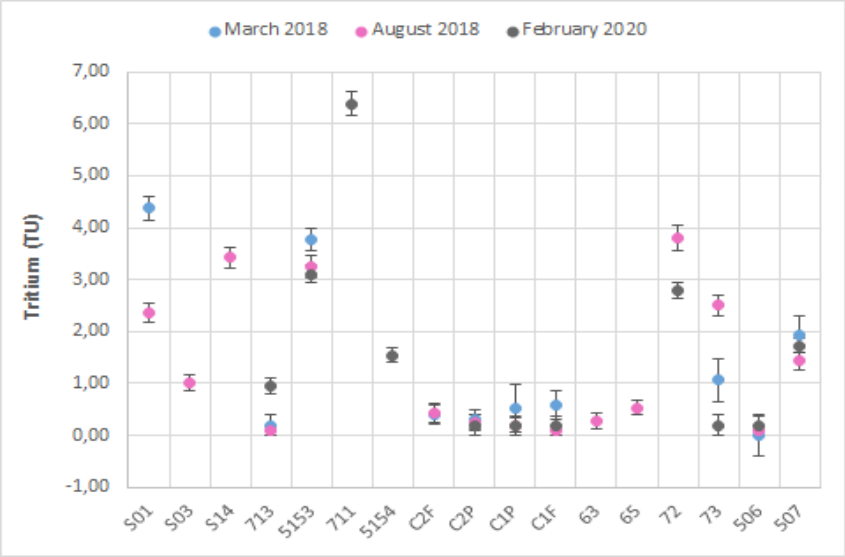

Fig. 2.25. Tritium values as a function of the sampling point.
March 2018 (blue marks), August 2018 (pink marks) and February 2020 (black marks)

2.4.5. Groundwater dating

2.4.5.1. T-^{3}He ages

Fig. 2.26 shows the relationship between the concentrations of Xe and Ne in water in equilibrium with the atmosphere at different temperatures (red points and red line) and the relationship between the concentrations of Xe and Ne measured in the different samples (blue points). The samples that are located on the left side of the red line have undergone a degassing process and the samples that are located on the right side present an excess of air. Therefore, no degassed samples are observed, and all samples show excess air: this result allows to calculate T-^{3}He ages.

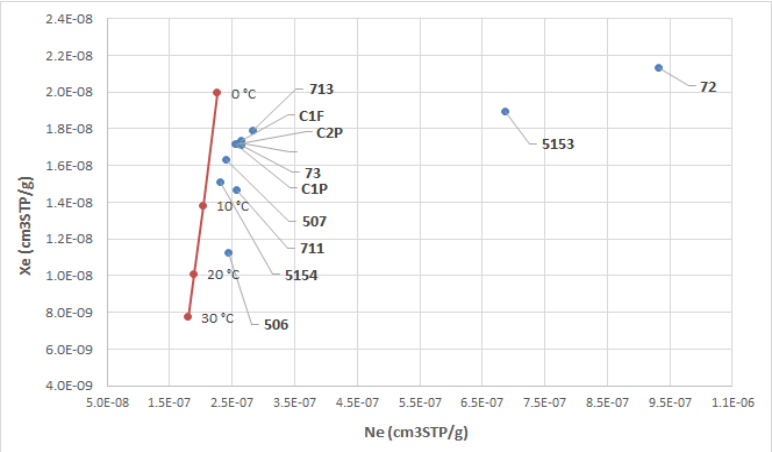

Fig. 2.26. Relationship between Xe and Ne concentrations measured in the samples (blue dots). Relationship between Xe and Ne expected in water in equilibrium with the atmosphere at different temperatures (red dots)

In Fig. 2.27, the samples C1F, C1P and 713 contain a significant excess of He with respect to Ne, and their $^{3}He/^{4}He$ ratio is less than this ratio in the atmosphere. This would indicate that in these samples the excess of He would be ^{4}He from the crust (due to the decay of uranium and thorium), which means that the age distribution of the water in these samples is mainly composed of old ages (> 500 years). This is consistent with the low tritium content observed in these samples and therefore it was not possible to calculate the T-^{3}He age in them.

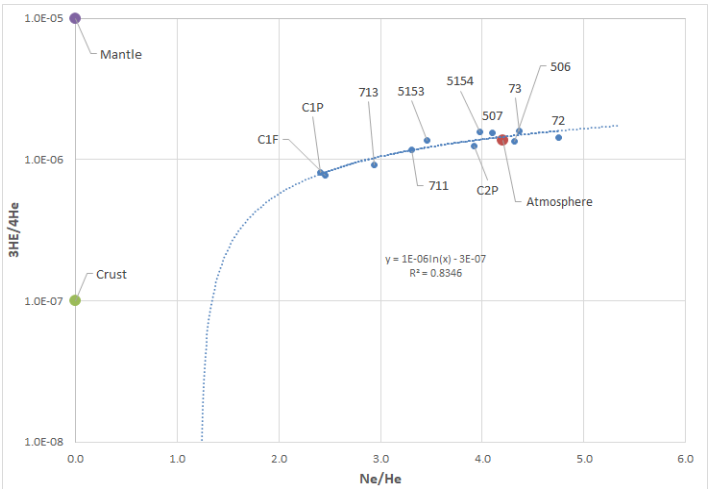

Fig. 2.27. $^{3}He/^{4}He$ ratio vs Ne/He ratio of the values obtained in the samples

The C2P and 506 samples presented negative calculated values in the content of tritiogenic ^{3}He, which would indicate that the age distribution of the water in these samples is composed mainly of ages that are above the technique limit (> 60 years). All the samples that correspond to old ages belong to the Puelche Aquifer (lower aquifer) which is consistent with antecedents of dating studies carried out in this aquifer (Hernández and González 1997; Panarello, Dapeña, and Auge 1994). The only exception is the C1F sample, which in theory corresponds to the Freático/Pampeano Aquifer but according to its apparent age (>500 years) corresponds to the Puelche Aquifer. This is in accordance with the results of the electrical conductivity analysis and the tritium content analysis.

Table 2.5 shows the calculated values (in those samples that it was possible) of T-^{3}He age. All the samples from the Freático/Pampeano Aquifer (upper aquifer), presented apparent ages between 16 and 26 years. The sample from well 73, which corresponds to the Puelche Aquifer, has an apparent age of 41 years. This would indicate that this well the water comes from the lower zone of the Freático/Pampeano Aquifer and not from the Puelche Aquifer. The sample collected from the well 711, that corresponds to the Puelche Aquifer, presents an apparent age of 6 years. This situation is considered anomalous since the tritium content in this sample is 6.38 UT, a value that is much higher than the tritium values observed in the other wells.

Table 2.5. T-^{3}He ages calculated on samples

					FINAL	
Well	Aquifer	Well depth (m)	^{3}He trit (TU)	Error (TU)	T-^{3}He age (yrs)	Error (yrs)
C1F	Freático/Pampeano (upper)	28	-3.7	0.9	> 500	
C1P	Puelche (lower)	59	-1.5	0.9	> 500	
713	Puelche (lower)	47	-4.7	1.1	> 500	
C2P	Puelche (lower)	56	-2.8	0.9	> 60	
506	Puelche (lower)	36	-2.9	0.8	> 60	
711	Puelche (lower)	47	0.8	0.9	5.9	2.6
507	Freático/Pampeano (upper)	22	3.4	1.2	19.4	4.2
72	Freático/Pampeano (upper)	16	4.8	0.6	17.7	1.6
73	Puelche (lower)	37	1.8	0.9	41.0	7.5
5153	Freático/Pampeano (upper)	20	4.4	2.6	15.6	6.2
5154	Freático/Pampeano (upper)	20	5.1	1.3	26.0	3.6

2.4.5.2. Mean residence time

Table 2.6 presents the values of the calculated mean residence time, the PEM parameter (relationship between the sampled and the unsampled depth), the relative error that arises from the adjustment process and the number of samples used in each calculation. The values of the mean residence time vary between 32 to 74 years. The order of these values coincides with that observed in the variation of the apparent ages.

Table 2.6. Average residence times calculated using a PEM model from the tritium data measured in the campaigns of March 2018, July 2018, and February 2020

Well	Mean residence time (yrs)	PEM parameter	Relative error	Samples used
507	47.06	0.82	26.2%	3
72	37.75	0.23	25.6%	2
73	74.26	0.32	57.2%	2
5153	32.62	0.21	13.3%	3
5154	52.92	0.48	0.0%	1

Table 2.7. Statistical description of the calculated age distributions

	Age distributions, g(t) (yrs)		
Well	Min (10% accumulated)	Max (90% accumulated)	Media (50 % accumulated)
507	20	85	37
72	9	78	27
73	21	149	56
5153	7	68	23
5154	20	100	41

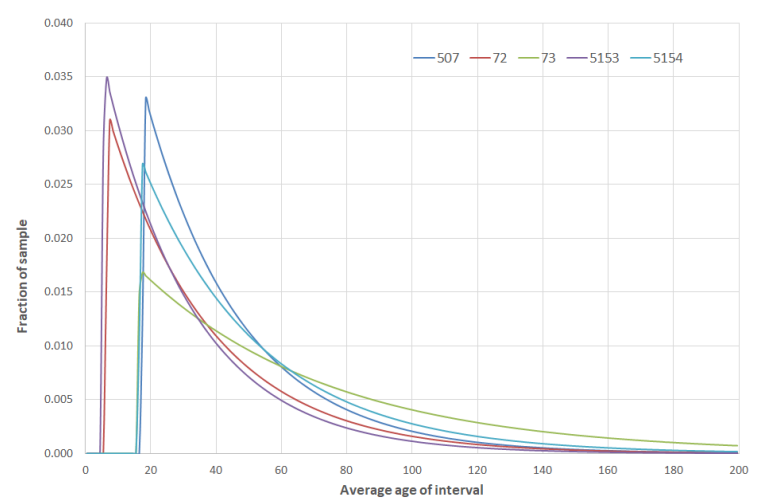

Fig. 2.28. Age distribution in wells 507, 72, 73, 5153 and 5154

From the calculated data (mean residence time and PEM parameter) the age distributions (g (t)) were determined for each sample. These distributions are summarized in Table 2.7 and are represented in Fig. 2.28.

2.4.6. ^{222}Radon

The ^{222}Rn activity values measured during the January 2019 campaign proved to verify that the activity of this isotope in groundwater is significantly higher than in surface water, which is a promising result to carry out the groundwater inflow analysis (Fig. 2.29). Unlike this, and in accordance with what was reported in section 4.2.1, the EC of groundwater and surface water are not significantly different.

The results obtained in August 2019, along a longer stretch of the stream, suggest that ^{222}Rn activity remains approximately constant from the entrance of the stream to the CAE (S01) to point S20. This may be due to the constant contribution of ^{222}Rn, either from the riverbed or from the continuous groundwater entry. ^{222}Rn activity increases from point S20 onwards (Fig. 2.30), which could be due to some groundwater ingress.

Based on these results, the next campaign was focused on the section between monitoring points S09 and S11. As in the previous results, there was an increase in ^{222}Rn activity from point S20 onwards, which could confirm an entry of groundwater. However, the EC seems to remain constant along this stretch of the creek (Fig. 2.31).

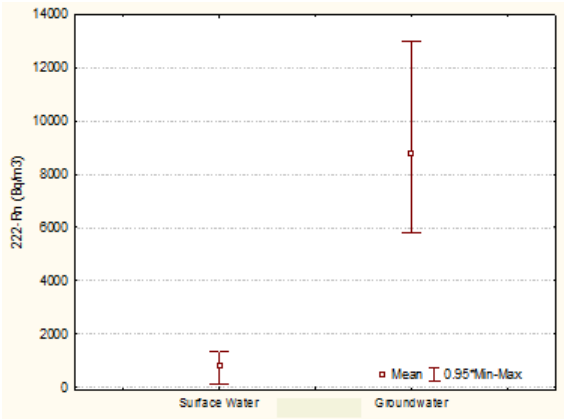

Fig. 2.29. ^{222}Rn activity in surface and groundwater (January 2019 campaign)

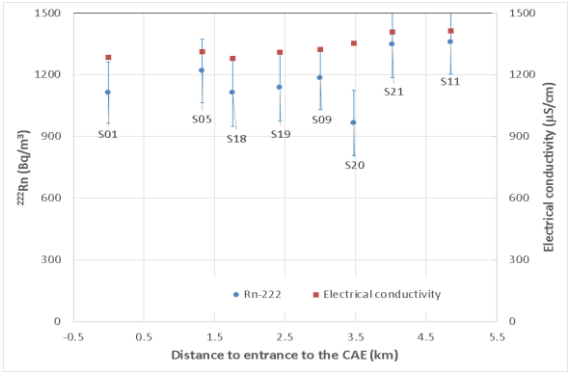

Fig. 2.30. ^{222}Rn activity and EC in Aguirre Creek sampled in August 2019

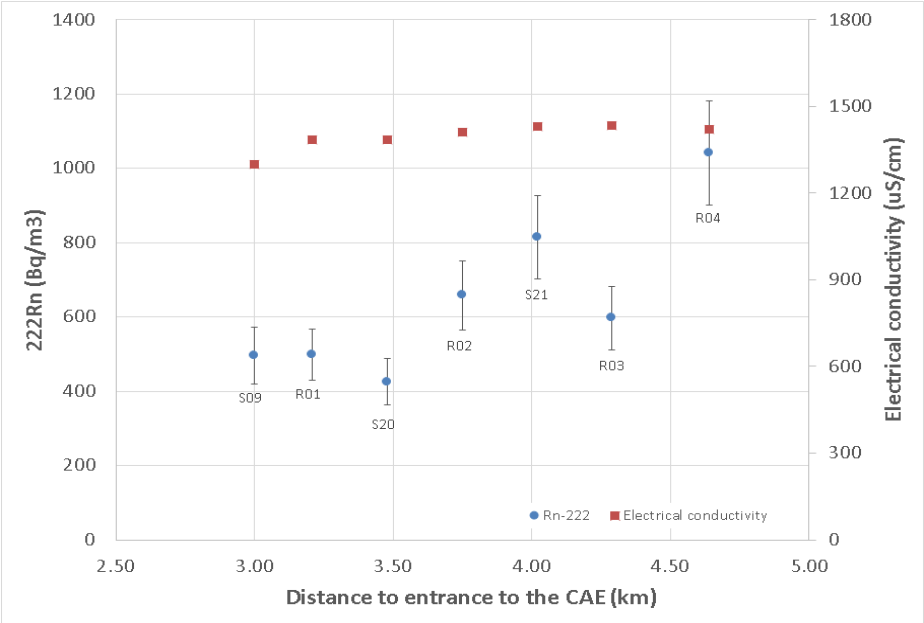

Fig. 2.31. ^{222}Rn activity in Aguirre Creek sampled in September 2019

2.5. Conclusions

The hydrogeological characterization of the groundwater system inside the CAE and its surroundings using physicochemical and geochemical data made it possible to determine the groundwater flow pathway, the water typology of surface and groundwater, and identify the hydrogeochemical processes responsible for groundwater chemistry. The use of stable isotopes, noble gas isotopes, and ^{222}Rn techniques allowed the characterization of recharge area, the assessment of surface and groundwater connections and the dating of groundwater.

Based on the results of this work a Conceptual Hydrogeological Model (CHM) (Fig. 2.32) can be defined as follows.

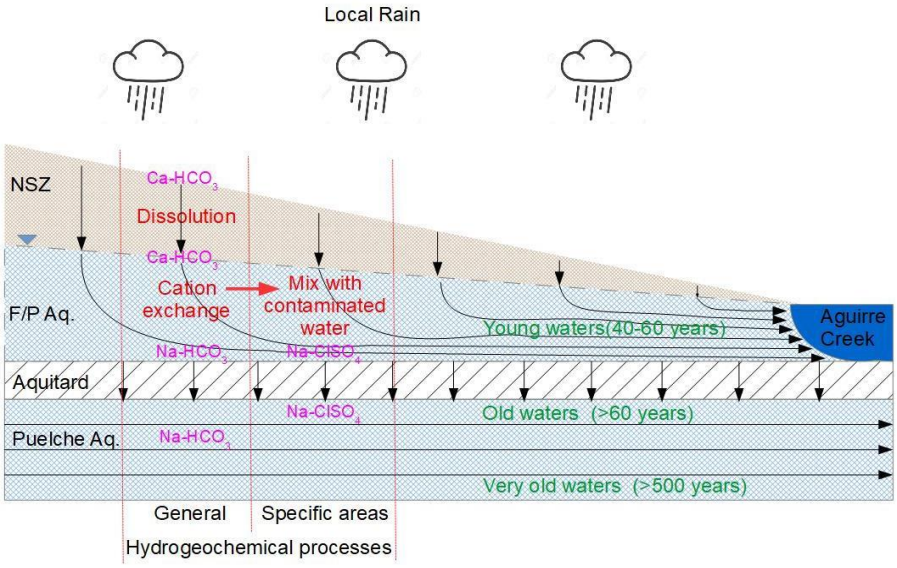

Fig. 2.32. Conceptual Hydrogeological Model scheme

The Freático/Pampeano Aquifer is recharged by local rainwater infiltration; in this aquifer the water is sodium bicarbonate type. There is a downward flow, and the ion concentration increases gradually through different hydrogeochemical processes: cation exchange, dissolution of carbon dioxide, carbonates (calcite and dolomite), albite and anorthite and, in certain areas, mixing with water with a high content of sulfate and chloride (contamination). The flow path is influenced by the topography and the Aguirre Creek that receives an inlet of groundwater. This aquifer has waters with T-^{3}He ages between 16 and 41 years and the mean residence time ranges from 32 to 74 years. The Puelche Aquifer is recharged by the upper aquifer through the aquitard and the flow lines follow a southwest-northeast direction. The water is, in general, sodium bicarbonate type. This aquifer has old waters (> 60 years) originated mainly from local recharge and very old waters (> 500 years) that come mainly from regional recharge water. This CHM is in accordance with the one presented by Vives, Mancino and Scioli (2012) for the Matanza-Riachuelo River basin area.

References

Aeschbach-Herting, W. and Solomon, K. 2013. Noble Gas Thermometry in Groundwater Hydrology. In the Noble Gases as Geochemical Tracers (pp. 1–391).

Armengol, S., Manzano, M., Bea, S., Pelizardi, F., Ormaechea, L. and Martínez, S. 2016. Aportes al modelo hidrogeoquímico conceptual de la cuenca del río Matanza-Riachuelo. ISBN: 978-987-661-222-7: Calidad del Agua Subterránea.

Armengol, S., Manzano, M., Bea, S. and Martínez, D. 2017. Identifying and quantifying geochemical and mixing processes in the Matanza-Riachuelo Aquifer System, Argentina. Science of the Total Environment 599-600, 1417-1432.

Auge, M. 1986. Hydrodynamic behavior of the Puelche aquifer in Matanza River Basin. Groundwater 25 (5), 636–642.

Auge, M. 2004. Hidrogeología de la Ciudad de Buenos Aires. Universidad Nacional de Buenos Aires. Available at: http://tierra.rediris.es/hidrored/ebooks/miguel/HidrogeoBsAS.pdf.

Dapeña, C. and Panarello, H.O. 2004. Composición isotópica de la lluvia de Buenos Aires. Su importancia para el estudio de los sistemas hidrológicos pampeanos. Revista Latino-americana de Hidrogeologia, n.4, 17-25, 2004. ISSN 1676-0999.

Hernández, M. and González, N. 1997. Impact of Rising Piezometric Levels on Greater Buenos Aires Due to Partial Changing of Water Services Infrastructure. Groundwater in the Urban Environment: Problems, Processes and Management 7.

IAEA. 2007. Sampling Procedures for Noble Gases to Be Measured at the Isotope Hydrology Laboratory. 1–16.

IAEA. 2020. Global Network of Isotopes in Precipitation (GNIP). https://www.iaea.org/es/servicios/red-mundial-sobre-isotopos-en-la-precipitacion-rmip (visited in 2020).

Instituto Nacional del Agua (INA). 2010. Balance de agua subterránea en la cuenca del Matanza-Riachuelo mediante modelación numérica. Proyecto INA 1.207. Informe LHA 01-1.207-10.

Jurgens, Bryant, Böhlke, J. and Eberts, S. 2012. TracerLPM (Version 1): An Excel ® Workbook for Interpreting Groundwater Age Distributions from Environmental Tracer Data. Reston, Virginia, USA: USGS.

Manzano, M., Zabala, M. and Martinez, S. 2013. El fondo químico natural del sistema acuífero de la cuenca del río Matanza -Riachuelo. Available at https://www.researchgate.net/publication / 306426004.

Panarello, H., Dapeña, C. and Auge, M. 1994. Mecanismos de salinización del agua subterránea de la zona de La Plata, Buenos Aires, Argentina: Su interpretación por medio de los isótopos ambientales. Investigations on Hydrology and Hydrogeology in Latin America on Water Resources and Groundwater Pollution. IAEA – TECDOC Series 835, 13–27.

Pritchard, J., Herczeg, A. and Lamontagne, S. 2003. Comparison of environmental isotopes for tracing groundwater-surface water interactions in a sand-bed stream (IAEA-CN--104). International Atomic Energy Agency.

Romanazzi, P.; Hernandez, M.; Angheben, E. 2016. Estudio hidrogeológico del Sitio Ezeiza - Etapa II. Informe Final. Convenio CNEA-UNLP; UIDET Hidrología, FI-UNLP.

Schlosser, P. 1992. Tritium/^{3}He Dating of Waters in Natural Systems. Pp. Isotopes of noble gases as tracers in environmental studies. Vienna, Austria: International Atomic Energy Agency. 123,145

Tangir. 2017. Modelo conceptual hidrogeológico del Sitio Ezeiza. Internal Report. CNEA.

Universidad Nacional de La Plata (UNLP). 2008. Estudio de las condiciones hidrogeológicas, capacidad de recarga y de la calidad de las aguas subterráneas en la cuenca Matanza - Riachuelo. Informe de Avance.

Universidad Nacional de La Plata. 2008. Estudio de las condiciones hidrogeológicas, capacidad de recarga y de la calidad de las aguas subterráneas en la cuenca Matanza - Riachuelo. Informe de Avance.

Vives, Mancino, and Scioli. 2012. Modelo conceptual y numérico del flujo de agua subterránea de la cuenca del río Matanza-Riachuelo. Proyecto de Aguas Subterráneas en la Cuenca Matanza Riachuelo. Informe Final. Available at http://www.bdh.acumar.gov.ar:8081/bdh3/publica.

Zabala, M; Martinez, S.; Manzano, M. y Vives, L. 2016. Groundwater chemical baseline values to assess the Recovery Plan in the Matanza- Riachuelo River basin, Argentina. Science of the Total Environment 541, 1516–1530.

BRAZIL

Central Nuclear Almirante Álvaro Alberto (CNAAA)
https://energiainteligenteufjf.com.br/biografia/almirante-alvaro-alberto/

3. ISOTOPIC AND RELATED TECHNIQUES FOR THE HYDROLOGICAL CHARACTERIZATION OF THE SITE AND VICINITY OF ANGRA DOS REIS NUCLEAR POWER PLANTS, RJ, BRAZIL

V. L. BOMTEMPO, C. A. CARVALHO FILHO, S. D. S. COTA, P. S. P. MINARDI, R. G. PASSOS

Nuclear Technology Development Center (CDTN/CNEN), Belo Horizonte, MG, Brazil

Abstract

The project "Use of Isotope Hydrology to Characterize Groundwater Systems in the Vicinity of the CNAAA NPP's, Rio de Janeiro, Brazil", carried out by CDTN in cooperation with Eletronuclear – ETN, the state-owned company in charge of the construction and operation of nuclear power plants in Brazil, aimed at the evaluation of the hydrologic and geologic conditions affecting the eventual contamination of groundwater by radioactive effluents released by normal or accidental operation of Almirante Álvaro Alberto Nuclear Power Plants (Angra I, Angra II and Angra III – this one, under construction), located in Angra dos Reis, Rio de Janeiro.

From July 2016 to November 2019, 67 water samples were collected from springs, piezometers, drilled and dug wells, streams, small reservoirs and ocean. Several physical-chemical parameters were measured on-site during the sampling procedures and twelve samples were selected for specific analyses: hardness; alkalinity; cations Ca^{++}, Mg^{++}, Fe^{++}, Mn^{++}, Na^{+}, NH_4^{+} and K^{+}; anions Br^{-}, Cl^{-}, F^{-}, NO_3^{-} and SO_4^{--}; quantitative determination of Mn, Fe, Sr, Ba, Cu, Si and B. Surface and groundwater samples, as well as twenty-four monthly integrated rainwater samples collected in two different spots, were analyzed abroad for stable isotopes (^{2}H and ^{18}O) and sixteen samples were also analyzed for environmental tritium.

The present research confirmed the presence of two types of aquifers in the study area: an unconfined and porous, free aquifer (0 to 50 m deep) over a fractured and semi-confined one (0 to unknown depth). It is also proposed to consider locally an expressive clay layer in the porous unit. The direction of the groundwater flow at the NPP's site is mainly from NNE to SSW, discharging into the ocean at Itaorna Bay, which is in agreement with the ground surface topography. The water table is kept about 2 m below the ground surface, with a slope of 0.5% towards the ocean, where it increases to a 1% gradient. Hydrochemical and isotopic data have confirmed that rainwater recharges the system locally, with little interaction with the local lithology, with some evidence of seawater intrusion. Groundwater around the nuclear power plants site showed tritium levels greater than regional environmental values.

3.1. Introduction

The nuclear power plants complex, known as "*Centrais Nucleares Almirante Álvaro Alberto – CNAAA*", comprises two nuclear power plants in full operation, Angra I and Angra II and another one under construction, Angra III (Fig. on this chapter cover page, Source: Eletronuclear, EIA/RIMA, 2005). Angra I (640 MWE), the first nuclear power plant of the Angra Complex, started to be operated definitely in 1985 and Angra II (1350MWE), the second plant, started operating in 2001. Angra III (1,405 MWE) is expected to be operational in 2026.

The complex is sited in the South Atlantic coastline, near the boundaries of the states of São Paulo and Rio de Janeiro, the two largest Brazilian states in economy and population (Fig. 3.1). The distance of the power plants site to the nearest town, Angra dos Reis (estimated population in 2019 of 204,000; according to *IBGE, 2020*) is 20 km. Angra dos Reis lies 100 km west of Rio de Janeiro and 220 km east-northeast of São Paulo city, right at the epicenter of one of the most active tourism places in Brazil. Highway BR-101 traverses the region at an average distance of 200 m north of the power plant site limits.

The Coordinated Research Project (CRP) named "*Use of Isotope Hydrology to Characterize Groundwater Systems in the Vicinity of the CNAAA Nuclear Power Plants, RJ, Brazil*", supported by the International Atomic Energy Agency (IAEA), was carried out by the Nuclear Technology Development Center (*Centro de Desenvolvimento da Tecnologia Nuclear-CDTN/CNEN*) in cooperation with *Eletrobrás Eletronuclear (ETN)*, the state-owned company in charge of operating the power plants. The main objective of the Project was the characterization of the groundwater system in the site of the NPPs and in its surroundings, encompassing the so-called "Direct Influence Area – DIA", a circle with a 15 km radius centered at Angra III (see Fig. 3.1).

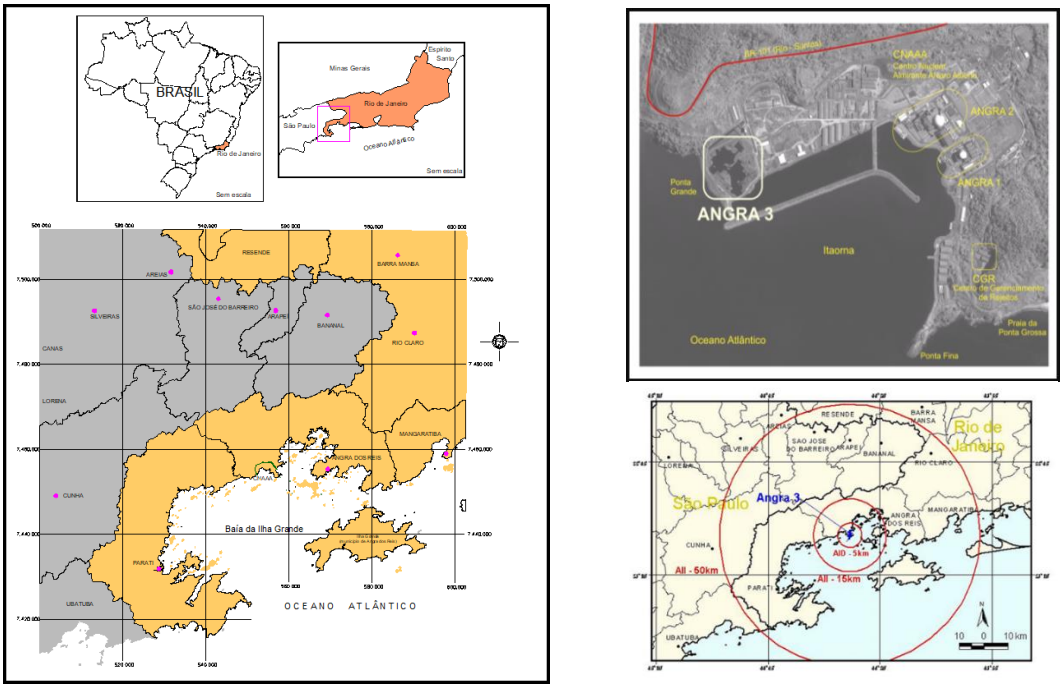

Fig. 3.1. Location of the CNAAA Nuclear Power Plants. (ELETRONUCLEAR, 2005)

3.2. Site description and previous studies

3.2.1. Climatology and meteorology

The site of the NPP's, located at the southern part of the State of Rio de Janeiro, presents a microclimate regime typical of a tropical coastal region, influenced by factors like latitude, longitude, proximity of the ocean, topographic features, nature of the vegetal cover and, in particular, the action of atmospheric circulation systems in large and mid-scales, such as cold fronts and sea/land wind regimes.

Presently the site has four towers for meteorological monitoring, providing measures of wind and air temperature at 10, 60 and 100 m (heights from the ground) and also precipitation in one location (Tower A), while the other towers measure only wind at 15 m (Towers B to D). Data and results can be found in Figueiredo et al. (2016) and Molnary (2017).

The highest values of air temperature fluctuate between 26–27 °C and 19–20 °C in summer and winter, respectively, between the three levels of height of Tower A (average annual thermal amplitude around 7 °C). The average daily temperature variation at the 10 m level (about 3 °C in the summer) is higher than at the higher levels (~ 1.5 °C), which is due to the greater efficiency of the heat exchange processes closer to the ground. At the 10 m height, air temperature at night is generally lower than the other levels, decreasing as soon as the air in contact with the surface is cooled by conduction and radiative loss, especially in winter. During the day, air temperature at 10 m rises above the values found at higher levels. Likewise, the reduction of temperature with height is also evident, so that temperature throughout the year at 60 m height is approximately 0.7 °C higher than temperature at 100 m, which is because the atmosphere is heated from below. Local atmosphere is predominantly stable

throughout the day, with more unstable conditions predominating between 8 a.m. and 16 h p.m. in the spring and summer.

The relative humidity in the meteorological station of Angra dos Reis presents a homogeneous profile along all the months of the year, without a clear definition of a dryer or a more humid period. This behavior is due to the continuous penetration of sea humidity into the continent and to the very frequent events of precipitation at the hillsides of Serra do Mar along the whole year. There is a large variation of consecutive daily values of relative humidity for the month of January (summer time in Brazil), from maxima of 85% to minima of 45%. During winter months (May to September), the relative humidity was kept below 40%, with extreme minima of 15% under special conditions of clear sky and absence of predominant maritime circulation and no precipitation.

Wind direction and speed are associated with the several scales of atmospheric circulation. As a rule, there is a predominance of the maritime regimes of circulation close to the ground surface in the coastal area, spreading from Sepetiba to the coast of Paraty, passing by Angra dos Reis. Registers from Tower A at 10 m level show most frequent directions from N/NE and S/SW during winter, spring and fall; the component from S was the most evident during fall. For the levels 60 m and 100 m for the same tower, the same configuration was maintained, but at 60 m the SW component was the most frequent during summer months.

Mean speed values for the period under consideration (2002–2003) were 3 m/s (10 m), from 3 to 8 m/s (60 m) and from 5 to 8 m/s (100 m). January and June were the months bearing the most frequent episodes of calm winds and March was the one with the less frequent values. The highest frequency occurs at intensities between 1 and 2 m/s. The maximum intensity occurs in the daytime period, reinforced by the turbulence component caused by the atmosphere heating. Katabatic winds produce strong vertical shear in the region. Stronger winds and rains were recorded in the fall, suggesting that this is the period of the most intense storms. Sea breeze action extends up to 100 m height, increasing intensity between 8 and 9 a.m., reaching a maximum around 3 p.m. and weakening thereafter.

The precipitation phenomena reaching Angra dos Reis and surroundings are associated with several atmospheric mechanisms, such as: cold fronts (all year round), lines of instability (spring-summer) and convective regional formations (spring, summer and fall times), originated from systems of the north-northwestern sector. Average precipitation is higher in late afternoon and evening, coinciding with the moment of reversal between sea and land breezes. Average precipitation is also higher in summer and lower in winter. Weak precipitation (up to 4 mm/h) predominates in the four seasons of the year. Moderate rains (between 4 and 24 mm/h) and strong rains (> 24 mm/h) occur predominantly in summer and fall. With regard to the frequency of precipitation occurrence throughout the day, it can be noted that rainfall occurs preferentially at night, regardless of its intensity and season. The arrival of cold fronts brings together more intense rains and winds, especially after passing by Paraty and entering Ilha Grande Bay. The rainy period extends from October to March, while the period from April to September represents the dryer months. Mean yearly precipitation values may be as high as 2,500 mm/year.

3.2.2. Geological and hydrological context

The crystalline basement of the study area consists of Proterozoic granite-gneiss rocks belonging to the Paraíba do Sul and Rio Novo Complexes (ELETRONUCLEAR, 2005; CPRM, 2007). These rocks are interbedded with Neoproterozoic porphyritic granitic bodies and small Cambro-Ordovician stocks and clusters of intrusive dykes of granite composition (Mambucaba Granite). Expressive systems of basic (tholeitic) rock dykes of Mesozoic age (Guedes et al., 2005) are also present in the study area. The quaternary units are represented by fluvial and marine deposits associated with the present-day and ancient sediments, with a great compositional diversity, consisting of gravel, fine and medium sand, silt and clay. The hillsides close to the NPP site present colluvial and talus deposits, consisting of sandy soils with several blocks and boulders rolled in the soil matrix and with intense vegetation. The study area has been the target of hydrogeological investigations in the last 20 years, mainly due to the studies for the licensing of NPPs (PROMON, 1974, 1989; NATRONTEC, 1999; UFRJ, 2003; ELETRONUCLEAR, 2005). These studies concluded that there are two main aquifers in the region. The first one (upper aquifer) is a free, porous and shallow aquifer type. In the

lowlands and beaches, it is represented by alluvial deposits and fluvial-marine sediments. The other aquifer is a fractured semi-confined type, characterized by fractures of crystalline rocks.

3.2.3. Hydrogeochemistry and isotopes

The hydrogeochemical characterization (ELETRONUCLEAR, 2005) of the DIA (Direct Influence Area) was carried out with a basis on a group of production wells and other water points, for which in-situ and laboratory physical and chemical essays were realized. At that occasion, waters were classified according to their major ions contents: Ca^{2+}, Mg^{2+}, Na^{+}, K^{+}, Cl^{-}, HCO_3^{-}, SO_4^{2-}. Three distinctive groups of waters were then identified (Observation: sample codes cited in this item are from the original reference, not related to the codes used in the present work):

1) waters with sodium-chloride (Na-Cl) characteristics, similar to rain waters; a sub-group of these waters can be distinguished, in which the concentration of calcium is a little greater, forming Ca^{2+}-Na^{+}-Cl^{-} waters;

2) waters from the tubular deep wells (ANG-24, ANG-32, ANG-33, ANG-42, ANG-43), with Ca^{2+}-Na^{+}--HCO_3-Cl^{-} (bicarbonated, chlorinated, calcic-sodium) characteristics;

3) one single sample (ANG-51) presented a bicarbonated-calcic (Ca-HCO_3) characteristic, different from the other groups.

Eight water points (springs, tubular wells, piezometers, rain water and a pond) were selected to be sampled aiming at evaluating the possible isotopic variations due to differences in altitude (elevation) and geographic location in relation to the site of CNAAA. This sampling work, realized in 2002, was simultaneously carried out with the sampling for hydrochemical purposes. Obviously, the data then collected for oxygen-18, deuterium and tritium represent very restricted information and the interpretation of the results, as issued by the authors at that time, has to be seen with great concern (Table 3.1).

Table 3.1. Previous data for stable isotopes and tritium (ELETRONUCLEAR, 2005)

Sample Code	Sampling Date	$\delta^{18}O$ (‰)	$\delta^{2}H$ (‰)	$\delta^{2}H$ Excess (‰)	Tritium (TU)
WP 2/X (ANG-24)	17.10.2002	-4.68	-29.9	7.5	-
WP 2/01 (ANG-34)	17.10.2002	-3.8	-26.3	4.1	3.0 ± 0.9
WP-F/1 (Fonte)	17.10.2002	-3.81	-23	7.5	4.0 ± 1.1
WP-3/08 (ANG-42)	18.10.2002	-4.53	-32.1	4.1	2.0 ± 0.9
WP–014 (ANG-33)	18.10.2002	-4.33	-22	12.6	2.1 ± 0.8
L1/01 (Lago AIII)	18.10.2002	0.59	-9.5	-14.2	19.0 ± 1.3
BR 1/01 (Branco)	21.10.2002	-6.16	-47.6	1.7	-
CH /1 (chuva)	24.10.2002	-1.39	-11.4	-0.3	16.2 ± 1.4

The Local Meteoric Water Line for Rio de Janeiro (LMWL-RJ), $\delta^{2}H = 7.6 * \delta^{18}O + 10.74$ ($R^2 = 0.93$), was obtained based upon isotopic data weighted by the precipitation for years 1961 to 1985 from GNIP, except for years 1972 and 1985, which presented extreme deuterium excess values of 25.8‰ and 6.6‰, respectively.

The slope of the LMWL-RJ is less than 8, mainly due to the relative humidity of the water vapor over the ocean, which will produce precipitation. The primary formation of atmospheric vapor and the precipitation are processes involving evaporation and kinetic mixture in a condition of non-equilibrium.

It can be observed that the LMWL-RJ falls plotted slightly above the GMWL, which indicates humidity values lower than 85%, once that for the GMWL the humidity considered is slightly greater than 85%. The humidity historical series for Rio de Janeiro in the period 1961 to 1990 presents a range between 77% and 80%. For Angra dos Reis the humidity range is between 80% and 82%, which will lead to the plotting of the local line closer to the GMWL.

The data for the campaigns of October/2002 and November/2017 (this project data) seem to be reasonably well adjusted to the GMWL, showing that these waters do not go through modifications in their isotopic composition. The only modifying phenomenon for this fitting is the evaporation observed in some samples from 2002.

3.3. Methodology

Following the work plan contracted with the Agency, four field trips to the survey area were accomplished. The first one, lasting from 13 to 16 September, can be considered an exploratory trip, in which discussions with the staff of the Environmental Monitoring Lab were held, preliminary visits to the site and to water points of interest (piezometers, production wells, springs, reservoirs, water courses) were made and technical material from previous studies were collected. These included geologic, hydrogeologic, topographic, hydrographic and climatological data, which were very useful in obtaining a better understanding of the area and in planning the future investigations.

The second trip to Angra dos Reis was in fact the first full campaign, carried out from 3 to 7 April, 2017, at the end of the rainy season. On that occasion, nine water samples were collected: surface water (streams), small reservoirs, springs and sea water. Some parameters were measured in the field: pH, Temperature – T (°C), Electric Conductivity – EC (µS/cm), Oxi-reduction potential – Eh (mV), Dissolved Oxygen – DO and Total Dissolved Solids – TDS. The samples were brought to CDTN´s labs for environmental tritium and stable isotopes analyses (^{18}O and ^{2}H).

Due to its geographic location between Serra do Mar and the coast of Angra dos Reis and Paraty, the region is very well supplied by surface water and most springs are located at hillsides, fairly away from the site of the plants and bearing difficult access by land. This reflects in the small number of perforated and/or tubular deep wells in the area, except those piezometers used for monitoring purposes (seven 8–10 m deep piezometers) at the construction grounds of Angra III, which were sampled by our partners in March, June, September and December 2017, or those existent in the grounds (yards) of the other two operating plants, Angra I and Angra II, to which our access was not granted at this occasion. Some others are scattered all over the region, in particular at the locality known as “Parque Mambucaba” or “Perequê”. Anyway, some of the waters are, in some degree, influenced by sea water, due to the penetration of the saline wedge. Some very shallow wells (4–8 m deep), known as “cacimbas” or “cisternas”, were identified, dug in porous terrain, intended for individual or collective domestic supply.

One more field campaign was realized from 20 to 24 November, 2017. Only six water samples were collected, due to the very bad weather conditions; the rainy season had started in October. For the first time it was possible to sample two control piezometers installed in the yards of power plants Angra I and II. Field measurements were once again made, including static water levels in the piezometers, and samples were taken to CDTN for environmental tritium and stable isotopes analyses.

The last field work was realized from 22 to 26 October, 2018. Eighteen water samples were collected and field parameters were measured for twelve of them; all samples were brought to CDTN for tritium, stable isotopes and physical-chemical analyses. Twelve (12) samples were selected for specific analyses in our labs, as follows: hardness (titulometry); alkalinity (titulometry); cations Ca^{2+}, Mg^{2+}, Fe^{2+} and Mn^{2+} (atomic absorption/spectrometry); cations Na^{+}, NH^{4+} and K^{+} (liquid chromatography); anions Br^{-}, Cl^{-}, F^{-}, NO_3^{-} and SO_4^{2-} (liquid chromatography); quantitative determination of Mn, Fe, Sr, Ba, Cu, Si and B (ICP-MS). Samples from the monitoring piezometers at Angra III were collected only in March 2018.

Additionally, along this year, our partners from the Environmental Lab collected seven samples in each month of March, June, September and December from the monitoring piezometers existent at the construction grounds of Angra III, neighboring the site of the other two plants.

Once again, the following field parameters were measured: pH, Temperature – T (°C), Electric Conductivity – EC (µS/cm), oxidation-reduction potential – Eh (mV), Total Dissolved Solids – TDS (ppm) and Dissolved Oxygen (DO). Samples were brought to our laboratories for tritium and stable isotope analyses (IRMS). Carbon-14 analyses were not demanded, for water in the region is basically modern. Fig. 3.2 shows the sampling net established for the project, in progressive levels of detail.

During the last campaign, two rain collectors (Model 1B Palmex Rain Samplers) were installed in the area. They are designed to store collected precipitation for several days or even weeks without evaporation and associated fractionation, thus particularly well suited to determine the isotopic composition of rain water. They are equipped with a 3L collecting bottle. One of them was installed in the grounds of the Environmental Monitoring Laboratory (LMA) of ELETRONUCLEAR close to the coastline, at an altitude of about 10 m. The other one was installed close to a water treatment station (EPTA), on the hillside of Serra do Mar facing the site of the NPP´s, at an altitude of 113 m. Forty

monthly integrated rain samples were collected from November 2018 to June 2020. Twenty-four samples from November 2018 to October 2019 were analyzed for stable isotopes.

The last field trip was scheduled to be realized in March-April 2020 but, unfortunately, due to the outbreak of the new coronavirus disease, Covid-19, which started in November 2019, it was not possible to accomplish the proposed work plan, which imposed a strong negative impact on the development of the last phase of the project.

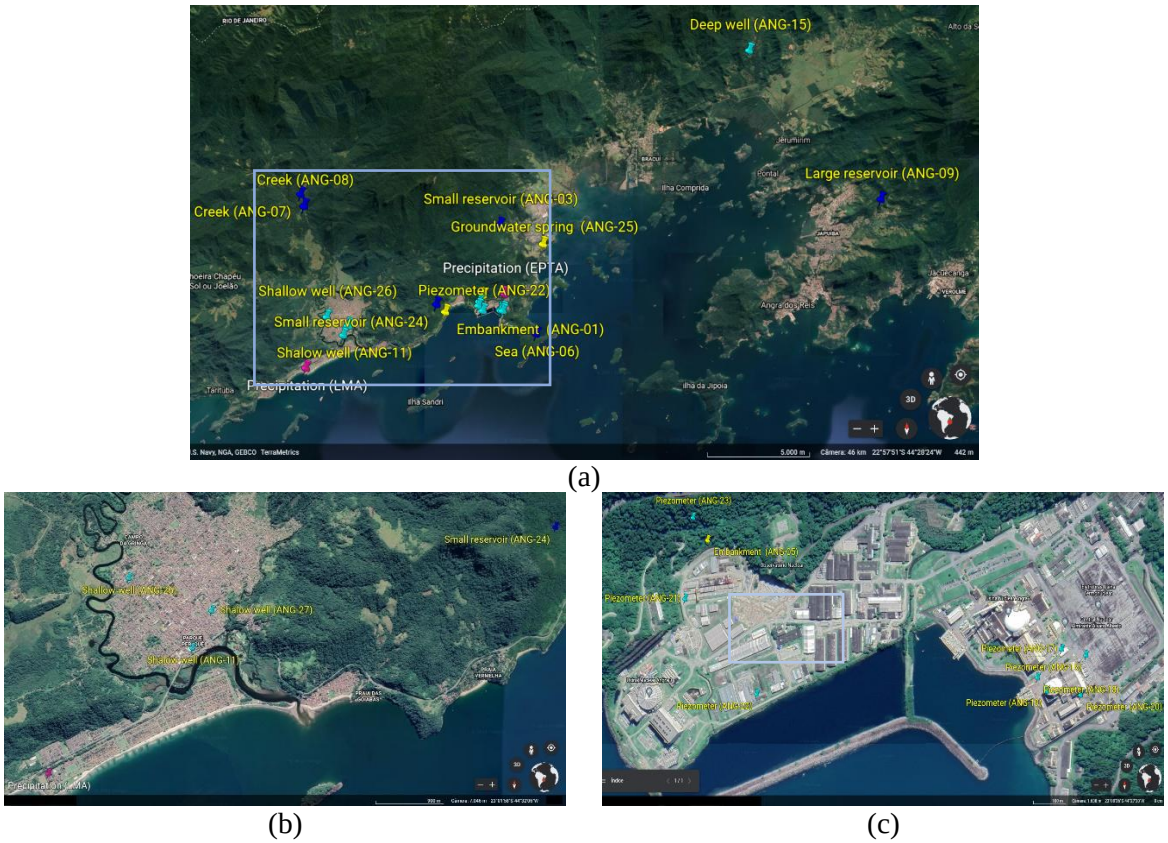

(a) (b) (c)

Fig. 3.2. Location of the sampling points for hydrochemistry and isotopes: (a) picturing the whole area; (b) vicinity of the NPPs; (c) NPPs detail. Light blue rectangles show the area of the following picture

All historical and new information collected during the project development were combined to review and improve the preliminary flow conceptual model of the area, using the software ROCKWORKS. A conceptual model of the interactions between the several water compartments can be applied in understanding the movement, extent and dilution factors of a contaminant plume eventually introduced in the groundwater (GDW) systems. This model can be a step for the future construction of numerical models aimed at protection and remediation actions.

3.4. Results and analysi

3.4.1. Geology and hydrogeology

The present research confirmed the presence of two types of aquifers in the study area, according to ELETRONUCLEAR (2005): a porous and free aquifer over a fractured and semi-confined one. However, it is proposed to consider locally an expressive clay layer in the porous unit. Then, the hydrogeological units identified in the site (Fig. 3.3) can be listed as follows.

Unconfined and porous aquifer (0 to 50 m deep): In the lowlands, river and coastal plains it is represented by river and marine sediments, composed in its upper portion by sandy sediments (locally silt-rich), containing fragments of sea shells. These fluvial-marine sediments occur over a sandy-clayey saprolite, containing fragments of the sound rock, pebbles and boulders resulting from the weathering of the granitic-gneiss basement, and which forms the basis of the porous aquifer. In the

area of the NPP facilities, this aquifer is commonly covered by a layer of landscaping material. On the hillsides, this aquifer is represented by the saturated portions of the talus and colluvium deposits, residual soil and saprolite. Locally, the fluvial-marine sediments are interspersed with layers of clay, one of which, of greater thickness (1 to 10 m thickness) and greater lateral continuity, is constituted by organic, dark and plastic clay, presenting fragments of shells, and that mainly occurs over the saprolite. This clay layer must be the result of sea level fluctuations, which are frequent in the quaternary (Martin et al., 1996). Due to the absence of more boreholes and piezometers, the lateral continuity of this clay layer can only be confirmed in the vicinity of the NPP facilities. Undoubtedly, it is a clay aquifuge or aquitard that, when present, acts as a confining layer for the groundwater below. According to ELETRONUCLEAR (2005) this porous aquifer is in hydraulic connection with the superficial portions of the fractured aquifer.

Fractured and semi-confined aquifer (0 to unknown depth). It is represented by the fractured network of the crystalline basement rocks. It occurs both on the surface (outcrops) and in depth, under the porous aquifer. According to ELETRONUCLEAR (2005) the gradients and the hydraulic load are high, as the recharge is frequently at the top of the hillsides (up to 500 m high) located north of the NPP's site. This aquifer is unconfined in the elevated portions of the hillsides occupied by extensive outcrops of the crystalline basement. According to ELETRONUCLEAR (2005) it becomes confined where it occurs under the layers of saprolite and colluvium/talus deposits, as well as under the fluvial-marine deposits in the coastal region. Sometimes this aquifer has its piezometric level at or above the land surface (ELETRONUCLEAR, 2005). This fractured aquifer in granitic-gneiss crystalline rocks is very common in the coastal region of southeastern Brazil, with the recharge areas located in the highest parts of the hills (Silva-Filho et al., 2009).

Regarding the groundwater flow at the NPP's site, its direction is mainly from NNE to SSW and discharging into the ocean at Itaorna Bay, which is in agreement with the ground surface topography. The water table is kept about 2 m below the ground surface, with a slope of 0.5% towards the ocean, where it increases to a 1% gradient (NATRONTEC, 1999).

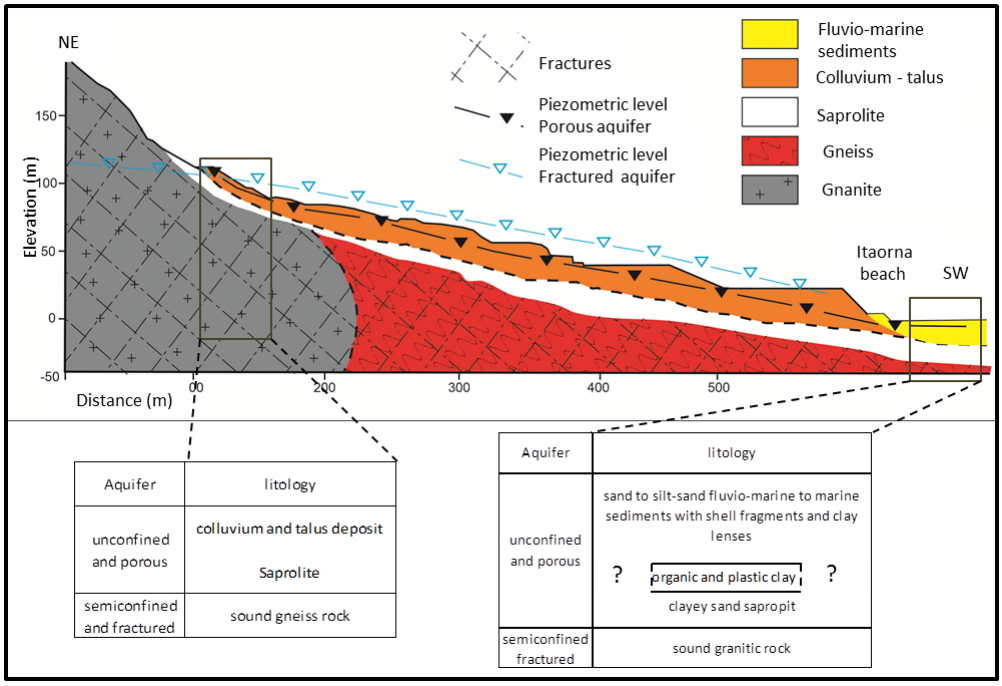

Fig. 3.3. Hydrogeological schematic section. Modified from ELETRONUCLEAR, (2005) and with updates made by the current research

Fig. 3.4 shows an image of Itaorna Beach where two clusters of water table curves of the local groundwater were plotted. These curves were inferred from measurements of water levels in piezometers taken during field campaigns and from a technical report (Tecnol, 2011). The absence of static level measurements in the entire area prevented the elaboration of a more detailed map.

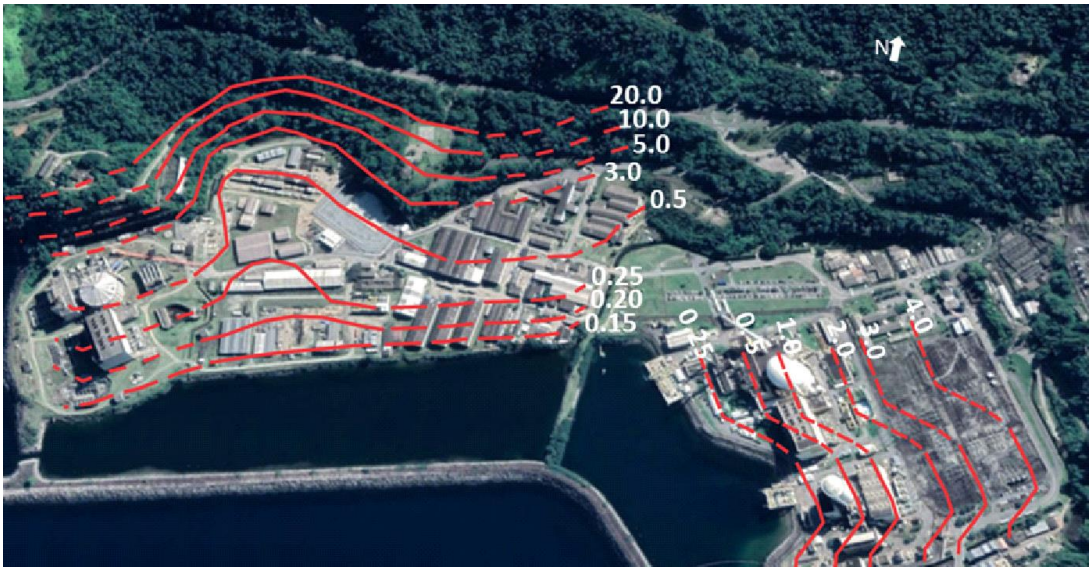

Fig. 3.4. Water level curves of groundwater at Itaorna Beach

3.4.2. Hydrochemistry

Based upon the Piper diagram (Piper, 1944), the waters under investigation can be classified in four major groups (Fig. 3.5): **Group 1** – **Ca-Na-HCO_3 water type.** It is constituted by a groundwater sample (ANG-23), a sample from a small reservoir (ANG-24) and a sample from a groundwater spring (ANG-25). These samples were collected in the hillside environment, where predominate granitic-gneissic basement outcrops, residual soil, talus deposits and dense vegetation. This area represents the main aquifer recharge zone, but with occurrences of discharge points from the fractured aquifer. **Group 2 – Ca-HCO_3 waters type.** It is represented by samples ANG-16, ANG-17, ANG-18, ANG-19, ANG-20 and ANG-21. These are all groundwater samples, collected at Itaorna Beach, very close to the present and future NPP facilities.

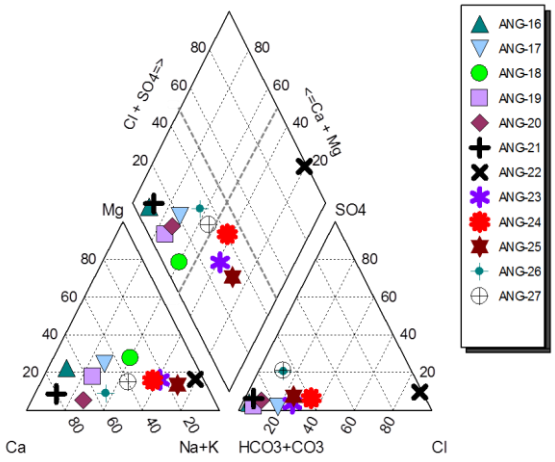

Fig. 3.5. Piper diagram of the waters from the study area

Group 3 – Ca-(Na)-HCO_3 waters type. According to Piper Diagram this group could be classified as a subgroup of **Group 2**. But due to other geochemical evidences, it is better to consider it as a separate group. This group seems to represent an intermediate stage (flow and chemical composition) between the waters of groups 1 and 2. It is represented by two samples (ANG-26 and ANG-27) of groundwater collected in *Jardim Mambucaba* (see Fig. 3.2, b), in the Perequê River basin. These samples were collected from the sandy porous aquifer on a coastal plain where past and

present-days fluvial and marine sediments occur. **Group 4 – Na-Cl waters type**. It is represented by one single sample (ANG-22), bearing an ionic composition typical of great seawater influence. This group corresponds to group 1 defined by the previous researches (UFRJ, 2003; ELETRONUCLEAR, 2005).

The Stiff diagram (Fig. 3.6) shows the ionic composition of the samples and the spatial distribution of the four groups. **Group 1** samples were collected on hillsides, where the crystalline basement outcrops. In comparative terms, this group is the one with the lowest ionic concentration. **Group 2** exhibits a water pattern predominantly Ca-HCO_3. According to the ionic concentration, **Group 3** exhibits more ionically enriched or mineralized waters than **Group 1**, but it is much poorer compared to **Group 2**. **Group 4** exhibits an extremely ion-rich water pattern, mainly in Na^+ and Cl^-, indicating strong influence of seawater.

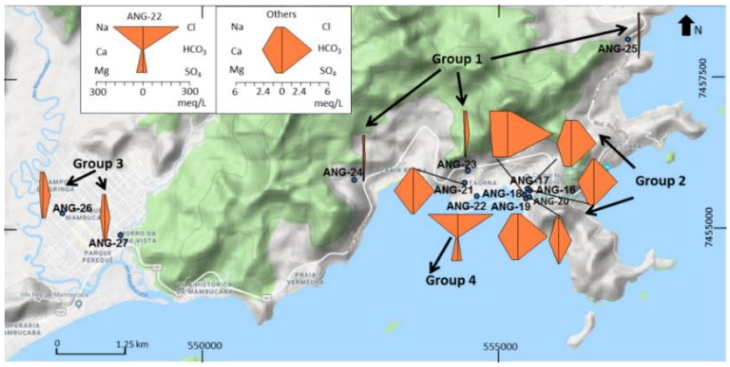

Fig. 3.6. Stiff diagrams of samples from the study area

The Gibbs diagram (Fig. 3.7, Gibbs, 1970) shows that the ANG-22 sample (**Group 4**) fell in the evaporation domain, which is one more indication that this sample has influence from seawater. Most of the samples **(Group 2**) fell into the rock dominance zone, which indicates that the rock-water interactions are the main factor that controls the chemical composition of these samples. In the zone of rainfall domain are the **Group 1** samples (ANG-23, ANG-24 and ANG-25).

Fig. 3.8, a shows that the sample ANG-22 (**Group 4**) has an excess of (Ca+Mg). This is due to the influence of seawater, enriched mainly in Mg^{2+} (Millero, 2013). This is indicative of the influence of seawater and the reverse ion exchange process or hardening (Appelo & Postma, 2005). Regarding the other samples, it is observed that most of them (**Group 2**) fall on the 1:1 stoichiometric equilibrium line (Ca^{2+}+ Mg^{2+}) versus HCO_3^-, suggesting dissolution of dolomite or Mg-rich calcite (Appelo & Postma, 2005). But some of them (**Groups 1 and 3**) fell slightly below line 1:1, suggesting a base ion exchange process or softening (Appelo & Postma, 2005).

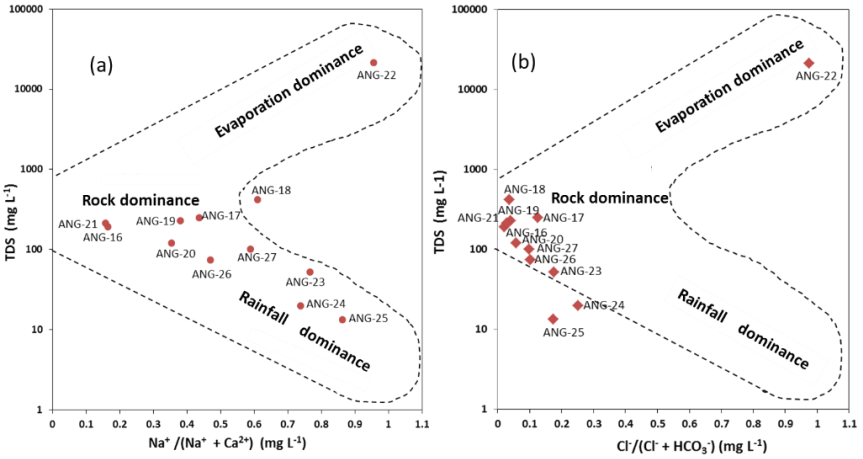

Fig. 3.7. Gibbs diagrams of the study area samples. TDS vs (a) $Na^+/(Na^+ + Ca^{2+})$ and (b) $Cl^-/(Cl^- + HCO_3^-)$

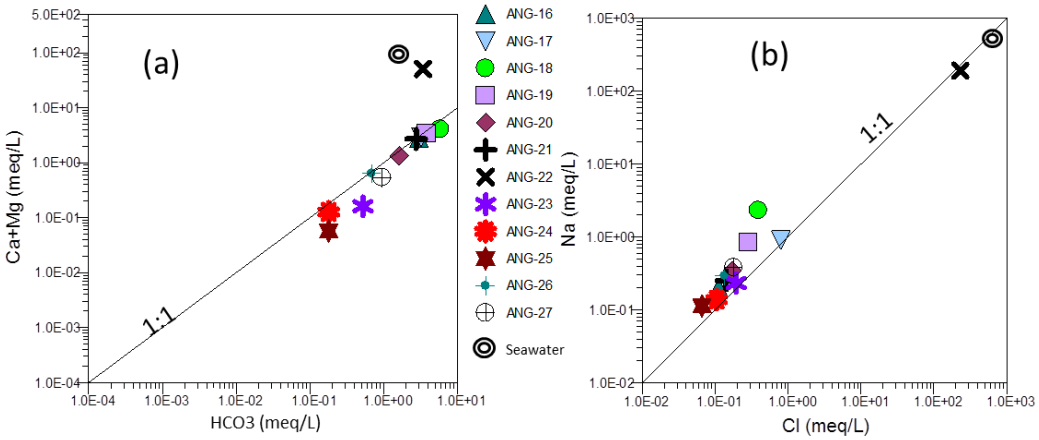

Fig. 3.8. Scatter plots of (a) Ca + Mg versus HCO_3^- and Na^+ versus Cl^- (b)

Fig. 3.8, b clearly shows that for the ANG-22 sample (**Group 4**) the source of Na^+ and Cl^- is the seawater, which confirms once again the strong influence of seawater on the ionic composition of this sample. Most of the data are slightly above the halite dissolution line. The Na^+/Cl^- ratio greater than 1 indicates either the presence of silicate weathering or base ion exchange (softening) between Na^+ and Ca^{2+} (Shansi et al., 2018; Appelo & Postma, 2005). For **Group 2** samples, it is suggested that ion exchange (Ca-Na) is the main cause for Na^+ excess. For samples from **Groups 1 and 3**, both processes must occur, whereas for samples ANG-23 to ANG-25 (**Group 1**) it is suggested that the excess of Na^+ is predominantly due to the weathering of sodium-rich silicates (Na-rich plagioclases).

The water quality was certified based on the Brazilian Standards for human consumption (Brazil, 2011). The ANG-22 was the sample that presented the largest number of parameters in non-compliance: TDS, Cl^-, SO_4^{2-}, Na^+ and hardness. The reason for this is that this water sample has a chemical composition very similar to seawater. Iron and manganese showed non-conforming values in the samples ANG-18 (Mn only), ANG-19, ANG-21 (Mn only), ANG-23 and ANG-27 (Fe only). Iron and manganese are common elements in waters and have similar hydrochemical behavior. The absence of regional background values for Fe and Mn in the local groundwater prevents an assessment of the cause of these enrichments: geogenic or anthropogenic.

3.4.3. Stable isotopes

Two local meteoric water lines (LMWL) were obtained based on isotopic data from local precipitation samples: one was calculated by the non-weighted regression model (ordinary least squares regression, OLSR) (IAEA, 1992), and the other by a precipitation weighted ordinary least squares regression (PWLSR) method, in order to reduce the influence of the precipitation amount (Hughes and Crawford, 2012). From November 2018 to October 2019, 24 monthly integrated precipitation samples from two points of the area (at sea level – LMA, and at 113 m of altitude – EPTA) were taken for establishing the LMWL's. In addition, twelve environmental samples were collected in October/2018, comprising one sample from a small reservoir; one sample from a groundwater spring; samples from two shallow pumping wells (about 6 m deep) located externally to the NPP area; and eight samples from internal monitoring wells, piezometers (10 m deep). The samples were analyzed at Beta Analytics Laboratory (USA) and results were reported in ‰ versus VSMOW standard (Vienna, Standard Mean Oceanic Water).

There was no significant difference between the lines obtained by the two methods (weighted or not). Using the OLSR method, the LMWL was represented by the equation $\delta^2H = \delta^{18}O\ (7.74 \pm 0.35) + (16.43 \pm 0.50)$ ($R^2 = 0.960$). The PWLSR method resulted in the equation $\delta^2H = \delta^{18}O\ (7.98 \pm 0.39) + (17.02 \pm 1.53)$ ($R^2 = 0.954$). According to Song et al. (2021) differences between the corresponding linear regression coefficients when applying weighted and nonweighted regression in tropical climate areas can be very small. This may be due to higher precipitation amount that makes the tropical regions more susceptible to the amount effect, which cancels out the effect of the weighting method. Song et al. (2021) suggest that there is no need to apply weighted regressions in tropical climates.

Fig. 3.9 shows the data of the isotopes in the precipitation samples from the two monitoring points (solid circles in the Fig., in blue and green colour, from LMA and EPTA monitoring points respectively) distributed along the local meteorological lines (dashed lines), as well as the global meteoric water line, GMWL, represented by the equation $\delta^2H = \delta^{18}O\ 8 + 10$ (black solid line in Fig.), for comparison. Two data points were excluded from the regression (probable outliers, indicated in the Fig.), in order to improve the fit of the equation. The Fig. also shows the isotopic data from the small reservoir sample (ANG-24), groundwater spring (ANG-25), shallow pumping wells (ANG-26 and ANG-27) and piezometers (ANG-16, ANG-17, ANG-18, ANG-19, ANG-20, ANG-21, ANG-22 and ANG-23).

From the available data, it was not possible to observe a significant difference in the stable isotopes signature between the two stations (LMA and EPTA). The mean values of $\delta^{18}O$ and δ^2H for the LMA station were –2.9 and –8.6 ‰, respectively, and –3.4 and –10.0 ‰ for the EPTA station. The slope values of the LMWLs were slightly lower than GMWL, so that the lines are practically parallel. Considering the standard deviations, they can be considered equal. Values below the GMWL slope could be explained mainly due to the relative humidity of the water vapour over the ocean, which produces precipitation. It can be also observed that the LMWLs fall above the GMWL, which indicates relative humidity (RH) values lower than 85%, once that for the GMWL the RH considered is slightly greater than 85%. For Angra dos Reis, the mean monthly RH value in 2019 ranged from 76.2% in January to 87.7% in September (the mean value considering all the data in the months under analysis was 83.2%). In addition, there was no apparent relationship between isotope data and precipitation or temperature. According to IAEA (1992), "Isotopic compositions of precipitation at stations with a mean annual air temperature higher than about 18 °C (mainly tropical stations) do not show a discernible temperature dependence". The mean monthly temperature in 2019 ranged from 20.0 °C in August to 28.5 °C in January (the mean value considering all the data in the months under analysis was 23.6 °C). Meteorological data were obtained in the meteorological station of the Angra dos Reis Airport (INMET, 2021).

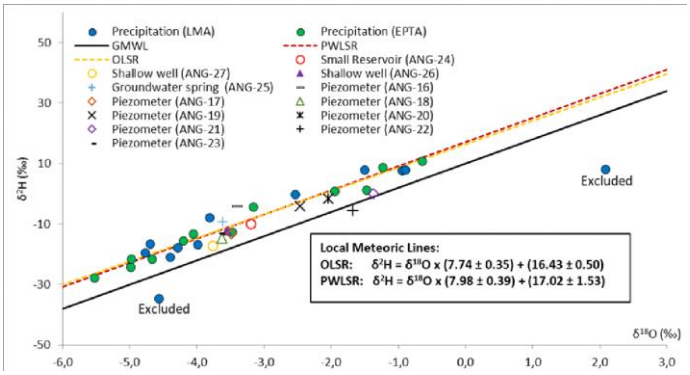

Fig. 3.9. Isotopic data of the water samples (δ^2H vs. $\delta^{18}O$) and MWL's (OLSR and PWLSR) for the site

All the valid values seem to fit reasonably well the LMWL, indicating that rainwater recharges the system locally, i.e., the water that supplies the groundwater sampling points (shallow, porous and unconfined aquifer) is basically from meteoric origin, with little interaction with the local lithology. Results of the hydrochemical composition suggest that the samples ANG-23, ANG-24 and ANG-25 are the ones that receive the greater influence from the rainwater composition (no significant interaction with the lithologies). Sample ANG-22 deviated a little more from the LMWL, which can be due to the probable seawater intrusion and mixture with the groundwater.

3.4.4. Environmental Tritium

According to the data assessed in the campaigns realized in April, November and December 2017 and March and October 2018 (Fig. 3.10), surface and groundwater around the nuclear power plants site showed tritium levels greater than regional environmental values. The regional background tritium value can be obtained at point ANG-09, a large reservoir located about 20 km from the NPPs, with 2.18 TU. Two samples were taken from a river located about 10 km (ANG-07 and 08) that provide also a good reference for the background level, with values of 2.57 and 2.73 TU (respectively, from upstream to downstream). There is no present data from the Rio de Janeiro GNIP station (which

operation was interrupted in 1984) and the most updated value for the tritium in precipitation (2.5 TU) is obtained for the CDTN GNIP station, located about 400 km from the site. Then, values of tritium concentration ranging from 2.5 to 3.0 TU may be considered as the regional background for surface and groundwater not impacted by the operation of the power plants.

The lowest tritium value of the sampled locations was measured at a deep tubular well (90 m depth, 20 m in fissural rock), located at 18 km, with the value of 1.65 TU. Other than this well, all other wells in the region were very shallow wells and piezometers. The main reason for this is the abundance of surface water which makes groundwater exploitation unnecessary. Located 8 km westward from the NPPs, three shallow wells (ANG-11, 26 and 27) presented the lowest values for the groundwater samples, between 2.63 and 3.38 TU, very close to the background level. As expected, the closer they get to the operating NPPs, the larger are the values. At one kilometer westward, the piezometer samples (ANG-21, 22 and 23) have values ranging from 6.29 to 37.44 TU. Larger values were still found at piezometers closer to the operational Angra I and II NPPs (see Fig. 3.10), with values close to 100 TU. The two largest concentrations (2,893.63 TU and 154.76 TU) were measured in two piezometers located very close to the Angra I reactor building, just outside of the building containing the pool for storage of the spent nuclear fuel and outside the building hosting the generators.

Since most of the groundwater samples are at or above the environmental background for the area, it is not possible to obtain the groundwater age of the samples based on fitting data using lumped parameter models. It can be considered that the mean transit times for groundwater samples around the NPPs are no greater than 5 years. Anyway, all the above mentioned Fig.s are raw values and should be interpreted with some concern, even because previous studies, dating from the first surveys for the installation of the third plant had already identified some high values of tritium concentration in the vicinity of the other two plants already in operation, but at that time it was predicted by the authors that the mean residence time for the shallow aquifers would be very variable and it was also estimated that a 20% of the total precipitation would be recharged into the aquifer system.

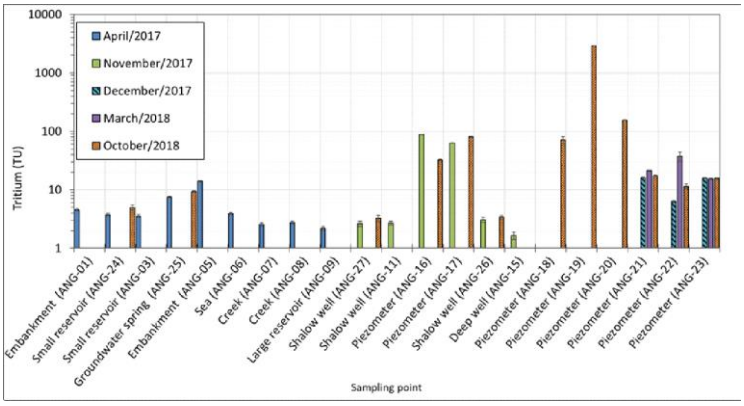

Fig. 3.10. Tritium results for the five sampling campaigns. Measure errors in black lines

3.5. Conclusions

As a result of the investigations carried out during the development of this project, and taking into account primary and secondary data, obtained from previous works and documentation, some relevant aspects of the site and its vicinity should be mentioned.

The present research confirmed the presence of two types of aquifers in the study area: an unconfined and porous, free aquifer (0 to 50 m deep) over a fractured and semi-confined one (0 to unknown depth). However, it is proposed to consider locally an expressive clay layer in the porous unit. The direction of the groundwater flow at the NPP's site is mainly from NNE to SSW, discharging into the ocean, which is in agreement with the ground surface topography. The water table is kept about 2 m below the ground surface, with a slope of 0.5% towards the ocean, where it increases to a 1% gradient.

The waters under investigation could be classified in four major groups: Group 1 – Ca-Na-HCO3 waters type (hillside environment, where predominate granitic-gneissic basement outcrops,

residual soil, talus deposits and dense vegetation; rainfall domain); Group 2 – Ca-HCO3 waters type (groundwater samples, very close to the present and future NPP's facilities; rock dominance domain); Group 3 – Ca-(Na)-HCO3 waters type (intermediate flow and chemical composition between the waters of groups 1 and 2, groundwater); Group 4 – Na-Cl waters type (strong influence of seawater).

Two local meteoric water lines (LMWL) were obtained based on isotopic data from local precipitation samples: one was calculated by the non-weighted regression model (ordinary least squares regression, OLSR) and the other by a precipitation weighted ordinary least squares regression (PWLSR) method, but there was no significant difference between the lines obtained by the two methods.

From the available data, it was not possible to observe a significant difference in the stable isotopes signature between the two stations for precipitation sampling (LMA and EPTA). The slope values of the LMWLs were slightly lower than GMWL. Considering the standard deviations, they can be considered equal. All the valid values seem to fit reasonably well the LMWL, indicating that rainwater recharges the system locally, i.e., the water that supplies the groundwater sampling points (shallow, porous and unconfined aquifer) is basically from meteoric origin, with little interaction with the local lithology.

Values of tritium concentration ranging from 2.5 to 3.0 TU may be considered as the regional background for surface and groundwater not impacted by the operation of the power plants. Groundwater around the nuclear power plants site showed tritium levels greater than regional environmental values. The closer the sampling gets to the operating NPPs, the larger are the values for tritium concentration, with contents close to 100 TU at piezometers located one kilometer westward and a maximum value of 2,893 TU just outside of the building containing the pool for storage of the spent nuclear fuel.

Since most of the groundwater samples are at or above the environmental background for the area, it is not possible to obtain the groundwater age of the samples based on fitting data using lumped parameter models. An estimate made by using the exponential model for the mean transit time for groundwater around the NPPs site suggests that it is no greater than 5 years.

As a result of all the time, money, personnel and effort applied to develop the project, an important question arises, and that is the need to plan in great detail all the investigations to be made in order to accomplish the positive expected results. Sometimes, not all that has been planned can be achieved and there has to be some alternative actions to cover eventual fails and blanks.

Even dedicating special concern to the groundwater compartment, as was the case in this project, it is perceived that the entire water resources system should be considered, because integrated studies tend to yield more consistent results to enable a most efficient management of the whole water bodies.

One particular concern should be given to the elaboration of a consistent conceptual model because it will represent the starting point for the development of a more robust and trustable mathematical (analytical or numerical) model which will, in turn, be able to predict with greater certainty the fate of the radioactive contaminants eventually introduced in the hydrological system, and how it will affect the public and the environment.

References

IBGE - Instituto Brasileiro de Geografia e Estatística. *População Angra dos Reis* – RJ, 2019. Available at https://cidades.ibge.gov.br/brasil/rj/angra-dos-reis/panorama (Accessed 20 August 2020).

FIGUEIREDO, J. B. A.; CHAN, C. S.; DERECZYNSKI, C. P.; LYRA, A. A. SILVA FILHO, P. P. L.; ALMEIDA, P. M. P. Climatologia no Entorno da Central Nuclear de Angra dos Reis, RJ. Revista Brasileira de Meteorologia, v. 31, n. 3, p. 298-310, 2016.

MOLNARY, L. Principais características da Climatologia e Meteorologia para a Central Nuclear Almirante Álvaro Alberto (CNAAA). Relatório Técnico, IPEN-CEN-PSE-ETN-213-00 RELT-001-00, IPEN – CENTRO DE ENERGIA NUCLEAR, Rio de Janeiro, 65 p. 2017.

APHA. Standard methods for the Examination of water and wastewater, (American Public Health Association, Washington, DC), 1999.

APPELO, C.A.J., POSTMA, D. Geochemistry, Groundwater and Pollution. Balkema, Rotterdam, 2ND edition, 2005. p. 634.
BRAZIL - Brazilian Ministry of Health. Drinking water standards for human consumption. Portaria Nº 2.914, de 12 de dezembro de 2011, 2011.
CPRM – Serviço Geológico do Brasil. Geologia da Folha angra dos Reis SF.23-Z-CII (escala 1:100.000): Ministério das Minas e Energia, Brasília, 2007.
ELETRONUCLEAR, Estudo de Impacto ambiental Unidade 3 da Central Nuclear Almirante Álvaro Alberto – ANGRA 3 – volume 2, maio, 2005.
GIBBS, R.J. Mechanisms controlling world water chemistry. Science 170:1088–1090, 1970. https ://doi.org/10.1126/science.170.3962.1088
GUEDES, E., HEILBRON, M., VASCONCELOS, P.M., VALERIANO, C.M., ALMEIDA, J.C.H., TEIXEIRA, W., THOMAZ FILHO, A., K-Ar and 40Ar/39Ar ages of dikes emplaced in the onshore basement of Santos Basin, Resende area, SE Brazil: implications for the South Atlantic opening and Tertiary reactivation. J. S. Am. Earth Sci. (18) 371-382, 2005.
HUGHES, C.E., CRAWFORD, J. A new precipitation weighted method for determining the meteoric water line for hydrological applications demonstrated using Australian and global GNIP data. Journal of Hydrology, 464-465: 344-351, 2012. https://doi.org/10.1016/j.jhydrol.2012.07.029
IAEA - International Atomic Energy Agency. Statistical treatment of data on environmental isotopes in precipitation, Technical Reports Series 331. IAEA, Vienna, pp. 1–781, 1992.
INMET - Instituto Nacional de Meteorologia. Banco de dados Meteorológico. Data requested in https://bdmep.inmet.gov.br/, 2021.
MARTIN, L., SUGUIO, K., FLEXOR, J., DOMINGUEZ, J.M.L., BITTENCOURT, A.C.S.P. Quaternary sea-level history and variation in dynamics along the Central Brazilian Coast: consequences on coastal plain construction, An. Acad. Bras. Ciências. v. 68(3); p. 303-354, 1996.
MILLERO, F.J. Chemical Oceanography. CRC Press; 4ª edição, 2013. 591 p.
NATRONTEC ESTUDOS E ENGENHARIA DE PROCESSOS LTDA. Estudo de Impacto Ambiental da Unidade 2 da Central Nuclear Almirante Álvaro Alberto – Angra 2. Rio de Janeiro, 8v, 1999.
PIPER, A.M. A graphic procedure in the geochemical interpretation of water analyses. Trans. Am. Geophys Union 25, 914-923, 1944.
PROMON ENGENHARIA S.A. Considerações sobre a Hidrogeologia da Região de Angra dos Reis, Operação Promon FR01H. RL. 3246-C.1, 1974.
PROMON ENGENHARIA S.A., 1989. Central Nuclear de Angra – Unidade 3 –Relatório Geotécnico Doc. BP-3-6502-850100 – RI: Volume 1.
TECNOL – AMBIENTAL TECNOL CONSULTORIA. Execução de 7 poços de monitoramento de águas subterrâneas em Angra 03. Relatório final, 2011.
SHAMSI, A; KARAMI, G. H., HUNKELER, D. TAHERI, A. Isotopic and hydrogeochemical evaluation of springs discharging from high-elevation karst aquifers in Lar National Park, northern Iran. Hydrogeology Journal, Volume 27, Issue 2, pp.655-667, 2019. https://doi.org/10.1007/s10040-018-1873-4.
SILVA-FILHO, E.V., SOBRAL BARCELLOS, R.G., EMBLANCH, C., BLAVOUX, B., SELLA, S.M., DANIEL, M., SIMLER, R., WASSERMAN, J.C. Groundwater chemical characterization of a Rio de Janeiro coastal aquifer, SE e Brazil. J. South Am. Earth Sci. 27, 100e108, 2009.
SONG, Y., WANG, S., ARGIRIOU. A., ARGIRIOU, A., ZHANG, M., SHI, Y. Global perspective of local meteoric water lines based on daily and monthly data: a consideration of climate types. Authorea. 2021. https://doi.org/10.22541/au.161606496.64265677/v1
TIWARI, A. K., ANTONINO PISCIOTTA, A., DE MAIO, M. Evaluation of groundwater salinization and pollution level on Favignana Island, Italy. Environmental Pollution 249 (2019) 969-98, 2019. https://doi.org/10.1016/j.envpol.2019.03.016
UFRJ - Universidade Federal do Rio de Janeiro. IGEO, Levantamento e Diagnóstico Ambiental (Meio Físico) da Área de Influência da Central Nuclear (CNAAA) – Volume II, Eixo 2 – Geologia e Recursos Hídricos. UFRJ, Instituto de Geociências (IGEO), Rio de Janeiro, 2003.

CHINA

4. THE MIGRATION OF RADIONUCLIDES IN GROUNDWATER SYSTEM IN THE VICINITY OF AN INLAND NUCLEAR POWER PLANT, EASTERN CHINA

DONG YIHUI (董一慧), LIU XIANHUI (刘显辉), ZAN JINJING (咎金晶), LIU CHUNHUANG (刘春篁), XU WEIDONG (徐卫东), LI JIALE (李佳乐)

State Key Laboratory of Nuclear Resources and Environment & School of Water Resources and Environmental Engineering, East China University of Technology, No. 418 Guanglan Road, Nanchang City, Jiangxi Province, P. R. China, 330013

Abstract

This project took Hekui NPP, a pre-selected site of inland nuclear power plant in Jiangxi province of China, as the research area, to reveal the migration of radionuclides in groundwater system in the vicinity of Hekui NPP. The project was carried out by field survey, groundwater hydrochemical analysis, hydrogen and oxygen stable isotopic analysis, activity concentrations analysis of radionuclides (uranium-238, thorium-232, and strontium-90), column experiments and modeling work. Distribution, spatial and temporal variation of regional groundwater hydrochemistry and radionuclides were stated based on hydrological investigation and hydrochemical analysis. The distribution characteristics of radionuclides were explained by the combination of geological settings, hydrological conditions, their activity concentrations analysis, distribution and the dominant geochemical processes in the groundwater system. The major groundwater recharge sources and water-rock reactions influencing the migration of radionuclides were discussed by both hydrogeological processes and hydrogen-2 and oxygen-18 stable isotopic compositions. Laboratory column experiments and modelling work were conducted to better theoretically understand the migration mechanism of radionuclides in groundwater system in case of unforeseen incidents. The project provides a theoretical basis for monitoring residential health risk near the nuclear power plant.

Keywords: δD, $\delta^{18}O$, radionuclides, groundwater, Hekui nuclear power plant.

4.1. Introduction

Nuclear projects have been constructed more and more in recent years with the rapid development of nuclear application technology. In China, the completed 13 NPPs have been put into service and are all distributed in the coastal areas, such as Shandong province, Guangdong province, and Fujian province, while planned NPPs are not only located in coastal areas, but in inland areas as well, including Hekui NPP in Jiangxi province, eastern China. Although NPPs provide convenience for human production activities and daily lives, they will impact the surrounding environment and even cause harm to human health and lead to groundwater contamination by radionuclides. In Japan, the Fukushima nuclear accident caused serious radioactive pollution to the surrounding environment of the NPP, and the total amount of radioactive material leakage was 520 PBq (Dantong et al., 2014; Wuhui et al., 2015). The study on the comprehensive characteristics of groundwater system in the vicinity of NPPs is a worldwide scientific issue and is of great importance for NPPs site selection and groundwater environment evaluation.

Hekui NPP, a pre-selected site of inland NPP in Jiangxi province, eastern China, is the research area in this project to study the migration of radionuclides in groundwater system in the vicinity of this inland NPP. This work was funded by the IAEA Coordinated Research Project F33022.

The project will provide a theoretical basis for water resources development and environment protection in the vicinity of the inland NPPs and will assist in controlling the pollution of water resources if unforeseen incidents happen.

4.2. Site description, geological and hydrogeological setting

4.2.1. Site description

Hekui village is chosen as a pre-selected site of inland NPP in Jiangxi province, eastern China (Fig. 4.1), located in E 115°03′19.57″ ~ E 115°04′08.43″, N 27°30′45.63″~ N 27°31′19.95″, with an area of 3.57 km^2 (Fei, 2014).

The area has a subtropical humid climate with distinctive four seasons. The annual average temperature is 18 ℃. The highest temperature is in July, with an average of 29–30 ℃ and up to 38–40 ℃, while the lowest temperature is in January with an average of 6 ℃. The climate of the region is warm and humid subtropical, with an abundant annual rainfall of 1,547.8 mm. The wet season is between April to June, accounting for 46.4% of the whole year's atmospheric precipitation, and the dry season is from September to January, with 19.9% of the whole year's precipitation. The annual average evaporation is 1,089.0 mm and it accounts for 32.3% and 10.9% of the whole year's evaporation from July to August, from December to February, respectively.

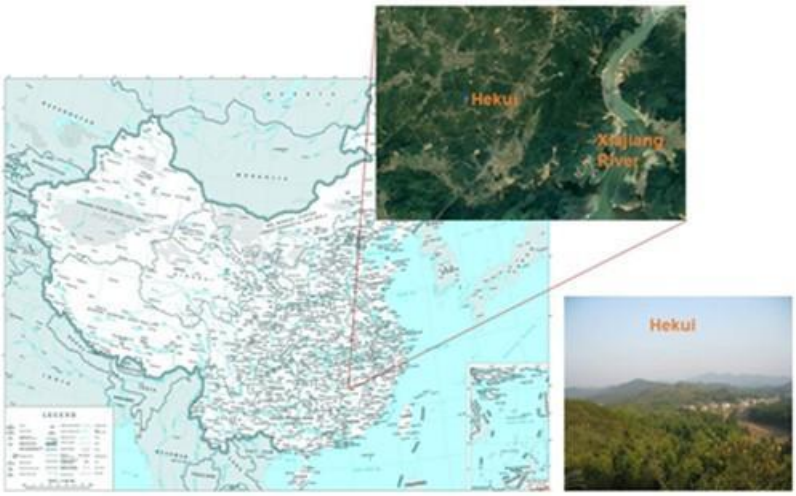

Fig. 4.1. The location of Hekui NPP

4.2.2. Geological and hydrogeological setting

In the study area, there are four aquifer units, a loosely porous aquifer group, a clastic pore fissure aquifer group, a magmatic pore fissure aquifer group, and a metamorphic aquifer group (Fig. 4.2). The strata are mainly divided into two layers, the overburden layer is Quaternary unconsolidated sediment and the underlying bedrock is Triassic granite (Fig. 4.3). The lower aquifer is 4~6 m thick and the groundwater is with a buried depth of 0.05–5.65 m.

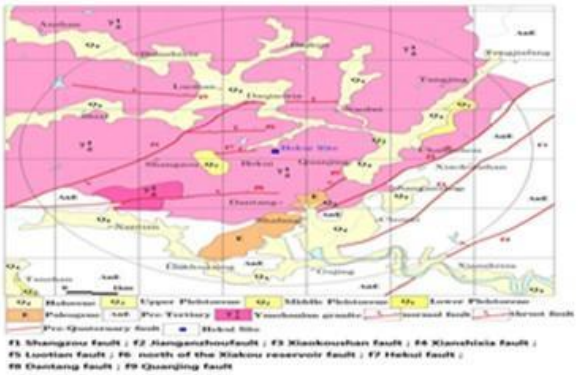

Fig. 4.2. The regional geology of in the Vicinity of Hekui NPP

Groundwater in this area is mainly bedrock fissure water. The permeability coefficient of intense weathered rock, with a moderate permeable capacity, is $3.945\times10^{-4} \sim 5.72\times10^{-3}$ cm • s^{-1}. The permeable rate of the moderate and weak weathered rock is 0.63~0.96 Lu and the permeability coefficient is $7.0\times10^{-6} \sim 1.17\times10^{-5}$ cm • s^{-1}, indicating they are slightly permeable rock, which is the major type of rock in Hekui NPP (Xiaochuan et al., 2013). Water from wells and springs is utilized extensively for livestock feeding and potable drinking water. Groundwater is non-corrosive to the concrete structure. Due to the poor amount, low level of exploitation and utilization of groundwater,

and local simple hydrogeological conditions, the influence of engineering construction activities on the geological environment is under control.

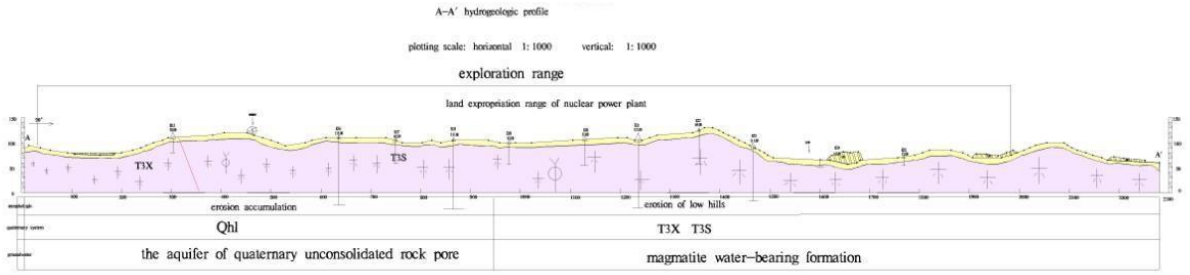

Fig. 4.3. Regional hydrogeological cross-section map of Hekui NPP

4.3. Method and sampling analysis

4.3.1. Sampling and measurements

Twenty-nine well water, eight spring water, and five surface water samples were collected within 12 km of the Hekui NPP in November 2017. Based on previous work in 2017, according to different water types and hydrochemical characteristics of samples, 21 well water, 3 spring water and 2 surface water samples were re-collected in September 2018 and December 2019 (Figs. 4.4 and 4.5). Wells are located in the shallow aquifer. Most wells were constructed in the past 10 years, and some were over 100 years.

Fig. 4.4. Sampling sites in the vicinity of Hekui NPP, eastern China in 2017, 2018, and 2019 (samples including groundwater water samples from well, spring water samples, and surface water samples including water from Xiajiang River, and some small rivers)

Fig. 4.5. Field sampling work in 2017, 2018, and 2019 in the vicinity of Hekui NPP

The temperature, pH, electrical conductivity (EC), dissolved oxygen (DO) and ORP of groundwater samples was monitored by a portable parallel analyzer (HQ40d, HACH). Groundwater samples were collected and filtered through membrane filters with 0.45-μm pore diameter for

chemical analysis. Alkalinity was determined using the Gran titration method within 24 h after sampling. The wells were typically pumped for approximately 10 minutes before sampling. Water samples were firstly filtered (<0.45μ m) on site and stored in 50 ml acid-washed HDPE bottles and acidified by ultra-pure HNO_3 to pH=2 or less for cations analysis. Those used for anions, ^{238}U and ^{232}Th concentrations analysis were not acidified but only filtered using 0.45 μm membrane filters. Samples for oxygen and hydrogen stable isotopes analysis were not filtered and directly stored in 100 ml HDPE bottles, full of water without any bubble. Samples for ^{90}Sr activity concentration were collected in 10 L HDPE bucket and acidified by ultra-pure HNO_3 to pH<2. All samples were kept at 4 ℃ and measured within 7 days.

Cations and anions were measured by inductively coupled plasma atomic emission spectrometry (ICP-AES, iCAP-7400) and ion chromatography (IC, ICS-1100), respectively. Oxygen-2 and hydrogen-18 stable isotopes were analyzed using a MAT 253 mass spectrometer. The activity concentration of radionuclides (uranium-238, thorium-232) were determined by Ensemble multi-detector alpha spectrometry (Ortec HPGe γ spectrometer, USA). The tritium analyses of water samples were completed with a liquid scintillation counting method (1220 Quantulus Ultra Low Level LSC), after enrichment by electrolysis. The tritium concentration was expressed in tritium units (TU), where 1 TU indicates a T/H abundance ratio of 10–18. The accuracy of low-level tritium measurement was 0.1 TU coupled with an average standard deviation of 0.6 TU. ^{90}Sr activity concentration was measured using the low background beta measuring instrument.

4.3.2. Lab experiments

Batch experiments were conducted in a shaking water bath with a temperature controller and performed in 100 mL centrifuge tubes containing soil collected from Hekui NPP and 50 mL of Cs solution ($CsNO_3$) with different initial concentrations (50 $mg \cdot L^{-1}$, 100 $mg \cdot L^{-1}$, 200 $mg \cdot L^{-1}$), different solution pH values (pH=4.0, 7.0), and different reaction times (3 h, 6 h, 12 h, 24 h, 36 h). The shaker speed was controlled at 210 rpm (Qinqin et al., 2019).

Column experiments were performed in the laboratory using the shallow sediment samples collected from the Hekui NPP. 50 $mg \cdot L^{-1}$ of $CsNO_3$ solution was pumped at a constant flow rate 2.04 $mL \cdot min^{-1}$ to flow through the column filled with the sediments. The effluent was collected for Cs concentration measurement (APHA, 2005).

4.3.3. Modelling work

The modelling work was carried out using the software GMS. ^{137}Cs was chosen as the objective to simulate its migration in groundwater system in case of unforeseen incidents.

4.4. Results and discussion

4.4.1. Groundwater chemistry

As can be seen from Fig. 4.6 and Table 4.1, major cations and anions in surface water are Ca^{2+}, Na^+, and HCO_3^-, respectively. The major types of well water are HCO_3-Na and HCO_3-Ca. The major cations and anions in spring water are Na^+ and HCO_3^-, respectively.

The major chemical compositions in well water and spring water are mainly from the dissolution of minerals. The relationship between the hydrogen and oxygen isotopic compositions of the groundwater reflects groundwater that originated from atmospheric precipitation. By comparison of hydrochemical compositions of the same water samples both collected in 2017 and 2018, 6 well water samples differed in cations, while four well samples differed in anions.

Chloride is an important indicator for hydrochemical variations in different seasons (Fig. 4.7). With the increase of TDS in groundwater, the content of chloride also increased, indicating that chloride ions may come from mineral dissolution. From Cl vs. Cl/Br plot, the wide variation of Cl to Br ratios in shallow groundwater may result from differences in the amount of halite dissolution in vertical recharge water (Zan et al., 2019). Therefore, dissolution of halite in the unsaturated zone was the most likely mechanism responsible.

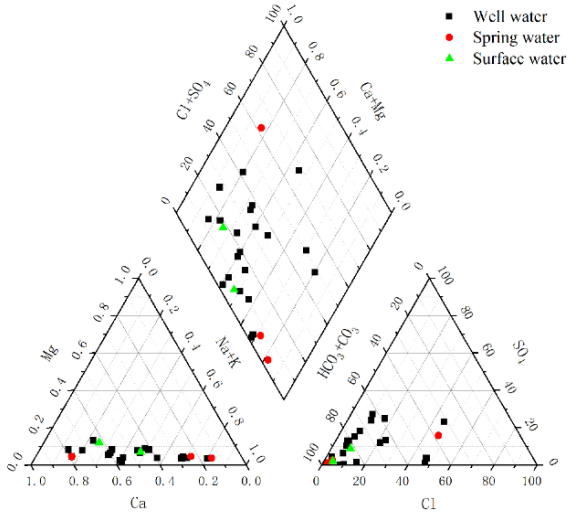

Fig. 4.6. The piper diagram of water samples collected from vicinity of Hekui NPP

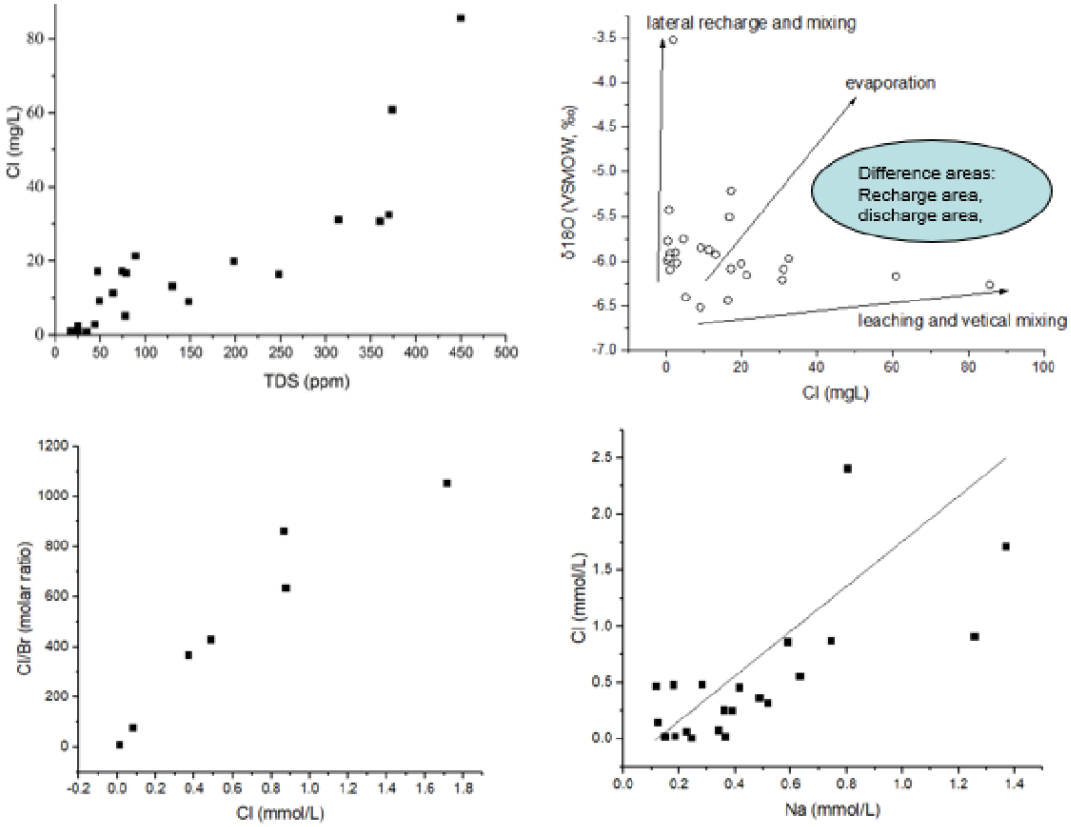

Fig. 4.7. The relationship of TDU vs Cl, Cl vs $\delta^{18}O$, Cl vs Cl/Br, and Na vs Cl, indicating the major hydrochemical processes in shallow groundwater

Table 4.1. Hydrochemistry of groundwater, surface water, and spring water

	Well water			Spring water			Surface water		
	MAX	MIN	AVE	MAX	MIN	AVE	MAX	MIN	AVE
Elevation	104	41	71	102	53	74	65	46	55
Well depth (m)	12.92	1.14	5.09	-	-	-	-	-	-

Groundwater level (m)	6.50	0.10	2.45	-	-	-	-	-	-
pH	7.26	6.01	6.71	7.73	5.93	6.95	7.84	7.22	7.60
ORP (mv)	329.4	162.5	258.0	327.6	240.0	291.6	313.3	173.8	250.7
EC ($\mu s \cdot cm^{-1}$)	652.00	7.81	230.29	198.00	16.89	91.16	187.30	49.70	119.44
T (℃)	23.60	17.10	20.78	20.50	16.90	19.30	20.50	16.40	18.48
DO ($mg \cdot L^{-1}$)	19.40	1.60	6.29	11.23	6.38	8.79	10.27	8.27	9.37
TDS ($mg \cdot L^{-1}$)	364.00	11.00	119.17	96.00	8.00	40.88	71.00	23.00	47.40
Ca ($mg \cdot L^{-1}$)	82.00	1.33	28.59	11.20	0.21	4.96	15.20	3.10	9.99
K ($mg \cdot L^{-1}$)	68.70	0.63	15.74	13.00	2.57	5.46	3.65	2.92	3.30
Mg ($mg \cdot L^{-1}$)	13.00	0.28	3.11	3.69	0.12	1.07	2.85	0.76	2.06
Na ($mg \cdot L^{-1}$)	24.20	1.44	8.29	11.20	2.49	5.92	7.64	4.32	5.41
HCO_3 ($mg \cdot L^{-1}$)	277.64	10.98	78.67	34.78	11.29	20.92	42.10	36.00	38.73
Cl ($mg \cdot L^{-1}$)	52.60	0.18	9.56	19.40	0.12	4.98	11.30	1.70	4.25
SO_4 ($mg \cdot L^{-1}$)	51.30	0.22	14.84	7.24	0.39	2.80	12.70	1.13	8.23
^{238}U ($\mu g \cdot L^{-1}$)	5.17	<0.04	0.64	1.11	0.05	0.27	<0.04 ug•L^{-1}		
^{232}Th ($\mu g \cdot L^{-1}$)	0.74	0.45	0.48	0.58	0.45	0.47	0.47	0.46	0.47

4.4.2. Isotopic characteristics of water samples

The relationship between δ18O and δD (Fig. 4.8) demonstrated a close hydraulic connection between surface water and well water, indicating that atmospheric precipitation is the main source of shallow groundwater recharge (Jinjing et al., 2019; XIAO et al., 2019).

In the study area, tritium concentrations ranged from 2.1 TU to 3.6 TU (Fig. 4.9). Vertically, there was a relatively weak linear varying trend for tritium concentrations, which was probably caused by various exchange with the surface end members in different sites.

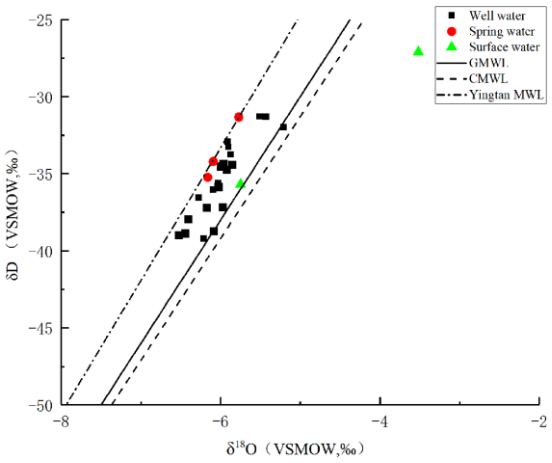

Fig. 4.8. $\delta^{18}O$ and δD isotopic composition in water collected in 2018

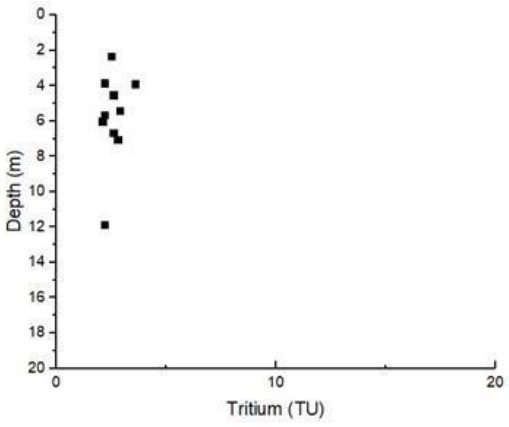

Fig. 4.9. A relationship between the tritium concentrations and well depth of shallow groundwater samples

Natural radioactive isotopic compositions are shown in Table 4.2. As shown in the table, radioactive concentration of Th-232 was all below the BLD. Radioactive concentrations of U-238, Ra-226, K-40 were BLD-3.22 Bq·L-1, BLD-13.85 Bq·L-1, and BLD-4.43 Bq·L-1. Both of the radioactive concentrations of U-238 and Th-232 were below the standard for drinking water 10 Bq·L-1 and 1 Bq·L-1 (WHO). Most water had higher radioactive concentration of Ra-226 than the drinking water standard 1 Bq·L-1.

Table 4.2. Natural radioactive isotopic compositions of water samples (unit: $Bq{\cdot}L^{-1}$)

Sample ID	U-238	Ra-226	Th-232	K-40
G05	1.86	1.37	BLD	3.63
G06	1.68	13.85	BLD	3.02
G09	3.22	1.30	BLD	2.53
G11	BLD	2.40	BLD	2.51
G22	1.74	1.11	BLD	2.56
G25	BLD	1.27	BLD	2.94
G26	BLD	BLD	BLD	2.84
G28	BLD	BLD	BLD	4.43
Q08	BLD	4.81	BLD	BLD
S01	BLD	BLD	BLD	BLD
G03	BLD	0.15	BLD	2.46

BLD: below the limit of detection. BLD for U-238, Ra-226, Th-232, K-40 was 1.12 $Bq{\cdot}L^{-1}$, 0.53 $Bq{\cdot}L^{-1}$, 0.48 $Bq{\cdot}L^{-1}$, and 2.45 $Bq{\cdot}L^{-1}$.

Radioactive concentration of ^{90}Sr in four groundwater samples, one spring water sample and one surface water sample were all below 10 $mBq{\cdot}L^{-1}$, providing a background value of ^{90}Sr in Hekui NPP.

4.4.3. Batch experiments and column experiments

4.4.3.1. Batch experiments

As can be seen from Fig. 4.10, when the solution pH was 7.0, the initial concentration of Cs was 50 $mg{\cdot}L^{-1}$, dose of shallow sediments was 40 g·L-1, the optimum adsorption rate of Cs reached 55.45%.

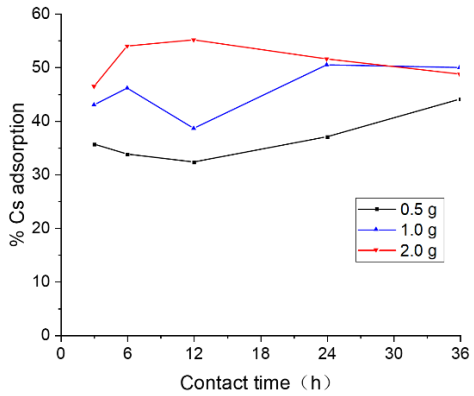

Fig. 4.10. Effect of soil dosage on Cs adsorption (initial Cs concentration=50 $mg{\cdot}L^{-1}$, pH=7, solution volume=50 mL)

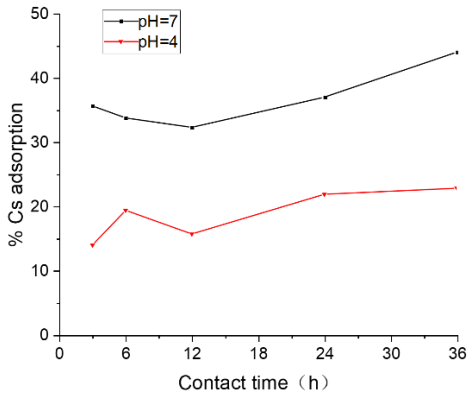

Fig. 4.11. Effect of pH on Cs adsorption onto soil (initial Cs concentration=50 mg·L-1, soil dosage=0.5 g, solution volume=50 mL)

As can be seen from Fig. 4.11, when Cs concentration was 50 $mg{\cdot}L^{-1}$, soil dosage was 0.5 g in 50 mL of solution, the soil had an obviously better sorption rate when pH=7 than in acid condition.

As shown in Fig. 4.12, in the first 3 h of the reaction, the Cs adsorption rate increased with increasing time. When the reaction exceeded time3 h, changes in the adsorption rate were not obvious in conditions of initial Cs concentration of 100 mg·L^{-1} and 200 mg·L^{-1}. For initial Cs concentration of 50 mg·L^{-1}, the Cs adsorption rate increases after 12 h (Table 4.3).

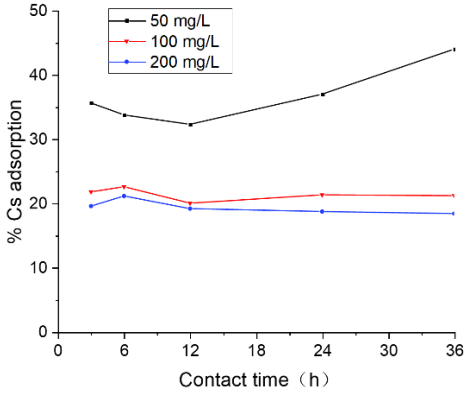

Fig. 4.12. Effect of initial Cs concentration on Cs adsorption
(pH=7, soil dosage = 0.5 g, solution volume = 50 mL)

Table 4.3. Results of Cs adsorption by shallow sediments collected from Hekui NPP

Initial Cs concentration, mg·L^{-1}	Dose of sediments, g	Adsorption rate, %
50	0.5	44.04
100	0.5	21.54
200	0.5	17.88
50	1	43.93
50	2	55.45

4.4.3.2. Column experiments

With the same hydraulic load, soil dosage and pH, the Cs adsorption are shown in Fig. 4.13. The higher the initial Cs concentration was, the higher the adsorption of Cs on soil particles. When the Cs concentration was 50 mg·L^{-1}, the adsorption capacity of the column was larger than the Cs concentration of 10 mg·L^{-1}. Under the experimental conditions, the increase in Cs concentration was beneficial to Cs adsorption by soil particles.

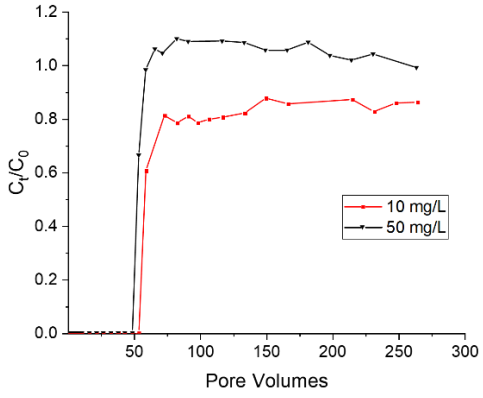

Fig. 4.13. Effect of initial Cs concentration on the breakthrough curve of the column used for Cs adsorption (hydraulic load = 23.39 m^3· m-1·d-1, pH = 7)

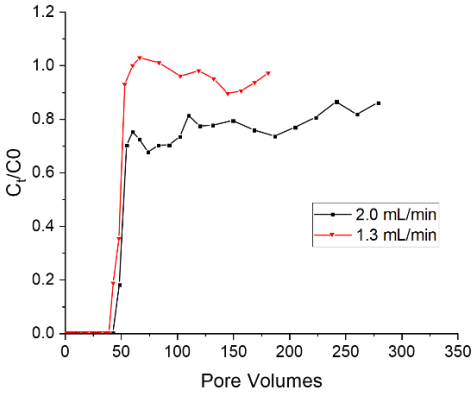

Fig. 4.14. Effect of hydraulic load on the breakthrough curve of the column used for Cs adsorption (initial Cs concentration = 50 mg·L-1, pH = 7))

Fig. 4.14 shows the breakthrough curves of the column under different hydraulic loads. With the same soil particle, initial U(VI) concentration and solution pH, Cs adsorption rate by soil under the

two hydraulic loads were both above 80%, indicating that changes in hydraulic loads had no obvious effect on Cs adsorption.

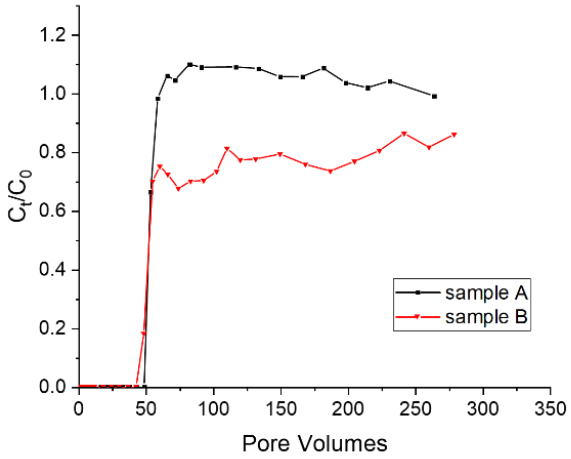

Fig. 4.15. Effect of different soils on the breakthrough curve of the column used for Cs adsorption (initial Cs concentration = 50 mg·L^{-1}, hydraulic load = 23.39 m^3· m^{-1}·d^{-1}, pH=7)

Fig. 4.15 shows the effect of different soil samples on Cs adsorption. For the two samples A and B, the Cs adsorption rate were both above 80%, indicating local soils was able to adsorb Cs in solution when initial Cs concentration was 50 mg·L^{-1}, hydraulic load was 23.39 m^3· m^{-1}·d^{-1}, and pH=7.

4.4.4. Modelling work

Through data collection and field survey to obtain the evaluation scope aquifer distribution characteristics, and according to the scope and discharge conditions of groundwater, unconfined aquifer was chosen as the target aquifer for simulation.

4.4.4.1. Hydrogeological conceptual model

The modelling area is a relatively complete hydrogeological unit, with an area of 55.43 km^2. The boundary is watertight, and the middle XiangJiang river is the fixed head boundary. The main source of groundwater recharge in the area is atmospheric precipitation. There is pore water and bedrock fissure water in the Quaternary aquifer, and the study area can be generalized into one aquifer.

4.4.4.2. Mathematical model

A mathematical model of homogeneous anisotropic 3-d unsteady flow and a mathematical model of pollutant migration were used in the modelling.

$$\theta \frac{\partial C}{\partial t} = \frac{\partial}{\partial x_i}\left(\theta D_{ij} \frac{\partial C}{\partial x_j}\right) - \frac{\partial}{\partial x_i}(u_i C) + q_s C_s + \sum_{n=1}^{N} REA_n \quad (1)$$

$$\frac{\partial}{\partial x}(K(h-z)\frac{\partial h}{\partial x}) + \frac{\partial}{\partial y}(K(h-z)\frac{\partial h}{\partial y}) + \frac{\partial}{\partial z}(K(h-z)\frac{\partial h}{\partial z}) + W = \mu \frac{\partial h}{\partial t} \quad (2)$$

4.4.4.3. Model grid subdivision

The visualization software GMS was used to solve the numerical simulation model, and the finite difference method was used when the MODFLOW module was used to solve the groundwater flow problem. The modelling area was subdivided as shown in Fig. 4.16.

4.4.4.4. Model calibration and verification

The simulation results of groundwater flow are shown in Fig. 4.17. Compared with the observation results, the model can reflect the overall direction of groundwater flow.

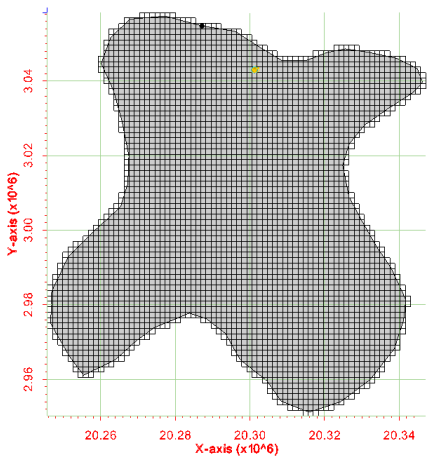

Fig. 4.16. Diagram of the model grid subdivision in the study area

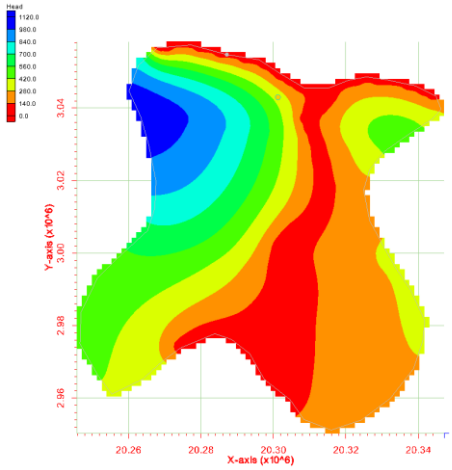

Fig. 4.17. Simulation of groundwater flow field

4.4.4.5. Prediction and evaluation of environmental impact on groundwater quality

^{137}Cs was selected for the evaluation of environmental impact in this study. In the event of an accident, 300 m^3 of radioactive waste water are all revealed for 72 h at a flow rate of 100 $m^3 \cdot d^{-1}$. According to the China Drinking Water Standard, total β radioactivity is 1 $Bq \cdot L^{-1}$, and the corresponding concentration of Cs is 2.27E-12 $mol \cdot L^{-1}$, which is used as the standard for migration distance and impact of ^{137}Cs. If the modelling result is below this value, it is considered that the concentration of ^{137}Cs has little or almost no impact on the environment (Figs. 4.18 and 4.19).

Table 4.4. Pollution area characteristics (Distance: km ; Area: km^2)

	100 days		1000 days		10 years		15 years	
	Distance	Area	Distance	Area	Distance	Area	Distance	Area
^{137}Cs	1.017	3.021	1.031	1.785	0.997	-	0.997	-

Fig. 4.18. Concentration and groundwater pollution range of ^{137}Cs after pollutant leaking for 100 days

Fig. 4.19. Concentration and groundwater pollution range of ^{137}Cs after pollutant leaking for 1,000 days

According to the modelling results, evaluation can be concluded as follows: 1) in normal condition, groundwater pollution would not happen; 2) after 100 days, 1,000 days, and 10 years, ^{137}Cs will spread following groundwater flow in the direction of the southeast. After 15 years, the concentration of ^{137}Cs will decrease to the standard value.

4.5. Conclusion

The groundwater hydrochemistry showed that groundwater had a good quality with low TDS and suitable pH for daily drinking, and with low radioactive background. Shallow groundwater was mainly from atmospheric precipitation and had a hydraulic connection with rainfall and surface water. Natural radioactive concentration of Th-232 was all below the BLD. Radioactive concentrations of U-238, Ra-226, K-40 were BLD-3.22 $Bq{\cdot}L^{-1}$, BLD-13.85 $Bq{\cdot}L^{-1}$, and BLD-4.43 $Bq{\cdot}L^{-1}$. Both of the radioactive concentrations of U-238 and Th-232 were below the standard for drinking water 10 $Bq{\cdot}L^{-1}$ and 1 $Bq{\cdot}L^{-1}$ (WHO). Most water had higher radioactive concentration of Ra-226 than the drinking water standard 1 $Bq{\cdot}L^{-1}$. In condition of accident happens that 300 m^3 of radioactive waste water are revealed for 72 h at a flow rate of 100 $m^3{\cdot}d^{-1}$, evaluation based on the modelling results of unconfined aquifer can be concluded as following: ^{137}Cs will spread following groundwater flow in the direction of southeast after 100 days, 1000 days, and 10 years, while concentration of ^{137}Cs will decrease to below the standard value (2.27E-12 $mol{\cdot}L^{-1}$ or 1 $Bq{\cdot}L^{-1}$) after 15 years.

Acknowledgements

This work was supported by Coordinated Research Project of the International Atomic Energy Agency (IAEA No. 21122), Fundamental Science on Radioactive Geology and Exploration Technology Laboratory, East China University of Technology (RGET1807), and Research Funding of East China University of Technology (DHBK2017136).

References

APHA, 2005. Standard Methods for the Examination of Water and Wastewater, 19th ed. American Public Health Association, Washington, DC, USA.

Awual, Rabiul M. Ring size dependent crown ether based mesoporous adsorbent for high cesium adsorption from wastewater. Chemical Engineering Journal, 2016, 303: 539–546.

D Zhong, Liao, X., Liu, Y., Zhong, N., & Xu, Y. Enhanced electricity generation performance and dye wastewater degradation of microbial fuel cell by using a petaline nio@ polyaniline-carbon felt anode. Bioresource Technology, 2018, 125.

Dantong Liu. Distribution and migration characteristics of typical radionuclides in China coastal environment after the Fukushima nuclear power plant accident. East China Normal University, 2014, Shanghai, China.

Fei Qin. A study on the hydro-geological conditions and permeability features of Hekui nuclear power plant in Jiangxi province. East China University of Technology, 2014, Nanchang, China.

He, Liu; Gao, Bai*; Luo, Xin; Jiao, Jimmy; Qin, Huanhuan; Zhang, Chunyan; Dong, Yihui. Health Risk Assessment of Heavy Metals in Surface Water near a Uranium Tailing Pond in Jiangxi Province, South China. Sustainability, 2018,10(4): 1113.

Hongji Wu. Kinetics of absorption of cesium in red soil in southeast Area. Chengdu University of Technology, 2007, Chengdu, China.

Jinjing Zan, Yihui Dong*, Weimin Zhang, Weidong Xu, Jiale Li, Bai Gao, Fawang Hu, Qiaohuan Wang. Distribution characteristics of dissolved oxygen and stable isotope compositions of shallow groundwater in the vicinity of an inland nuclear power plant, HK, China. E3S Web of Conferences 2019(98) :09035.

Lee J O, Cho W J, Chi H. Sorption of cesium and iodide ions onto KENTEX-bentonite. Environmental Earth Sciences, 2013, 70, 1(5): 2387-2395.

Qinqin Tao, Xu Zhang, Krishnamoorthy Prabaharan, Ying Dai. Separation of cesium from wastewater with copper hexacyanoferrate film in an electrochemical system driven by microbial fuel cells. Bioresource Technology, 2019, 278: 456-459.

Wuhui Lin, Liqi Chen, Jianghua He, Hao Ma, Shi Zeng, Shi Zeng. Review on monitoring marine radioactivity since the Fukushima Nuclear Accident. China Environmental Science, 2015, 35(1):269-276.

Xiaochuan Xu, Huahui Xu, Fei Qin. Research of hydrological geological condition in nuclear power plant inland. Journal of East China Institute of Technology (Natural Science), 2013, 36: 101-104.

XIAO Lili, WANG Zhifen*, HUA Rong*, LIU Xiaojian, LI Yang, DONG Yihui, ZHU Jiannan, HE Feifan, DAI Yahong, YUE Zhanggao. Progress on the Migration of Key Radionuclides in Geological Materials. Environmental Science & Technology, 2019, 42(4): 53-60.

Yaoqin Wang. Studies on the sorption behaviors of strontium and cesium onto sandy soil. Lanzhou University, 2011, Lanzhou, China.

Zan Jinjing, Dong Yihui*, Zhang Weimin, Li Jiale, Gao Bai, Chen Gongxin. Occurrence and migration of uranium in groundwater system. Nonferrous Metals (Mining Section), 2019, 71(6): 69-77.

Zheng, Y., Qiao, J., Yuan, J., Shen, J., & Li, N. Electrochemical removal of radioactive cesium from nuclear waste using the dendritic copper hexacyanoferrate/carbon nanotube hybrids. Electrochimica Acta,2017, 257.

Zhong, D., Liao, X., Liu, Y., Zhong, N., Xu, Y. Enhanced electricity generation performance and dye wastewater degradation of microbial fuel cell by using a petaline NiO@ polyaniline-carbon felt anode. Bioresources Technology, 2018, 258: 125–134.

ITALY

Centrale del Garigliano
https://www.sogin.it/it/chiusuradelciclonucleare/sitinucleariitaliani/centraledigarigliano/Pagine/default.aspx

5. GROUNDWATER SYSTEM ASSESSMENT IN THE VICINITY OF GARIGLIANO NUCLEAR POWER PLANT (SOUTHERN ITALY)

L. STELLATO[1], F. MARZAIOLI[1], F- TERRASI[1], B. DI RIENZO[1], C. SABBARESE[1], A. D'ONOFRIO[1], A. PETRAGLIA[1], M. MASTROCICCO[2], D. GRANATA[2], D. RUBERTI[3], A. M. ESPOSITO[4]

[1] Dipartimento di Matematica e Fisica, Università degli Studi della Campania "Luigi Vanvitelli", Caserta, ITALY
[2] Dipartimento di Scienze e Tecnologie per l'Ambiente, la Biologia e il Farmaco, Università degli Studi della Campania "Luigi Vanvitelli", Caserta, ITALY
[3] Dipartimento di Ingegneria, Università degli Studi della Campania "Luigi Vanvitelli", Aversa, ITALY
[4] SoGIN, Società Gestione Impianti Nucleari, Garigliano NPP, Sessa Aurunca, Caserta, ITALY

Abstract

In Italy the nuclear technology to produce electric power has been abandoned since 1987, one year after the Chornobyl nuclear accident. Among the four Italian nuclear power plants (NPPs) are in decommissioning. During the decommissioning phase, environmental monitoring plans are carried out according to prescriptions of the Ministry of Environment (MATTM) in agreement with the Ministry of Cultural Heritage and Tourism (MiBACT). In particular, for the Garigliano NPP, a semi-annual environmental impact assessment is prescribed in order to monitor the atmosphere, water bodies (river and groundwater), soil, ecosystems (vegetation, flora and fauna), environmental noise and ionizing radiations.

Although monitoring plans usually take into account the groundwater and the surface water components as a possible way of release of radionuclides to the environment, no guidelines are available on techniques for proper characterization of groundwater spatial and temporal dynamics to understand in detail the conceptual groundwater model in the vicinity of a NPP and to evaluate potential pathways for radionuclide migration, hydrogeological aspects, such as recharge and discharge areas and rates, interactions between surface and/or groundwater bodies, infiltration or leakages of water, either from reservoirs constructed for the needs of the NPP, or due to natural recharge by precipitation with the aim to plan effective countermeasures for protection of public and the environment in case of accidental release of radioactive materials.

In the framework of the existing and fruitful collaboration among the Department of Mathematics and Physics of the SUN and the Sogin, a project is proposed to integrate the already acquired knowledge about the environment surrounding the GNPP with hydrogeological, hydrochemical and isotopic data to characterize the groundwater and the river in the vicinity of the nuclear power plant and finally obtain a conceptual model of the temporal and spatial patterns of groundwater flow.

The main scope of the proposed project are i) the study of groundwater flow pathways, residence times, recharge zones in the vicinity of the Garigliano NPP, ii) the study of temporal and spatial surface water-groundwater interactions nearby the Garigliano NPP, iii) the identification of suitable artificial and/or natural isotopic tracers to identify groundwater preferential pathways by means of an integrated methodological approach based on hydrogeologic, hydrochemical and isotopic techniques in order to define a conceptual model of groundwater recharge rate, residence times, interactions with local surface water bodies (sea and rivers).

Keywords: Groundwater, Surface water-groundwater interactions, Natural and artificial tracers, Isotopes, Nuclear Power Plant decommissioning.

5.1. Introduction

Nuclear technology to produce electric power has been developed since 1950s. Today, the world produces as much electricity from nuclear energy as it did from all sources combined in the early years of nuclear power. Civil nuclear power can now boast over 16,000 reactor years of experience and supplies almost 11.5% of global electricity needs, from reactors in 31 countries. Nowadays 31 countries host over 435 commercial nuclear power reactors with a total installed

capacity of over 375,000 MWe. About 70 further nuclear power reactors are under construction, equivalent to 20% of existing capacity, while over 160 are firmly planned, equivalent to half of present capacity. (source: http://www.world-nuclear.org/info/Current-and-Future-Generation/Nuclear-Power-in-the-World-Today/). The expansion of new plants and the management of the existing ones is subject to the application of safety and monitoring plans, in order to ensure an adequate protection to the public and the environment, usually based on the assessment of radioactive releases and the doses to the population.

In this general context, after the Tokyo Electric Power Company's (TEPCO) Fukushima Daiichi Nuclear Power Station (NPS) accident a Technical Meeting has been convened at IAEA headquarters in Vienna in September 2014 in order to discuss and share experiences in terms of countermeasures adopted to reduce the risk of groundwater and surface water contamination (http://www-naweb.iaea.org/napc/ih/documents/other/Meeting_Summary_%20Final.pdf). The most important outcome from the meeting was the acknowledged need of a groundwater characterization in the vicinity of NPPs in order to define a conceptual model of groundwater recharge rate, residence times, interactions with local surface water bodies (sea and rivers) and create a basic knowledge for the application of transport models and a better management of the situation in case of accidental releases.

In Europe the situation is controversial, since many Member States decided to phase out the nuclear power while others continue to expand their capacity to produce nuclear power. Among the states who decided to abandon nuclear generated energy, there is Italy. Nuclear power phase-out started in Italy in 1987, one year after the Chornobyl accident. Following the outcome of a referendum in that year, Italy's four nuclear power plants were closed down, the last in 1990. A moratorium on the construction of new plants, originally in effect from 1987 until 1993, has since been extended indefinitely. In Table 5.1, the specifications of the existing Italian NPP are reported.

Table 5.1. Italian Nuclear Power Plants

Reactor	Model	Net MWe	First power	Shutdown
Latina	GCR	153[k]	05/1963	12/1987
Garigliano	BWR	150	01/1964	03/1982
Enrico Fermi (Trino Vercellese)	PWR	260	10/1964	07/1990
Caorso	BWR	860	05/1978	07/1990
Montalto di Castro (Alto Lazio) 1 & 2	BWR	982 each	Cancelled	-
Total operated (4)		1423 MWe		

When the government decided to end the country's nuclear power program in 1990, a deferred decommissioning (or 'Safstor') strategy was adopted. However, in 1999, the government changed to an accelerated decommissioning strategy. This strategy envisaged all decommissioning of nuclear facilities by 2020, subject to the availability of a low- and intermediate-level waste repository that can also be used for temporary storage of high-level wastes. In 2004, the deadline for decommissioning was put back to 2024, with the option of reprocessing allowed. In October 2005, there was a seminar sponsored by the government about the possibility of reviving Italian nuclear power but a referendum held in June 2011 stopped definitively any project.

The decommissioning activities of a nuclear site, in Italy entrusted to the Sogin (Società di Gestione degli Impianti Nucleari), is the last phase of its life cycle are related to the maintenance of the plants' safety, the removal of spent nuclear fuel, the process of decontamination and dismantling of nuclear installations, as well as the management and safety of radioactive waste pending their transportation to the National Repository. All these activities are intended to decontaminate the

nuclear sites and turn them into “green field”, i.e. to a condition free from restrictions linked to the presence of radioactivity, making them suitable for any other use (source: http://www.Sogin.it/en/Pages/default.aspx).

During the decommissioning phase, environmental monitoring plans are carried out according to prescriptions of the Ministry of Environment (MATTM) in agreement with the Ministry of Cultural Heritage and Tourism (MiBACT). In particular, for the Garigliano NPP, a semi-annual environmental impact assessment is prescribed in order to monitor the atmosphere, water bodies (river and groundwater), soil, ecosystems (vegetation, flora and fauna), environmental noise and ionizing radiations.

Although monitoring plans usually take into account the groundwater and the surface water components as a possible way of release of radionuclides to the environment, no guidelines are available on techniques for proper characterization of groundwater spatial and temporal dynamics to understand in detail the conceptual groundwater flow and transport model in the vicinity of a NPP. Evaluating the potential pathways for radionuclide migration, the hydrogeological aspects such as recharge and discharge areas and rates, the interactions between surface and/or groundwater bodies, and the infiltration or leakages of water either from reservoirs constructed for the needs of the NPP or due to natural recharge by precipitation, is of crucial importance to plan effective countermeasures for protecting public health and the environment in case of accidental release of radioactive materials.

Stable and radioactive isotopes have been extensively used to identify water residence times, components of stream discharge (Rodgers et al., 2005; Stellato et al., 2009; Vitvar et al., 2005), nutrient biodegradation processes (McMahon and Böhlke, 1996), and quantify groundwater inflows to rivers (Genereux and Hemond, 1990; Lee and Hollyday, 1991), resulting in the development of very useful tools in the comprehension of effluent river ecosystems. Among radioactive tracers, ^{222}Rn (radon), a naturally occurring noble gas, is particularly useful for detecting groundwater discharge to streams because of its different concentrations in surface water and groundwater (Cook et al., 2003; Ellins et al., 1990; Genereux and Hemond, 1990; Genereux et al., 1993; Lee and Hollyday, 1991; Rogers, 1958; Stellato et al., 2008), as well as for characterizing hyporheic exchange (Cook et al., 2006; Lamontagne and Cook, 2007), and to trace river infiltration into an adjacent alluvial aquifer in order to determine the mean residence time and flow velocity of freshly infiltrated water (Bertin and Bourg, 1994; Freyer et al., 1999; Hoehn and Cirpka, 2006; Hoehn and von Gunten, 1989; Hoehn et al., 1992, Stellato et al., 2013).

Moreover, lately the development of ultra-sensitive techniques like Accelerator Mass Spectrometry to measure concentrations and isotopic ratios of elements, and in particular actinides, at levels below ppq (fq/g) and 10^{-12}, respectively, opens great possibilities to trace liquid releases from routine decommissioning activities (Quinto et al., 2015). For example, the isotopic ratio of plutonium (^{240}Pu/^{239}Pu) is a key to distinguish weapons-grade from power reactor nuclear material (Hotchkis et al., 2012). The long half-lives of the most abundant isotopes of plutonium, 24.110 and 6.561 years for ^{239}Pu and ^{240}Pu, respectively, imply that no significant decay has occurred since its release into the environment, in contrast to ^{137}Cs ($T_{1/2}$= 30.1 y).

^{236}U/^{238}U has been demonstrated to be a valuable tool to identify the anthropogenic origin of a radionuclide contamination. Several orders of magnitude of difference between the ^{236}U/^{238}U isotopic ratios in naturally occurring uranium (10^{-9}–10^{-14}) (Steier et al., 2008) and in spent nuclear fuel (10^{-2}–10^{-4}) imply that also a small contamination from irradiated nuclear fuel in a natural sample is able to increase the ^{236}U/^{238}U significantly. Quinto et al. (2009) carried out a field study at Garigliano NPP (GNPP) where they found that the ^{236}U/^{238}U isotopic ratio measured in sediment cores sampled in the drain channel of the GNPP, and 1 m downstream, was slightly but significantly higher than several km upstream and 1 km downstream (Fig. 5.1). This finding increases the sensitivity of ^{236}U as fingerprint of releases from nuclear facilities, even at levels much below alarm levels, owing also to the AMS detection technique.

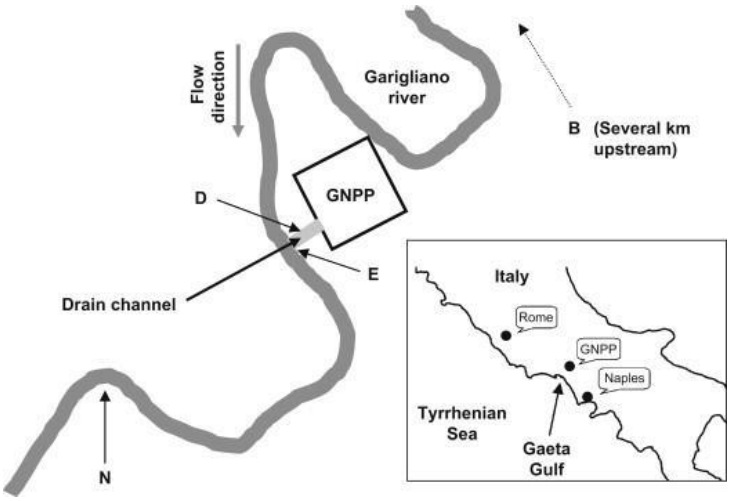

Fig. 5.1. Schematic representation of the sampling points; the insert shows the location of the Garigliano Nuclear Power Plant in Southern Italy (from Quinto et al., 2012)

In the framework of the environmental impact assessment at the Garigliano NPP, scientific research agreements have been stipulated between the Sogin and the Department of Mathematics and Physics of the Second University of Naples (i.e., Contracting Institution) since 2001. In the framework of the existing and fruitful collaboration among the Department of Mathematics and Physics of the SUN and the Sogin, a project has been realized to integrate the already acquired knowledge about the environment surrounding the GNPP with hydrogeological, hydrochemical and isotopic data to characterize the groundwater and the river in the vicinity of the nuclear power plant and finally obtain a conceptual model of the temporal and spatial patterns of groundwater flow.

5.1.1. Overall research objectives

The overall objectives of the project are:

1. The study of groundwater flow pathways, residence times, recharge zones in the vicinity of the Garigliano NPP.
2. The study of temporal and spatial surface water-groundwater interactions nearby the Garigliano NPP.
3. The identification of suitable artificial and/or natural isotopic tracers to identify groundwater preferential pathways.

The integrated monitoring of groundwater in the vicinity of the Garigliano NPP (Objective 1) has been carried out to understand the groundwater flow dynamics and to identify preferential groundwater pathways, recharge areas and groundwater residence times with the aim to develop a conceptual model of groundwater flow.

The study of surface water-groundwater interactions (Objective 2) clarified spatial and seasonal sw-gw exchanges. In particular, the main results are the identification of stream water recharge areas of the local aquifer nearby the Garigliano NPP.

Finally, the development of tools based on trace elements of anthropogenic origin, in particular the actinides and their isotopic ratios (Objective 3), will allow to follow the fate of the NPP releases in water bodies during ordinary operation phases and consequently could be of big help in the identification of preferential pathways in case of accidental releases.

5.2. Description of the study site

The Garigliano nuclear power plant (GNPP) is located in a bend in the lower course of the Garigliano river (Fig. 5.2) about 7 km from its mouth, in the Gulf of Gaeta on the Tyrrhenian Sea in the territory of the municipality of Sessa Aurunca (Caserta), and about 5 km downstream of the Garigliano-Suio hydroelectric power plant. The alluvial plain, through which the final part of the river runs, is enclosed between the limestone masses of the Aurunci mountains, the volcanic massif of

Roccamonfina and the Tyrrhenian Sea. A geological complex, the Roccamonfina, within which an intense water circulation takes place with also thermo-mineral characteristics.

The land use shows an abundance of areas cultivated with irrigated, non-irrigated arable land and stable meadows dominating the allunional plain, unlike the piedmont belt, where arboreal phytocoenoses predominate.

5.2.1. Climatic and hydrological framework

From the point of confluence between the Liri and Gari rivers, the Garigliano river flows for 38 km until it flows into the Gulf of Gaeta (Tyrrhenian Sea), at the ancient Roman city of Minturnae and receives as tributaries the Peccia river, the Fosso Coccuruzzo from the left and the Ausente river from the right. The average flow rate at the mouth is 120 m^3 s^{-1} (ranging from 25 m^3 s^{-1} to a maximum of 1,200 m^3 s^{-1} when during winter the atmospheric precipitation reaches the highest peaks (PGRA Liri-Garigliano Volturno, 2013) so as to be considered the Italian river with the greatest discharge southward of the Tiber river.

Downstream of the town of Suio, where the river plain widens rapidly, the riverbed has a meandering course up to the ancient bridge, where it has extensive flooding areas in the lower Garigliano course. The first of these areas, the one hosting the electronuclear site, is not directly floodable, but nevertheless presents emergency management problems as it is completely surrounded by the river and floodable areas (PGRA Liri-Garigliano Volturno, 2013).

5.2.2. Geological and hydrogeological framework

The oldest formations present in the area of the Garigliano nuclear power plant are the Cretaceous-Miocene ones (Elaborated GR GM 00511 Sogin). They constitute the reliefs of the Aurunci Mountains and are represented by the following formations (Fig. 5.2):

✓ well stratified detrital and fine-paste limestones, sometimes with interspersed clay-silty levels (Tuoronian-Senonian);

✓ fine-textured and finely detrital limestone well stratified alternating with limestone with a conglomerate structure and sometimes with thin clayey-silty levels (Senonian-Paleocene);

✓ debris-organogenic limestones in layers and large banks (Langhiano-Elveziano);

✓ layered clayey and calcareous marl passing down to well layered marly limestone and finely detrital limestone (Elveziano-Tortonian);

✓ sandstones stratified with silty clays, marl and marly limestone (Tortonian-Messinian).

Due to the dislocations undergone, these same formations, or similar formations, are also found deep below the Quaternary deposits of grabens and products of the Roccamonfina volcanic complex.

The Quaternary deposits that make up the plain are represented:

✓ aeolian sands with weakly cemented horizons (Pleistocene). They constitute a fossil dune probably set on an ancient coastline;

✓ clayey, silty and subordinately sandy deposits, with frequent, slow peat levels and rare gravelly levels (Pleistocene-Holocene). It is the formation that emerges most extensively in the area under examination, and it is the one on which the site is located. Below this formation, deposits with coarse granulometry such as gravels, pebbles, conglomerates and pyroclastic intercalations can be seen more frequently up to the Miocene marine formations that constitute the bottom of the tectonic depression;

✓ travertines (Holocene); it is a small outcrop located about 4 km north-west of the site, linked to the presence of mineralized springs on the slopes of the Aurunci Mountains;

✓ humiferous soils, sands and river pebbles (Holocene); They emerge from the north-western part of the area in question on the slopes of the Aurunci mountains;

✓ loose or weakly cemented groundwater debris (Holocene); it emerges at the foot of the Aurunci Mountains about 3 km north and north-west of the site;

From the hydrogeological point of view, on the other hand, the soils described above can be grouped into the following complexes (Saroli et al., 2017):

✓ carbonate complex, consisting of the limestone formations outcropping on the Aurunci Mountains. It has an overall high degree of permeability due to cracking and karst, although it varies

from area to area. It represents the most important aquifer in the area as it hosts a “regional” aquifer that feeds numerous high-flow springs located at the foot of the Aurunci Mountains. The hydrogeological map of the Lazio region (Boni et al., 1988) provides, for these springs, average flow values between 110 and 250 l/s and also indicates the presence in the same area of a series of springs in the Garigliano river bed, whose overall flow rate has been estimated at 1,000 l/s;

✓ arenaceous-marly-clayey complex: consists of the Miocene formations that emerge, overlapping the carbonate complex, on the Aurunci mountains and which are found deep under the recent cover of the Garigliano plain. Very low permeability;

✓ lava-pyroclastic complex: coincides with the Roccamonfina volcanic series which, being made up of lavas and pyroclastic deposits, has a very variable permeability from place to place according to the degree of fracturing of the lavas and the granulometry and cementation degree of the pyroclasticites;

✓ coastal dune complex: it consists of the aeolian sands of the coastal dunes. Although it presents a fair permeability, it is of little hydrogeological importance given the limited extension of the outcrops;

✓ fluvio-marsh, lagoon and marine detrital complex: it is made up of all the remaining formations that are present in the plain, including the decomposition products of volcanites. As a whole it has average permeability values, but with significant local variations both vertically and horizontally, depending on the granulometry of the sediments. The coarser granulometry levels constitute a series of overlapping aquifers which therefore host interconnected aquifers. These aquifers receive power not only from effective infiltration, but also from the aquifers contained in the lava-pyroclastic complex, but above all from the “regional” aquifer of the carbonate complex. The more superficial groundwater is also in direct relationship with the surface waters and usually appears to be drained by the Garigliano river (Elaborated GR GM 00511 Sogin).

In the study area, the surface of the aquifer is closely linked to the water level in the Garigliano river and is normally located around 8–9 m depth from the ground level. In phases of strong flood, pressure gradients from the river to the water table are limited to the area of the power plant, even if only for the duration of the flood peak, with significant increases in the water table level (GR GM 00511 Sogin).

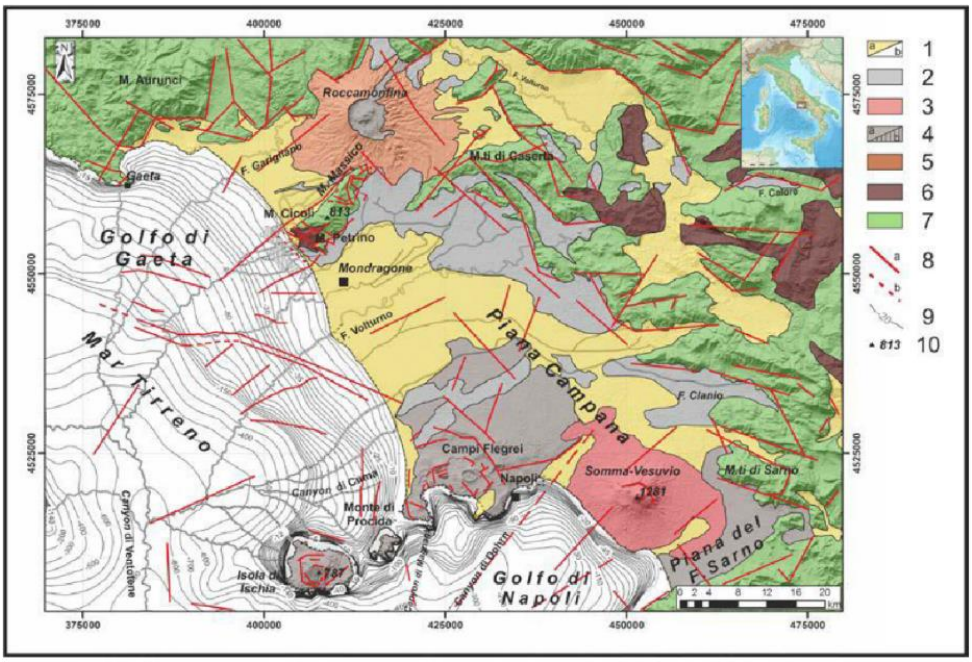

Fig. 5.2. Geological map of the northern sector of Campania (taken from Pennetta et al., 2016). In the area of interest of the GNPP, the following formations are distinguished: sedimentary rocks (1a) such as reworked pyroclasticites, fluvial-marine, lake and aeolian deposits of the Piana Campana; and exposed faults (8a)

5.3. Methods and materials

Four sampling campaigns have been carried out from November 2016 to December 2018 where water table levels, field parameters, major ions, trace elements, water stable isotopes (^{18}O and D), ^{222}Rn have been measured in surface water, groundwater and rainwater samples. Moreover, continuous measuring EC/T, level/T probes have been installed in three selected piezometers and one stilling well in the river at the Garigliano NPP site. Moreover, chemical purification protocols for $^{234}U/^{238}U$, $^{235}U/^{238}U$ and $^{236}U/^{238}U$ have been implemented in order to find a reliable tracer for gw flowpath studies. The latter analytical development has been applied to groundwater and surface water samples collected at the NPP site.

After a preliminary study of the existing documents and studies, a monitoring network has been established in an area of 3 km radius around the Garigliano NPP (Fig. 5.3). The monitoring network consisted of 30 piezometers within the Garigliano NPP site (Fig. 5.4) and 33 domestic and agricultural wells, 4 river water stations, 1 rainwater collector installed at the GNPP site.

Fig. 5.3. Study site and sampling network in the vicinity of the Garigliano Nuclear Power Plant in Southern Italy

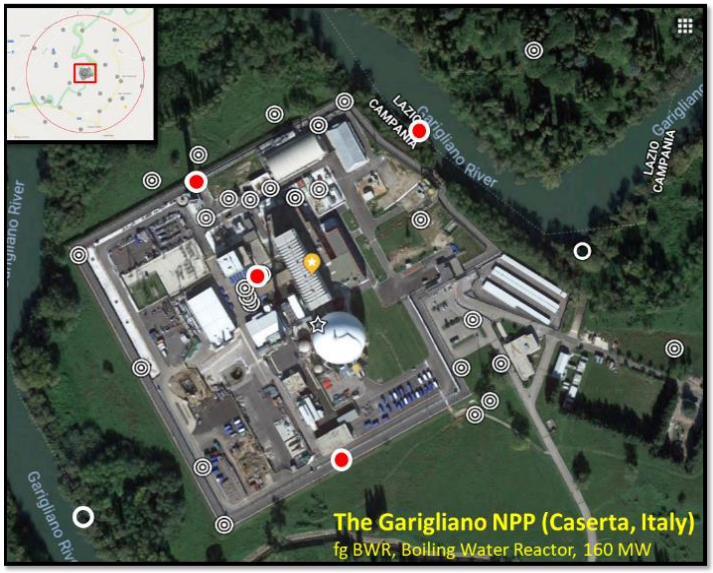

Fig. 5.4. Sampling network within the Garigliano Nuclear Power Plant site. The red dots indicate the piezometers equipped with data loggers

Water table levels measurement in monitoring points (wells and piezometers) have been carried out by a water level meter (BFK-100 model, PASI, Italy). Ground elevations of the wells were measured by GPS techniques (K9 Series RTK, KOLIDA Instrument, China). Water table measurements have been collected weekly in 2018 in the piezometers of the GNPP in order to elaborate water surface maps by means of Surfer15 (Golden Software).

Continuous monitoring of water level and temperature was performed in 3 selected piezometers (P2, P6, P30), while continuous monitoring of EC was performed in 2 selected piezometers (P2, River) by means of multi parametric probes (U20 and U24, HOBO Onset, MA, USA).

Physico-chemical parameters as pH, electrical conductivity (EC, μS/cm) and temperature (T, °C) were measured in situ by a multi-parametric probe (WTW Multi 340i, WTW GmbH, Weilheim, Germany). Alkalinity was determined in the laboratory by a titrimetric method.

In order to determine major anions and cations (i.e., HCO_3^-, SO_4^{2-}, Cl^-, Br^-, F^-, Ca^{2+}, Mg^{2+}, Na^+, K^+) and trace elements (i.e., As, B, etc.) water samples were collected in 1 L high-density polyethylene (HDPE) bottles avoiding air bubbles and stored at +4°C. The samples were filtered (0.45 μm) in the laboratory. Anions and cations were determined by ion chromatography (IC Metrohm 850 Professional). The accuracy of the analyses was checked by the ionic balance within ±5% range. For trace elements determinations the filtered samples were acidified with a 3% v/v HNO_3 solution and analyzed by inductively coupled plasma with mass spectrometry (ICP-MS, Aurora M90, Bruker, USA) at the Regional Environmental Protection Agency of Campania laboratories (Benevento, Italy).

Water samples for ^{222}Rn determinations were sampled in 100 mL bottles and measured by a RAD7 detector (Durridge Company ltd, Billerica, MA, USA).

Water samples for $\delta^{18}O$ and δD analyses were collected in 50 mL narrow necked high-density polyethylene bottles, leaving no headspace to avoid contact with air and horizontally stored at 4 °C. $\delta^{18}O$ and δD isotopic ratios of 0.45 μm filtered samples, reported as permil (‰) relative to Vienna Standard Mean Ocean Water, were analyzed by a TC/EA-ConfloIII-IRMS system (DeltaV, Thermo Fisher) at the Centre for Isotopic Research on Cultural and Environmental heritage, Dept. of Mathematics and Physics, University of Campania "Luigi Vanvitelli" (Caserta, Italy). The precision of the measurements was 0.1‰ and 1‰ for $\delta^{18}O$ and δD, respectively.

$^{234}U/^{238}U$ and $^{235}U/^{238}U$ isotopic ratios measurement protocols have been developed (measured by MC-ICP-MS, Neptune plus, Thermo Fisher, Bremen, Germany) at the Centre for Isotopic Research on Cultural and Environmental heritage, Dept. of Mathematics and Physics, University of Campania "Luigi Vanvitelli" (Caserta, Italy).

Noble gases measurements have been carried out on selected water samples at the Stable Isotope Laboratory of IAEA (Vienna, Austria).

5.4. Results and Discussion

5.4.1. Water table reconstruction

In this project, Surfer 15 (Golden Software) was used for the representation of the piezometric surface in order to build a piezometric morphology map for the study of groundwater circulation. The interpolation algorithm used for the construction of the piezometric map was the kriging. Kriging is a geostatistical method that produces maps from irregularly distributed data interpolated on a spatial basis. With each map a variogram was created, to interpolate the spatial autocorrelation of geo-referenced points, i.e. the degree of variance between the values in two positions, x and y. The factors affecting the variogram are: the quality of the data, the level of dispersion presented by the spatial variable and the distance between the sampled points within the domain (Fig. 5.5).

In Table 5.2 the water table levels measured in the piezometers of the GNPP are reported.

Table 5.2. Water table levels measured in the piezometers of the GNNP and in the river in 2018

Piezometri monitorati	Gennaio "m.s.l.m"	Febbraio "m.s.l.m"	Marzo "m.s.l.m"	Aprile "m.s.l.m"	Maggio "m.s.l.m"	Giugno "m.s.l.m"	Luglio "m.s.l.m"	Agosto "m.s.l.m"	Settembre "m.s.l.m"	Ottobre "m.s.l.m"	Novembre "m.s.l.m"	Dicembre "m.s.l.m"
P1	0.68	1.81	2.37	1.18	0.76	0.58	0.40	0.40	0.31	0.32	1.47	1.37
P2	0.76	1.43	2.26	1.20	076	0.56	0.39	0.40	0.33	0.37	1.46	1.43
P3	0.56	1.47	2.28	1.08	0.60	0.33	0.11	0.14	0.16	0.23	1.39	1.37
P4	0.82	1.34	2.25	1.29	0.78	0.52	0.36	0.36	0.32	0.36	1.46	1.44
P5	0.77	1.22	2.15	1.27	0.82	0.50	0.29	0.30	0.27	0.34	1.39	1.27
P6	1.21	1.73	2.72	1.80	1.39	0.98	0.78	0.78	0.68	0.80	1.86	1.82
P7	1.50	1.70	2.92	2.43	2.18	1.60	0.36	0.63	1.35	1.34	2.52	1.43
P8	1.36	2.01	3.63	2.85	1.75	1.41	0.87	0.94	1.06	1.03	2.80	0.96
P9	0.89	1.67	2.38	1.50	1.08	0.77	0.64	0.63	0.45	0.65	1.85	1.23
P12	1.35	1.72	2.62	1.50	1.10	1.02	0.53	0.58	0.70	0.68	1.81	2.32
P13	0.95	1.44	2.32	1.26	0.93	0.69	0.23	0.25	0.37	0.93	1.61	1.71
P14	2.24	2.03	3.56	2.86	2.86	2.38	1.95	1.83	1.56	1.65	2.78	2.22
P16B	0.89	1.04	2.09	1.20	0.92	0.93	0.51	0.52	0.49	0.52	1.71	1.49
P17	0.83	1.42	2.22	1.19	0.92	0.87	0.31	0.34	0.46	0.46	1.70	1.57
P18	1.03	1.49	2.29	1.22	0.98	1.08	0.89	0.50	0.12	0.43	1.60	1.80
P19a	1.42	1.67	2.38	1.77	1.40	1.08	0.57	0.68	0.75	0.83	2.02	1.96
P19B	1.25	1.69	2.18	1.46	1.09	0.90	0.48	0.46	0.41	0.50	1.82	1.73
P20A	1.08	1.42	2.29	1.49	1.03	1.14	0.43	0.49	0.50	0.58	1.79	2.17
P21A	1.32	1.72	2.67	1.57	1.22	0.76	0.51	0.60	0.73	0.66	1.77	1.83
P21B	1.22	1.66	2.48	1.44	1.06	0.75	0.45	0.49	0.51	0.50	1.75	1.90
P35 ODP Fiume	0.63	2.85	2.78	0.80	0.53	0.49	0.38	0.40	0.40	0.46	1.90	0.72

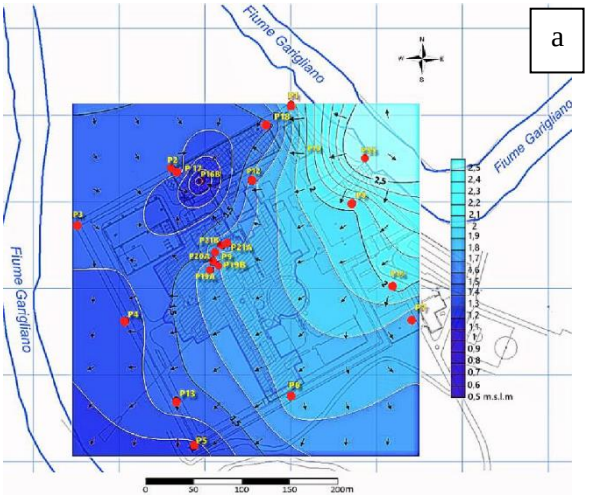

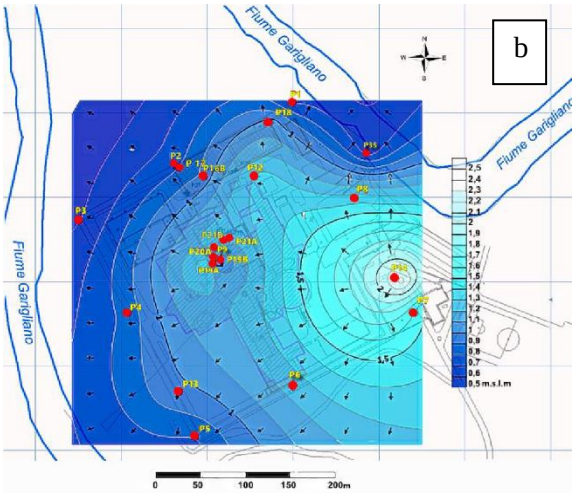

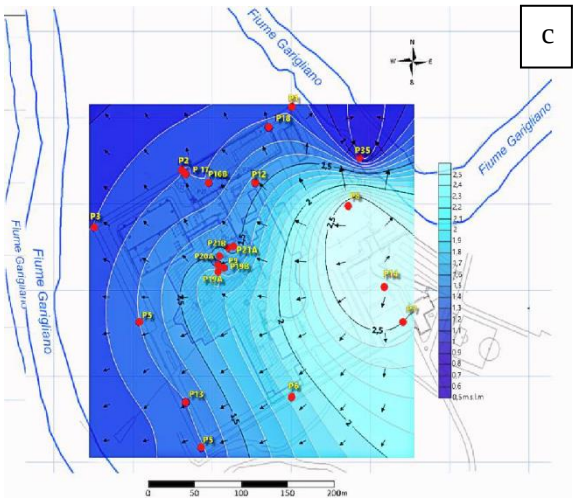

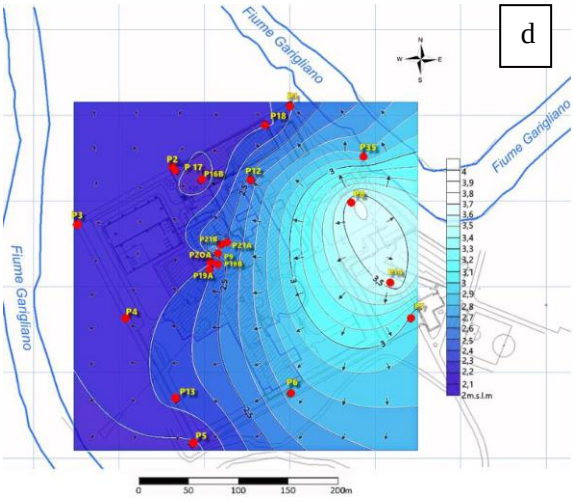

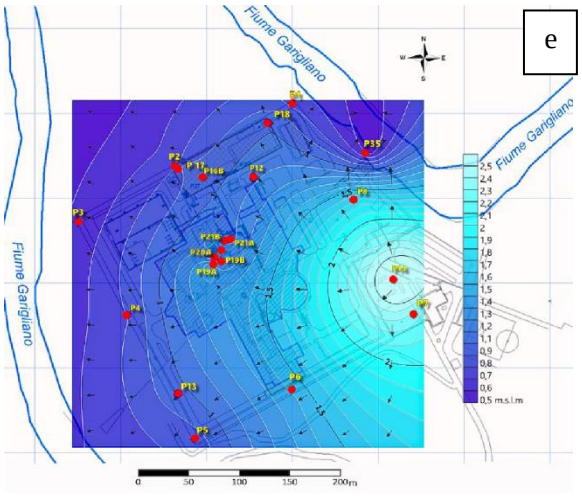
e
Fiume Garigliano
Fiume Garigliano
Fiume Garigliano
0 50 100 150 200m

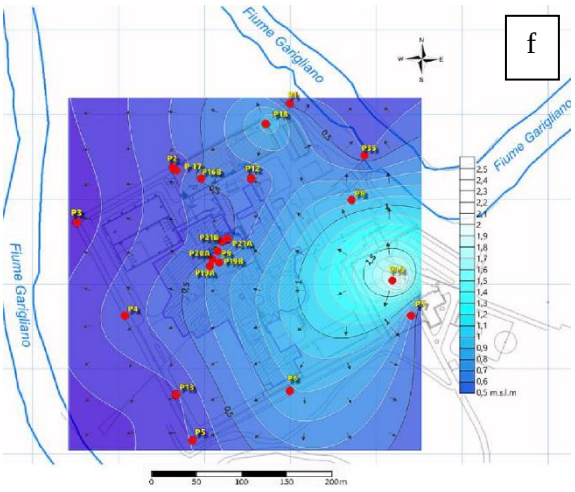
f
Fiume Garigliano
Fiume Garigliano
Fiume Garigliano
0 50 100 150 200m

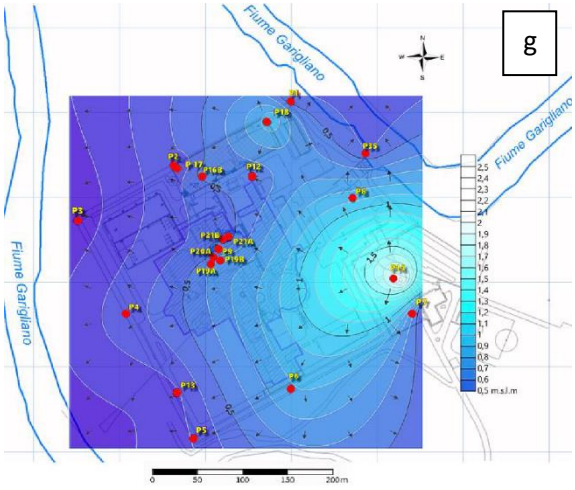
g
Fiume Garigliano
Fiume Garigliano
Fiume Garigliano
0 50 100 150 200m

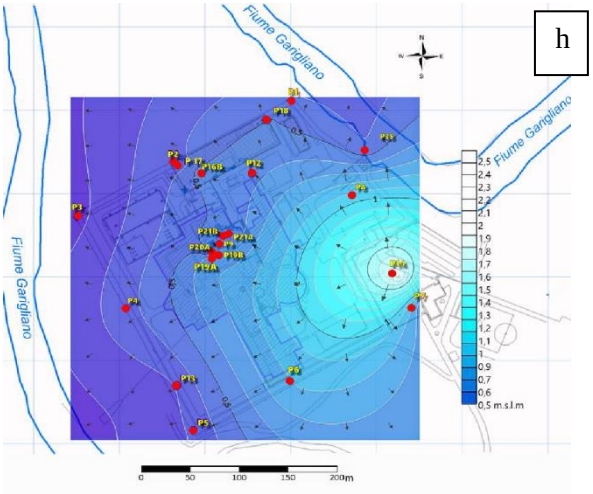
h
Fiume Garigliano
Fiume Garigliano
Fiume Garigliano
0 50 100 150 200m

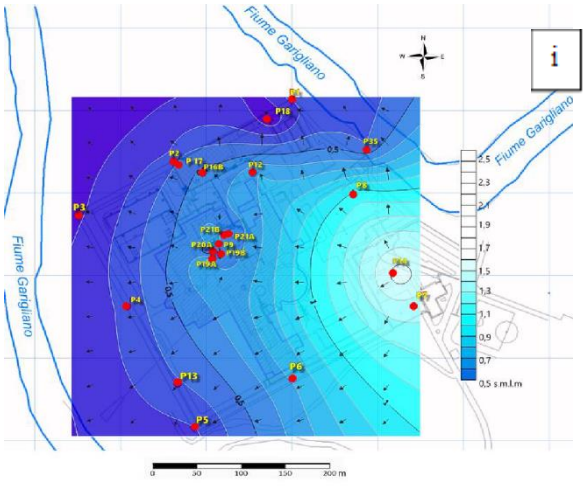
i
Fiume Garigliano
Fiume Garigliano
Fiume Garigliano
0 50 100 150 200m

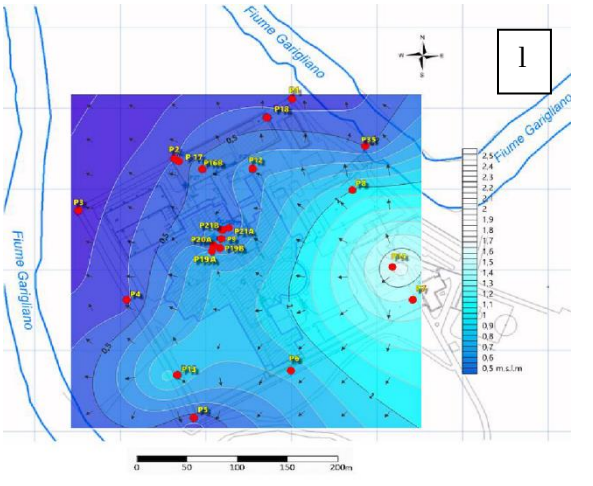
l
Fiume Garigliano
Fiume Garigliano
Fiume Garigliano
0 50 100 150 200m

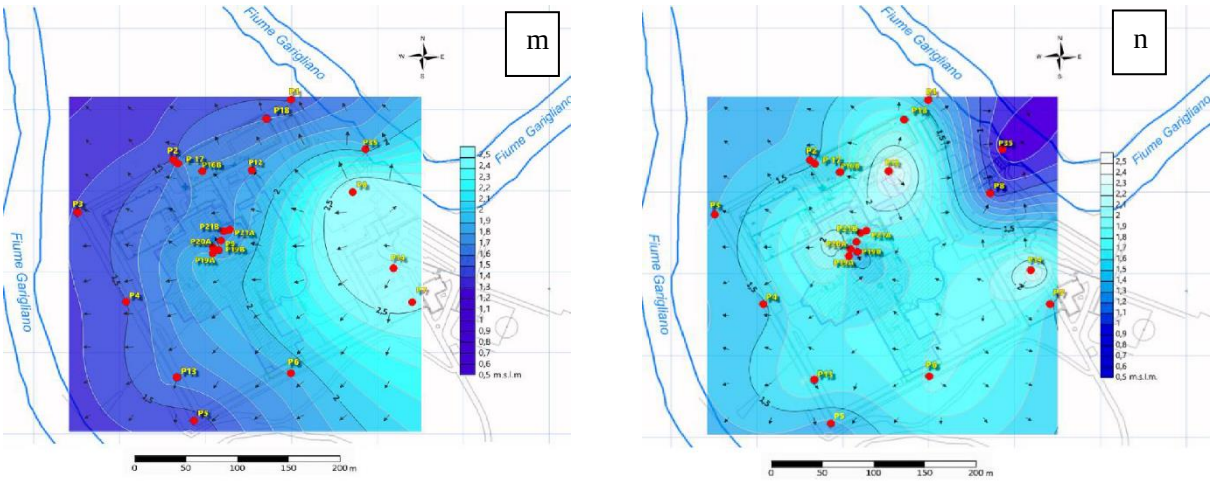

Fig. 5.5. Piezometric contour maps at the site of the GNPP from January (a) to December (n) 2018

To evaluate how atmospheric precipitation influenced the piezometric level of the site aquifer, the monthly atmospheric precipitation was related to the course of the aquifer for some piezometers in the study area, as illustrated in the graphs in Fig. 5.6. In each graph the precipitation expressed in mm is shown in orange, while the dashed line in light blue indicates the piezometric level expressed in m asl. For piezometers P1, P3, P6, P7, P13 and P17 (shown respectively from top to bottom in Fig. 5.6) Looking at the graphs shown, it can be seen how the trend of the aquifer is strongly influenced by atmospheric precipitation, with sudden increases in the piezometric altitude precisely in correspondence with the 2 precipitation peaks previously identified. Similarly, in the summer months, a decrease in rainfall corresponds to a lowering of the piezometric surface in all the piezometers considered. While generally following the trend described above, each of the piezometers taken into consideration shows dissimilar temporal responses to the charging events, with some piezometers (P3, P7, P13 and P17) showing minimum values in July and others (P1 and P6) which present them in October. This behavior is most likely to be attributed to local anisotropy which can give rise to different geological and stratigraphic characteristics between the different monitoring points considered.

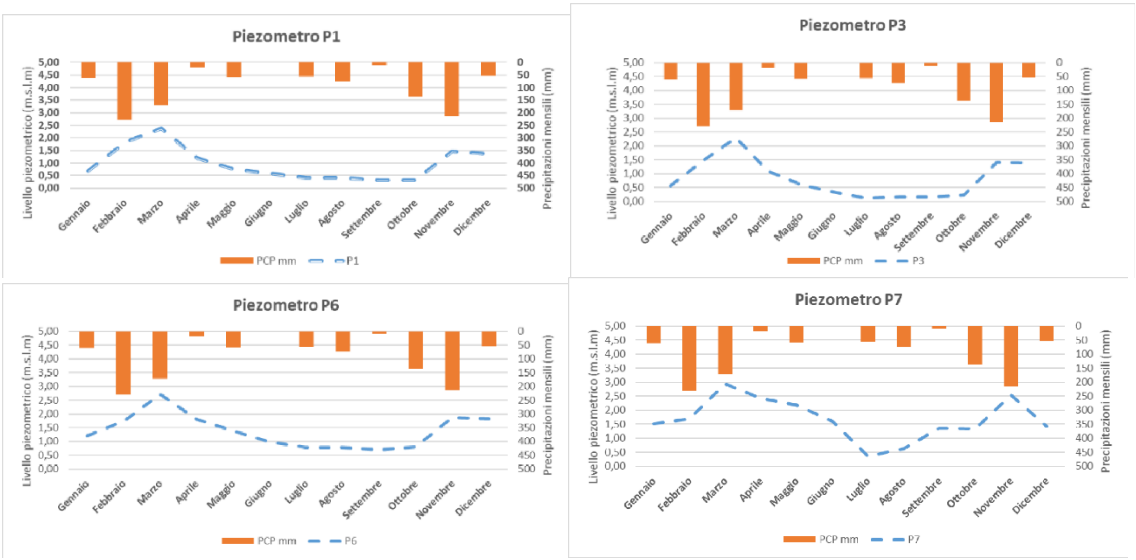

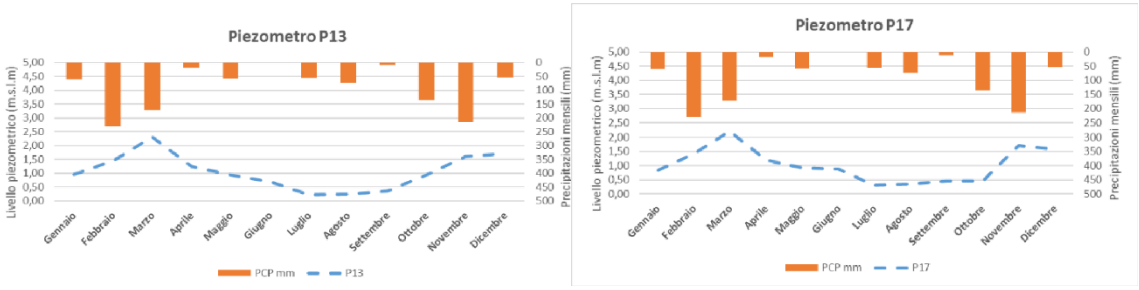

Fig. 5.6. Trend of groundwater levels (m a.s.l.) in piezometers P1, P3, P6, P7, P13 and P17 and of monthly rainfall (mm)

The plot in Fig. 5.7 shows how the maximum peak of the hydrometric level in the river was reached in the winter months, February and March 2018, influenced by the abundant atmospheric precipitation of the same graph months (Table 5.4), and then stabilized in the remaining months of the year 2018. A level of about 4.3 m, with a lower intensity peak observed in the months of October and November at the monitoring point P35 ODP located on the left bank of the Garigliano river taken as a reference for this study.

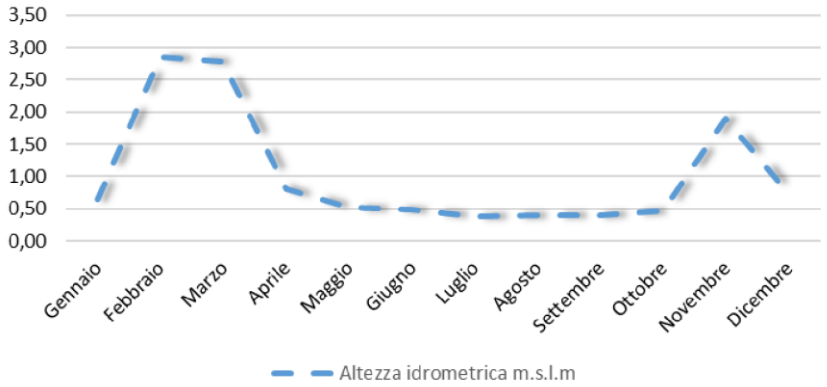

Fig. 5.7. Hydrometric height at P35 ODP located inside the Garigliano river (stilling well) for the year 2018

The study shows that during the year 2018, the aquifer has always been feeding the Garigliano river except for the month of February, the only month in which the height of the hydrometric level of the river was higher than the level of the piezometric surface of the aquifer.

With reference to the monitoring period of the hydrological year 2018, the interaction between the aquifer and the Garigliano river was assessed, taking into consideration the 20 piezometers for which the piezometric level measurements and the monitoring point P35 ODP, located inside the Garigliano river. In relation to the piezometric level measured in the field, it was possible to reconstruct the monthly piezometric surfaces, which made it possible to establish the direction of the hydrogeological flow and understand how the surface water of the Garigliano river can influence the groundwater of the site where the water table is located. former Nuclear Power Plant or vice versa. To this end, through the application of the Darcy Law, the exchange volumes between the two water bodies in question were estimated: groundwater below the power plant and the Garigliano river. In order to estimate these exchanges, two wet sections were considered, one upstream and one downstream, with dimensions of 200 × 2 m (estimated through the Google Earth software) which theoretically allow the interaction between the two water bodies. The hydraulic gradients for each month of monitoring were estimated, both upstream and downstream, from the analysis of the monthly piezometries, while the hydraulic conductivity of the aquifer was estimated on the basis of the stratigraphic reconstruction.

In Table 5.3 the fluxes of exchange water between groundwater and the Garigliano river are reported.

Table 5.3. Average monthly flows in m^3/d from the aquifer to the Garigliano river (positive values) and from the Garigliano to the aquifer (negative values) for the year 2018 for the upstream and downstream section of the nuclear power plant

	G	F	M	A	M	G	L	A	S	O	N	D	2018
Monte	5.2	-4.0	5.0	15.0	10.0	7.2	3.2	3.3	3.3	2.9	4.0	1.6	56.9
Valle	1.2	0.9	1.3	0.7	1.2	1.6	0.8	0.7	0.5	1.6	1.0	0.8	12.3

Furthermore, the sum for the whole of 2018 shows that in the upstream section there is a much greater flow than in the downstream (56.9 m^3/d versus 12.3 m^3/d) one due to the greater hydraulic gradients in the upstream area. Finally, it should be noted that these flows are several orders of magnitude lower than the average flow rates of the Garigliano river, which being equal to about 120 m^3/s is equal to more than 10 million m^3/d, against a total flow from the aquifer to the Garigliano equal to only 69.2 m^3/d (both in the upstream and downstream sections, close to the GNPP). Even if the absolute minimum flow rate measured in the Garigliano is used, equal to about 60 m^3/s, equal to more than 5 million m^3/d (Boni et al., 1996), the supply due to the groundwater below the plant is in any case negligible.

5.4.2. Hydrogeochemistry

In general, it has been seen that the aquifer in the study area can have a feeding or draining behavior and that it can alternate these types of interaction with the Garigliano river, both along the development of the river shaft, and over time depending on the hydraulic gradients.

The study also shows that during the year 2018, the aquifer has always been feeding the Garigliano river except for the month of February, the only month in which the height of the hydrometric level of the river was higher than the level of the piezometric surface of the aquifer. The temperature and electrical conductivity values indicate that in 2018 the two water bodies, the aquifer and the Garigliano river, tend to have different characteristics, thus demonstrating that the water table/river interaction is not continuous throughout the year, and in any case that the interaction between the two water bodies is quantitatively limited.

During the three monitoring campaigns carried out in June, August and October of the year 2018 and with the aid of the continuous monitoring probes HOBO U20 (Onset) and HOBO U24 installed since the beginning of the hydrological year, in 3 strategic piezometers (P2 equipped with U20 and U24 probes, P6 equipped with U20 probe and P30 equipped with U20 probe) and in the measuring point P35 River ODP (equipped with U24 probe), the groundwater temperature was monitored and related to the temperature of the Garigliano river. As can be seen from Fig. 5.8, groundwater temperature measurements show very regular fluctuations in the study area.

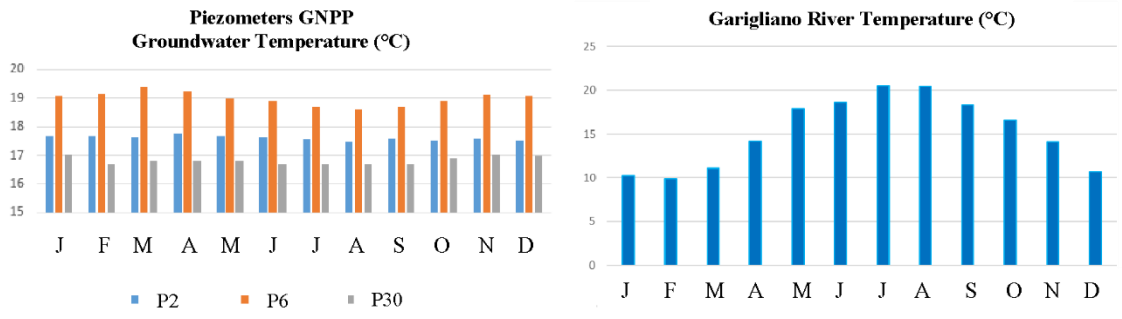

Fig. 5.8. Temperature measured in selected piezometers (P2, P6 and P30) and in the Garigliano River in 2018

The maximum values measured are equal to 19 °C while the minimum values are just below 17 °C. The main evidence is certainly represented by the P6 piezometer which is further away from the river and shows an increase in temperature of about 1.5 °C compared to the P2 and P30 piezometers. The different temperatures may be due to multiple factors, including the subsidence of the

groundwater, the vertical positioning of the probes in the relative piezometers or groundwater with different temperatures for different origins (originating from upstream areas with different temperatures) or for any upwelling of thermal fluids from the depths of the aquifer.

The temperature trend of the Garigliano river measured in P35 ODP is of a different nature (Fig. 5.8), in fact here the temperature shows evident fluctuations that fluctuate by about 10 °C in the hydrological year. In particular, there are minimum peaks below about 10 °C in the autumn/winter months and maximum peaks in summer of about 20 °C. Therefore, any arrival of water from the Garigliano should cause marked increases and decreases in temperature in the monitoring piezometers.

In particular, the P30 piezometer, the closest to the Garigliano river (at about 100 m), should be affected by any water table / river exchanges more than the P2 and P6 piezometers (respectively positioned at about 200 m and 300 m from the river), showing a temperature trend consistent with the temperature trend at measuring point P35 ODP. Comparing the temperature trends of the P30 (gray bar in Fig. 5.8) and of the river, it is actually evident that the two water bodies show completely dissimilar, even opposite, trends, which would seem to exclude that the groundwater/river interactions are particularly intense in the area under study.

The values of electrical conductivity (Fig. 5.9) vary in the P35 ODP between 450 µS/cm in winter, when atmospheric precipitation is heavier and the hydrometric level of the Garigliano is maximum, and about 600 µS/cm in summer, when atmospheric precipitation are almost absent. In the Piezometer P2, representative of the aquifer, the fluctuations in electrical conductivity vary between 700 µS/cm in the winter and 800 µS/cm in the summer. Considering the electrical conductivity data, it is noted that the P35 ODP well is generally characterized by lower values throughout the examination period, while the P2 piezometers shows a rather constant value between 700/800 µS/cm, reporting lower values in the months of February and March when the hydrometric level of the river is maximum. The decrease in the electrical conductivity of the aquifer recorded in the month of February, coinciding with the only moment in which, from the analysis of the water table the Garigliano river is responsible for feeding the aquifer, seems to confirm a direct interaction (exchange) between surface and groundwater, at least in the northern area of the plant where the monitoring points considered for this analysis are located.

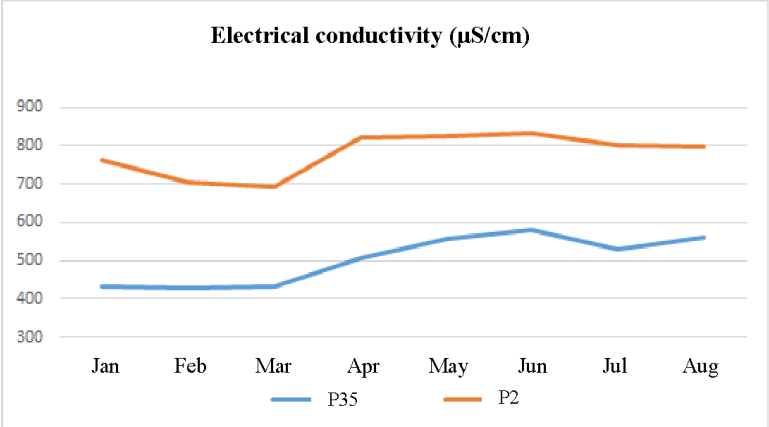

Fig. 5.9. Electrical conductivity measured in a selected piezometers (P2) and in the Garigliano River in 2018

Water stable isotopes were measured in rain water, groundwater and river water in order to study the different water pools and eventually identify possible mixing and recharge dynamics.

In Fig. 5.10, the $\delta^{18}O$ and δD measured in river water and groundwater samples in the sampling campaigns of July and December 2018 are reported in order to study the isotopic features in the low flow period (July) and the recharge period (December). The Local Meteoric Water Line is also reported, as a reference.

The ^{222}Rn measurements reported in Fig. 5.11 indicate that in the upstream northern part of the GNPP site (piezometers P6 and P23) groundwater is more mineralized, as also supported by hydrochemical data, probably due to an upwelling of hydrothermal waters.

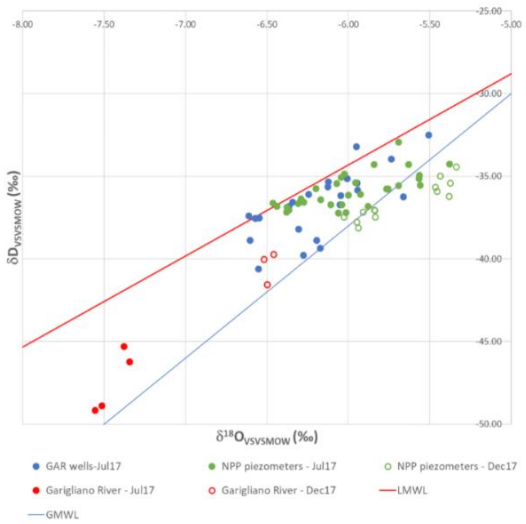

Fig. 5.10. $\delta^{18}O$ vs δD diagram measured in river water and groundwater at the NPP site

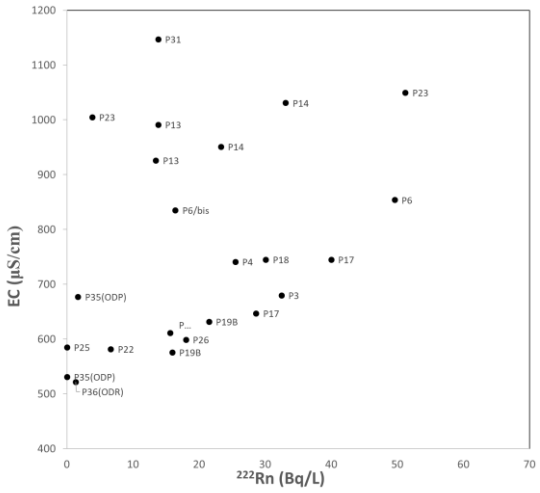

Fig. 5.11. ^{222}Rn (Bq/L) versus EC measured in GNPP piezometers and the Garigliano river at the NPP site

5.5. Concluding remarks

Environmental monitoring programs nearby nuclear sites usually consider groundwater and surface water as possible transport routes for radionuclides released into the environment. At the moment, however, no guidelines are available on the use of techniques for an appropriate characterization of the spatial and temporal dynamics of water flow in order to understand in detail conceptual models of transport and flow near a nuclear site. The evaluation of potential radionuclide migration paths, the consideration of hydrogeological aspects such as the knowledge of the areas and groundwater recharge rates, the average residence times of the water in the aquifer, the groundwater-river interactions are crucial points of interest for the planning of activities for the protection of public health and the environment in the event of accidental releases of radionuclides.

The multi-disciplinary study based on hydrogeological, hydrogeochemical and isotopic monitoring allowed us to assess the interactions between the aquifer and the Garigliano river at the site of the Garigliano NPP. Thanks to the activities carried out in the field and the continuous monitoring of the groundwater level, it was possible to reconstruct the monthly trend of the piezometric surface. The interactions between the two water bodies (groundwater and river) were evaluated by taking into account: atmospheric precipitation, hydrometric level of the river, hydraulic load of the aquifer, temperature and electrical conductivity of both water bodies.

In general, it has been seen that the aquifer can have a feeding or draining behavior and that it can alternate these types of interaction with the Garigliano river, both along the river course and over time depending on the hydraulic gradients.

The study also shows that during the year 2018, the aquifer has always been feeding the Garigliano river except for the month of February, the only month in which the height of the hydrometric level of the river was higher than the level of the piezometric surface of the aquifer. The temperature and electrical conductivity values as well as chemical and isotopic data indicate that the two water bodies, the aquifer and the Garigliano river, tend to have different characteristics, thus demonstrating that the groundwater/river interaction is not continuous throughout the year, and in any case that the interaction between the two water bodies is quantitatively limited.

As regards the aspects that could be further considered and implemented, they are essentially linked to a more in-depth characterization campaign of the hydraulic conductivities of the aquifer and to a more detailed estimate of the extension of the interaction surface between two water bodies considered. In fact, there are some aspects that could be explored in more detail through the use of natural tracers and heat propagation methods, to evaluate the interaction dynamics of river water and groundwater.

References

Bertin, C., and Bourg, A.C.M., 1994. Radon-222 and chloride as natural tracers of the infiltration of river water into an alluvial aquifer in which there is significant river/groundwater mixing. Environ. Sci. Technol., 28, 794-798.

Cook et al., 2003, Determining natural groundwater influx to a tropical river using radon, chlorofluorocarbons and ionic environmental tracers, J. Hydrol. 227 (2003) 74-88.

Cook et al., 2006, Quantifying groundwater discharge to streams using dissolved gas tracers ^{222}Rn and SF6, Cockburn River, Southeastern Australia, Water Resour. Res. 42: W10411, doi: 10.1029/2006WR0049921.

Ellins, K.K., Roman-Mas, A., Lee, R., 1990. Using 222Rn to examine groundwater/surface discharge interaction in the Rio Grande de Manati, Puerto Rico. J. of Hydrology, 115, 319-341.

Freyer, K., Treutler, H.C., Dehnert, J., Kuhn, K., Nestler, W., 1999. Investigation of river bank infiltrationusing Rn-222 as radiotracer, in Isotope techniques in water resources development and management, Proceedings of a symposium, Vienna 10-14 May 1999.

Genereux, D.P., and Hemond, H.F., 1990. Naturally occurring radon-222 as a tracer for streamflow generation: steady state methodology and field example. Water Resour. Res., 26 (12), 3065-3075.

Genereux, D. P., et al, Use of radon-222 and calcium in a three-end-member mixing model for streamflow generation on the west fork of Walker Branch watershed, J. Hydrol. 142 (1993) 167-211.

Hoehn, E., and Cirpka, O.A., 1996. Assessing residence times of hyporheic ground water in two alluvial flood plains of the Southern Alps using water temperature and tracers. Hydrol. Earth Syst. Sci. 10: 553–563.

Hoehn, E., and von Gunten, H.R., 1989. Radon in groundwater: A tool to assess infiltration from surface waters to aquifers. Water Resour. Res., 25, 1795-1803.

Hoehn, E., von Gunten, H.R., Stauffer, F., Dracos, T., 1992. Radon-222 as a groundwater tracer. A laboratory study. Environ. Sci. Technol., 26, 734-738.

Hotchkis et al., 2012. Applications of Accelerator Mass Spectrometry in Nuclear Verification. Journal of Nuclear Materials Management, volume XL, No.4, 60-68.

Lamontagne, S., Cook, P.G., Estimation of hyporheic water residence time in situ using 222Rn disequilibrium, Limnology and Oceanography: Methods, 5 (2007) 407-416.

Lee, R., Hollyday, E.F., "Use of radon measurements in Carter's Creek, Maury County, Tennessee, to determine location and magnitude of groundwater seepage", Field studies of radon in rocks, soil and water, (Gundersen, L.C., Wanty, R.B., Eds), C.K. Smoley, Boca Raton, Florida (1991) 237–242.

McMahon, P.B., Böhlke, J.K. Denitrification and mixing in a stream-aquifer system: effects on nitrate loading to surface water, Journal of Hydrology 186 (1996) 105-128.

Quinto et al. 2009. The first use of 236U in the general environment and near shutdown nuclear power plant. Applied Radiation and Isotopes, 67, 1775-1780.

Quinto et al., 2015. Accelerator mass spectrometry of actinides in ground- and sea water: as innovative method allowing for simultaneous analysis of U, Np, Pu, Am and Cm isotopes below ppq levels. Analytical Chemistry, 87, 5766-5773.

Rodgers, P., et al., Using stable isotope tracers to identify hydrological flow paths, residence times and landscape controls in a mesoscale catchment, Hydrol. Earth Syst. Sci. Discuss. 2 (2005) 1–35.

Rogers, A.S., Physical behaviour and geologic control of radon in mountain streams. Geological Bulletin No. 1052-E, U.S. Geological Survey (1958).

Steier et al, 2010. Nucl. Instrum. MethodsPhys. Res., Sect. B, 268, 1045-1049.

Steier et al., 2008. Nucl. Instrum. MethodsPhys. Res., Sect. B, 266, 2246-2250.

Stellato, L., et al., Some limitations in using ^{222}Rn to assess river–groundwater interactions: the case of Castel di Sangro alluvial plain (Central Italy), Hydrogeology Journal, 16(4) DOI 10.1007/s10040-007-0263-0 (2008) 701-712.

Stellato et al., 2013. Is ^{222}Rn a suitable tracer of stream – groundwater interactions? A case study in central Italy. Appliead Geochemistry, 32 (2013), 108-117.

Tims et al., 2010. Plutonium as a tracer of soil and sediment movement in the Herbert River, Australia. Nucl. Instrum. MethodsPhys. Res., Sect. B, 268, 1150-1154.

Vivtar, T., et al., A review of isotope applications in catchment hydrology, In (P.K. Aggarwal, J.R. Gat, and K.F.O. Froehlich, eds), Isotopes in the Water Cycle. IAEA/Springer, Dordrecht, The Netherlands, 151-169.

JAPAN

The combination of two photos shows the Fukushima Dai-ichi nuclear power station in Fukushima Prefecture before, top, and nearly one year after a devastating earthquake and tsunami hit Japan's northeast on March 11, 2011 and sent three of its reactors into meltdown. The top photo was taken in October, 2008 while the bottom photo was taken on Feb. 26, 2012. (Kyodo News)
https://cryptome.org/2012-info/daiichi-12-02-05/daiichi-12-02-05.htm

6. TEN YEAR REPORT OF FUKUSHIMA DAIICHI NPS, JAPAN

ATSUNAO MARUI

Geological Survey of Japan, AIST

6.1. Introduction

East Japan great earthquake (Magnitude 9.0) occurred at 14:46 on March 11, 2011, and the Fukushima Daiichi NPS was attacked by the 16-m tsunami. As a result, three of six nuclear reactors caused the hydrogen detonation in three days after the tsunami caused by the electricity loss (no supply of cooling water to reactors). Actually, four reactors were damaged hardly by this accident. This report describes that the main countermeasures by the Japanese government and TEPCO (Tokyo Electric Power Company), its evaluation, the current condition, and the policy in the future work though the influence has been left now.

6.2. Geomorphology and geology

The Fukushima Daiichi NPS had been constructed on a marine terrace with a height of 35 m originally. Sand beach of about 50 m in width placed between the terrace and shore. This marine terrace was not suitable to construct NPS from the view point of ground strength because the nuclear plant must be obligated to construct on the stable geology, so that the flat artificial plain of the 10-m high was made for the NPS base (cut the marine terrace). The reactor and turbine buildings were based on a stable layer (-10 m below the sea level) below the sand layer which composes the marine terrace. The structure of the area was shown in Figs. 6.1 and 6.2, the all stratums are Tertiary. The geology was deposited almost horizontally and three sand layers existed as aquifer. The mudstone layer below the top sand layer is the support base of buildings. The top sand layer which composes the marine terrace is the main aquifer of the NPS site. And the groundwater of the aquifer is thought to be recharged by rainfall brought on the NPS site.

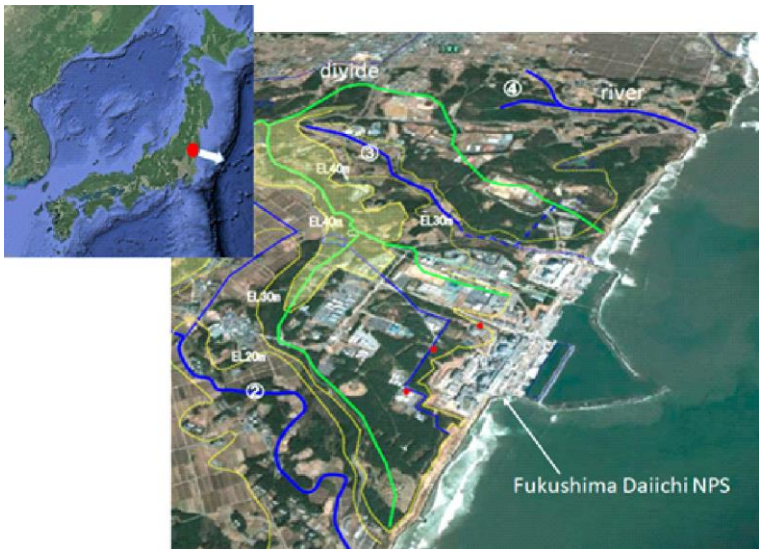

Fig. 6.1. Fukushima Daiichi Nuclear Power Station (before the accident), from TEPCO HP

There are three aquifers named mid-grain sand layer (former top sand layer), alternated sand layer and sand layer from the top, and the hydraulic conductivity is almost the same in the order of 10^{-5} m/s. In the first stage of the accident, the pollution was extended to the top mid-grained sand layer, and the muddy stable layer just below the sand layer hold block the contamination to the alternated sand layer. The top mid-grained sand layer and its groundwater was the target of the countermeasures in the first stage. However, the base of the 3rd and the 4th reactor buildings were reached to the alternated sand layer, so that the expanded countermeasures were necessary in shortly.

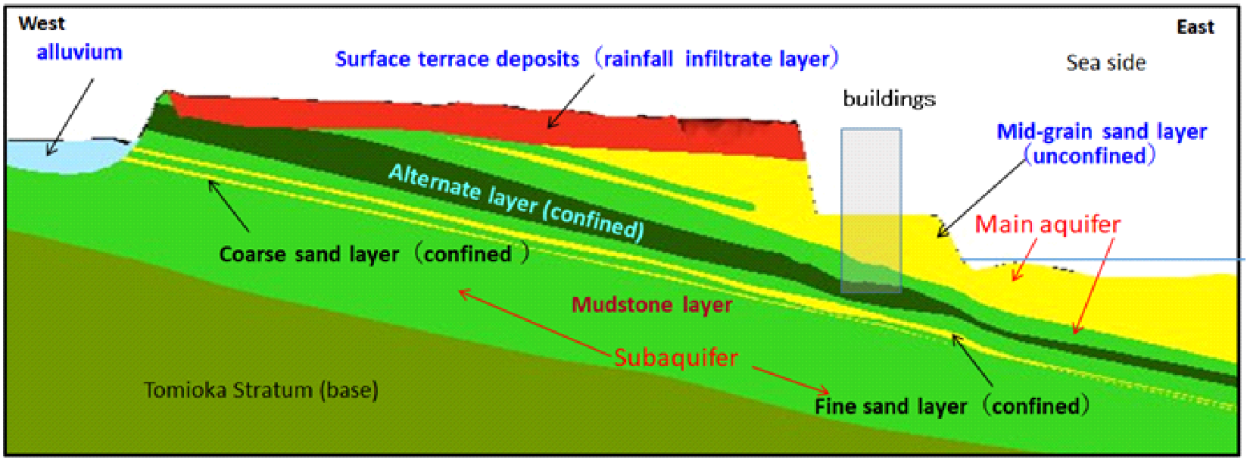

Fig. 6.2. Geological cross section of Fukushima Daiichi NPS

6.3. Main countermeasures by Japanese government and TEPCO

The government settled on three basic policies of countermeasures in consideration of the problem of coming out one after another in May, 2013. That are ① Remove the source of pollution, ② Prevent the water touch to the source of pollution, and ③ No leak of polluted water. In the original plan, the buildings will be dried up in early 2020's. The main countermeasures are as follows (Fig. 6.3).

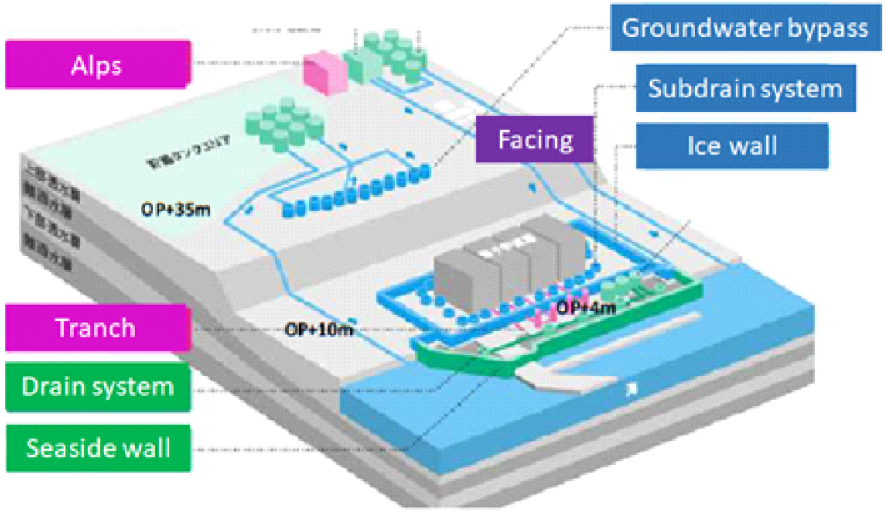

Fig. 6.3. Main countermeasures by the government and TEPCO (ANRE HP #1)

1) Seaside wall (Fig. 6.4): It is a wall of the iron tube installed just outside in an original coast line, preventing the polluted groundwater discharge to the ocean. The entire completion is in October, 2015. The wall cut off the groundwater flow of the mid-grained and the alternated sand layers.

2) Ice wall (Fig. 6.5): The wall is made by freeze water in the soil and strata surrounds of the 1st to 4th reactors and turbine buildings and neighbor polluted area. The total length was over 1,400 m. Over 30 m length treble structure pipe were settled underground the area through the brain of minus 35 ℃. Partially linking to the seaside wall, the polluted groundwater flow was blocked. It was a challenging business done on an unprecedented scale through the groundwater control was easy because it froze at a dash after all pipes were driven.

3) Subdrain system (pumping up system of groundwater around the buildings) (Fig. 6.6): To keep the water table around the buildings for a stable running of reactors, amount of 850 to 1,200 m^3 of groundwater has been pumped up in a day and released to the ocean, before the earthquake. After the accident, the groundwater is polluted, so the groundwater around the buildings is transported to the decontamination processing unit. The final goal of this countermeasure is to dry up the buildings.

Fig. 6.4. Picture of the seaside wall (after TEPCO HP).
This wall cut the groundwater discharge from the main two aquifers in Fig. 6.2.

Fig. 6.5. Ice wall construction, over than 30 m length freezing pipes were settled by every 1.0 m on the mountain side and 1.2 m on the seaside (after TEPCO HP)

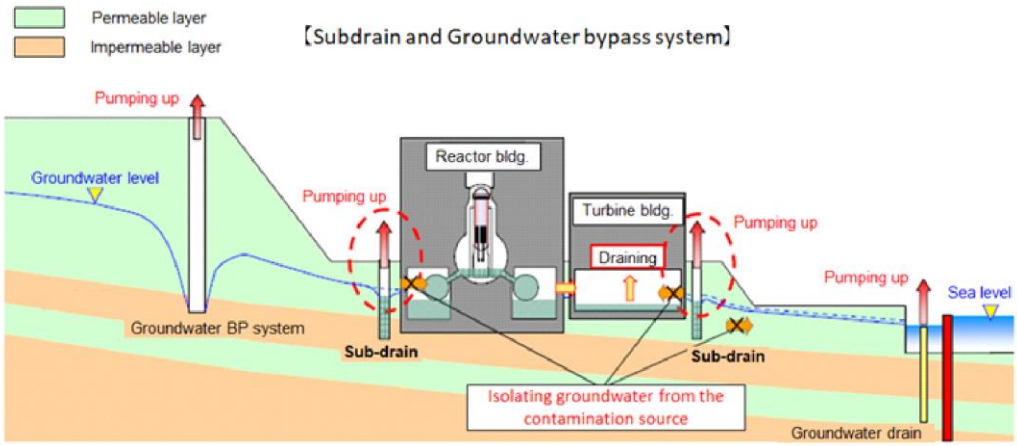

Fig. 6.6. Subdrain and groundwater bypass system to keep the low water table (small injection to the buildings, after Ohnishi, 2014

4) Groundwater bypass (12 drawing up wells in front of ice wall): Groundwater flow of the NPS area is from marine terrace (west) to ocean (east) through the reactor and the turbine buildings. The groundwater bypass plays the important role of groundwater drawing up before the reach to the ice wall area. The government thought the groundwater before the touch to the area is clean, then the pump up water seemed to be able to release to the ocean. However, the plan was canceled by the fishermen.

5) Facing: This is the measure which covered surface by asphalt etc. to recharge groundwater by rainfall. Over 1,500 mm/y rainfall was brought to the area and thought to be over 10,000 m^3/day groundwater yielded, if the half of rainwater is evaporated. The purpose of facing is dumping the rainwater to the ocean stay clean. But concerning about land subsidence and seawater intrusion was discussed before the measurement.

6) Decontamination processing unit and tanks of treated water: The government and TEPCO operate a multi nuclide removal device that is called ALPS, and it is thought that it will discharge water that removes the contaminant into the ocean, first. However, tritium is not removed by ALPS, the treated water through ALPS is still stored in the NPS area. The total volume of the water is over 1,100,000 m^3 now. The volume of the water has exceeded the capacity of the NPS area.

6.4. Countermeasures not to achieve though given as candidate

1) Hardener injection to decrease the permeability: The main problem is controlling groundwater in the mid-grained sand layer (top sandy layer). It is thought about 10 years, the duration time of groundwater to discharge to the ocean. Decreasing the permeability is an idea of groundwater control to avoid water attack on the reactors.

2) Second wall around or inside of ice wall: The government (decommissioning countermeasures promotion conference) announced the necessity of "Multiple countermeasures". The ice wall needs the lot of electricity to keep the big ice. The usual wall e.g. clay cement wall was thought as a candidate to support the ice wall.

6.5. Evaluation of the countermeasures

1) Seaside wall: The iron tube wall was completed in four and half years after the accident, mentioned above. The polluted water had been leaked to the ocean from the port of NPS. However, the impact of the wall was proved, the contamination of the sea water is shown in Fig. 6.7.

2) Ice Wall: Ice wall has been completely success, frozen wall was made by soil water from the bottom to top, in almost all the site (less than two percent of the area remaining near the surface). The groundwater flow into the buildings was blocked by the ice wall, and contributed to drying out the buildings (it is on the way, now). The water level of inside and outside the ice wall is changed clearly (Fig. 6.8).

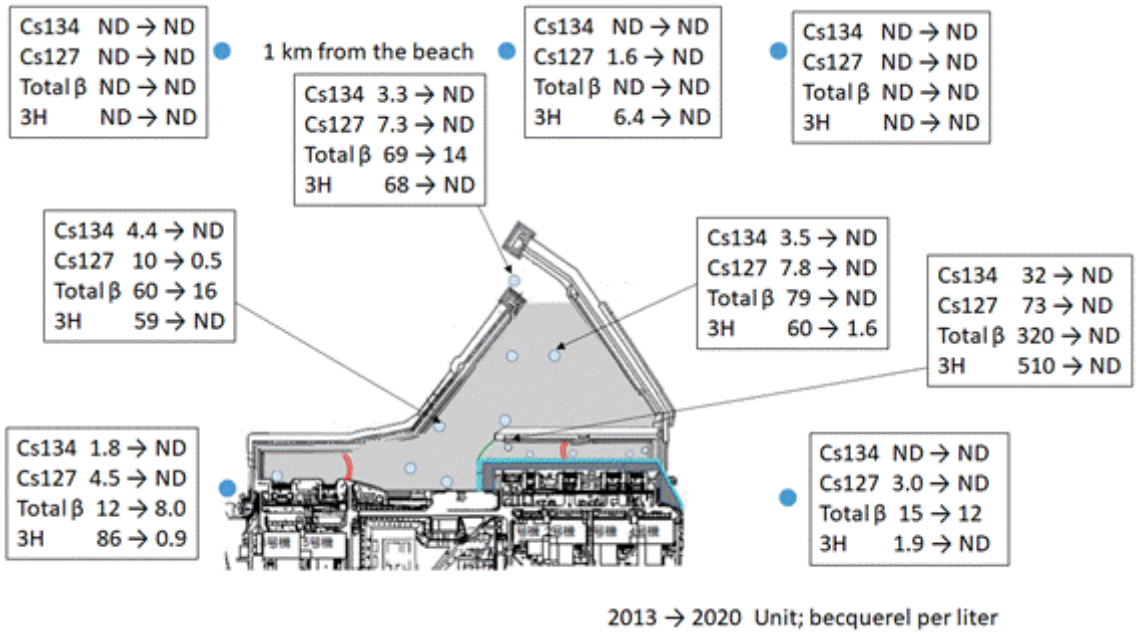

Fig. 6.7. Impact of seaside wall and countermeasures to leak the polluted water to the ocean, between 2013 and 2021 (ANRE #2)

3) Subdrain system: Pump up system of groundwater gives an effect to the water level control around the buildings. It could be seen in the rate of polluted water yield shown in Fig. 6.5.

4) Facing: outside of the ice wall, almost 100% of the area was done in 2020, but only 25% in the ice wall area was covered in 2021. Totally 95% of the NPS area is finished now (see Fig. 6.5). And about 70% of the roof are covered now. These countermeasures are contributed to prevent the rainwater invasion to the buildings and increase the polluted water. Especially, groundwater outside the ice wall has been thought to be controlled.

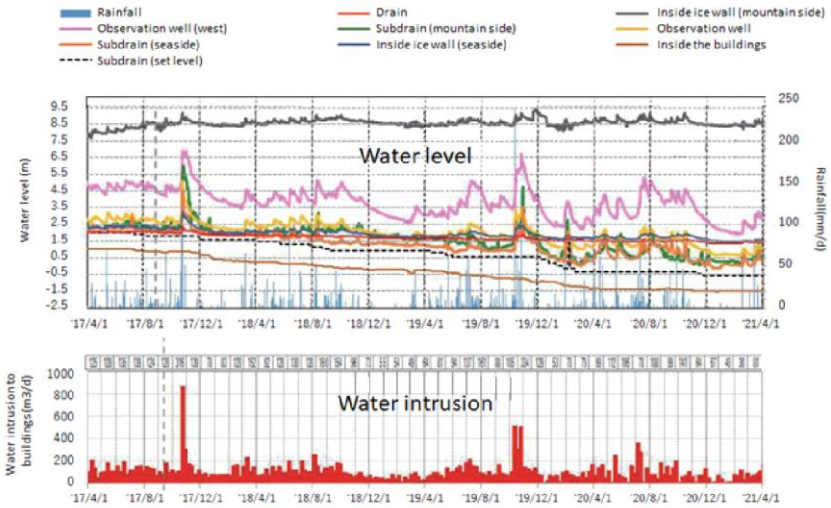

Fig. 6.8. The ice wall has cut off the groundwater from mountain side to buildings (inside the wall). Water level difference is cleared from the begin and effects of the rainfall is also cut. Water level inside the building is influence of rain water intrusion through the broken roof (ANRE #3)

5) ALPS: Polluted water from the buildings has been processed by the decontamination processing unit (represented ALPS), steadily. However, over 1,100,000 m^3 of treated water (almost all is tritium water) has been stored in the tanks on the NPS site. But the place which settled tanks reaches to the limit, no exceed area, in 2021 (Fig. 6.9).

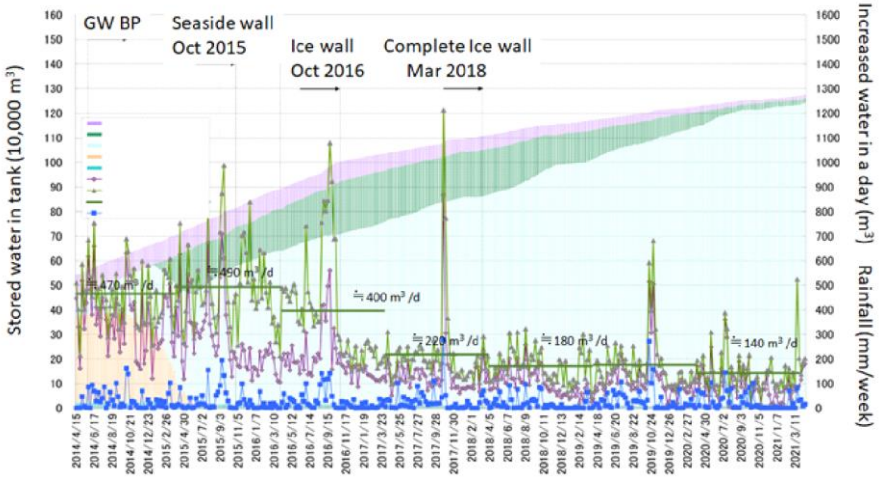

Fig. 6.9. Change of stored water in the tank. It already reaches the limit of capacity (ANRE #4)

6.6. Problems passing ten years

1) Polluted water stored in tanks: Huge volume of tritium water was remaining on the NPS site. It is thought the various danger in this situation. The government decided to release the treated water to the ocean from 2022, by following recommendation of the countermeasure board. The government will establish Japanese own standard as tighter than world (IAEA) standard. However, people think more discussion should be done to get a consensus.

2) Taking out of debris: The first step is drawing the water level in reactor containment vessel. But the total volume of debris thought to become 880 t and they need 200 to 300 m^3 cooling water every day. The water will become the polluted water. In this condition, the operation test and the verification test are advanced by a robotic arm developed in England.

3) Description and discussion about risk communications and rumor: People still have a tendency to avoid the marine and agricultural products of the area. The government and TEPCO should make a polite explanation and enough scientific discussion to have a consensus and trust.

6.7. Conclusion

To secure the transparency to the international society, an international review will be required to IAEA for the ensuring safety about the treatment of the ALPS processing water. The conversation activity incl. scientific discussion is necessary to avoid the rumor damage and the risk communications.

References

ANRE HP (Agency for Natural Resources and Energy at Ministry of Economy, Trade and Industry) #1: https://www.meti.go.jp/english/earthquake/nuclear/decommissioning/index.html

ANRE #2: https://www.meti.go.jp/earthquake/nuclear/decommissioning/committee/osensuitaisakuteam/2021/04/4-1-4.pdf

ANRE #3: https://www.meti.go.jp/english/earthquake/nuclear/decommissioning/index.

ANRE #4: https://www.meti.go.jp/earthquake/nuclear/decommissioning/committee/osensuitaisakuteam/2021/04/2-2.pdf

TEPCO HP (Tokyo Electric Power Company): https://www.tepco.co.jp/decommission/progress/about/

Marui, A. (2014): Discussion about groundwater problem on Fukushima Daiichi NPS, Sekai (World) by Iwanami press., No. 852, 2014 (in Japanese)

Ohnishi, Y. (2014): Summary of the Measures for Contaminated Water that the Committee Compiled, UNESCO workshop of countermeasures for the groundwater of Fukushima Daiichi Nuclear Power Station in 2014.

LITHUANIA

Ignalina Nuclear Power Plant Lithuania with two towers
https://commons.wikimedia.org/wiki/File:Ignalina_Nuclear_Power_Plant_Lithuania_two_towers.JPG

7. INTEGRATED STUDIES OF CRUSTAL PERMEABILITY BASED ON ENVIRONMENTAL ISOTOPES, NOBLE GASES DATA AND SHALLOW - DEEP GROUNDWATER FLOW AND MASS-TRANSPORT MODELING IN THE SURROUNDING AREA OF IGNALINA NUCLEAR POWER PLANT (NPP)

R. MOKRIK, V. SAMALAVICIUS, M. GREGORAUSKAS, V. MASELIENE-JAKIMAVICIUTE, J. ARUSTIENE

Vilnius University, 3 Universiteto St., LT-01513 Vilnius, Lithuania

Abstract

Within the IAEA Research Program F33022 work plan the task for Baltic region was to prepare a new approach of deep aquifer investigation that will be focused on using a wide complex of environmental isotopes, noble gases, groundwater chemistry and hydraulic data via coupled analysis of groundwater flow numerical models. The project main aim was to analyze crustal fracturing and hydraulic migration properties of sedimentary cover related with the faults systems and aquifers reservoir role in noble gas and fluid distribution of the surrounding area of Ignalina NPP. The study was emphasized on groundwater circulation system using stable and radioactive isotopes of the Baltic artesian basin (BAB) and comparing revealed particles' travel times along with flow and mass-transport simulation model results for Ignalina NPP surrounding sites. In this study modeled particle travel time in intermediate and deep aquifers which are covered by thick impermeable aquitards was compared with ^{4}He and ^{81}Kr dating results. To improve the reliability of 3D groundwater flow model verification, the isotopic age of deep groundwater was compared to the MODPATH modeled times of particle tracking.

We had widely studied helium gas concentration of boreholes and their distribution peculiarities in the BAB using INGEM-1 device. For this project aim from the 6 Lithuanian deep boreholes which depth varies from 300 to 1,011 m. $^{3}H/^{3}He$ ratio was estimated at the IAEA Isotope Hydrology Section Laboratory. Tritium was estimated in the Lithuanian Nature Research Centre. Stable isotopes analyzed at the Institute of Geology, Tallinn University of Technology, Estonia. At the Institute of Geosciences of Vilnius University in 2016–2019 a numerical 3D steady-state and transient groundwater models of the BAB was created and calibrated with groundwater head and hydraulic parameters data of boreholes. Modeled areas include around 500,000 km², grid size 5x5 km, total cell number 614823 and have 31 separated layers from the crystalline basement aquifer up to the Quaternary aquifer system. In 2013–2017 radio krypton age was estimated for the BAB by the cooperation of international team for samples of seven boreholes of deep groundwater using ATTA method (Gerber et al., 2017).

7.1. Introduction of hydrogeologic framework of the Baltic Artesian Basin

The BAB is a multistoried geological structure of aquifers and aquitards. In western and northern marginal parts, it is inundated by the Baltic Sea which is one of the main groundwater discharge areas. The vertical sequence of groundwater bodies forms three hydrogeological units or zones – active, delayed and stagnant, separated by regional scale aquitards and formed by boundary conditions for hydrogeochemical-isotopical composition and flow direction during geotectonic development of sedimentary basin (Fig. 7.1). Geodynamic loading processes, hydrogeochemical interactions between groundwater and rocks, groundwater flow features from meteoric recharge area to discharge area and partitioning processes of isotopic composition have predetermined the evolution of stable oxygen-18 isotope ratio values and its localization sites inside of these zones. A zone of an active water exchange extends from an inland meteoric water recharge area to a coastal submarine discharge area which is separated in a nearshore with transitional zone, where inversion of the groundwater heads takes place. In the inland part, meteoric water infiltration predominates downwards up to depths of 400 to 450 m. Here the fresh carbonate type groundwater reaches in the total dissolved solid (TDS) value no more than 2–4 g/l. The zone of delayed groundwater is located at the depths from 0.5 up to 1.8 km. The carbonate-chloride and sulfate types' groundwater of this zone reaches in TDS from 5 to 60–100 g/l. Below the 1.8 km depth, stagnant chloride type groundwater zone with

more than 100 g/L in TDS is formed. Thus, the three main zones according to $\delta^{18}O$ values distribution in above mentioned groundwater zones were distinguished in the BAB.

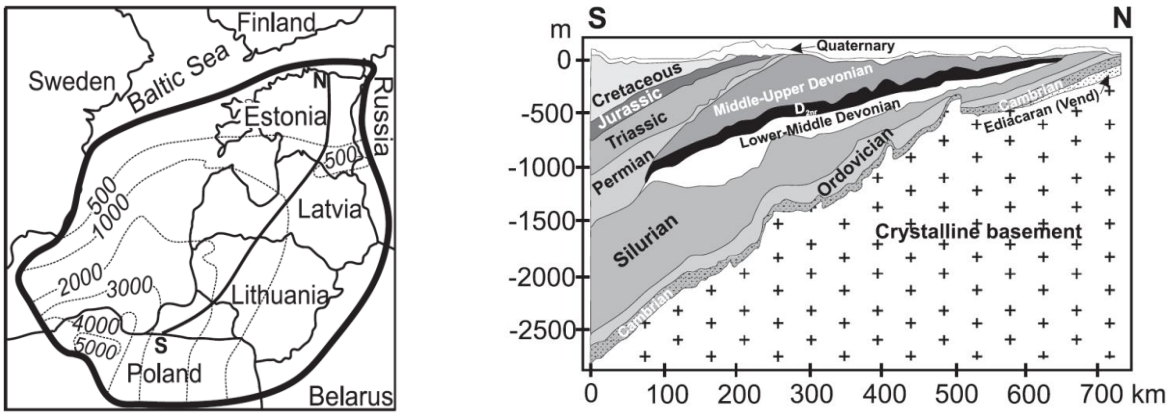

(a) (b)

Fig. 7.1. Location of the Baltic Artesian Basin, dotted lines represent depth of crystalline basement in metres, below sea level (a), longitudinal cross-section of the BAB (b) (after: Juodkazis, 1980; Pärn et al., 2016; Virbulis et al., 2013)

In the active zone near surface dominated $\delta^{18}O$ values from –8.2 up to –11.6‰, which are related with the modern meteoric water recharge and by features of lateral partitioning of $\delta^{18}O$ isotope ratio of precipitations across the region (Raidla et al., 2016). More positive zones with $\delta^{18}O$ values from –8.2 to –10.5‰ are located mostly in southwestern part of the Baltic region. Extremely depleted zones with $\delta^{18}O$ values from –14 to –22.5‰ are located in the Estonian territory which reflects palaeorecharge during cold climate Pleistocene time. These differences in $\delta^{18}O$ of groundwater reflect changes of global paleoclimatic conditions and their impact onto the groundwater formation during the Pleistocene and Holocene (Mokrik, 2003) (Fig. 7.1, b). The $\delta^{18}O$ values of groundwater in most aquifers in North Poland, Kaliningrad District of Russia, Lithuania and Latvia territory range from –7.7 to –13.9‰ (Mokrik, 2003; Rozanski and Zuber, 2000). However, in Gotland Island (Sweden monocline) at the same depths groundwater has significantly higher $\delta^{18}O$ values (from –5.7 to –6.1‰) (Mokrik, 1997).

The delayed zone is dislocated in the western part of BAB where the TDS of groundwater gradually rise from 5–7 g/L up to 90–100 g/L. Under the impact of lithostatic load and tectonic activities, compaction flow of this zone is moving toward the periphery part of artesian basin. This zone includes three hydrogeochemical facies of groundwater: bicarbonate chloride calcium sodium, chloride magnesium sodium (marine) and chloride sodium groundwater facies with intermediate isotopic ratio $^{18}O/^{16}O$ values –9 to –6 ‰. In this zone the $\delta^{18}O$ isotope ratio values are formed like transitional media between shallow active and deep stagnant groundwater motion and mixing adaptation.

Stagnant zone brines are under closed system thermodynamically in complete equilibrium with sedimentary rocks of artesian basin. Theirs salinity reaches up to 140–300 g/l and value of the isotopic ratio $^{18}O/^{16}O$ enriched –4.5 to –3‰.The temperature at the top of Cambrian – Ordovician rocks varies from 98 °C in the southwestern Lithuania epicenter, to 21 °C at the Jelgava site located close Riga. The geothermal anomaly promotes the processes of ultrafiltration, dehydration and ion-exchange because enrichment of deep groundwater with calcium ions, i.e., waters of strongly chloride calcium facies are formed.

7.2. Description of study area

Ignalina NPP is located in the north-eastern part of Lithuania, near the borders with Belarus and Latvia (Fig. 7.2). Previous investigations of NPP fixed following safety relevant external factors for analyzing: seismic factors; near surface geotechnical conditions; meteorological conditions; possibility of flooding in the area; external risks caused by human activity. The Strategy on Radioactive Waste Management was approved by the Government of Lithuania in 2008. Its objective is to define a

radioactive waste management policy. This strategy is approved to implement the provisions of the Law of the Republic of Lithuania for Radioactive Waste Management, which establishes basic principles of Radioactive Waste Management. New management facilities, which are or will be built under the Decommissioning Programme, such as solid radioactive waste management and storage facility, spent nuclear fuel storage, landfill and near surface disposal facilities and others, are being financed by the Ignalina International Decommissioning Support Fund, Ignalina Programme and co-financed by the National Ignalina NPP Decommissioning Fund.

According to the geological section near Ignalina NPP in the upper zone active meteoric water exchange is spread which is separated from the deeper aquifers by regional Silurian-Ordovician aquitard. Meteoric water infiltration predominates downward to the depths of 300–400 m. Here mostly bicarbonate sodium-calcium-magnesium facies of groundwater reaches in TDS from fresh up to 2–4 g/L. From the 500 m depth below the regional aquitard is located the delayed groundwater zone. The TDS of chloride sodium type groundwater of this zone rise up to 64 g/L. Under the impact of lithostatic compression load on groundwater flow from this zone are resulted brines moving toward modern recharge area. The counteraction of these two opposite flows forms a hydro-chemical/hydrodynamic trap like a hydrogeological barrier which is fixed at a depth of 250–320 m.

Fig. 7.2. Ignalina NPP location site on the Lithuania map

Groundwater investigations by environmental isotopic research methods have been made in few east Lithuanian areas: Varėna and Druskininkai surroundings, Rykantai site near Vilnius, near Ignalina NPP and in Virinta river basin. Isotopic zones are mostly expressed according to the changes in tritium and radiocarbon contents in groundwater. Complicated isotopic distribution of zones is often formed by a number of factors associated with groundwater exchange near the river valleys and tectonic fault zones. Radioisotope research was also used to assess the percolation time in aeration zone. Thus, three main zones according to $\delta^{18}O$ distribution in groundwater can be distinguished: 1) near subsurface zone with $\delta^{18}O$ values from –10.0 to –10.6‰ (close to local meteoric water), which are related to the modern meteoric water percolation on watersheds of highlands (eastern part of the Baltic Basin); 2) zones up to 150–250 m depth with $\delta^{18}O$ values from –10.5 to –11.5‰ (more negative values than modern meteogenous water); 3) zone with $\delta^{18}O$ more reached values –7‰ (more positive values than modern and Late Pleistocene time meteogenous water). The differences in $\delta^{18}O$ of groundwater reflect changes of paleoclimatic conditions and their impact onto the groundwater formation from the Early Pleistocene to Holocene.

7.3. Tritium methods application for shallow groundwater age estimation

For shallow groundwater dating using conventional tritium dating method is incorrect, because initial tritium activity values are usually absent and many sources of water mixing affects tritium concentration. The $^{3}H/^{3}He$ ratio is more independent of the initial tritium concentration of the groundwater sample which is one of the advantages. But the problem for the correctly quantitative interpretation of the $^{3}H/^{3}He$ for residence time in multilayered complex is the fact that it is affected also by mixing via leakages from the separated by aquitards aquifers and by degassing neglect. For quantitative studies of modified conventional model by trend analyzing for quasi stable state of tritium

monitoring data and coupled $^{3}H/^{3}He$ method for resident time's evaluation at Lithuanian sites was made.

Table 7.1. Tritium decrease gradients in Quaternary aquifer system

Well No.	Well depth, m	Location	^{3}H volumetric activity, TU		Gradient, TU/year
ag II-III md-gr			2008	2012	
955/1	37.5	Medininkai	7.5	6.2	0.325
28809/2	23.7	Vilnius	10.2	9.1	0.275
29708/3	25.0	Vievis	5.5	4.1	0.350
30000/4	32.0	Kaunas	7.3	6.1	0.300
ag II žm-md				Average	0.313
42169/5	76.0	Medininkai	8.5	8.3	0.050
6442/6	64.0	Vievis	2.6	1.7	0.225
43515/7	60.0	Kaunas	2.3	<0.1	0.575
ag II dn-žm				Average	0.285
4121/8	130.0	Medininkai	<2	<0.1	0.000
28811/9	51.0	Vilnius	4.4	2.1	0.575
6446/10	93.0	Vievis	<2	<0.1	0.500
25940/11	98.0	Kaunas	<2	2.5	–0.125
				Average	0.238

Southeastern Lithuania unconfined layer and precipitation water tritium activity decrease rate is dominated by radioactive decay for the period 1980–2013. Confined aquifers are more affected by mixing, but in some cases tritium activity values in time can be predicted if the tritium gradient trend is close to stabilizing. The monitoring type of sampling was applied in order to calculate tritium activity gradient value. Aquifer ag II-III md-gr groundwater gradient values in different sampling points along the water pathway are very similar. It is necessary condition to proceed on exponential decay curves comparing with actually calculated. Modern groundwater dating, using tritium isotope, was conducted in southeastern Lithuania Quaternary aquifer system. Cross-section represent the full path of groundwater from recharge to discharge areas (Štuopis et al., 2012). Numbering starts with first aquifer and proceeds from recharge area: ag III md-gr – 1–4 points, ag II žm-md – 5–7 points, ag II dn-žm – 8–11 points. Additional sample points (12–20) were taken in 2013 from wells located near the earlier (Tables 7.1 and 7.2). ag III md-gr aquifer spreads locally, but linked hydraulically in all groundwater path. Its area covers 8,570 km² (Fig. 7.3). Aquifers, ag II žm-md (15,600 km²) and ag II dn-žm (12,360 km²), spreads almost the entire south-eastern Lithuania region (Štuopis et al., 2012). Hydrogeological stratus units represented in cross-section are schematizing to solid layers, in defiance of disruptions.

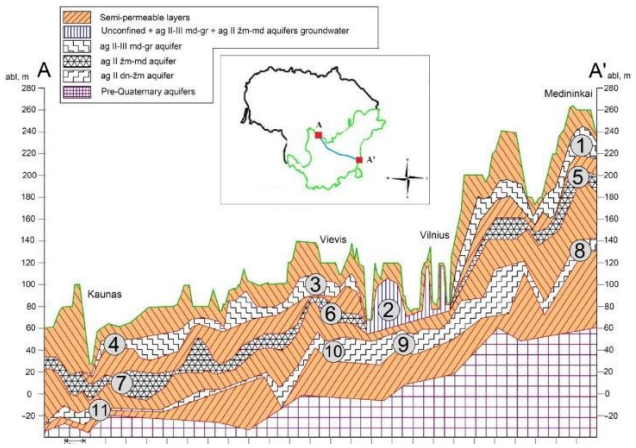

Fig. 7.3. Cross-section of Quaternary aquifer system Medininkai-Vilnius-Vievis-Kaunas

In previous studies groundwater age was also deduced using numerical modeling, statistical data extrapolation and gradient method. For these studies tritium activity monitoring in the Quaternary aquifer system began in 2008. All these methods according to tritium dating were very problematic and made significant difficulties determining modern groundwater age (Mokrik et al., 2014;

Samalavičius and Mokrik, 2016; Štuopis et al., 2012). Initial tritium values in aquifers is usually unknown, therefore the gradient must be reconstructed for quasi stationary state trend site. Gradient method showed promising results, for determining initial tritium value on the quasi stable state trend intervals. For obtaining actual gradient value at least two samples must be collected and analyzed. The gradient is a difference of tritium activity per time in the particulate site and aquifer. Theoretically calculated tritium decay curve compared with calculated results enables quantifying initial tritium activity (Fig. 7.4). Best fitting theoretical curve enables us to predict for future or extrapolates for the past (until apparent initial tritium activity) in a specific aquifer and site, t – time, αT – tritium activity, $\alpha_0 T$ – initial tritium activity, $T_{grad.}$ – tritium gradient in time:

$$T_{grad.} = \frac{\alpha_0 T - \alpha_t T}{t}.$$

For the first time in Lithuania $^3H/^3He$ conventional dating technique was used for groundwater residence time estimation and calibration of gradient method. In this study $^3H/^3He$ age was used to backward calculate tritium gradient and initial tritium activity in three Quaternary aquifers and results to previously collected monitoring data (Mokrik et al., 2014).

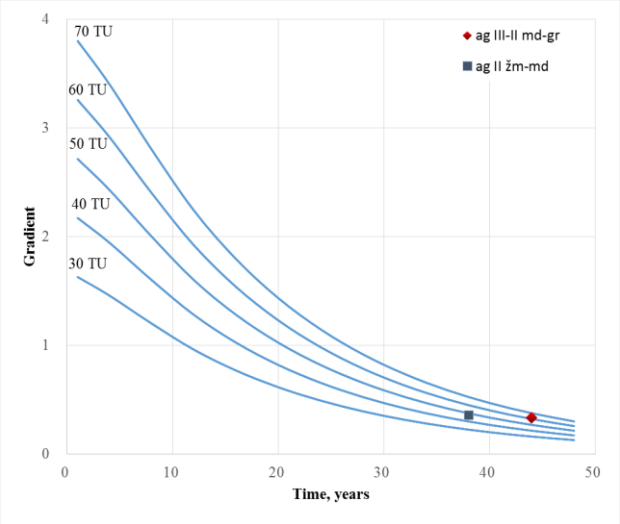

Fig. 7.4. Tritium decreases gradient curves

Groundwater age (Table 7.2) calculated by conventional and with $^3H/^3He$ method is almost identical in all three Quaternary aquifers (49–53 years). Other factors such as: recharge with precipitation or leakage from other aquifers in this case is not excluded and is stabilized during residence time. Gradient method provides results which include mixing and radioactive decay in groundwater. Analyzing monitored tritium trend and age data in southeastern Lithuanian in the shallow groundwater up to depth 50–60 m shows close equilibration state with precipitation and possible leakages mixing from the lower aquifers in river valleys sites in period 1980–2012 for conventional tritium and in 2017 for $^3H/^3He$ ratio. These methods ages difference varies 8–22% and that can be also related by monitored wells sampling times differences (see Table 7.2). Groundwater tritium activity gradients show that main decrease rate factor is radioactive tritium decay process which is affected by mixing of their concentrations dynamic in precipitation and groundwater reserves

Table 7.2. $^3H/^3He$ and gradient dating results in Quaternary aquifer system

Well No.	Site	Index	Depth, m	^3H, TU	^3He, TU	Groundwater age, a	
						$^3H/^3He$ method	Gradient method
26368	Rūdiškės	ag II -III md-gr	51	5.4	79	49	38
487	Trinkuškiai	ag II dn-žm	60	4.7	90	53	–
47520	Salininkai	ag II žm-md	45	4.8	70	49	45

during approximately 50 years. For multilayered aquifer systems particle track models must be coupled for tritium and helium studies additionally. Coupled tritium gradient method and $^{3}H/^{3}He$ are useful for verifying tritium decrease factors in Quaternary groundwater. Numerical modeling could also be included as a valuable asset for determination of groundwater flow, balance and boundary conditions.

7.4. Noble gas and coupled flow modeling methods application for intermediat and deep groundwater age estimation

Deep and intermediate aquifer investigation of BAB was carried out using a wide complex of environmental isotopes, noble gases, groundwater chemistry and hydraulic data via coupled analysis of groundwater flow numerical models. For 40 years helium distribution peculiarities in the BAB was studied using INGEM-1 device (Juodkazis and Tibar, 1989; Mokrik et al., 2002). A numerical 3D steady-state and transient groundwater models of the BAB were developed at the Institute of Geosciences of Vilnius University in 2016–2018 (Fig. 7.5). A measured groundwater head and hydraulic parameters of boreholes were used to calibrate the model. Area of the digitized model is 500,000 km² and grid size is 5x5 km with total cell number of 614823. Total number of aquifers and aquitards is 31 layers starting from the crystalline basement aquifer up to the Quaternary aquifer system. Regional hydraulic ages have been assessed by using particle tracking from well sites up to the recharge area endpoints (MODPATH simulation). In case of a few flow paths crossing in the site, two most significant recharge areas were picked: Riga well No. 50194 and Likėnai, Aukštaitija well No. 21965. Thus, two particle track ages are obtained (Table 7.3). An average value of both hydraulic ages is presented in a diagram of dating method comparison (see Fig. 7.6). Deep groundwater seepage velocity estimated by particle tracking for BAB varies for intermediate depth up to 500 m $5 \cdot 10^{-3}$ m/y and for 1 km depth ~ $8 \cdot 10^{-4}$ m/y. That result is significantly lower as modeled by BAB steady state condition with Darcy hydraulic conductivity of ~1 m/y (Virbulis et al., 2013). Modeled particle travel time in aquifers confined with regional scale impermeable aquitards and was compared with ^{4}He and ^{81}Kr dating results. Groundwater reservoirs where elevated helium values were observed coincide with steep fault blocks which transect the basin sedimentary cover.

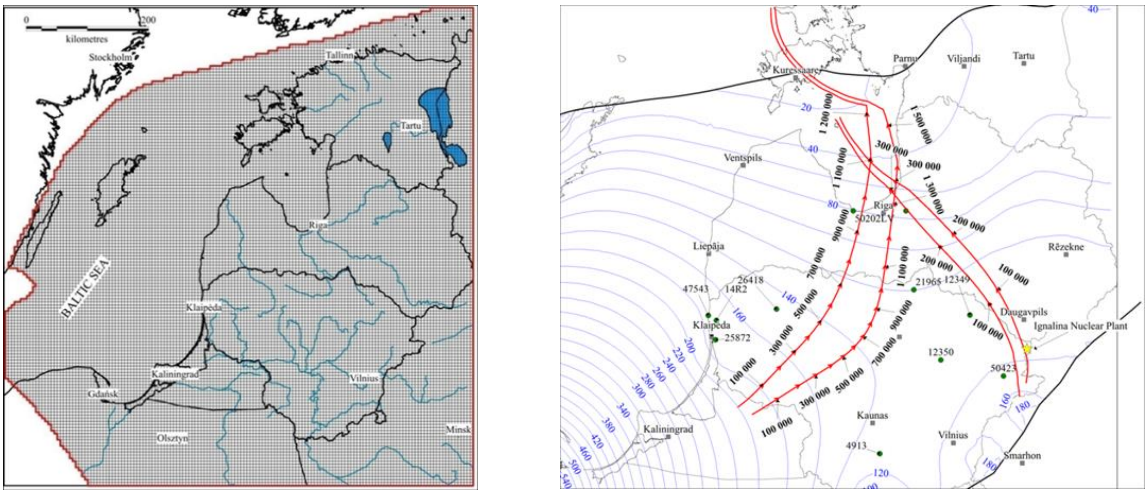

Fig. 7.5. Numerical 3D steady-state and transient groundwater model grid of the BAB (a).
An illustration of MODPATH modeled particle tracks for the O-Cm aquifer (b).
Particle were released in two recharge areas: Eastern Lithuania and northern part of Kaliningrad district

Radio krypton age was estimated in deep and intermediate groundwater samples collected from seven boreholes using ATTA method in 2013–2017 (Gerber et al., 2017). Helium was measured at the IAEA Isotope Hydrology Section Laboratory samples of Lithuania, Latvia and Estonia. The dissolved helium concentration data was obtained during fieldwork sampling and previous publications (Gerber et al., 2017; Juodkazis and Tibar, 1989; Mokrik et al., 2002). For ^{4}He age calculation, average uranium

(440 ppm) and thorium (1,500 ppm) content in the crystalline basement at the northern part of the BAB were used (Raudsep, 1997). Helium age and correction for the helium production to the calculation of accumulation rate (Torgersen and Stute, 2013) was made using average rock density (2.5 g/cm^3), void ratio was calculated for porosity of reservoir aquifers (n_e – 0.15) and release factor Λ_{He} – 1.

Deuterium and oxygen-18 stable isotopes were measured in the Laboratory of mass spectrometry at the Department of Geology, Tallinn University of Technology. Major and trace element analysis were performed in Lithuania, Latvia and Estonia accredited laboratories.

Table 7.3. Intermediate and deep BAB aquifers groundwater ages determined using helium-4, krypton-81 and particle track modeling

Well no.	Site	Index	Depth, m	Particle travel time (modeled), ka recharge from south/east	^{4}He age, ka	^{81}Kr age, ka
12350	Anykščiai	D_{1-2}	360	70	76	-
47543	Palanga	D_2	522	250	225	-
12349	Rokiškis (Vaiva)	D_{1-2}	440	100	31	-
21965	Likėnai (Aukštaitija)	O-Cm	1,011	900/180	308	-
11978	Likėnai (Likėnai)	D_{1-2}	434	180	55	-
50423	Ignalina	O-Cm	500	100	129	320
25872	Klaipėda, Geoterma	D_{1-2}	1,100	400	597	1,157
50194	Riga, Hospital	O-Cm	1,027	1,100/300	326	929
8021	Häädemeeste	O-Cm	610	500	150	408
4613	Värska	O-Cm	460	360	81	550

A selective database was compiled from data collected during research of the BAB in the past 40 years. Criteria for data selection were to pick samples, which are exclusive in the contest of the other BAB groundwater. In case of intermediate and deep aquifers additional criteria for groundwater dating results (^{4}He, ^{81}Kr or particle travel time) were necessary. All data were divided into groups considering groundwater depth (modern-shallow, intermediate, deep), location and structural features of crystalline basement. Saturation indices for calcite, gypsum and halite were modeled using software Phreeqc, wateq4 database. In case the data was not available, initial conditions were applied: temperature – 10°C, pe – 0, density –1 g/mL. All stable oxygen and deuterium isotope data are expressed in the Vienna Standard Mean Ocean Water (VSMOW) system (Craig, 1961).

7.4.1. Intermediate and deep aquifers dating results

Radio krypton is meteoric in origin and has the same downward-lateral flow trajectory as modeled particle track. This statement is applicable for the multilayered aquifer systems and confined aquifer isolated from above by regional scale aquitards where groundwater flow direction is predominantly lateral from recharge area toward discharge places. For BAB hydraulic conductivity values of such aquitards, which confine aquifers from meteoric water leakage on regional scale, is below 5E-7 m/d (Mokrik, 2003). Source of emanation of ^{4}He occurs due to decay of uranium and thorium in minerals of the crystalline basement rock. Helium diffuses through fractures and tectonic faults to sedimentary reservoirs where it accumulates. Cases where vertical local uplift blocks confine groundwater aquifers (offset from 100 to 600 m) could prevent lateral migration of fluid. Accumulation rates of crustal origin noble gases could increase significantly. Helium amount in the deep and intermediate groundwater of the BAB vary considerably: 4.6E-8 up to 9.0E-4 ccSTP/g (Mokrik, 2003). High helium accumulation rate in groundwater is observed at the periphery margin of the Estonian Homocline and Belarus-Mazurian Massif, Polish-Lithuanian Trough (at depth 500 – 600 m), Liepaja-Riga-Pskov Ridge and other Rapakivi granite massifs in basement (Mokrik, 2003). Mentioned tectonic structures are bounded by Paldisk-Pskov, Middle Estonian, Liepaja-Saldus-Riga and East Lithuanian fault zones. These fault zones separate regions where groundwater movement

rates are relatively fast from stagnant in the deepest parts of the BAB. Seepage velocity in the peripheral part of BAB varies from 0.2 to 1 m/y.

Table 7.4. Aggregate ^{4}He age in Klaipėda site multilayered aquifer systems (Gerber et al., 2017; Juodkazis and Tibar, 1989; Mokrik, 2003; Mokrik et al., 2002)

System	He, ccSTP/g	Age, ka
T	Regional scale aquitard	–
P_2	4.56E-08	Modern
D_2	3.06E-04	225
D	Regional scale aquitard	–
D_{1-2}	8.12E-04	597
O-Cm	9.00E-04	662
Σ	2.02E-03	1484

Helium age modeling shows that older groundwater may originate in an intermediate depth aquifer compared to located deeper (Tables 7.4 and 7.5). It contradicts groundwater chemical composition and dating results obtained using other techniques, therefore should be considered while interpreting helium ages. Aggregate helium age in a multilayered aquifer matrix unit is a sum of all groundwater helium ages in a particular site. This approach could be a tool for analyzing and interpreting helium dating results. Sum of accumulated helium should be equal to its total bulk emanation released from the crystalline basement into an aquifer matrix up to the shallowest regional aquitard. Two cases of helium distribution and aggregate helium age are presented in this study. A cross-section of Klaipėda-Palanga site, Lithuania coastline, distribution of helium content ccSTP/g in following aquifers is: O-Cm – 9.0E-4, D_{1-2} – 8.1E-4, D_2 – 3.1E-4, P_2 – 4.6E-8. The sum of helium is 20.2E-4 ccSTP/g and aggregate helium age is 1,484 ka (see Table 7.4). The value of aggregate helium age could suggest more reliable dating of the deepest aquifer, which in this case is O-Cm. Groundwater age of 1.5 Ma is more likely than 0.6 Ma (conventional helium dating) considering that radio krypton measured in overlaying D_{1-2} aquifer dates groundwater up to 1.2 Ma.

Table 7.5. Aggregate ^{4}He age in Värska site multilayered aquifer systems (Gerber et al., 2017; Juodkazis and Tibar, 1989; Mokrik, 2003; Mokrik et al., 2002)

System	He, cc STP/g	Age, ka
D	Regional scale aquitard	–
D_{1-2}	4.75E-05	35
O-Cm	1.10E-04	81
V_2vr	1.17E-04	86
V_2gd	3.09E-06	2
Σ	2.78E-04	204

A case of Värska, in southern Estonia presents an even more extreme case, where the deepest aquifer (of V_2gd) groundwater contains more than 40 times less helium than overlaying aquifers (see Table 7.5). Helium amount in aquifer of Värska (ccSTP/g): V_2gd – 3.1E-06, V_2vr – 1.2E-04, O-Cm – 1.1E-04, D1-2 – 4.8E-05. The sum of helium in Värska site is 2.8E-04 ccSTP/g and aggregate helium age is 204 ka (see Table 7.5). A similar estimation of deepest V_2gd aquifer groundwater age could be deduced applying aggregate helium age of 0.2 Ma. Conventional helium method dates groundwater to 0.002 Ma, almost 100 times younger. It is necessary to mention that this approach is not necessarily accurate. Radio Krypton age in Värska O-Cm aquifer dates groundwater up to 0.6 Ma, which is 3 times older than aggregate helium age. The most likely reason for that is a loss of helium which escapes to the atmosphere due to insufficient aquitard confining capacity. In such cases the sum of

accumulated helium is not equal to its total bulk emanation. The role of confining regional scale aquifers is the most important factor considering this approach.

Groundwater residence times in intermediate and deep aquifers are increase with depth (Fig. 7.6). Oldest groundwater age is obtained using radio krypton tracer. Particle tracking and ^{4}He dating results show good correlation and are significantly younger as compared with radio krypton method in most sites. Linear equations of age correlation vs. depth are presented in Fig. 7.6.

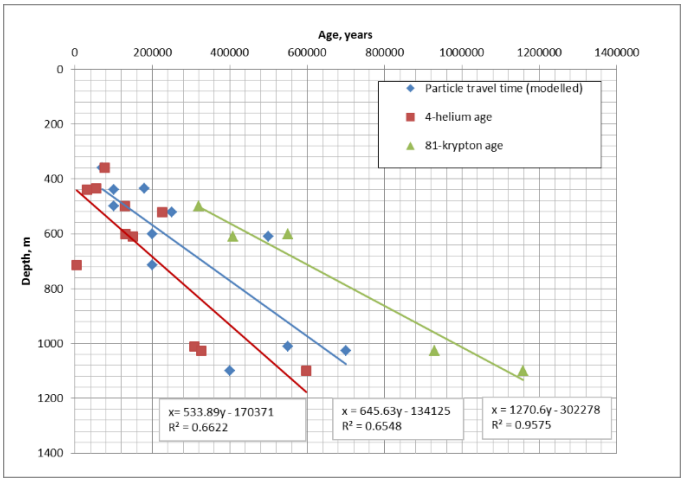

Fig. 7.6. Intermediate and deep BAB aquifers groundwater age distribution in depth.
Linear groundwater age trends are plotted for ^{4}He, ^{81}Kr and particle travel time dating results

The greatest differences of groundwater dating results are in deep (>1000 m) aquifers where ^{81}Kr obtained age is more than 2 times greater compared to helium and particle tracking methods. These aquifers are well confined with at least one regional scale aquitards. The differences between ages could be explained by reduced helium amount in aquifer. It is most likely that helium escapes deep aquifers through tectonic faults and diffuses upwards. Modeled particles tracking results are slightly higher than ^{4}He and lower than radio krypton. Unlike ^{4}He, radio krypton and particle track paths are moved mostly on lateral flow towards discharge. Modeled aquifers are smooth, without any geological structures which can immobilize groundwater, therefore radio krypton dating shows more stagnant groundwater.

Particle travel time and ^{4}He age are very similar in the Lithuania intermediate aquifers (see Table 7.3). Intermediate depth of Estonian and Latvian groundwater show very young ^{4}He age compared to radio krypton and particle travel time. Structural features of intermediate aquifers located in the Lithuanian-Poland Trough may result in higher accumulation of helium than on the Saldus-Riga-Pskov Ridge (Latvia) and southern Estonian High. Uneven distribution of uranium and thorium in crystalline basement could partly explain low helium content in Latvia and Estonia as well, yet this hypothesis is inconclusive because elevated content of radioactive elements are in many places of the BAB basement (Juodkazis and Tibar, 1989; Mokrik et al., 2002; Raudsep, 1997). High helium values in groundwater reservoirs coincide with a crystalline basement deformation zone near Rapakivi granite massifs (Juodkazis and Tibar, 1989; Mokrik, 2003; Mokrik et al., 2002; Raudsep, 1997). Two sites in Lithuania Lower-Middle Devonian aquifer system show 3 times younger ^{4}He age than particle track: Likėnai (well No. 11978) and Rokiškis (well No. 12349).

7.4.2. Isotope-geochemistry anomalies of groundwater, their ages and origin

Groundwater of deep aquifers in Lithuania and Latvia (Fig. 7.7, a) are usually enriched with oxygen-18 and deuterium isotopes in respect to the current modern water in shallow aquifers (δ^{18}O –11.2 to –10.5‰). Utmost enrichment is in deep brines, where δ^{18}O varies between –5.8 to –4.4 per mil. A deuterium excess could be explained by the evaporation factor, which took place during the brine evolution. Other hypotheses could suggest that groundwater isotope fractionation occurs by means of ultrafiltration through the thick aquitards. Deep groundwater age is from a few hundred thousand to more than a million years old, which is sufficient for a significant stable isotope fractionation due to

the ultrafiltration (Mokrik, 2003). Evaporation trend and enrichment of stable isotopes are shown in Fig. 7.7, a. Stable isotope values of groundwater collected near the tectonic faults fall exactly between modern freshwater and brine, as do one intermediate aquifer site (well No. 47543, Palanga). This supports opinion that groundwater in these hydrogeological conditions is formed by means of binary mixing, brine groundwater discharge into freshwater aquifers (Gregorauskas et al., 2017; Juodkazis, 2003, 1989; Mažeika, 1999; Zuzevičius, 2010; Zuzevicius et al., 2007).

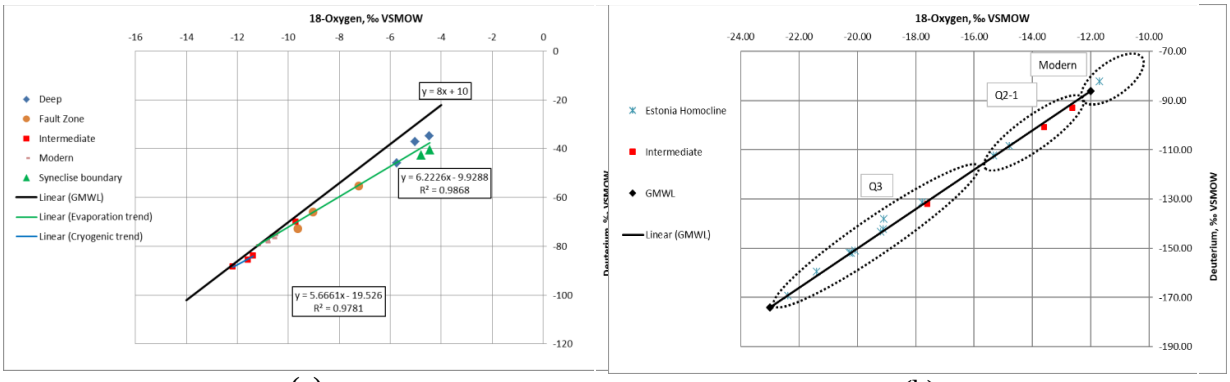

(a) (b)

Fig. 7.7. (a) Craig diagram of the BAB Lithuanian and Latvian groundwater. Green line represents evaporation trend, blue line – cryogenic trend. (b) Craig diagram of the BAB Estonian groundwater. Estimated groundwater formation periods (dotted circles) Q3 – the Late Pleistocene, Q2-1 – the Early-Middle Pleistocene, Modern – modern meteoric water recharge

A few sites of intermediate aquifer groundwater located in northern Lithuania are slightly depleted with stable isotopes ($\delta^{18}O$ –11.6 to –12.2‰). A minor deuterium excess is observable. A few hypotheses could be forwarded to explain this phenomenon. Depletion of stable isotopes could be recharge of glacial meltwater or caused by permafrost induced Rayleigh distillation (Clark and Fritz, 1997; Lehmann and Siegenthaler, 1991; O'Neil, 1968). Based on groundwater age, it is suggested that Likėnai and Rokiškis groundwater were formed during the Pleistocene.

The highest accumulation rates of helium in BAB deep aquifers are located near the Baltic Sea coast and islands, lowland areas and of lakes or rivers valleys where groundwater flow is from above tightly protected from meteoric water leakage and transected by wide low amplitude fault system networks, which are able to reduce or interrupt regional flow path. Radiogenic helium flux from crystalline basement at local level have good conditions for accumulation below regional confining aquitard layers situated reservoir traps depending on hydraulic features of aquifers. High helium values in groundwater reservoirs coincide with a deformation zone in the crystalline basement and dipping separated steep fault blocks transecting the sedimentary cover.

The helium age obtained in the intermediate and deep groundwater of the BAB is significantly lower than radio krypton dating results: ages differ 2–3 times. An aggregate helium age is best fitted to correct the age of the deepest sedimentary aquifer groundwater because of the loss of helium into overlaying aquifers. A sufficient confining capacity of regional aquitards is the most important factor for obtaining reliable aggregate helium age. Modeled particle travel trajectory and atmospheric origin ^{81}Kr pathway should be similar in the well confined aquifer system, but radio krypton reveals significantly older groundwater. This is due to vertical fault zones interrupting lateral groundwater flow in the BAB while numerical model is neglected that. Absence of fault zones in numerical model should be reflected by fault zone geometry and certain aperture or barrier parameters for layers. Noteworthy that the diffusive loss of ^{81}Kr to stagnant water reservoir may be dispersion, which mixes water masses of different ages that might impact groundwater ages deduced from radio krypton content.

In the eastern part of Lithuania for borehole no. 50423, which are located near the Ignalina NPP radio krypton dating age is equal to 319 ka and the helium noble gas age is 129 ka. To improve the reliability of steady and transient states of 3D groundwater flow model calibration, the helium and radio krypton isotopic ages of deep groundwater were compared to the MODPATH modeled times of elementary particle tracking for all BAB. The modeled particle travel time from the research area on

the Belarus-Masurian Anteclise up to Ignalina NPP site is 100 ka. In the eastern part of Lithuania, low helium values in deep groundwater are related to ancient deformation zones in the crystalline basement.

7.5. Conclusion

Within the IAEA Research Program F33022 workplan, the main aim for Lithuania was to prepare a new approach of deep aquifer investigation that will be focused on use of wide complex of environmental isotopes, noble gases, groundwater chemistry and hydraulic data via coupled analysis of groundwater flow numerical models.

The shallow groundwater analysis of monitored tritium trend and age data in the southeastern part of Lithuania shows a close to the equilibrium state with precipitation. Shallow groundwater is affected by the leakage from underlying aquifers in the river valleys sites. These results are supported with conventional tritium (data collected during 1980–2012), and $^{3}H/^{3}He$ obtained ages (data collected during 2017). The difference between ages obtained by these methods varies 8–22 percent and could be related to water sampling time. Monitored groundwater tritium activity gradients show that the main decrease rate factor is radioactive tritium decay process, which is affected by mixing of their concentrations dynamic in precipitation and groundwater reserves during approximately 50 years.

During 40 years we had studied dissolved in groundwater helium gas concentration of boreholes and their distribution peculiarities in the Baltic Artesian Basin using the INGEM-1 device. At the Institute of Geosciences of Vilnius University in 2016–2019, the numerical 3D steady-state and transient groundwater models of the BAB were created and calibrated with groundwater head and hydraulic parameters data of boreholes. In 2013–2017, radio krypton age was studied from samples of seven boreholes of deep groundwater using ATTA method (Gerber et al., 2017). In Lithuanian eastern part for well no. 50423, which is located near the Ignalina NPP shows estimated radio krypton age of 319 ka. Helium noble gas age and modeled particle travel time is 129 and 100 ka correspondingly. To improve the reliability of steady and transient states 3D groundwater flow model calibration, the helium and radio krypton isotopic age of deep groundwater were compared to the MODPATH modeled times of elementary particle tracking for all BAB. High helium values in groundwater reservoirs coincide with deformation zones in the crystalline basement and dipping separated steep fault blocks transecting the sedimentary cover.

Acknowledgements

We would like to thank LGS (Lithuanian Geological Survey) staff for assistance in sampling campaigns. We are grateful to colleagues at the Tallinn Technology University laboratory for analysing the chemical and isotope content.

References

Clark, I., Fritz, P., 1997. The environmental isotopes, in: Environmental Isotopes in Hydrogeology. p. 328. https://doi.org/10.1002/047147844X.gw211

Craig, H., 1961. Isotopic variations in meteoric waters. Science (80-.). 133, 1702–1703. https://doi.org/10.1126/science.133.3465.1702

Gerber, C., Vaikmäe, R., Aeschbach, W., Babre, A., Jiang, W., Leuenberger, M., Lu, Z.T., Mokrik, R., Müller, P., Raidla, V., Saks, T., Waber, H.N., Weissbach, T., Zappala, J.C., Purtschert, R., 2017. Using 81Kr and noble gases to characterize and date groundwater and brines in the Baltic Artesian Basin on the one-million-year timescale. Geochim. Cosmochim. Acta 205, 187–210. https://doi.org/10.1016/j.gca.2017.01.033

Gregorauskas, M., Kaušinis, K., Bujanauskas, M., Samalavičius, V., Mokrik, R., 2017. Cenomanio-apatinės kreidos sluoksnio požeminio vandens išteklių ir hidrocheminių anomalijų modelinis įvertinimas. Geol. Geogr. 3. https://doi.org/10.6001/geol-geogr.v3i2.3538

Juodkazis, V., 2003. Regional hydrogeology foundations, In Lithuan. ed. Vilnius University Publishing House, Vilnius.

Juodkazis, V., 1989. Regional hydrogeology of the Baltic region, In russian. ed. Mokslas, Vilnius.

Juodkazis, V., 1980. Hydrogeological Map of the Pre-quaternary Deposits of the Soviet Baltic Republics. Ministry of Geology of the USSR.
Juodkazis, V., Tibar, K., 1989. Helium in groundwater on the northern flank of the Baltic Artesian Basin. Int. Geol. Rev. 31, 736–743.
Lehmann, M., Siegenthaler, U., 1991. Equilibrium oxygen- and hydrogen-isotope fractionation between ice and water. J. Glaciol. 37, 23–26. https://doi.org/10.3189/S0022143000042751
Mažeika, J., 1999. Regularities of Radionuclide Migration and Transformation in Lithuanian Geological Environment. Vilnius University.
Mokrik, R., 2003. The paleohydrogeology of the Baltic basin. Vilnius University Publishing House, Vilnius.
Mokrik, R., 1997. The Palaeohydrogeology of the Baltic Basin. Vendian and Cambrian. Tartu University Press.
Mokrik, R., Juodkazis, V., Štuopis, A., Mažeika, J., 2014. Isotope geochemistry and modelling of the multi-aquifer system in the eastern part of Lithuania. Hydrogeol. J. 22, 925–941. https://doi.org/10.1007/s10040-014-1120-6
Mokrik, R., Puura, V., Floden, T., Petkevičius, R., 2002. Peculiarities of helium distribution in the Baltic Basin. Litosfera 6, 121–123.
O'Neil, J.R., 1968. Hydrogen and oxygen isotope fractionation between ice and water. J. Phys. Chem. https://doi.org/10.1021/j100856a060
Pärn, J., Raidla, V., Vaikmäe, R., Martma, T., Ivask, J., Mokrik, R., Erg, K., 2016. The recharge of glacial meltwater and its influence on the geochemical evolution of groundwater in the Ordovician-Cambrian aquifer system, northern part of the Baltic Artesian Basin. Appl. Geochemistry 72, 125–135. https://doi.org/10.1016/j.apgeochem.2016.07.007
Raidla, V., Kern, Z., Pärn, J., Babre, A., Erg, K., Ivask, J., Kalvāns, A., Kohán, B., Lelgus, M., Martma, T., Mokrik, R., Popovs, K., Vaikmäe, R., 2016. A $\delta^{18}O$ isoscape for the shallow groundwater in the Baltic Artesian Basin. J. Hydrol. 542, 254–267. https://doi.org/10.1016/j.jhydrol.2016.09.004
Raudsep, R., 1997. Mineral occurrence, in: Raukas, A., Teedumäe, A. (Eds.), Geology and Mineral Resources of Estonia. Estonian Academy Publishers, Tallinn, p. 436.
Rozanski, K., Zuber, A., 2000. Glacial infiltration in Europe – myth or reality. Przegląd Geol. 48, 796–803.
Samalavičius, V., Mokrik, R., 2016. Tritium activity trend formation in groundwater of Quaternary aquifer system, south-eastern Lithuania. Geol. Geogr. 2, 173–181. https://doi.org/https://doi.org/10.6001/geol-geogr.v2i4.3399
Štuopis, A., Juodkazis, V., Mokrik, R., 2012. The quaternary aquifer system flow model by chemical and tritium isotope data: Case of south-east Lithuania. Baltica 25, 91–98. https://doi.org/10.5200/baltica.2012.25.09
Torgersen, T., Stute, M., 2013. Helium (and other noble gases) as a tool for the understanding long time-scale groundwater transport, in: ISOTOPE METHODS FOR DATING OLD GROUNDWATER. International Atomic Energy Agency, Vienna, p. 376.
Virbulis, J., Bethers, U., Saks, T., Sennikovs, J., Timuhins, A., 2013. Hydrogeological model of the Baltic Artesian Basin. Hydrogeol. J. 21, 845–862. https://doi.org/10.1007/s10040-013-0970-7
Zuzevičius, A., 2010. The groundwater dynamics in the southern part of the Baltic artesian Basinduring the Late Pleistocene. Baltica 23, 1–12.
Zuzevicius, A., Mažeika, J., Baltrunas, V., 2007. A model of Brakish groundwater formation in the Nemunas River Valley. Geologija 60, 63–75.

MOROCCO

Centre National de l'Energie, des Sciences et des Techniques Nucléaires (CNESTEN)
https://www.cnesten.org.ma/index.php

8. USING ISOTOPE HYDROLOGY TOOL TO CHARACTERIZE GROUNDWATER SYSTEMS IN THE VICINITY OF SIDI BOULBRA NUCLEAR POWER PLANT SITE OF MOROCCO

M. QURTOBI[1], F. RAIBI[1], T. EL GHALI[1], U. SARAVANA KUMAR[2]

[1] Centre National de l'Energie, des Sciences et des Techniques Nucléaires / Rabat, MOROCCO
[2] Isotope Hydrology Section. International Atomic Energy Agency / Vienna, AUSTRIA

Abstract

Sidi Boulbra site, selected to host the first Moroccan Nuclear Power Plant (NPP), is located in the south-western part of Morocco and largely open to the Atlantic Ocean. In this area, the groundwater constitutes a vital water source for the population. The groundwater is used for water supply and development of traditional agriculture. The groundwater is intensively pumped for the aforesaid purposes, which increases its vulnerability to salinization and affects its quality.

The specific objective of this research is to assess and improve the use of environmental isotopes to investigate the groundwater recharge source(s), recharge area, recharge and discharge relationships, to determine groundwater flow directions, ages and velocity in the proximity of Sidi Boulbra NPP, in order to define transport paths and travel times of radioactive material to reach the source of consumption from the point of release in case of an accident.

A total of 23 water samples were collected during two sampling campaigns, carried out in 2017 and 2018, including 11 samples from upper shallow aquifer and 12 samples from lower deep aquifer. Two groups of groundwater are distinguished with stable isotope of water. The difference observed is due mostly to the difference in altitude of the recharge area. The ^{3}H data from shallow and deep aquifers, show very low values ranging from 0.3 to 0.9 TU. The activities of carbon-14 determined for 6 boreholes are relatively low, within a range of 28 to 64 pMC. According to correction models, groundwater sampled have typical apparent older ages of 4,000 to 10,000 years BP. Groundwater is expected to flow from SSE to NNW and discharging along the Atlantic coast of Sidi Boulbra with a velocity ranging from 0.41 to 1.88 m/y with an average value of about one meter per year.

Keywords: coastal aquifers, hydrochemistry, isotope techniques, groundwater age, Morocco.

8.1. Overview and historical development of the Moroccan NPP project

Morocco has very limited local resources of energy and depends almost totally on external sources for its energy supply.

In the framework of the policy of diversification of energy primary sources and in compliance with governmental orientations, the National Office of Water and Electricity (ONEE) considers the nuclear power option as one potential technically viable solution able to meet the future electrical energy needs of Morocco.

Sidi Boulbra site, located on the Atlantic coast between the cities of Safi and Essaouira (300 km south of Casablanca) (Fig. 8.1), as the appropriate and qualified site able to receive the first Moroccan NPP under the required nuclear safety conditions. This conclusion was validated by IAEA experts after an expert mission conducted in September 1994.

Currently, the Sidi Boulbra site is being subjected to a continuous monitoring programme, the goal of which is to monitor the evolution of the site characteristics in the relevant areas (hydrology, meteorology, demography, industrial environment, etc.).

After thirty years, the proposed research aims, is to update characterization of groundwater resources in the vicinity of Sidi Boulbra site, using isotope hydrology and conventional techniques.

Indeed, in the context of semi-arid climate, groundwater represents a strategic resource that can sustain socio-economic development efforts. However, increasing abstractions may lead to depletion and degradation of these resources. The Sidi Boulbra site is a case where such phenomenon had reach drastic levels with major socio-economic consequences. The groundwater in this region is intensively pumped for the domestics and agricultural purposes, which increases its vulnerability to salinization and consequently affects its quality.

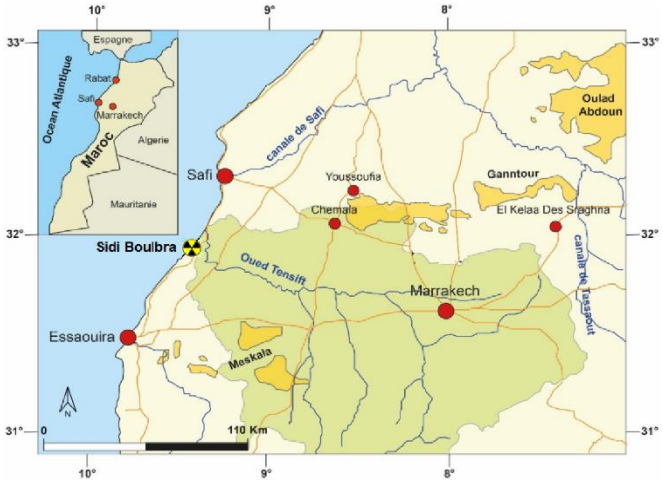

Fig. 8.1. Location of Sidi Boulbra site within the Moroccan map

The specific objectives of this study are:

✓ use of conventional techniques to better understand the hydrogeological conditions at the vicinity of Sidi Boulbra site, by determining type of water, origin of mineralization and processes responsible for groundwater mineralization;

✓ use of environmental isotopes to investigate origin of recharge and discharge relationships;

✓ use of noble gases, tritium and carbone-14 to determine the water age and velocity in the vicinity of Sidi Boulbra site, in order to define transport paths and travel times of radioactive material to reach the source of consumption from the point of release in case of an accident.

8.2. Introduction and site description

Sidi Boulbra NPP site is a part of Akermoud coastal plain, which extends along the Atlantic Ocean coast on a wide strip of 15 km and lengthy of 45 km (Fig. 8.2). It's limited in the east and south-east by jbel Hadid and jbel Kourati mountains, in the north and north-east by the Tensift Wadi river and opening to the Atlantic Ocean in the west. The Akermoud plain has a population of 10000 inhabitants and is predominantly rural.

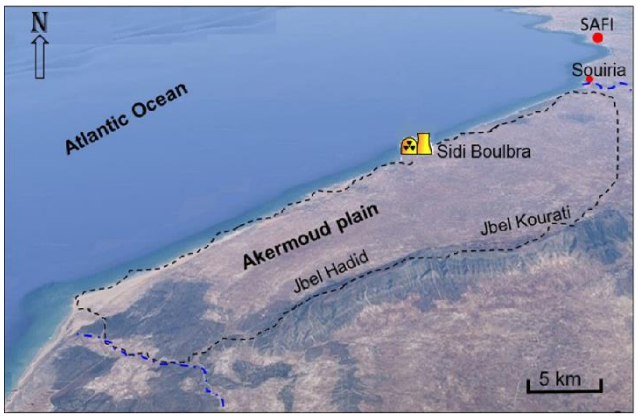

Fig. 8.2. Location of Sidi Boulbra site within the coastal plain of Akermoud

Sidi Boulbra site has a warm Mediterranean climate with dry summer according to the Köppen-Geiger classification (Fig. 8.3). The mean annual temperature in Essaouira is 17.8 °C and the average rainfall is 251.1 mm occurring during the short cold season (October to April). The average of potential evaporation ranges from 780 mm in the mountains and near the Atlantic coast to 920 mm in the plain. The decrease of winter precipitation may have resulted in a degradation of the soil moisture content and a depletion of the groundwater level. The climatic pattern in this area is frequently characterized by a relatively "cool" dry season, followed by a relatively "hot" dry season, and ultimately by a "moderate" rainy season. In general, there are significant diurnal temperature

fluctuations within these seasons. Quite often, during the "cool" dry season, these diurnal temperature fluctuations restrict the growth of plant species.

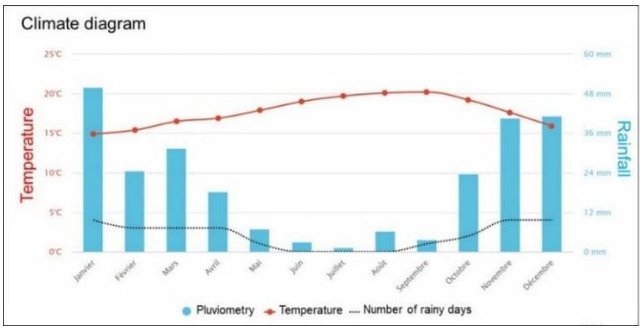

Fig. 8.3. Climatic diagram of Essaouira city located at 45 km south of study area

The geological map of the study area (Fig. 8.4) shows that the geological formations consist in Tertiary and Quaternary sedimentation. The sedimentary units consist mainly in detrital deposits of Upper Miocene, Pliocene and Quaternary ages, which overlay uncomfortably the middle Miocene bed rock.

The Triassic deposits crops out in the Eastern and Southern parts of the region, and marl sediments of Lower Cretaceous to Cenomanian overlie the Jurassic layers composed by carbonate rocks, with presence of Senonian gypsy marls covered by the Plio-Quaternary detrital deposits of sands, conglomerates and sandstones (Duffaud et al, 1966). The geological structures delineate a syncline bordered by the Hadid and Kourati diapirs, of Triassic age, outcropping east and south.

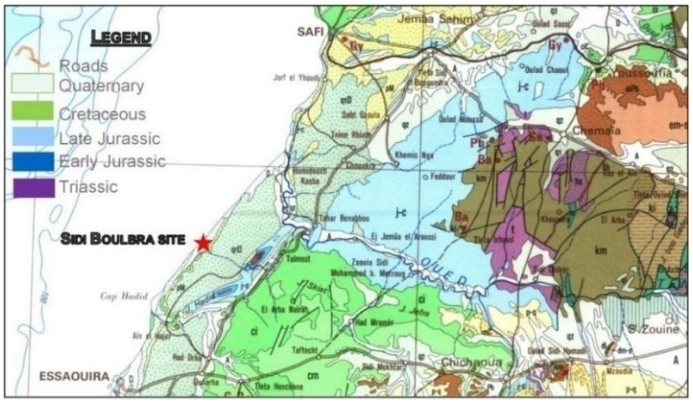

Fig. 8.4. Geological map of study area (extract from the geological map of Morocco, 1985)

In this area, the groundwater constitutes a vital water source for the population. The reservoir water is used for water supply and development of agriculture. The pumping of the water from reservoirs is ensured either by motor-driven pumps or by tanks. The groundwater is intensively pumped for aforesaid purposes, which increases its vulnerability to salinization and affects its quality (Fadili, A. et al, 2015).

From the hydrogeological point of view, two main aquifers constitute the system (Fig. 8.5):

✓ The Mio-Plio-Quaternary upper aquifer represents an unconfined aquifer which is mainly composed of sand, sandstone and conglomerates, whose thickness ranges from 15 to 65 m and a hydraulic conductivity by porosity of about $3.2*10^{-2}$ m/s. This aquifer provides the bulk of the water supply to the population. It's crops out between the sea level and 300 m above sea level (a.s.l).

✓ The Cenomanian-Turonian lower aquifer is mainly calco-dolomitic. This carbonate formation represents a confined and discontinuous aquifer at a depth of more than 80 m. However, it becomes unconfined and outcrops locally at the Jbel Hadid and Jbel Kourati Mountains between 300 and 600 m a.s.l. The thickness ranges from 80 to 180 m. This carbonate formation has high porosity and permeability due to fissures and karstification. This aquifer is tapped by many boreholes with artesian flow.

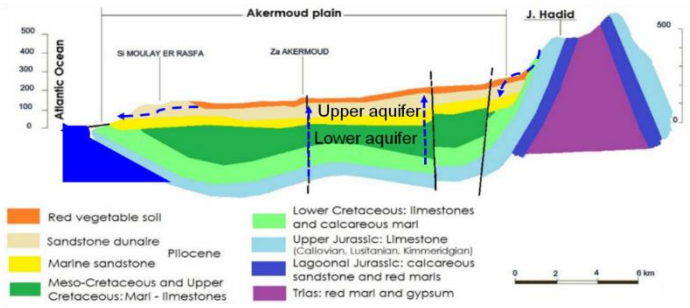

Fig. 8.5. Schematic cross section illustrating the main aquifers of the coastal plain of Akermoud

Fig. 8.6. Potentiometric map (in metre a.s.l) of Plio-Quaternary upper aquifer, showing the general groundwater flow directions in coastal plain of Akermoud in 2017–2018

The piezometric head survey of the Plio-Quaternary upper aquifer, shows a groundwater flow direction ESE to WNW from Jbel Hadid and Jbel Kourati mountains toward the Atlantic Ocean, which constitute the natural discharge area of the aquifers (Fig. 8.6).

The major drainage axis appears along the river beds, which have good permeability and constitute an appropriate site for numerous pumping wells. This structure represents the area where the risk of salinization of the groundwater by seawater intrusion is high, in particular in the coastal areas fringe.

The piezometric map reveals that the upper aquifer is recharged by recent flood water infiltration in the plain of Akermoud and by direct infiltration of rain water through the local carbonate outcrops of the basin and partially from vertical leakage of the lower aquifer.

8.3. Method and sampling analyses

In order to improve the management of the water resources, to better understand the hydrological functioning and to define the relationship between sea water and groundwater of the aquifers system in the coastal plain of Akermoud, an investigation of the sources and dynamics of groundwater is being conducted with geochemical tracers (Major and trace elements) and environmental isotopes including $\delta^{18}O$, $\delta^{2}H$, ^{3}H, ^{14}C and $^{3}H/^{3}He$.

Two sampling campaigns for the geochemical and isotopic analyses were carried out during august 2017 and during November 2018. A total of 23 samples were collected from Sidi Boulbra NPP area (Fig. 8.7 and Table 8.1). The pumping method was used for collection of water samples. The measurements of pH, temperature and electrical conductivity (EC) were performed in the field. Water samples were collected in 1000 ml polyethylene bottles with poly-seal caps for major elements after the stabilization of pH, E.C and temperature.

Chemical analyses and isotopic measurements were determined in the Isotope Laboratories of the National Centre for Nuclear Energy, Science and Techniques, (Morocco). Analytical error as inferred from the balance between cations and anions did not exceed 5%. The noble gases analysis ($^{3}H/^{3}He$) was conducted in the IAEA Isotope Hydrology Section Laboratory (Vienna, Austria). Major elements (Cl^{-}, SO_4^{2-}, NO_3^{-}, Na^{+}, Mg^{2+}, Ca^{2+} and K^{+}) analysed using ion liquid chromatography (HPILC, Dionex DX100). The overall detection limit for ions was 0.04 mg/L and HCO_3^{-} concentrations were analysed by titration using 0.1 N HCl acid. The ionic balance for all samples is within ± 5%. Trace elements were performed using Inductively Coupled Plasma Mass Spectrometer (ICP-MS X-Series 2).

Stable isotope ratio ($^{18}O/^{16}O$, $^{2}H/^{1}H$) analyses were performed by using the Laser Absorption Spectrometry measurements LGR DLT 100 (Penna et al., 2010). Analyses are reported in ‰ versus VSMOW standard (Vienna-Standard Mean Oceanic Water).

Six groundwater samples were selected to be analysed for Carbon-14 dating activities. Precipitation of $BaCO_3$ from groundwater samples was done in the field. ^{14}C activities were determined by scintillation counting on C_6H_6 (Fontes, 1972; Stuiver and Polach, 1977).

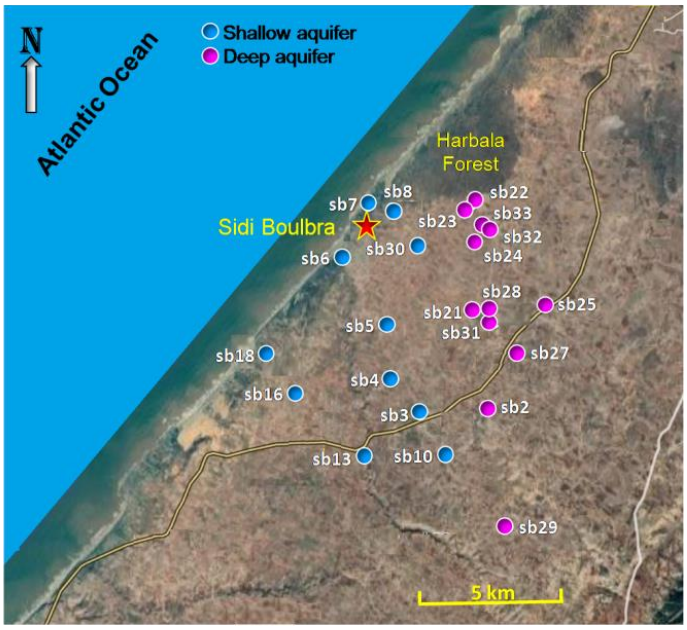

Fig. 8.7. Sampling points of wells and boreholes in Akermoud coastal plain, sorted by type of aquifers (defined as water groups, see Table 8.1)

Eighteen samples were analyzed for Tritium content using electrolytic enrichment and liquid scintillation spectrometry (Taylor, 1976). ^{3}H levels are expressed in Tritium Units (TU). One TU is defined as the isotope ratio $^{3}H/^{1}H=10^{-18}$. Six samples sb5, sb13 and sb2, sb21, sb29, sb33 along the flow lines of upper and lower aquifers respectively, were analysed for ^{14}C. Results are expressed in percent modern carbon (pmC), representing the proportion of ^{14}C activity in the sample with respect to the ^{14}C standard. Standard activity is defined as 95% of the activity of Oxalic Acid I in AD 1950 (Mook *et al*. 1999), and 120 pmC = 271.2 Bq/kg C. (Table 8.2) presents the ^{14}C values of the analysed samples and their apparent age. The analytical precision of measurement for stable isotope and radioactive analyses were ±0.2 ‰ for $\delta^{18}O$, ±1‰ for $\delta^{2}H$, ±0.2 TU for ^{3}H and 0.5 pmC for ^{14}C.

8.4. Results and discussion

8.4.1. Groundwater hydrochemical facies

Groundwater hydrochemical facies depend on lithology, residence time and regional flow pattern of water (Jamshidzadeh and Mirbagheri, 2011). The most known method for determining groundwater chemical facies is Piper diagram (Piper, 1944).

Chemical analyzes results of sampled water are projected on two ternary triangles, either for cations or anions, which extend to a third diagram diamond shaped. Results of chemical analyses can be interpreted to identify groundwater hydrochemical facies as well as the possibility of freshwater seawater mixture (Arslan et al., 2012; Singhal and Gupta, 2010; Tomaszkiewicz et al., 2014). Hydrochemical results from groundwater samples of Sidi Boulbra NPP area were plotted in Piper diagram (Fig. 8.8). The most affected wells by seawater intrusion are the upper aquifer samples, which are characterized by chloride and sodium water types. As demonstrated in Table 8.1, all wells of this part of the upper aquifer have high values of ECs, which vary from 1400 to 4200 µS/cm with dominance of Na^{+} and Cl^{-} ions. Almost of these wells are located in downstream at about 0.5 km from the coastal fringe (see Fig. 8.7).

Table 8.1. In situ measurement, geochemical and isotopic data of groundwater samples in the Sidi Boulbra NPP area (<LOD: below limit of detection)

Aquifer type	Nom	pH	Depth (m)	EC (µS/cm)	T (°C)	HCO_3^- (mg/l)	Cl^- (mg/l)	NO_3- (mg/l)	SO_4^{2-} (mg/l)	Na^+ (mg/l)	K^+ (mg/l)	Ca^{2+} (mg/l)	Mg^{2+} (mg/l)	^{18}O (‰ (VSMOW)	^{2}H (‰ (VSMOW)	^{3}H (TU)	^{14}C (pmC)	^{13}C (‰ (VPDB)
Upper aquifer	SB03	7.23	39	2200	22.6	233.01	407.11	79.14	188.13	212.11	1.81	125.0	46.34	-4.3	-24.5	0.78		
	SB04	7.86	43	2570	22.3	286.73	382.93	58.93	307.11	302.84	3.28	156.6	61.50	-4.36	-23.9	0.63		
	SB05	7.70	38	2210	22.9	259.35	418.66	60.51	199.87	219.17	1.95	107.1	38.24	-4.34	-23.9	0.84	53.1	-11.6
	SB06	7.49	15	3280	22.9	250.12	805.92	66.06	274.06	508.57	7.26	168.4	79.17	-4.19	-24.4	0.97		
	SB07	7.57	20	4220	22.0	311.18	997.86	54.54	394.10	680.01	12.01	126.4	75.99	-4.33	-24.4	0.93		
	SB08	7.65	40	3220	22.1	325.76	901.62	71.73	291.84	520.69	4.64	121.9	57.32	-4.28	-24.5	1.06		
	SB10	7.92	56	2540	22.4	222.77	404.73	75.09	245.76	226.82	3.36	181.5	61.82	-4.39	-24.2	0.74		
	SB13	7.40	65	2910	22.0	256.23	589.33	49.62	404.82	333.25	3.83	193.8	58.87	-4.39	-24.6	0.92	44.0	-11.8
	SB16	7.80	32	1379	21.5	301.39	538.28	82.25	230.45	267.49	17.67	55.9	35.24	-4.22	-24.2	1.36		
	SB18	7.40	60	3350	22.8	372.21	558.91	67.52	424.52	428.07	3.60	72.0	36.32	-4.29	-23.7	1.02		
	SB30	7.24	80	2360	22.1	405.75	629.86	61.73	371.89	439.55	4.42	151.9	67.31	-4.48	-25.7	0.75		
Lower aquifer	SB2	7.28	160	1351	24.6	225.71	283.81	57.2	232.33	154.96	1.92	86.1	34.56	-5.38	-32.5	<LOD	54.0	-11.8
	SB21	7.21	130	2220	24.1	262.32	362.35	43.4	347.66	206.92	2.10	139.0	55.58	-5.01	-30.1	<LOD	51.6	-11.3
	SB22	7.91	84	2480	24	253.84	459.21	45.5	256.28	229.61	3.14	151.3	55.94	-5.15	-31.3	0.24		
	SB23	7.82	94	1993	23.5	268.43	350.39	40.8	168.20	199.23	1.66	113.2	35.81	-5.19	-31.9	<LOD		
	SB24	7.94	126	2410	23.8	239.17	460.52	46.2	246.33	240.17	2.37	136.3	50.97	-5.08	-30.7	0.75		
	SB25	7.88	126	2140	24.7	225.74	415.43	29.7	206.86	212.20	1.83	120.6	48.23	-5.36	-33.2	0.69		
	SB27	8.03	130	2420	24.6	228.87	429.66	32.2	388.14	232.55	2.32	168.6	60.18	-5.43	-33.5	0.47		
	SB28	7.85	140	2440	24.2	242.83	425.12	37.3	389.9	224.28	3.47	144.2	50.13	-5.18	-31.4	<LOD		
	SB29	7.39	175	1107	24.4	249.60	275.82	41.2	271.8	160.58	2.19	95.5	55.77	-5.33	-32.1	<LOD	28.6	-11.7
	SB31	7.18	150	2140	22.1	391.51	441.37	31.5	326.7	281.83	4.44	136.2	78.13	-5.34	-32.9	<LOD		
	SB32	7.29	75	1798	21.8	241.56	415.40	42.2	248.1	209.17	2.26	143.8	48.35	-5.05	-31.2	<LOD		
	SB33	7.36	136	1722	23.5	259.33	401.24	43.5	215.1	208.23	2.62	129.2	45.10	-5.17	-31.6	0.22	64.3	-11.2

Cations diagram indicates a water mixture between different aquifers and shows enrichment in Na^+ and K^+ passing from lower aquifer towards the upper aquifer. In addition, anions diagram suggests a migration of points to the chlorinated pole, which can be a consequence of seawater intrusion effect.

However, lower aquifer wells are primarily freshwater characterized by abundance of calcium, magnesium and bicarbonate ions with ECs, which range from 1100 to 2480 µS/cm (see Table 8.1). These wells are located in the East and the upstream parts of the area (recharge zone).

In the Piper diagram, it seems clear a hydrochemical evolution of groundwater samples from Sidi Boulbra NPP area, towards more Cl-Na (Fig. 8.8).

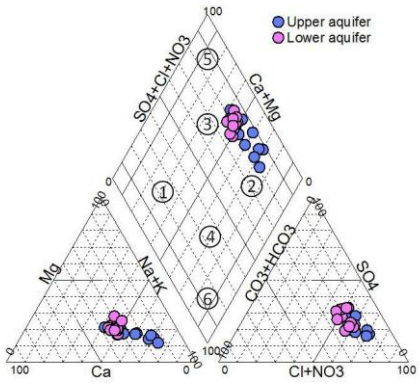

Fig. 8.8. Piper diagram of groundwater samples from Sidi Boulbra NPP area

Generally, we can classify the sample points in the piper diagram into 6 fields:

- ✓ Type 1. Ca-HCO_3;
- ✓ Type 2. Na-Cl;
- ✓ Type 3. Ca-Mg-Cl;
- ✓ Type 4.Ca-Na-HCO_3;
- ✓ Type 5. Ca-Cl;
- ✓ Type 6. Na-HCO_3.

In the present study water types were confined to the 2 and 3 types. Majority of the samples (52%) are plotted in the Na-Cl field and (48%) of the samples showed Ca-Mg-Cl type.

To better understand the hydrochemistry and comparing the water types, Chadha´s diagram was plotted (Fig. 8.9). In order to define the primary character of groundwater, the rectangular field is divided into eight sub-fields, each of which represents water types as given below in Table 8.2, Chadha (1999).

Table 8.2. Geochemical classification and hydrochemical parameters of groundwater (D. K. Chadha, 1999)

Classification groups		**Notations**
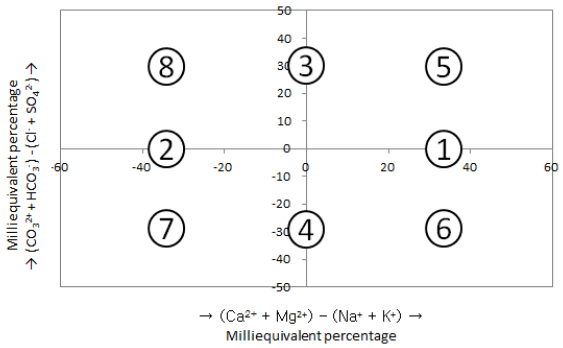	Fields	Water types
	1	Alkaline earths exceed alkali metals
	2	Alkali metals exceed alkaline earths
	3	weak acidic anions exceed strong acidic anions
	4	Strong acidic anions exceed weak strong acidic anions
	5	Alkaline earths and weak acidic anions exceed both alkali metals and strong anions, respectively. (Ca-Mg-HCO_3 type, Ca-Mg-dominant HCO_3 type, HCO_3-dominant Ca-Mg type)
	6	Alkaline earths exceed alkali metals and strong acidic anions exceed weak acidic anions (Ca-Mg-Cl type, Ca-Mg-dominant Cl type, Cl-dominant Ca-Mg type)
	7	Alkali metals exceed alkaline earths and strong acidic anions exceed weak acidic anions (Na-Cl type, Na_2SO_4-type, Na-dominant Cl type, Cl-dominant Na type)
	8	Alkali metals exceed alkaline earths and weak acidic anions exceed strong acidic anions (Na-HCO_3 type, Na-dominant HCO_3 type, HCO_3^- dominant Na type)

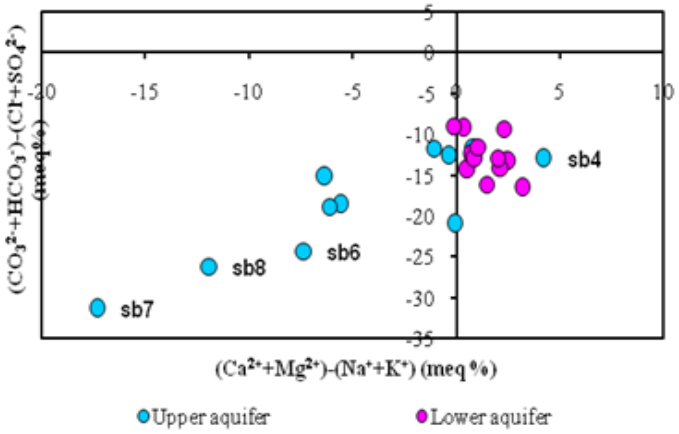

Fig. 8.9. Geochemical classification and hydrochemical parameters of groundwater from Sidi Boulbra NPP area (D. K. Chadha, 1999)

The tracing study of ion based on the Chadha diagram indicated that there is an interaction between the alkaline earths and alkali metals that originate from soil or rock interactions with strong acidic anions exceed weak acidic anions in groundwater as shown in Fig. 8.9. All the samples from lower and upper aquifer are confined to **6** and **7**th fields respectively. A majority of the samples from upper aquifer are plotted in the **7**th field, representing the ***Na-Cl*** type of water and the samples from lower aquifer are plotted in the **6**th field which represents a **Cl**-dominant **Ca–Mg** type waters. This is exactly similar to the results obtained from the piper plot diagram.

8.4.2. Hydrogeochemistry and controlling processes

8.4.2.1. Groundwater mineralization processes

To emphasize and to identify origin and processes contributing to groundwater mineralization, some plots of relations between major elements are presented.

The graph (Fig. 8.10, a) presents a correlation between K^+ and NO_3^- concentrations, and shows nitrate enrichment with respect to potassium accompanied by simultaneous increase of both ions with a correlation coefficient of 0.69. This result is due to K^+ fixation and NO_3^- release by the aquifer matrix (Nasher et al., 2013; Fadili et al., 2015), which reveals that groundwater contamination by nitrate ions as a consequence of human activities (Dutta et al., 1997; Kumar et al., 2006; Reddy, 2013; Fadili et al., 2015). Such findings are in agreement with literature ones, where nitrates ions are mainly generated by anthropogenic activities such as leachate, wastewater and agriculture activities (Park et al., 2005; Kass et al., 2005; Nasher et al., 2013; Reddy et al., 2013).

In addition, correlation between calcium and sulfate is plotted in Fig. 8.10, b, which shows two groups.

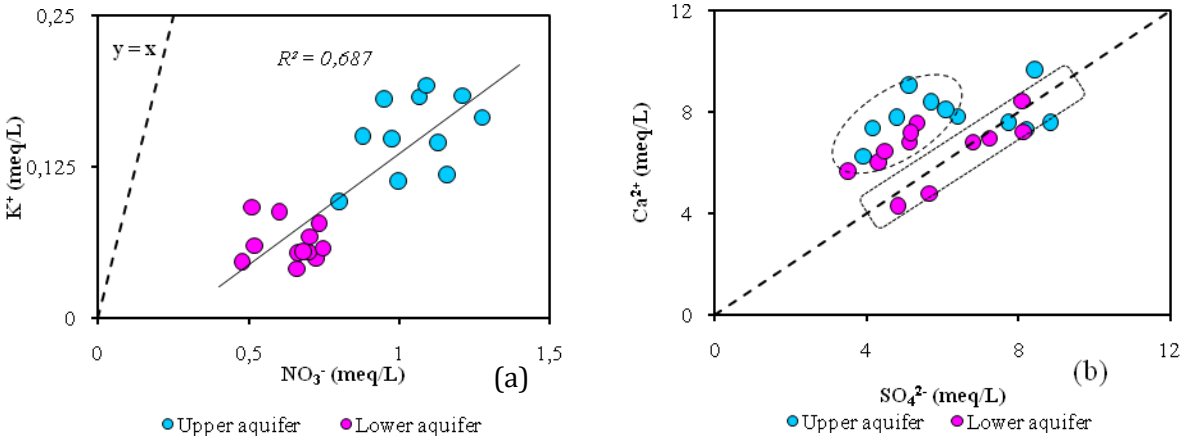

Fig. 8.10. Correlations between analyzed major elements: (a) K^+ vs NO_3^-, (b) Ca^{2+} vs SO_4^{2-}

The first group represents sample points plotting near the 1:1 line (gypsum dissolution line) and showing a simultaneous increase of calcium and sulfate ions. This pattern indicates the same origin of the mentioned ions which is the likely dissolution of gypsum and or anhydrite. Similarly, positive correlation between Ca^{2+} and SO_4^{2-} with a correlation coefficient of 0.53 implies that gypsum dissolution, present in cretaceous formations, can be further source of these elements in water (Awad et al., 2011; Lachaal et al., 2011; Marimon et al., 2013; Ledesma-Ruiz et al., 2015).

As confirmed by Fig. 8.11, the points representing the both aquifers samples fall either on, or just above 1 : 1 stoichiometric equilibrium line Ca^{2+} vs HCO_3^-. The abundance of carbonate rocks (sandy limestone of Cretaceous age) and the erosion rates in the central area of Sidi Boulbra NPP site, suggest that the dissolution of carbonate minerals may potentially add significant amounts of Ca^{2+} and Mg^{2+} to the groundwater of the lower and upper aquifers. The Mg^{2+}/Ca^{2+} ratio in these groundwaters is maintained at around of 0.43 to 0.96. This pattern is consistent with an equilibrium control governed by calcite mineral (Appelo and Postma, 1993).

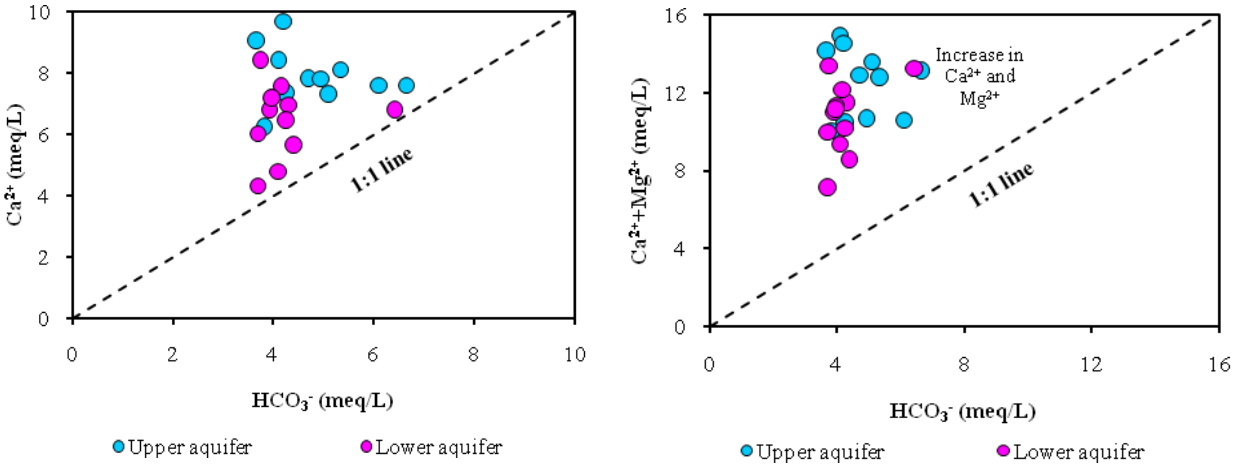

Fig. 8.11. Relationships between Ca^{2+}, Mg^{2+} and HCO_3^-

8.4.2.2. Use the relationships between major elements and Cl- to determine the origin of groundwater salinity

In order to determine possible mixture with seawater, Fig. 8.12 performs a correlation between major elements and Cl^- ions, which can characterize salinity origin and form a mixture tracer (Ako et al., 2012; Re et al., 2013; Xing et al., 2013).

The positive linear correlation indicates freshwater-saltwater mixture (FW-SW) (Mercado, 1985). Besides, major elements show different behavior with respect to FW-SW mixture line. Magnesium and calcium indicate enrichment, while bromides, sodium, sulfates, and potassium present depletion with respect to the mixture line. However, Ca^{2+} ions are in the upper side, whereas Na^+ ions are in the down side of freshwater-seawater mixing line. This result is due to cation exchange under seawater intrusion effect, which leads to Na^+ ions fixation in opposition to Ca^{2+} ions release by the aquifer clayey matrix as shown in Eq. (1) (Giambastiani et al., 2013; Srinivasamoorthy et al., 2013; Han et al., 2014).

$$Na^+ + \frac{1}{2}Ca^{2+} - X \rightarrow Na^+ - X + \frac{1}{2}Ca^{2+} \quad (1)$$

Furthermore, K^+ ions depletion is the consequence of its exchange with NO_3^- ions in the aquifer matrix as was demonstrated in Fig. 8.10, a.

Bromide ions show also depletion with respect to mixture line, suggesting that this element is provided from evaporation process rather than FW-SW mixture (Giambastiani et al., 2013).

Magnesium ions are abundant in carbonate and dolomite minerals that characterize coastal Akermoud aquifers. Their excess can be explained by its exchange with Na^+ under seawater intrusion effect.

Sulfate ions show depletion for most sampled wells. Such depletion is commonly observed in aquifers affected by saltwater intrusion (Andersen et al., 2005; Giambastiani et al., 2013).

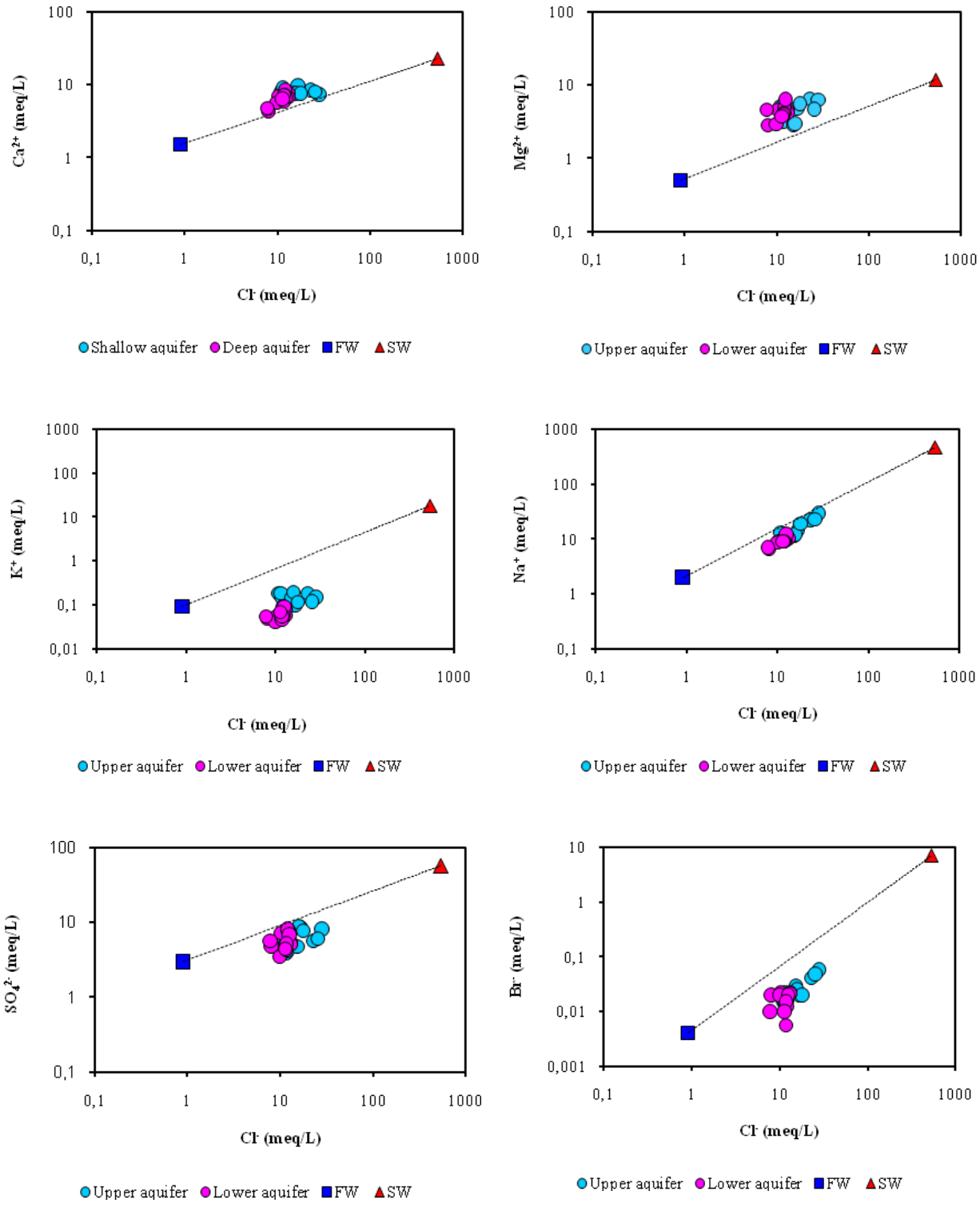

Fig. 8.12. Plot of major elements (Ca^{2+}, Mg^{2+}, K^+, Na^+, SO_4^{2-}, Br^-) as function of chloride ion (in meq/L)

8.4.2.3. Use the major elements ratio to trace source of groundwater salinity

Na^+/Cl^- ratio can characterize seawater presence in water table. Ratios lower than 0.86 characterize salinization associated with seawater intrusion (Vengosh et al., 1997; Askri, 2015). In this study, most groundwater samples have a Na^+/Cl^- ratio which range from 0.77 to 1.08, with a decrease trend versus Cl^- increase (57% of samples have a Na^+/Cl^- ration ≤ 0.86 and 43% of samples have a Na^+/Cl^- ratio > 0.86) (Fig. 8.13, a). This result may be due to seawater intrusion influence mainly in coastal fringe (Vengosh et al., 1997; Mondal et al., 2008; Singaraja et al., 2014).

Additionally, the use of bromide anion contents is an essential complement to chloride measurements in order to explain the salinity anomalies in groundwater. Chloride (Cl^-) and Bromide (Br^-) ions are considered as conservative elements in groundwater, which not participate either in ion exchange or redox reactions and not form insoluble precipitate (Davis et al., 1998; Daniele et al., 2011). Therefore, ratio (Cl^-/Br^-) can be used as a tracer to identify groundwater salinity origin (Alcalà and Custodio, 2008; Dror et al., 1999; Lorenzen et al., 2012; Giambastiani et al., 2013; Hofmann and Cartwright, 2013). However, constant and aligned Cl^-/Br^- ratio with seawater ratio indicates that Cl^- and Br^- ions have a marine origin. The Cl^-/Br^- ratio upper than 300 can be related to anthropogenic sources such as industrial wastewater or agricultural fertilizers. Low ratio values, less than 50, are due to precipitation contributions (Whittemore, 1988; Davis et al., 1998; Alcalà and Custodio, 2008).

Fig. 8.13, b, which presents Cl^-/Br^- ratio of sampled groundwater, indicates values ranging from 213 to 946 with an average of 546 above seawater ratio level. These values demonstrate human activity contribution in groundwater salinization. Lorenzen et al. (2012) and Giambastiani et al. (2013) suggest, for such ratio, evaporate dissolution, salts present in the soil, and mixture with brackish or salt seawater as further sources of these elements.

Decreasing of Cl^-/Br^- ratio versus seawater (272.17) can originate in marine aerosols (Duce and Hoffman, 1976) and also partly in percolation of seepage water through the bromide-rich organic horizons of soils (Gerritse and George, 1988).

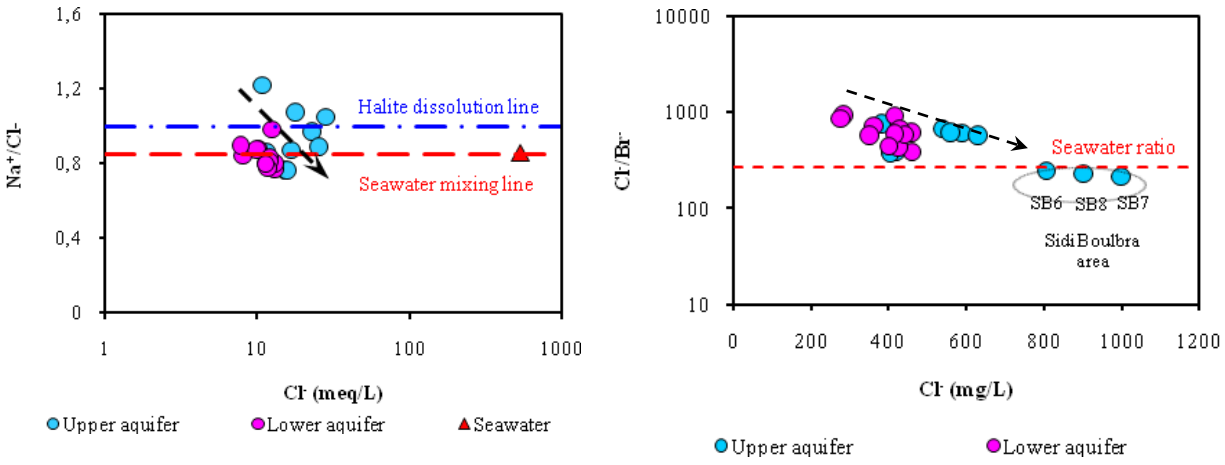

(a) (b)

Fig. 8.13. Ratios of Na^+/Cl^- vs Cl^- (a) and Cl^-/Br^- vs Cl^- (b) in sampled groundwater of Sidi Boulbra site

8.4.2.4. Use the ionic deltas for identification of groundwater salinity source

Ionic deltas calculation allows identifying hydrochemical processes in the water table via the comparison of major element concentrations and theoretical mixture composition. This calculation,

can confirm ion exchange process within the aquifer (Andersen et al., 2005; El Yaouti et al., 2009; Daniele et al., 2011; Giambastiani et al., 2013). Seawater percentage determination for each sample using chloride concentration in seawater and freshwater is the first step for ionic deltas calculation. This percentage is determined the following Eq. (2) (Appelo and Postma, 1993, 2005):

$$\%sea = \frac{Clsample - Clfresh}{Clsea - Clfresh}, \qquad (2)$$

where Cl_{sample} is sample chloride concentration, Cl_{fresh} is freshwater chloride concentration and Cl_{sea} is seawater chloride concentration.

Seawater percentage, which is used in the calculation of theoretical mixture concentration for each ion (i) resulting from seawater and freshwater mixture, is given in Eq. (3):

$$i_{mixture} = \%_{sea} * i_{sea} + (1 - \%_{sea}) * i_{fresh}, \qquad (3)$$

where $\boldsymbol{i_{sea}}$ is the ion (***i***) concentration in seawater, and $\boldsymbol{i_{fresh}}$ is the ion (***i***) concentration in freshwater.

However, ionic delta (**Δ**) for each ion (***i***) is the difference between concentration of conservative mixture ($\boldsymbol{i_{mixture}}$) and measured concentration for each sample ($\boldsymbol{i_{sample}}$) as shown in Eq. (4) (Fidelibus 2003):

$$\Delta_i = i_{sample} - i_{mixture}. \qquad (4)$$

Where Δ_i is positive, groundwater is enriched by ion under consideration, while negative value indicates ion depletion relative to theoretical mixture (Andersen et al., 2005).

Obtained results indicate that most samples from upper and lower aquifers, present Na^+, K^+ and Br^- deficit with respect to theoretical mixture, while Ca^{2+} and Mg^{2+} present a main excess for all samples (Fig. 8.14). In coastal aquifers, subject to seawater intrusion, ion exchange process is of great significance in the modification of groundwater chemical concentrations (Andersen et al., 2005; Appelo and Postma, 2005; Daniele et al., 2011 Giambastiani et al., 2013). As well, clays, which form the groundwater matrix, are the expected ions exchanger, organic material layers found in the aquifer have also a higher ions exchange capacity (Appelo and Postma, 2005; Giambastiani et al., 2013). Moreover, the excess, relative to theoretical mixture, of SO_4^{2-} in all groundwater samples can be interpreted as a new dissolution of precipitated gypsum according to (Gomis-Yagues et al. 2000 and Daniele et al. 2011).

8.4.2.5. Seawater intrusion estimation

Regarding human uses, mixing only 2% seawater in a freshwater aquifer exceeds organoleptic objectives for the upper limit of chloride (water tastes salty). If the mix exceeds 4%, the water becomes mostly unusable, and if the mix exceeds 6%, the water can only be used for cooling and flushing purposes. In this context, an estimation of average seawater contribution to collected samples was carried out using Cl^- and Br^-, two halides known for their conservative behavior in groundwater (Flury and Prapitz, 1993). Assuming that there were no contributions other than fresh groundwater or seawater, and that both anions behave in a conservative way, the seawater contributing fraction to a particular sample can be computed according to Eq. 5 (Appelo and Postma, 1993, 2005):

$$f_{sea} = \frac{m_{sample} - m_{fresh}}{m_{sea} - m_{fresh}} \qquad (5)$$

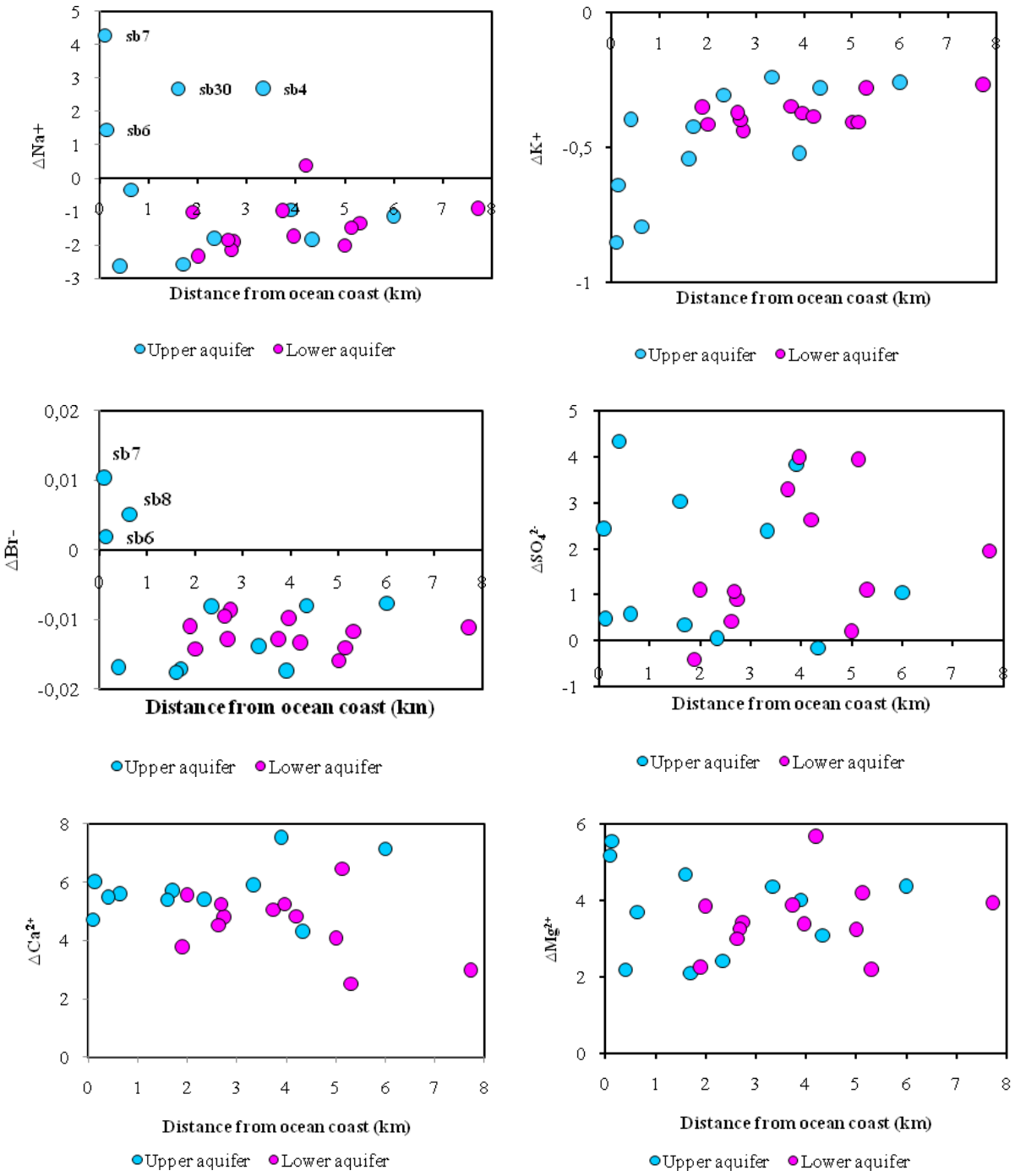

Fig. 8.14. Ionic deltas of analyzed sample in function of distance from the ocean

Where, m is the molar concentration of the anion tested (Cl^- or Br^-) in the sample, freshwater (f) or seawater (s). However, some increase in groundwater salinity in the aquifer is expected as a consequence of the recirculation of groundwater (pumping for irrigation purposes and infiltration of irrigation return flows).

The intrusion rate of marine water estimated based on the chloride conservation equation (chloride mass balance) Eq. (2), proves that the contribution of seawater to upper and lower aquifers ranges between 1.3 and 5.1% at about 8 km from the Atlantic coast. The wells located at a distance less than 2 km to the coastal fringe, are the most affected by seawater intrusion. It is significant in the wells located at Sidi Boulbra NPP site (eg. ***sb6***, ***sb7*** and ***sb8***) (Fig. 8.15).

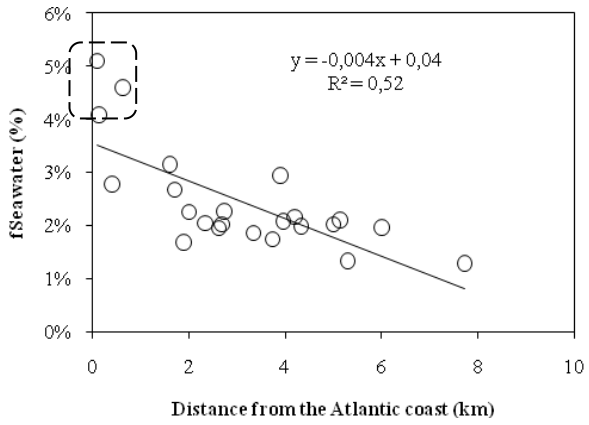

Fig. 8.15. Seawater percentage mixing of analyzed samples
in function of distance from the ocean

Results obtained for both Cl^- and Br^- anions were in reasonable agreement given the uncertainties of this estimation, with a slope of 1.6 and a regression coefficient of 0.87, as depicted in Fig. 8.16, a. The mean of both estimates is used as a measure of seawater contribution. According to this estimate, 83% of the studied wells and boreholes presented seawater contributions below 2%, while 17% surpassed this threshold (Fig. 8.16, b).

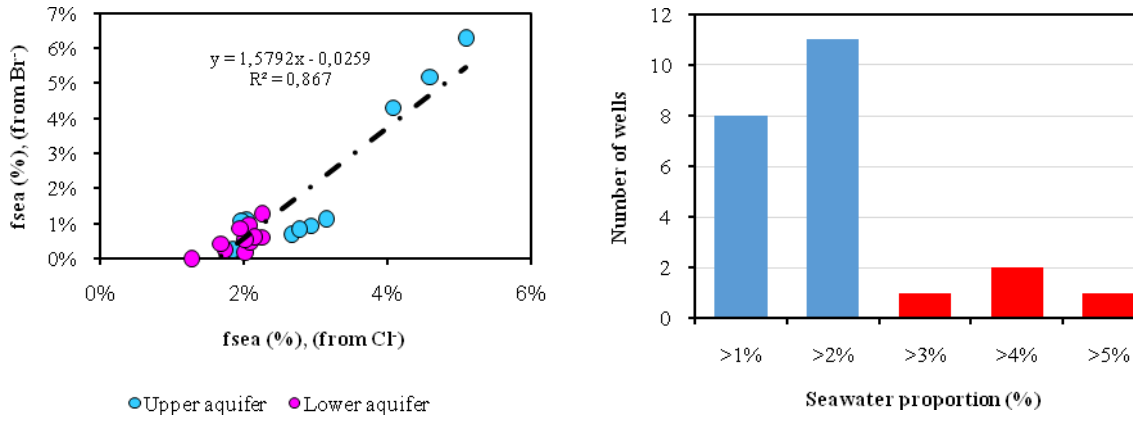

(a) (b)

Fig. 8.16. Agreement in the proportion of seawater estimation with Cl^- and Br^- tracers (a). Histogram of seawater proportion in the sampled production wells and boreholes in Sidi Boulbra NPP aquifers system (b)

It is notable that 2% of seawater in freshwater implies about 14 mmol L^{-1} of Cl^-, two times higher than the Moroccan guideline value for drinking water (300 mg L^{-1} or 8 mmol L^{-1}). Three samples contained at least 4% seawater (sb6, sb7 and sb8) located in the area of Sidi Boulbra NPP, being severely affected not only for drinking purposes but also for irrigation of most crops (Ayers and Westcot, 1992). These seawater contributions are expected to increase since measures against groundwater overexploitation are lacking in the study area.

8.4.3. Isotope data

Isotope geochemistry techniques are valuable tools in investigating many problems in hydrology and evaluating hydrogeological and hydrochemical controlling mechanisms in any groundwater system (Clark and Fritz, 1997). They provide significant insights into water origin, recharge circumstances (time and location), water flow directions and residence times, augmenting evidence provided by the major ions (Geyh, 2000).

8.4.3.1. Stable isotopes $\delta^{18}O$ and $\delta^{2}H$

8.4.3.1.1. Origin of recharge

Stable isotope compositions of samples representing the upper aquifer are within the range from –4.5 and –4.2‰ and between –25.7 and –23.7‰ for $\delta^{18}O$ and $\delta^{2}H$, respectively. The stable isotope compositions of groundwater in the lower aquifer fluctuate between –5.4 to –5.0 ‰ for oxygen-18 and between –33.5 and –30.1 ‰ for deuterium (see Table 8.1).

The mean isotopic composition of the sampled groundwater from the upper aquifer system is similar to local precipitation recorded in the Sidi Boulbra NPP station (–4.4 for $\delta^{18}O$ and –25 ‰ for $\delta^{2}H$) (Fig. 8.17). This similarity in isotopic composition between upper aquifer groundwater and local precipitation indicates that the groundwater has been recharged under climatic conditions, which are similar to those prevailing at present in the region (Carreira et al., 2018) (see Fig. 8.17).

On the other hand, the samples representing the lower aquifer are relatively more depleted in heavy isotopes than the mean weighted values of ^{18}O and ^{2}H observed at the Sidi Boulbra NPP station. This in turn suggests that the individual aquifers of the studied plain have been recharged at altitudes higher than elevation of the local rainfall station of Sidi Boulbra NPP (E = 27 m a.s.l.).

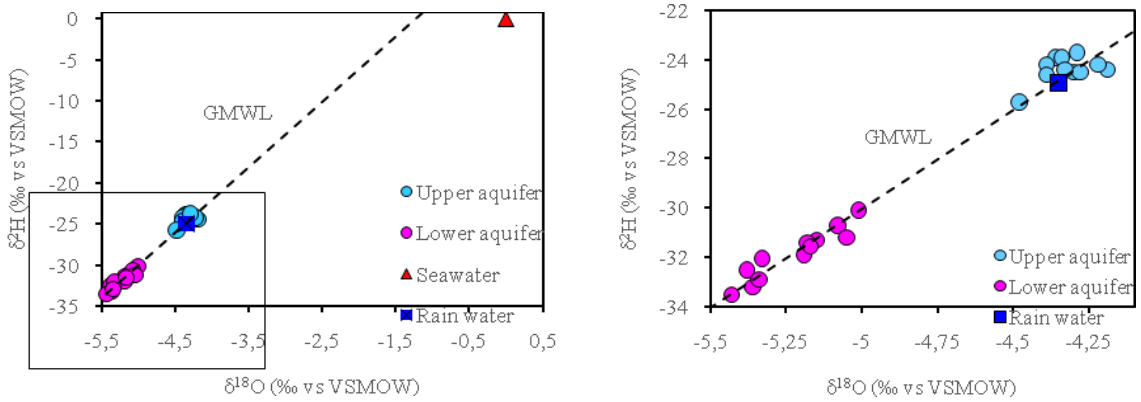

Fig. 8.17. Stable isotope composition of groundwater samples in Sidi Boulbra NPP area

The different isotopic concentrations found between the two aquifers systems are due to the different recharge altitudes. The main recharge area of the Plio-Quaternary upper aquifer is located on Sidi Boulbra area plain, while recharge of the Turonian lower aquifer probably takes place in Jbel Kourati and Jbel Hadid Mountains (elevation range from 242 to 725 m a.s.l.). Considering the $\delta^{18}O$ altitudinal gradient (G) of 0.27 ‰/100 m (Bouchaou et al., 1995; Qurtobi et al., 2010), the lower aquifer recharge altitude (R_A) is estimated according to the following equation.

$$R_A = E + \frac{100 * (d18O mean\ local\ rainfall - d18O groundwater)}{G}, \qquad (6)$$

where E is the elevation of the local rainfall station of Sidi Boulbra (E = 27 m a.s.l).

The calculated values, ranging between 280 and 440 m a.s.l., which coincide with the elevation of the aquifer outcrops in the Jbel Kourati and Jbel Hadid Mountains.

It seems that mountain recharge is not available for the coastal groundwater of the upper aquifer and thus the water resources of this aquifer system are more limited for predominantly local recharge. At the same time, the source of groundwater in the lower aquifer system is derived from the lateral groundwater flow originated in the Mountains. This contribution is favored by the high permeability and soil structure in this area.

8.4.3.1.2. Origin of salinization

In groundwater salinization studies, it is common to try to identify a relation between the isotopic and hydrogeochemical groundwater evolution along the flow paths i.e., in dissolution processes the stable isotope concentration of the water remains invariable, while the water salinity increase is noticed. A different trend is observed when seawater intrusion is occurring or has occurred, with a parallel isotopic and mineralization enrichment. This unique characteristic enables the identification of the main processes based on isotopic and geochemical data (Araguás-Araguás and Gonfiantini, 1989; Edmunds and Droubi, 1998; Carreira et al., 2014).

Plotting the oxygen-18 concentration as function of the chloride concentration, (Fig. 8.18, a), a clear trend in the seawater/freshwater characteristics is found for the samples with the highest mineralization of upper aquifer, which clearly indicates that the salinity is derived from seawater intrusion.

On the other hand, we observed a good correlation between nitrate and $\delta^{18}O$ values (Fig. 8.18, b). This correlation could indicate that the increase of the salinity is derived from slightly evaporated agricultural return flow.

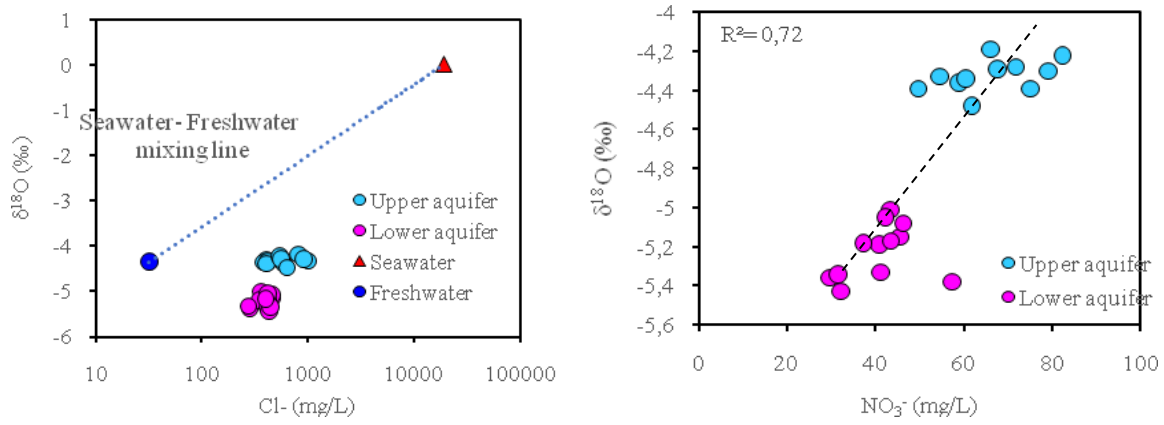

(a) (b)

Fig. 8.18. Variations of $\delta^{18}O$ values (‰) vs chloride concentrations (mg/L) (a), and $\delta^{18}O$ values (‰) vs nitrate concentrations (mg/L) of groundwater investigated in this study (b)

8.4.3.2. Radioactive isotopes (^{3}H and ^{14}C)

8.4.3.2.1. Tritium

For several decades, tritium has been regarded as being the simplest and most convenient tracer method for determining young groundwater ages (Dulinski et al., 2003). The occurrence of tritium in groundwater indicates the extent of migration of modern post-1950s recharge, but its use is limited by its short half-life (12.43 years) (Edmunds and Smedley, 2000; Zuber, 1986; Szabo et al., 1996; Plummer et al., 1998). Tritium content in groundwater depends primarily on the initial atmospheric concentration at the time of recharge and the radioactive decay that has occurred since infiltration (Maduabuchi et al., 2006).

The measured ^{3}H contents varied between 0.63 TU and 1.36 TU for the upper aquifer, while for the lower aquifer they ranged from 0 to 0.75 TU.

As it is shown on $^{3}H/^{18}O$ diagram (Fig. 8.19), most of the groundwater samples have very low, mostly zero tritium levels, which indicate that both the vertical and lateral recharge process are longer than about 30 years (Clark and Fritz, 1997).

The lack of high tritium activities in groundwater suggests that the 1960's tritium peak (Schlosser et al., 1988; Mook, 1980; Michel, 2005; Plummer, 2005; Yechieli et al., 2001) has already depleted in that groundwater system.

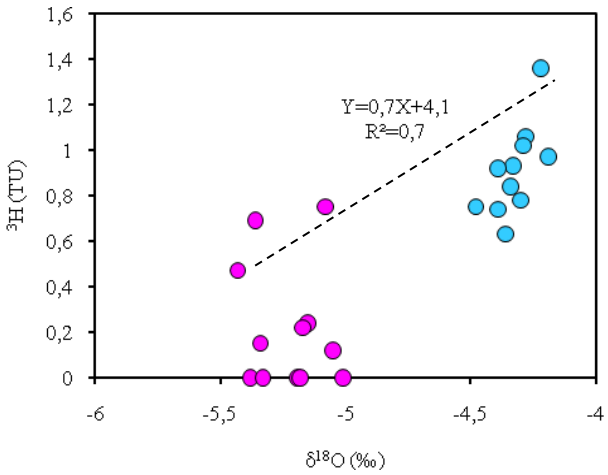

Fig. 8.19. Relation between $\delta^{18}O$ and ^{3}H in groundwater samples in Sidi Boulbra NPP area

8.4.3.2.2. Radiocarbon

Radiocarbon, with a half-life of 5,730 years, allows the determination of water residence time over timescales to 30,000 years (Clark and Fritz, 1997). As ^{14}C is involved in many geochemical reactions, a detailed understanding of the origin of dissolved inorganic carbon (DIC) is required to convert the measured ^{14}C activities into the ages (Clark and Fritz, 1997).

Radiogenic isotope measurements were carried out only on a few selected wells and boreholes samples of the different aquifers. Measured activities of ^{14}C in analyzed water samples are within the ranges of 44 to 53.1 pmC and 28.6 to 64.3 pmC for the upper and lower aquifer, respectively (see Table 8.1).

In general, all analyzed samples are characterized by the high ^{14}C activities (higher than 50% of modern C) excepting sample sb 29 representing the lower aquifer at 175 m depth (see Fig. 8.7). Its low activity (28,62 pmC) is probably due to the substantially thicker clay beds in the lower aquifer, which hinder the flow of infiltration water and increase the age of groundwater. On the other hand, the relatively high ^{14}C activities provide the presence of waters of recent infiltration.

High ^{14}C activities remain in good agreement with low $\delta^{13}C$ values (Fig. 8.20) ranging from –11.76 to –11.64 and from –11.78 to –11.19 for the upper and lower aquifer, respectively, indicating domination of the soil-derived CO_2. This supports that the $\delta^{13}C$ content becomes depleted due to water-plant CO_2 interaction as the groundwater equilibrate with isotopically light CO_2 incorporated by C4 plants that have $\delta^{13}C$ values of –17 to –9‰ VPDB (Cerling et al., 1991; Romanek et al., 1992; Vogel, 1993).

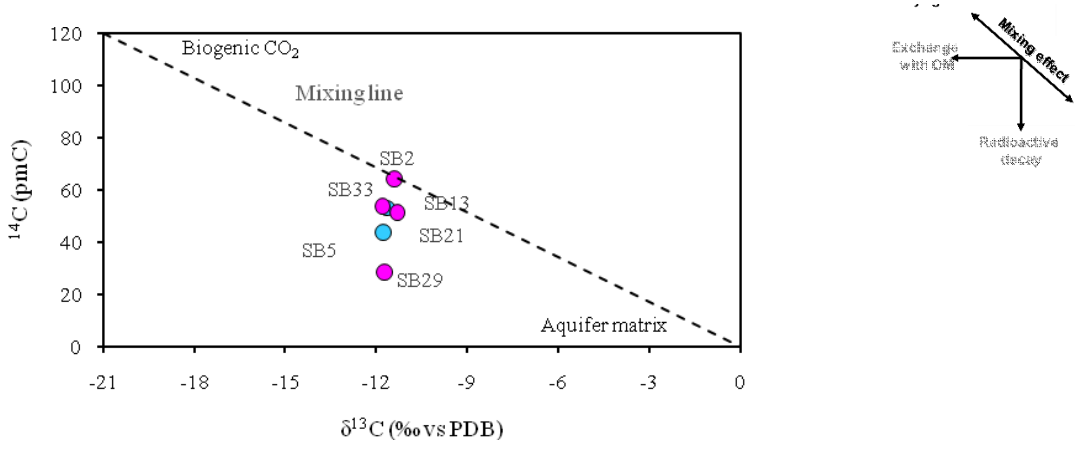

We use a Mixing line that represents a theoretical closed system mixing between modern DIC derived from soil CO_2 ($A^{14}C$~120 pmC; $\delta^{13}C$~21‰ PDB) and marine carbonate rock DIC (^{14}C~0 pmC; $\delta^{13}C$~0‰). Groundwater samples along this line are hypothesized to reflect the mixing between a biogenic end member and a mineral end member under a closed system, and thus are modern, whereas deviation from that mixing line is modeled to ^{14}C decay and thus residence time of the groundwater.

Most of our samples are located below this mixing line, indicating radioactive decay and therefore a long residence time. However, sb2 is located along this line and can be attributed to modern age recharge.

8.4.3.2.3. Estimation of Mean Residence Time

The determination of groundwater Mean Residence Time (MRT) is possible after an evaluation of the contribution of different carbon sources and isotopic exchange processes (Le Gal La Salle et al., 1996). The reliability of radiocarbon in estimating groundwater residence times depends on an accurate estimate of the initial ^{14}C activity (A) of the total dissolved inorganic carbon (TDIC) at the time of recharge and the assumption that the groundwater is closed to addition or removal of DIC in the saturated portion of the aquifer (Love et al., 1994; Darling et al., 2006).

In order to assess the initial activity (A_0), correction models are necessary for groundwater showing several sources of the TDIC. During previous decades, thorough ^{14}C correction models have been proposed (Ingerson and Pearson, 1964; Tamers, 1975; Evans et al., 1979; Fontes and Gamier, 1979; Salem et al., 1980 (IAEA); Eichinger, 1983). Most of these models indistinctly take into account the geochemical interactions occurring in both unsaturated and saturated zones and consider a mixing between biogenic CO_2 and ^{14}C-free carbonates (Darling et al., 2006). These models are based on different mixing reactions: models of purely chemical mixing (Tamers, 1975); isotopic mixing (Ingerson and Pearson, 1964) and models of chemical mixing and isotopic exchange (Fontes and Gamier, 1979; Evans et al., 1979; Mook, 1980; Salem et al., 1980; Eichinger, 1983).

Groundwater ages have been calculated and compared using six correction models: Pearson (Ingerson and Pearson, 1964), Evans (Evans et al., 1979), Eichinger (Eichinger, 1983), IAEA (Salem et al., 1980), Fontes and Garnier (Fontes and Gamier, 1979) and Tamers (Tamers, 1975). These models are based on the chemical evolution and/or isotope dilution of $^{13}C/^{12}C$ derived from soil CO_2 through interactions with the matrix carbonates. It is highlighted that ages proposed by Fontes and Garnier in equilibrium, (1979) and the IAEA (Salem et al., 1980) are globally in good agreement and provide almost similar ages.

According to these correction models (Table 8.3), groundwater sampled from Sidi Boulbra lower aquifer have typical apparent older ages of 4,000 to 10,000 years BP with a mean value of 6,300 years BP. This indicates the relatively old orgin of the water, resulting from a long groundwater flow path probably linked to the low permeability of the clayey levels, and/or from a mixture with deep old water of Jurassic (sb29), recharged during the early Holocene (<10000 YBP).

Table 8.3. Calculated ages [years BP] of selected groundwater samples in Sidi Boulbra NPP area

Aquifer type	Sample ID	$d^{13}C$ [‰ PDB]	Activity ^{14}C [pmC]	Uncorrected Age [years BP]	F&G eq Model			IAEA Model			Mean age [years BP]
					A_0 [pmC]	Age [years BP]	±1σ [years]	A_0 [pmC]	Age [years BP]	±1σ [years]	
Upper aquifer	SB05	-11.76	43.97	8300	103	7056	-36	109	7472	-36	7264
	SB13	-11.64	53.07	6745	101	5334	-387	108	5839	-387	5587
Lower aquifer	SB2	-11.39	64.32	5155	96	3295	-219	103	3898	-219	3596
	SB21	-11.29	51.57	6982	96	5106	-268	103	5736	-268	5421
	SB29	-11.72	28.62	11849	102	10518	-40	108	10994	-40	10756
	SB33	-11.78	53.95	6609	104	5401	-32	110	5920	-32	5661
MRT of all analysed samples											**6381**

The relative old age of the groundwater sampled from the upper aquifer may be a result of mixing between modern and Late Holocene waters (Clark and Fritz, 1997; Ma et al., 2009).

According to these data, the studied aquifer system of Sidi Boulbra NPP site is recharged by modern infiltration waters at the Oligocene-Miocene outcrops. This observation is also consistent with the ^{3}H data contents (~0 TU).

8.4.3.2.4. Flow velocity

The calculation of the transit velocity of water between two drillings A and B (Fontes et al., 1979) can be estimated according to the following equation:

$$Transit\ velocity = \frac{L}{T_B - T_A}, \qquad (7)$$

where L is the distance between drillings A and B in meters; (T_B - T_A) is the difference between ^{14}C mean ages of samples from drillings A and B in years BP.

Assuming a predominantly horizontal flow and a conservation of the initial isotopic marking during the transit of water in the reservoir (Huneau 2001, Fontes 1979), the flow velocity (Table 8.4), is calculated for several intervals along the presumed flow direction (from SB13 to SB5 for the upper aquifer and from SB2 to SB29, SB2 to SB21 and SB2 to SB33 for the lower aquifer).

The mean transit velocity in the Mio-Plio-Quaternary upper aquifer, composed mainly of sand, sandstone and conglomerates was 1.88 m/year. Whereas, in The Cenomano-Turonian lower aquifer, mainly calco-dolomitic was 0.72 m/year. These values were obtained taking care of differences between ^{14}C mean ages of samples from drillings SB2, SB5, SB13, SB21, SB29 and SB33 and distances between them.

Mean transit velocity is about 1.01 m/year, which is a specific value to both aquifers located in the sedimentary layers of Sidi Boulbra NPP area. Obtained results are presented in Table 8.4.

Table 8.4. Mean transit velocities of studied aquifers

	Presumed Flow direction	Transit time (Year)	Distance between sampling points (m)	Supposed Flow velocity (m/y)	Mean transit velocity (m/y)
Upper aquifer	SB13 to SB5	1678	3150	1.88	**1.88**
Lower aquifer	SB2 to SB29	7160	2940	0.41	**0.72**
	SB2 to SB21	1824	2340	1.28	
	SB2 to SB33	2064	4320	0.48	

8.4.4. Noble gas analyses

For noble gas isotope analyses, five water samples of about 40 cm^3 were collected in copper tubes with metal pinch-off clamps at both ends. All water samples were shipped to the Isotope Hydrology Laboratory (IHL) at the IAEA, Vienna (Austria), that houses two large sector static mass spectrometers for precise determination of noble gas isotope abundances dissolved in groundwater.

Concentrations of Ne, Kr, Ar and Xe in groundwater originate from the atmosphere, and usually serve for determining the temperature at the water table at the time of recharge after correcting for the so-called air excess and altitude (Mazor, 1972; Herzberg and Mazor, 1979; Heaton and Vogel, 1981; Stute and Schlosser, 1993, 2000; Aeschbach-Hertig et al., 1999). If the dependence of surface air temperature on altitude is known, noble gases can also be used for determining the altitude of recharge (Zuber et al., 1995; Manning and Solomon, 2003).

The temperature of recharged water derived from the concentrations of noble gases is usually called the noble gas temperature (NGT). Noble gas temperatures were mainly studied for well-known large groundwater systems to obtain paleoclimatic information (e.g. Stute and Deăk, 1989; Stute et al., 1993; Clark et al., 1997; Beyerle et al., 1998), or to confirm the pre-Holocene origin of water dated by other methods (e.g. Blavoux et al., 1993; Clark et al., 1997, 1998; Zuber et al., 2000).

Due to insufficient data to estimate the NGT for groundwater in Sidi Boulbra NPP site, we attempted to estimate groundwater ages using amounts of tritium and tritiogenic ^{3}He (^{3}He produced by tritium decay).

Tritiogenic ^{3}He was determined for each sample using a recharge temperature, excess air and terrigenic helium as determined by the (CE Aeschbach model) (Table 8.5). Because of very low tritium contents, the ages obtained from samples with <1 TU of tritium and/or <3 TU of tritiogenic ^{3}He showed significantly large uncertainties, making it impossible to treat these ages in a quantitative manner. Nevertheless, the $^{3}H/^{3}He$ results would indicate that groundwater within the Sidi Boulbra NPP site aquifers includes some younger component recharged within the last 50 years considering the analytical uncertainty of the age determinations. Ages determined by noble gases $^{3}H/^{3}He$ range from 45 to 47 years, and the age of the calendar of recharge of these groundwater is 1972 with an initial content of tritium that ranges between 1.29 to 3.19 TU (Fig. 8.21).

Table 8.5. T-^{3}He ages

Name	T (TU)	Tritiogenic ^{3}He (TU)	Initial Tritium (TU)	T-^{3}He age (years)	Date of Sampling	Age in Calendar Year
SB2	0	3	3.19	45	18/07/2017	1972
SB4	0.63	0	0.20	0	19/07/2017	2018
SB13	0.92	2	2.01	45	19/07/2017	1973
SB21	0.1	1	1.29	47	20/07/2017	1970
SB33	0.22	0	0.22	0	14/11/2018	2019

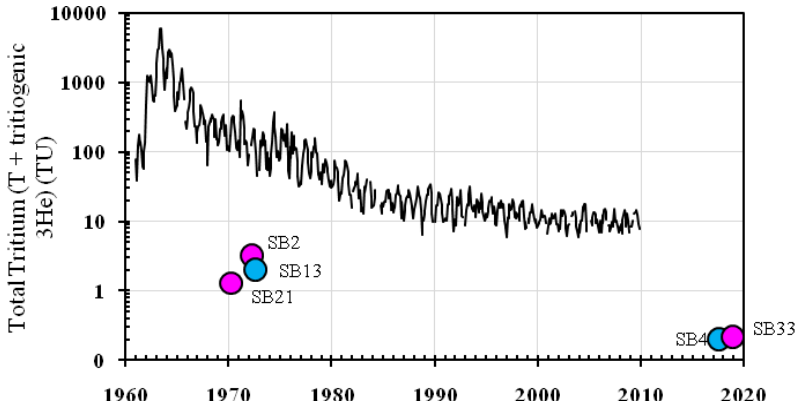

Fig. 8.21. Calculation of "Initial Tritium" and its comparison with tritium input curve (based on iNoble ver 2.6 model)

When mostly old groundwater is examined, as it is done in this paper, tritium often acts as a marker of admixed young groundwater.

8.5. Conclusion

A multi-tracer approach including the application of isotope techniques, noble gas isotopes, notably ^{3}He and ^{4}He, reveals a groundwater mixing scheme in the Sidi Boulbra aquifer system, which was not accessible by traditional tracer methods alone.

Stable and radioactive isotopes ($\delta^{2}H$, $\delta^{18}O$; ^{3}H, $^{3}H/^{3}He$, $\delta^{13}C$ and ^{14}C), together with physical and geochemical data, were used in the determination of the origin of groundwater salinization and geochemical evolution processes in coastal aquifers of Sidi Boulbra site located in the north of Essaouira sedimentary basin. In this region, groundwater degradation occurs by salinization increase to different concentrations and in relation to different origins. The main quality issues for the groundwater resources are related to seawater intrusion and/or brine dissolution at depth. Anthropogenic pollution ascribed to agricultural activities is another source for groundwater degradation, affecting mainly the shallow aquifer (Fig. 8.22).

Various isotopic age indicators show groundwater ages ranging from 4,000 to 10,000 years BP in the Cretaceous lower aquifer. This observation is also consistent with ^{3}H data that is below the detection limit (~0 TU). The Cretaceous lower aquifer contributes to recharge the Plio-Quaternary upper aquifer via a network of faults, leading to the observed pattern of mixed water types. The finding of mantle helium signature in shallow aquifer generally supports the assumption of the deep, permeable faults in the area of the Sidi Boulbra NPP site area (Fig. 8.23).

The isotopic results together with the geochemical data provided an effective label for tracing the mineralization origin and groundwater degradation processes.

This joint approach provided a better understanding of the variable nature of groundwater mineralization, which can help to optimize the use of groundwater resources in coastal regions. The results of this study can be used to guide alternative management practices enabling mitigation of the overexploitation and deterioration in water quality, thus leading to sustainable groundwater use.

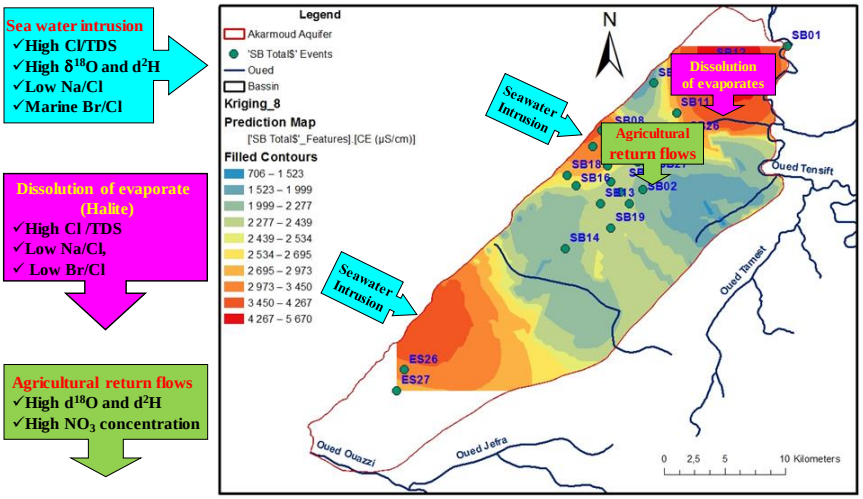

Fig. 8.22. The data generated within this project revealed several sources of salinity: (i) Sea water intrusion along the coastal area, (ii) Recycling of agricultural return flows and (iii) Dissolution of evaporates (Halite)

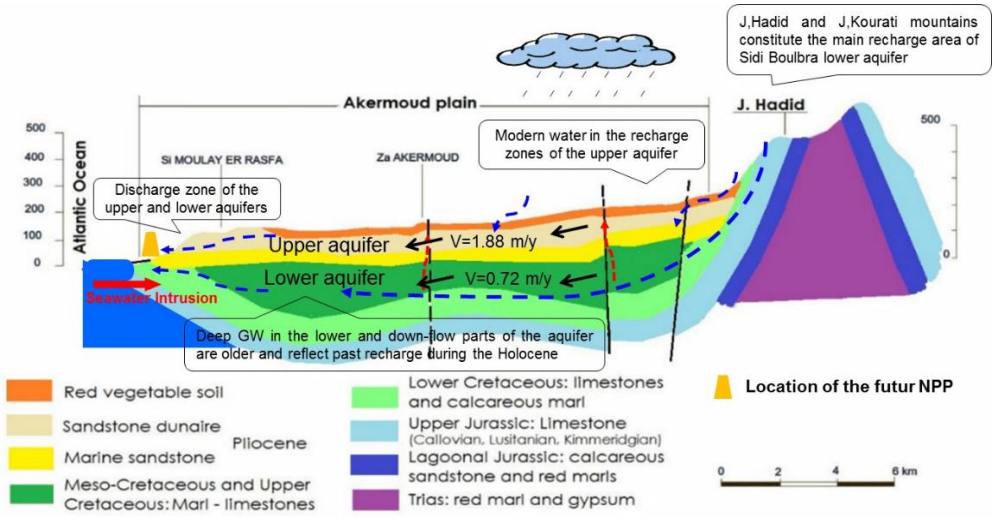

Fig. 8.23. Cross section showing the proposed groundwater flow scheme in the Sidi Boulbra NPP site system aquifer with major and supposed faults. The upper Plio-Quaternary, lower Turonian aquifers and Jbel Hadid-Kourati mountains are shown in brown-orange, green and sky-blue colors, respectively. Water from deep aquifer (red arrows), ascends along the Fault and admixes into shallow aquifer. Young waters are coming directly from recharge areas (Mountains and plain with blue arrows) and/or from irrigation water return (orange arrows). Water from lower aquifer (red arrows), ascends along the Fault and admixes into upper aquifer. Seawater intrusion has increased salinity in downstream, where one third of the samples showed significant seawater contribution and a significant exchange processes affected major cations

References

Aeschbach-Hertig, W., Peeters, F., Beyerle, U., Kipfer, R., 1999. Interpretation of dissolved atmospheric noble gases in natural waters. Water Resour. Res. 35, 2779–2792.

Ako, A.A., Shimada, J., Hosono, T., Ichiyanagi, K., Nkeng, G.E., Fantong, W.Y., Eyong, G.E.T., Roger, N.N., 2011. Evaluation of groundwater quality and its suitability for drinking, domestic, and agricultural uses in the Banana Plain (Mbanga, Njombe, Penja) of the Cameroon Volcanic Line. Environ. Geochem. Health 33 (6), 559-575.

Alcala, F.J., Custodio, E., 2008. Using the Cl/Br ratio as a tracer to identify the origin of salinity in aquifers in Spain and Portugal. J. Hydrol. 359, 189-207.

Andersen, M.S., Nyvang, V., Jakobsen, R., Postma, D., 2005. Geochemical processes and solute transport at the seawater/freshwater interface of a sandy aquifer. Geochem. Cosmochim. Acta 69, 3979-3994.

Appelo, C.A.J., Postma, D., 2005. Geochemistry, Groundwater and Pollution, second ed. A.A. Balkema Publishers, Rotterdam, Netherlands. 0-41-536428-0.

Araguás-Araguás L, Gonfiantini R. 1989. Environmental isotopes in sea water intrusion studies. International Atomic Energy Agency, Internal Report, IAEA, Vienna.

Arslan, H., Cemek, B., Demir, Y., 2012. Determination of seawater intrusion via hydrochemicals and isotopes in Bafra Plain, Turkey. Water Resour. Manag. 26 (13), 3907-3922.

Askri, B., 2015. Hydrochemical processes regulating groundwater quality in the coastal plain of Al Musanaah, Sultanate of Oman. J. Afr. Earth Sci. 106, 87-98.

Awad, S., 2011. Hydrochimie et faciès géochimiques des eaux souterraines, Plaine de Bekaa. Hydrol. Sci. J. J. Des. Sci. Hydrol. 56 (2), 334-348.

Ayers, R.S., Westcot, D.W., 1992. Water quality for agriculture. FAO Irrigation and Drainage

Beyerle, U., Aeschbach-Hertig, W., Hofer, M., Imboden, D.M., Baur, H., Kipfer, R., 1999. Infiltration of river water to a shallow aquifer investigated with H-3/He-3, noble gases and CFCs. J. Hydrol. 220, 169–185.

Blavoux, B., Dray, M., Fehri, A., Olive, P., Gröning, M., Sonntag, C., Hauquin, J.-P., Pelissier, G., Pouchan, F., 1993. Palaeoclimatic and hydrodynamic approach to the Aquitaine basin deep aquifer (France) by means of environmental isotopes and noble gases, In: Isotope Techniques in the Study of Past and Current Environmental Changes in the Hydrosphere and the Atmosphere, IAEA, Vienna, pp. 293–305.

Bouchaou, L., Michelot, J.L., Chauve, P., Mania, J.Et., Mudry, J.,1995. Apports des isotopes stables à l'étude des modalités d'alimentation des aquifères du Tadla (Maroc) sous climat semiaride. C.R. Acad. Sci. 320, 95-101.

Carreira PM, Bahir M, Ouhamdouch S, Galego PF, Nunes D. 2018. Tracing salinization processes in coastal aquifers using an isotopic and geochemical approach: comparative studies in western Morocco and southwest Portugal.

Cerling, T.E., Solomon, D.K., Quade, J., Bowman, J.R., 1991. On the isotopic composition of carbon in soil carbon dioxide. Geochimica et Cosmochimica Acta 55, 3403e3405.

Chadha DK. 1999. A proposed new diagram for geochemical classification of natural waters and interpretation of chemical data, Hydrogeology Journal; 7 :431-439.

Clark, I., Fritz, P., 1997. Environmental Isotopes in Hydrogeology. Lewis Publishers, New York.

Craig, H., 1961. Isotopic variation in meteoric water. Science 133, 1702-1703.

Daniele, L., Vallejos, A., Sola, F., Corbella, M., Pulido-Bosch, A., 2011. Hydrogeochemical processes in the vicinity of a desalination plant (Cabo de Gata, SE Spain). Desalination 277 (1), 338-347.

Darling, W.G., Bath, A.H., Gibson, J.J., Rozanski, K., 2006. Isotopes in water. In: Leng, M.J. (Ed.), Isotopes in Paleoenvironmental Research. Springer, Dordrecht, pp. 1-66.

Davis, S.N., Whittemone, D.O., Fabryka-Martin, J., 1998. Uses of chloride/bromide ratios in studies of potable water. Ground Water 36 (2), 338-350.

Dror, G., Ronen, D., Stiller, M., Nishri, A., 1999. Cl/Br ratios of Lake Kinneret, pore water and associated springs. J. Hydrol. 225, 130-139.

Duce R.A and Hoffman E.J, 1976. Chemical Fractionation at the Air/Sea Interface. Annual reviews Inc. Provided by the NASA Astrophysics Data System. Annual Review of Earth and Planetary Sciences. November 2003. DOI: 10.1146/annurev.ea.04.050176.001155.

Duffaud, F., Brun, L. et Plauchut, 6. 1966. Le bassin du Sud-Ouest marocain. In : Bassins sddimentaires du littoral africain (Editd par Reyre, D.) pp5-26. Publication de I'Association Services Gdologiques Africains, Paris.

Dulinski, M., Rozanski, K., Kania, J., Karlikowska, J., Korczynski-Jackowicz, M., Witczak, S., Mochalski, P., Opoka, M., Sliwka, I., Zuber, A., 2003. Groundwater dating with Sulfur hexafluoride: Methodology and Field Comparison with Tritium and Hydrodynamic Methods. International Symposium, International Atomic Energy Agency, Vienna, Austria, IAEA-CN-104/8.

Dutta, P.S., Deb, D.L., Tyagi, S.K., 1997. Assessment of ground water contamination from fertilizers in Delhi area based on 18 O, NO3 and K composition. J. Contam. Hydrol. 27, 249-262.

Edmunds WM, Droubi A. 1998. Groundwater salinity and environmental change. In: Isotope techniques in the study of environmental change. Vienna: IAEA, 503–518.

Eichinger, E., 1983. A contribution to the interpretation of 14C groundwater ages considering the example of partially confined sandstone aquifer. Radiocarbon 25, 347-356.

Evans, G.V., Otlet, R.L., Downing, A., Monkhouse, R.A., Rae, G., 1979. Some problems in the interpretation of isotope measurements in United Kingdom aquifer. Isotope Hydrology 2, 639-708. Proceedings of Symposium, Neuherberg, 1978, IAEA-SM 228/34.

Fadili, A., Mehdi, K., Riss, J., Najib, S., Makan, A., Boutayab, K., 2015. Evaluation of groundwater mineralization processes and seawater intrusion extension in the coastal aquifer of Oualidia, Morocco: hydrochemical and geophysical approach. Arab. J. Geosci.

Fidelibus, M.D., 2003. Environmental tracing in coastal aquifers: old problems and new solutions. In: López-Geta, J.A., Gómez, J.D., de la Orden, J.A., Ramos, G., Rodríguez, L. (Eds.), Coastal Aquifers Intrusion Technology: Mediterranean Countries. Serie: Hidrogeología y Aguas Subterráneas n° 8. Instituto Geológico y Minero de España, Madrid, Spain, 335 pp.

Flury, M., Prapitz, A., 1993. Bromide in the natural environment: occurrence and toxicity. J. Environ. Qual. 22, 747–758.

Fontes, J. Ch., Gamier, J.M., 1979. Determination of the initial 14C activity of the total dissolved carbon: a review of the existing models and a new approach. Water Resources Research 15, 399-413.

Gerritse R.G and George R.J., 1988. The role of soil organic matter in the geochemical cycling of chloride and bromide. Journal of Hydrology 101(1-4):83-95.

Geyh, M.A., 2000. An overview of 14C analysis in the study of the groundwater. Radiocarbon 42, 99-114.

Giambastiani, B.M.S., Colombani, N., Mastrocicco, M., Fidelibus, M.D., 2013. Characterization of the lowland coastal aquifer of Comacchio (Ferrara, Italy): hydrology, hydrochemistry and evolution of the system. J. Hydrol. 501, 35-44.

Gomis-Yagùes V., Boluda-Botella N., Ruiz-Bevia F. 2000. Gypsum precipitation/dissolution as an explanation of the decrease of sulphate concentration during seawater intrusion. Journal of Hydrology 228 (2000) 48–55.

Gonfiantini R, Araguás-Araguás LA. 1988. Los isotopos ambientales en los estudios de intrusión marina [The environmental isotopes in marine intrusion studies]. Proc. Symp. Tecnología de la Intrusión en acuíferos Costeros, Ponencias Internacionales, 1. IGME, Madrid, pp 135–190.

Han, D.M., Song, X.F., Currell, M.J., Yang, J.L., Xiao, G.Q., 2014. Chemical and isotopic constraints on evolution of groundwater salinization in the coastal plain aquifer of Laizhou Bay, China. J. Hydrol. 508, 12-27.

Heaton, T.H.E., Vogel, J.C., 1981. “Excess air” in groundwater. J. Hydrol. 50, 201–216.

Herzberg, O., Mazor, E., 1979. Hydrological applications of noble gases and temperature measurements in underground water systems: examples from Israel. J. Hydrol. 42, 217–231.

Hofmann, H., Cartwright, I., 2013. Using hydrogeochemistry to understand interaquifer mixing in the on-shore part of the Gippsland Basin, southeast Australia. Appl. Geochem. 33, 84-103.

Hollard H., Choubert G., Bronner G., Marchand J., Sougy J. 1985. Carte géologique du Maroc, scale 1/1,000,000. – *Servi. Carte géol. Maroc*, 1985, n° 260.

Huneau, F., Blavoux, B., Bellion, Y., 2001. Differences between hydraulic and radiometric velocities of groundwaters in a deep aquifer: example of the Valréas Miocene aquifer (southeastern France). Comptes Rendus de l'Académie des Sciences Series IIA. Earth Planet. Sci. 333, 163–170.

Ingerson, E., Pearson, F.J., 1964. Estimation of age and rate of motion of groundwater by 14C method. In: Recent Researches in the Fields of Hydrosphere. Atmosphere and Nuclear Geochemistry, Sugarawa Festival Volume Maruzen, Tokyo, pp. 263-283.

Jamshidzadeh, Z., Mirbagheri, S.A., 2011. Evaluation of groundwater quantity and quality in the Kashan Basin, Central Iran. Desalination 270, 23-30.

Kass, A., Gavrieli, I., Yechieli, Y., Vengosh, A., Starinsky, A., 2005. The impact of freshwater and wastewater irrigation on the chemistry of shallow groundwater: a case study from the Israeli Coastal Aquifer. J. Hydrol. 300 (1e4), 314-331.

Kim, Y., Lee, K.-S., Koh, D.-C., Lee, D.-H., Lee, S.-G., Park, W.B., Koh, G.-W., Woo, N.-C., 2003. Hydrogeochemical and isotopic evidence of groundwater salinization in a coastal aquifer: a case study in Jeju volcanic island, Korea. Journal of Hydrology 270, 282-294.

Kumar, M., Ramanathan, A.L., Rao, M.S., Kumar, B., 2006. Identification and evaluation of hydrogeochemical processes in the groundwater environment of Delhi, India. Environ. Geol. 50, 1025-1039.

Le Gal La Salle, C., Marlin, Ch., Savoye, S., Fontes, J. Ch., 1996. Geochemistry and 14C dating of groundwaters from Jurassic aquifers of North Aquitaine Basin (France). Applied Geochemistry 11, 433-445.

Ledesma-Ruiz, R., Pastén-Zapata, E., Parra, R., Harter, T., Mahlknecht, J., 2015. Investigation of the geochemical evolution of groundwater under agricultural land: a case study in northeastern Mexico. J. Hydrol. 521, 410-423.

Lorenzen, G., Sprenger, C., Baudron, P., Gupta, D., Pekdeger, A., 2012. Origin and dynamics of groundwater salinity in the alluvial plains of western Delhi and adjacent territories of Haryana State, India. Hydrol. Process 26, 2333-2345.

Love, A.J., Herczeg, A.L., Leaney, F.W., Stadter, M.H., Dighton, J.C., Armstrong, D., 1994. Groundwater residence time and paleohydrology in the Otway Basin, South Australia. Journal of Hydrology 153, 157-187.

Ma, J., Ding, Z., Edmunds, W.M., Gates, J.B., Huang, T., 2009. Limits to recharge of groundwater from Tibetan plateau to the Gobi Desert, implications for water management in the mountain front. J. Hydrol. 364, 128–141.

Maduabuchi, C., Faye, S., Maloszewski, P., 2006. Isotope evidence of paleorecharge and paleoclimate in the deep confined aquifers of the Chad basin, NE Nigeria.Science of the Total Environment 370, 467-479.

Manning, A.H., Solomon, D.K., 2003. Using noble gases to investigate mountain-front recharge. J. Hydrol. 275, 194–207.

Marimon, M.P.C., Roisenberg, A., Suhogusoff, A.V., Viero, A.P., 2013. Hydrogeochemistry and statistical analysis applied to understand fluoride provenance in the Guarani Aquifer System, Southern Brazil. Environ. Geochem. Health 35 (3), 391-403.

Mazor, E., 1972. Paleotemperatures and other hydrological parameters deduced from noble gases dissolved in groundwaters, Jordan Rift Valley, Israel. Geochim. Cosmochim. Acta 36, 1321–1336.

Mercado, A., 1985. The use of hydrogeochemical patterns in carbonate sand and sandstone aquifers to identify intrusion and flushing of saline water. Groundwater 23 (5), 635-645.

Michel, R.L., 2005. Tritium in the Hydrologic Cycle. In: Isotopes in the Water Cycle: Past, Present and Future of Developing Science, IAEA, Springer, pp. 53-66.

Mondal, N.C., Singh, V.S., Saxena, V.K., Prasad, R.K., 2008. Improvement of groundwater quality due to fresh water ingress in PotharlankaIsland, Krishna delta, India. Environ. Geol. 55 (3), 595e603.

Mook, W.G., 1980. Carbone14 in hydrogeological studies. In: Fritz, P., Fontes, J. Ch. (Eds.), Handbook of Environmental Isotope Geochemistry. The Terrestrial Environ., vol. 1. Elsevier, Amsterdam, pp. 49-74.

Nasher, G., Al-Sayyaghi, A., Al-Matary, A., 2013. Identification and evaluation of the hydrogeochemical processes of the lower part of Wadi Siham catchment area, Tihama plain. Yemen. Arab. J. Geosci. (6), 2131-2146. Paper 29. Food and Agriculture Organization of the United Nations, Rome, Italy.

Park, S.C., Yun, S.T., Chae, G.T., Yoo, I.Y., Shin, K.S., Heo, C.H., Lee, S.H., 2005. Regional hydrochemical study on salinization of coastal aquifers, western coastal area of South Korea. J. Hydrol. 313 (3-4), 182-194.

Penna, D., Stenni, B., Wrede, S., Bogaard, T.A., Gobbi, A., Borga, M., Fischer, B.M.C., Bonazza, M., Charova, Z., 2010. On the reproducibility and repeatability of laser absorption spectroscopy measurements for d^2H and $d^{18}O$ isotopic analysis. Hydrological Earth Systems Science 7, 2975-3014.

Piper, A.M., 1944. A graphic procedure in the geochemical interpretation of water analyses. Trans. Am. Geophys Union 25, 914-923.

Plummer, L.N., 2005. Dating of young groundwater. In: handbook: Isotopes in the water cycle. Past, Present and Future of Developing Science. IAEA. Springer, 193-218.

Qurtobi M., Marah H., El Mahboul A., Emblanch C., 2010. Groundwater Tracing Using Stable Isotope in the Western Mediterranean (Case of Rif Chain in the North of Morocco). In: Andreo B., Carrasco F., Durán J., LaMoreaux J. (eds) Advances in Research in Karst Media. Environmental Earth Sciences. Springer, Berlin, Heidelberg.

Re, V., Sacchi, E., Martin-Bordes, J.L., Aureli, A., El Hamouti, N., Bouchnan, R., Zuppi, G.M., 2013. Processes affecting groundwater quality in arid zones: the case of the Bou-Areg coastal aquifer (North Morocco). Appl. Geochem. 34, 181-198.

Reddy, A.G.S., 2013. Evaluation of hydrogeochemical characteristics of phreatic alluvial aquifers in southeastern coastal belt of Prakasam district, South India. Environ. Earth Sci. 68 (2), 471-485.

Romanek, C.S., Grossman, E.L., Morse, J.W., 1992. Carbon isotopes fractionation in synthetic aragonite and calcite: effects of temperature and precipitation rate. Geochemica et Cosmochimica Acta 56, 419-430.

Salem, O., Visser, J.H., Dray, M., Gonfiantini, R., 1980. Groundwater flowpatterns in the western Libyan Arab Jamahiriya. In: Arid Zone Hydrogeology: Investigations with Isotope Techniques. International Atomic Energy Agency, Vienna, pp. 165-179.

Schlosser P., Stute M., Dorr H., Sonntag C. and Munnich K.O., 1988. Tritiuml3He dating of shallow groundwater. Earth Planet. Sci. Lett. 89, 353-362.

Singaraja, C., Chidambaram, S., Anandhan, P., Prasanna, M.V., Thivya, C., Thilagavathi, R., Sarathidasan, J., 2014. Hydrochemistry of groundwater in a coastal region and its repercussion on quality, a case study-Thoothukudi district, Tamil Nadu, India. Arab. J. Geosci. 7 (3), 939-950.

Singhal, B., Gupta, R.P., 2010. Applied Hydrogeology of Fractured Rocks. Springer Science & Business Media.

Srinivasamoorthy, K., Gopinath, M., Chidambaram, S., Vasanthavigar, M., Sarma, V.S., 2014. Hydrochemical characterization and quality appraisal of groundwater from Pungar sub basin, Tamilnadu, India. J. King Saud Univ. Sci. 26 (1), 37-52.

Stuiver, M., Polach, H., 1977. Reporting of 14C data. Radiocarbon 19 (3), 355-363.

Tamers, M.A., 1975. Validity of radiocarbon dates on groundwater. Geophysical Survey 2, 217-239.

Stute, M., Deăk, J., 1989. Environmental isotope study (^{14}C, ^{13}C,^{18}O, D, noble gases) on deep groundwater circulation system in Hungary with reference to paleoclimate. Radiocarbon 31, 902–918.

Stute, M., Schlosser, P., J.F., C., Broecker, W.S., 1992. Paleotemperatures in the Southwestern United States derived from noble gases in ground water. Science 256, 1000–1003. Science (80-).

Tamers, M.A., 1975. Validity of radiocarbon dates on groundwater. Geophysical Survey 2, 217-239.

Taylor, C.B., 1976. IAEA Isotope Hydrology Laboratory. Technical Procedure Note No. 19. International Atomic Energy Agency, Vienna.

Tomaszkiewicz, M., Najm, M.A., El-Fadel, M., 2014. Development of a groundwater quality index for seawater intrusion in coastal aquifers. Environ. Model. Softw. 57, 13-26.

Vengosh, A., Gill, J., Reyes, A., Thoresberg, K., 1997. A Multi-Isotope Investigation of the Origin of Groundwater Salinity in Salinas Valley, California. American Geophysical Union, San Francisco, California.

Vogel, J.C., 1993. Variability of carbon isotope fractionation during photosynthesis. In: Ehleringer, J.R., Hall, A.E., Farquhar, G.D. (Eds.). Stable Isotopes and Plant Carbone Water Relations. Academic Press, San Diego, pp. 29-38.

Whittemore, D.O., 1988. Bromide as a tracer in ground-water studies: geochemistry and analytical determination. In: Proceeding of the Ground Water Geochemical Conference. Denver National Water Well Association, Dublin, OH, pp. 339-360.

Xing, L., Guo, H., Zhan, Y., 2013. Groundwater hydrochemical characteristics and processes along flow paths in the North China Plain. J. Asian Earth Sci. 70, 250-264.

Yechieli, Y., Sivan, O., Lazar, B., Vengosh, A., Ronen, D., Herut, B., 2001. Radiocarbon in seawater intruding into the Israeli Mediterranean coastal aquifer. Radiocarbon 43, 773-781.

Zuber, A., Weise, S.M., Osenbrück, K., Grabczak, J., Ciężkowski, W., 1995. Age and recharge area of thermal waters in La˛dek Spa (Sudeten, Poland) deduced from environmental isotope and noble gas data. J. Hydrol. 167, 327–349.

Zuber, A., Weise, S.M., Osenbrück, K., Pajnowska, H., Grabczak, J., 2000. Age and recharge pattern of water in the Oligocene of the Mazovian basin as indicated by environmental tracers. J. Hydrol. 233, 174–188.

PAKISTAN

Chashma units 1–4 (Image : CNNC)
https://world-nuclear-news.org/Articles/Pakistans-Chashma-4-officially-accepted

9. STUDY OF GROUNDWATER DYNAMICS AT AND AROUND CHASHMA NUCLEAR POWER PLANT COMPLEX AT CHASMA, PUNJAB, PAKISTAN

N. IQBAL, A. GHAFFAR, S. BUTT, M. ASIM

Isotope Application Division, Pakistan Institute of Nuclear Science and Technology (PINSTECH), Islamabad, Pakistan

Summary

The study was conducted on alluvium aquifer around Chashma NPPs to investigate the impact of NPPs operation on groundwater system. Stable isotope, major ion chemistry and organic compounds signature suggested recharge from canals, lake and river. Organic signature further explained most probable recharge sources for individual locations. Groundwater residence time using Tracer LPM, CFCs and noble gases isotopes was in the range of 14–59 years and was in good agreement. UA, CE and NGT models suggested recharge temperatures from 9–30 °C and absence of denitrifying or anoxic conditions. The real and filtration velocities of groundwater were found to be 22.2 cm/day and 10.94 cm/day respectively in south-west direction and in-situ effective porosity of the aquifer was 49.3%. The hydraulic conductivity of the aquifer was estimated using grain size analysis that varies from 48–278 m/day with an average value of 139 m/day. The flow pattern suggested that the south-western region of the study area was susceptible to contamination in case of any leakage. Hydro-geochemical facies, hydro-geochemical processes and rock weathering phenomena were clarified using Piper diagram, Gibb's diagram and bivariant plots respectively. Predominantly $Ca - Mg - HCO_3$ water type, water-rock interaction, silicate weathering and evaporative enrichment are the leading phenomenon controlling groundwater chemistry. A preliminary conceptual hydrological model is developed, which may help for the development of a groundwater flow and contaminant transport model for the study area. The study also revealed that the NPPs operation did not impose any adverse impact on groundwater system.

9.1. Introduction

Pakistan, like many other developing countries, is suffering from a 20–30 % shortfall of electricity demand. Because of limited water resources for power generation, it relies on oil/gas fired power plants to meet its growing energy requirements. However, economic, environmental and political pressure along with surging prices of imported oil cost are the major constraints to resolve the power crisis. Nuclear power generation is one of the available alternatives for clean, safe and environmentally friendly modes of electricity generation. Pakistan first nuclear reactor started its operation in 1972 at Karachi. However, two nuclear power reactors, i.e., C1 and C2 have been operational since 2000 and 2011 respectively. At the same site, two new Nuclear Power Plants (NPPs) C3 and C4 made operational recently will continue their power generation for the next 40 years. Hydrological assessment and changes in different parameters (recharge and discharge sources/areas, flow paths, interactions between surface and/or groundwater bodies, dynamics) is utmost important in the vicinity of any NPP because any accidental release of highly toxic/radioactive materials can spread in the environment through surface and groundwater systems. Baseline data of most hydrological parameters was generated during the site selection and construction of C1 and C2 reactors.

This data was compiled by the Isotope Hydrology Group, PINSTECH in 1992–1993 and 2005–2007 for C1 and C2. In these hydrological studies at the sites of the operational NPPs commonly used isotopes and conventional techniques were employed. After a long-term operation of these NPPs, there was a need to reinvestigate and evaluate the changes in various hydrological parameters and groundwater dynamics using advanced isotope techniques.

Participation in this CRP was an opportunity to investigate the changes in hydrological parameters of operational NPPs using common isotopic and conventional hydrology tools along with newly developed techniques e.g., noble gases isotopes and Emerging Organic Compounds (EOCs) for development of a groundwater conceptual model.

Among the numerous applications of noble gas geochemistry, the study of noble gases (He, Ne, Ar, Kr, and Xe) dissolved in groundwater can enhance understanding of surface and groundwater dynamics by providing indications of flow paths, connectivity between aquifers, and water residence times [Andrews J. N. and Lee D. J., 1979; Bottomley D. J. et al., 1984; Torgersen T. and Ivey G. N., 1985; Stute M. et al., 1992; Bethke C M. et al., 2000]. Being conservative tracers, the concentration of Ne, Ar, Kr, and Xe in the groundwater system and recharge areas is considered to be a function of temperature (T), pressure (P) (altitude of recharge area), salinity (S), and excess air (EA). Therefore, noble gas temperatures (NGTs) are regarded as a robust indicator of past climate as well (Kipfer R. et al., 2002).

Emerging Organic Compounds (EOCs) are being employed for identifying processes and sources for transport, occurrence and fate of the contaminants in subsurface systems [Glassmeyer S. T. et al., 2005; Stuart M. E. et al., 2014]. EOCs including Persistent Organic Pollutants (POPs) and organic hydrocarbons are very conservative in nature. Due to their hydrophobic nature and non-polarity, adsorption of EOCs on soil particles is minimal or ignorable. Being conservative nature of organic compounds, the signature of recharge source must have similarity with groundwater reservoir under recharge. The water coming through different geological strata/formations must have different organic signatures in case of non-point source. EOCs can be effectively used as supporting technique to strengthen the existing isotopic tools to estimate groundwater recharge and interconnectivity. This tool may be very effective where the isotopic signatures of multiple recharge sources are very similar and can provide strong evidences for more reliable results. Signatures of organic compounds can provide valuable information on the recharge mechanism and to differentiate the recharge of groundwater for a particular area.

Contaminant transport is the key hydrogeological parameter for site evaluation of any nuclear installation. This may not only provide the deriving mechanism to predict the fate of radionuclides transport in case of a nuclear accident, but also evaluate the vulnerability to human population in terms of groundwater contamination. Assessment of radionuclides contamination and transport in groundwater is imperative to estimate the groundwater flow velocity and flow direction. A combination of a very common radioactive tracer technique was also introduced to estimate in-situ effective porosity. These results will help to understand the changes in groundwater system in the vicinity of NPP site since the last study and will provide basic information that may be used to predict the fate of radioactive contaminants released into groundwater in case of an accident and/or during normal operations. Moreover, the findings of this study will also be useful to develop guidelines for better hydrogeological characterization and management of local and regional groundwater systems in the vicinity of nuclear power plants and to fulfill the safety requirements of Pakistan Nuclear Regulatory Authority.

9.2. Objectives

The Overall Objective of the study is to explore the use of Isotope Hydrology tools, like Noble gases isotopes, together with conventional nuclear tracers (e.g., ^{18}O, ^{2}H, ^{14}C, ^{3}H) for better understanding of hydrogeological conditions and prediction of radioactive contaminants released into groundwater in the vicinity of NPPs in case of a radiological accident and/or during normal operations.

9.2.1. Specific Objectives

✓ Impact of nuclear power plants operation on groundwater parameters for the assessment of radiological hazards

✓ Enhanced technical knowledge for better characterization of groundwater at and around the NPP site

✓ Dating of fast moving and old groundwater using modern techniques of noble gases and other isotope tools.

✓ A conceptual groundwater flow and contaminant transport model of the NPP site.

9.3. Study Area

The study area tectonically lies within the Mianwali Re-entrant, representing part of the northwest-ward dipping Punjab platform. It is located near the Chashma Barrage on the left bank of the river Indus in the Mianwali District, about 32 km south of Mianwali and 280 km south-west of Islamabad. The project site comprises Chashma Nuclear Power Plant Complex and the area in its vicinity covering total area of about 400 km^2. Initially a rectangular strip of approximately 260 km^2 area situated between geographical coordinates from Latitude $32°17' N$ to $32°28' N$ and Longitude $71°21' E$ to $71°33' E$ was sampled and defined as the "Project Area/Study Area". Taking into consideration results of the first sampling, study area was extended to about 400 km^2 between geographical coordinates from Latitude $32°15' N$ to $32°33' N$ and Longitude $71°18' E$ to $71°36' E$.

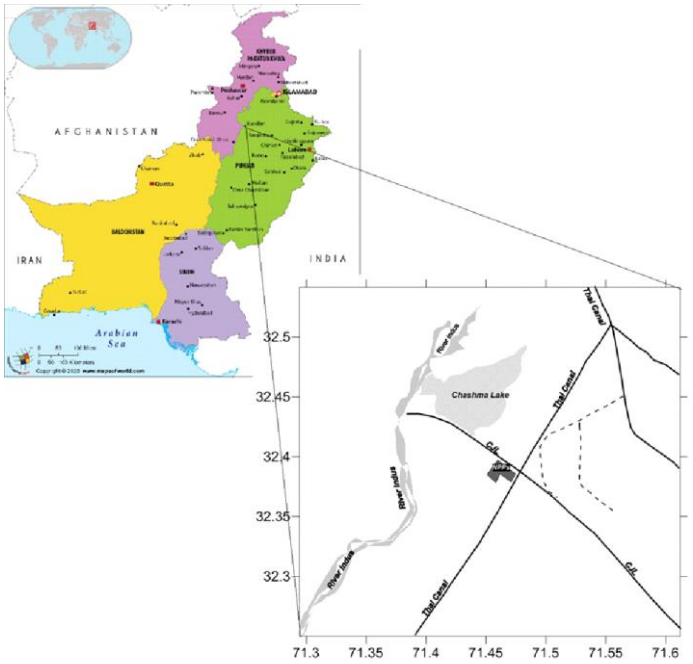

Fig. 9.1. Location Map of study area

The study area (Fig. 9.1) is located on the left bank of the river Indus, downstream of the Chashma Barrage, and extends from Chashma Barrage up to Harnoli and Piplan in the south. While the river Indus itself flows along the western boundary of the project area.

The sub-soil regime in the study area can be recharged by the local rains, the river Indus (higher reaches contributing to downstream sites), Thal canal system, Chashma Barrage reservoir and Chashma-Jhelum Link Canal.

9.3.1. Hydrogeology of study area

The study area makes a part of the upper Thal Doab, interfluding between rivers Indus and Jhelum. It is underlain by unconsolidated Aeolian and alluvial deposits of quaternary age. The Aeolian deposits in the study area are mainly composed of fine sands. These deposits overlie the alluvial sediments in the form of sand dunes. Due to development of agriculture, sand dunes are gradually disappearing and now exist in patches. The exploratory bore holes (160 to 366 m), drilled by WAPDA and PAEC in and around the study area bottomed in alluvium. Hence no definite information is available regarding the total thickness of alluvial deposits. However, deep bore holes drilled by WAPDA in the Punjab reveal that unconsolidated sediments have been deposited on semi-consolidated Tertiary rocks or on a basement of metamorphic and igneous rocks of Precambrian age and their thickness is generally more than 300 m.

The alluvial sediments were deposited in a subsiding trough by the present and ancestral tributaries of the river Indus. The trough was developed due to orogenic movements in the Himalayan Ranges. Contemporaneous filling and subsidence of the trough gave rise to a thick accumulation of alluvial sediments which generally exceed 300 m. In accordance with the mode of deposition i.e. by large streams in constantly shifting courses, the alluvial complex is heterogeneous in both vertical and lateral extent. The drilling indicates that the sand formations are intercalated with lenses of silt and clay of variable thickness and aerial extent [NESPAK, 1992].

9.3.2. Climate of the area

The climate of study site and its surroundings is generally arid and hot, with a long, hot summer season and cold, dry winters. Summer lasts from May to September and winter lasts from November till February. June is the hottest month with average temperatures of 42 °C (highest recorded temperature 52 °C); in winter, December and January monthly average temperatures can be as low as 3 to 4 °C. The average rainfall during 2000–2016 in the district was about 385 mm. The study area is about 200 m above mean sea level, and is located in the direction of north-east, at a distance of about 1,120 km from the Arabian Sea. Towards the west and immediately on the right side of the river Indus are the hills of the Khisor range with an average elevation of 950 m above mean sea level. These hills are devoid of any vegetation. On the north of the site, the land is generally flat and extends up to the foot-hills of the salt range. High mountain ranges lie farther to the north and north-west of the area, which provide an effective barrier, during the winter, to cool-air-masses moving southward from central Asia.

9.4. Materials and Methods

Water samples were collected from the surface bodies, pre-existed hand pumps, boreholes and tube wells located in the area under investigation. Temperature, EC, pH and dissolved oxygen (DO) were measured in-situ. The main concern during sampling, transport and storage was to avoid isotope fractionation through evaporation or diffusive loss of water vapor, and/or isotope exchange with the surroundings as well as with the bottle material. These effects were minimized by using appropriate collection methods and bottles.

Three sampling campaigns were launched, during March 2017 (Pre-monsoon), September 2017 (Post-monsoon) and December 2017 (transition period). In the pre-monsoon sampling campaign 42 water samples were collected for tritium, stable isotope (Deuterium & Oxygen-18) and major ion chemistry, whereas 52 and 54 water samples were collected during September and December sampling campaigns, respectively for the analysis of tritium, stable isotope (Deuterium & Oxygen-18), CFCs and major ion chemistry (Fig. 9.2). All the bottles were marked individually with waterproof marker (project code, location, date, sample number); the information was cross-referenced with the field notebook.

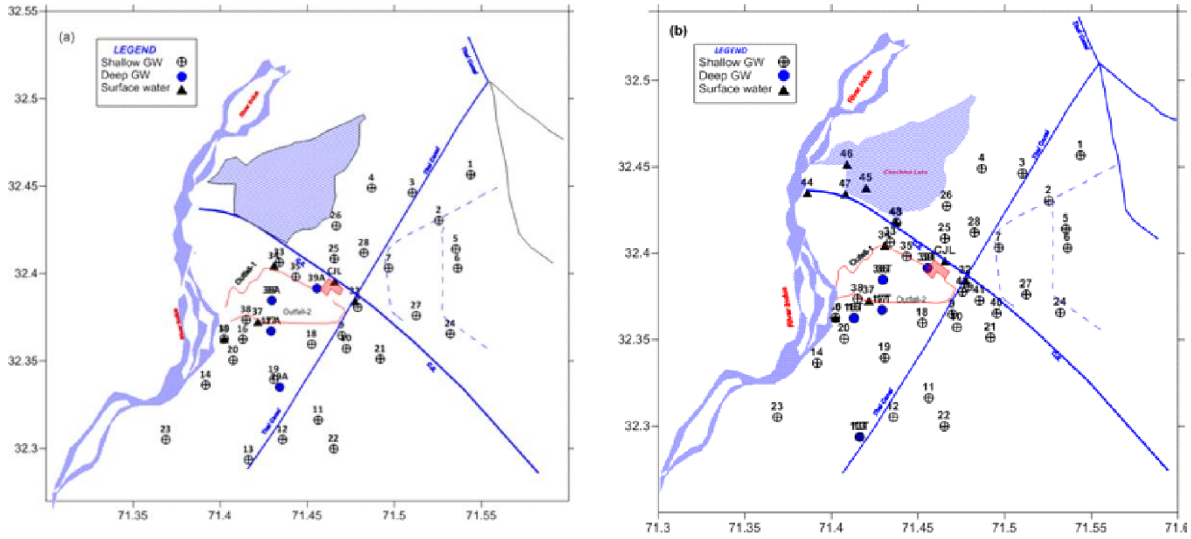

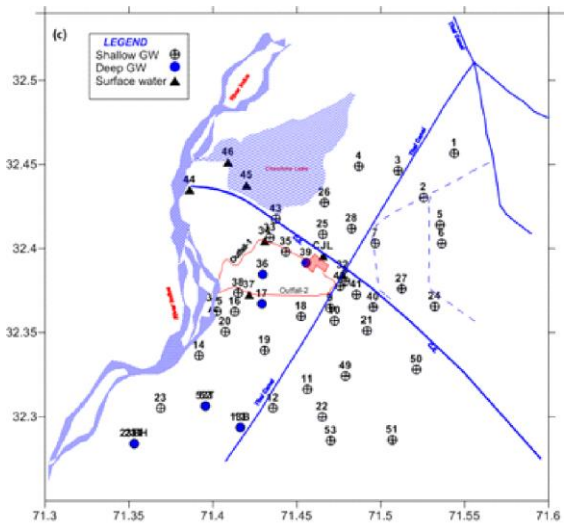

Fig. 9.2. Location of water samples (a - Pre-monsoon, b - post-monsoon, c - Transition period)

9.4.1. Stable isotope analyses

Stable isotope (^{18}O and ^{2}H) analysis was carried out as per the IAEA Standard Operating Procedure for the Liquid-Water Stable Isotope Analyser on Los Gatos Research (LGR) Liquid Water Isotope Analyzer.

9.4.2. Tritium analysis

Tritium analysis of water samples was performed by Liquid Scintillation Counter (LSC), Quantulus-1220 followed by electrolytic enrichment. The uncertainty in measurement was about 0.8 TU. All the samples were distilled on a routine basis to remove impurities. One gram Sodium peroxide is added to250 ml distillate and solution thus prepared is transferred to electrolysis cells for electrolytic enrichment. All the 20 cells were placed in a specially fabricated refrigerator and connected in series. A total charge of 700 AH was passed to get about 14–15 ml of enriched sample. The refrigerator is set to maintain a temperature of 0±1 °C around the cells. Three spikes were included in each run of electrolysis to determine the degree of enrichment. The average enrichment factor is about 16.

On completion of electrolysis, the electrolyte was neutralized by adding four gram Lead Chloride. The samples were again distilled to recover the sample water. Eight ml of enriched sample was taken in 20 ml polyethylene vial and 12 ml scintillation cocktail (Ultima Gold LLT) was added to it. The contents of the vial were mixed up thoroughly by vigorous manual shaking. A batch of samples comprising 3 background samples, 3 standard samples, 3 enriched spikes, 3 un-enriched spikes and 17 enriched samples having unknown tritium concentration were placed in the LSC. Unquenched standards of tritium supplied by Packard Instrument Co. were used to measure and optimize the counting efficiency of LSC. All the samples were counted for a preset time of 50 minutes and the whole batch was cycled 10 times.

Finally counting data was statistically evaluated and processed by excel template to calculate the tritium activity (TU). This template comprises the calculation of the mean background count rate, net count rate of enriched spike, net mean count rate of standard and net count rate of enriched unknown samples.

9.4.3. Emerging Organic Compounds (EOCs)

In order to evaluate EOCs signatures, 25 samples including four reference samples from available recharge sources in the area were collected for analysis. The major recharge sources included Chashma Jhelum Link Canal (CJL), Thal canal (TC), Chashma lake and river Indus. Organic compound signatures of all samples were compared with the reference samples to identify recharge sources.

Samples were filtered through 0.25 μm filter paper using vacuum assisted filtration assembly. Organic compounds in water samples were extracted/pre-concentrated by using solid phase extraction (SPE) techniques using C-18 cartridges under optimized extraction conditions and concentrated through visidry (drying with inert gas purging technique). Extracted samples for organic compounds were scanned using GC-MS and DB-5 column under optimized heating condition of injection port, column and MS detector temperature. The EOCs signatures of surface water sources and groundwater samples were developed under the same extraction and analytical conditions on GC-MS. Then the EOCs signature is compared to identify the recharge sources and interconnections between surface water and groundwater.

9.4.4. Noble gas isotope analysis

Twenty four groundwater samples for Noble gas isotope analysis were collected from a study site in copper tubes provided by IAEA according to IAEA SOPs. The collected samples were sent to IAEA, Vienna for NG isotopes analysis in March 2019.

The Nobel Gas Temperature (NGT) values were calculated using two different models. The Un-fractionated Air (UA) model which assumes that groundwater has equilibrated at 100% relative humidity and any excess noble gas derived from the incorporation of air bubbles has atmospheric composition (Stute M. and Schlosser P, 1992), and the Continuous Equilibration (CE) model of (Aeschbach-Hertig W. et al. 1999) which allows for partial dissolution of trapped air, thereby leading to noble gas fractionation. Mean Residence time (age) in years was calculated applying a total dissolution model considering the recharge temperature and excess air parameters.

9.4.5. Radon concentration around NPPs

The radioactivity of water samples collected around the NPPs was measured using RAD-7. Twenty water samples were collected in 250 ml vials from different sources i.e. bore holes, tube wells, canals, hand pumps as well as the outfalls of power plants. The water samples were collected in a vial from selected borehole/well using an electric pump, so that the accurate radon content of water in deep water is measured. The activity of Radon gas was estimated with RAD-7 detector as per standard protocol.

9.4.6. CFCs analysis

Field sampling for CFCs was carried out during September and December 2017. Forty groundwater samples were collected for CFCs during the sampling campaigns. The sampling bottle was purged according to the USGS National Field Manual. The bottle was placed into a 3 liter SS beaker and then inserted the end of the copper tubing from the pump all the way into the bottom of the sampling bottle. The sample was allowed to pass into the bottles and continued to overflow the bottle while it's sitting in the outer beaker until one liter of water has flushed through the bottle from the bottom. Tapped the bottle to dislodge air bubbles and tightly capped the bottle while submerged in water.

9.4.7. Major ion chemistry

All the samples collected from the study area were analyzed for physico-chemical parameters (EC, pH, temperature) in the field and for major ions Na, K, Ca, Mg, Cl. HCO_3, CO_3, SO_4 analysis were performed in the laboratory. Chloride contents were determined by Titration ($AgNO_3$) method. Carbonate and bicarbonate contents were determined by the titrimetric method. Sulfate concentrations were determined by spectrophotometric method using Hitachi 220-A Double Beam Spectrophotometer. All the major cations were analyzed using Thermo Scientific, ICE-3000 Atomic Absorption Spectrophotometer (AAS).

9.4.8. Groundwater dynamics

Twenty-four (24) boreholes around NPPs site were constructed and investigated to monitor water table fluctuation over a period of one year and to determine the general groundwater flow

direction in the study area. Portal elevations and horizontal coordinates of all the boreholes with reference to a benchmark were determined to correct the values of hydraulic heads accordingly. Water depths from the portal of each borehole were measured using a depth meter. Measurements were plotted on a map of the area and contour lines were drawn connecting points of equal elevation. These lines represent equal pressure between connected points and are called equipotential lines (Fetter C. W., 1990).

Water table contour maps of the study area were generated with respect to the temporal variation in static water level from which the major and minor flow directions were delineated. After assessment of general flow direction a setup for groundwater real and filtration velocities was constructed at the central place between NPPs site and the river Indus (anticipated discharge area). The setup comprising a set of boreholes for multi-well technique and a borehole for point dilution technique (PDT) to determine local groundwater flow direction and velocity. The setup for multi-well technique comprised of an injection borehole at the center and two semicircles of satellite boreholes at 200 cm and 500 cm, which were used as detection boreholes. The semicircle pattern was selected on the basis of groundwater flow direction estimated from the water table contour map described as above. The inner semicircle comprises of 07 observation wells from T1 to T7, with each well located at 26° 45^{0} apart from one another, while the outer semi-circle has 09 monitoring wells from T8 to T16, 20°30^{0} apart from each other (Fig. 9.3).

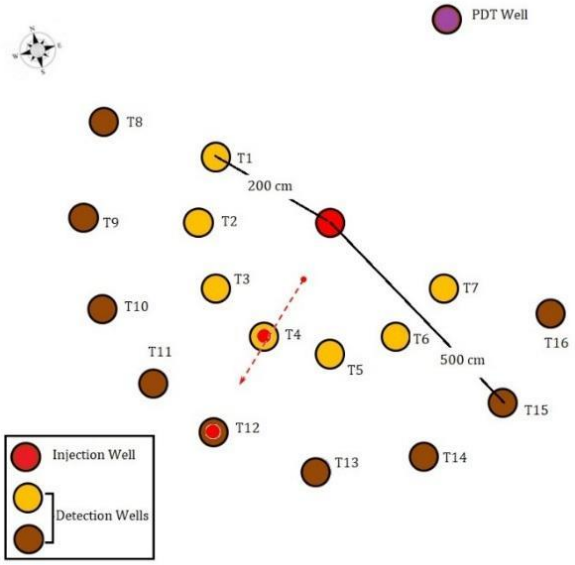

Fig. 9.3. Schematic diagram of experimental setup for groundwater dynamics

About 280 mCi Iodine-131 (^{131}I) in the form of Sodium Iodide solution was injected in the injection well D_0 on 3rd November, 2019 at 1645 hours by using an indigenously designed injection system. Background radiation in air and water was also measured well before the injection of radiotracer (^{131}I). Monitoring of radioactivity in all the detection wells was initiated just after the injection of the tracer and continued until the count rate reached in the limit of three times the standard deviation (σ) in the detection wells. The response of the detectors in the form of CPM was recorded after every 6 hours

An additional borehole for point dilution technique (PDT) was also constructed at 500 cm distance from the central borehole in general groundwater flow direction on the rear (North-East) direction of setup.

The point dilution test (PDT), also called the borehole dilution test, was employed to estimate the groundwater Darcy velocity (Tazioli G.S., 1973). Radiotracer (^{99m}Tc) with a half-life of 6 hours was introduced and homogeneously distributed into a confined section of a well, which was continuously diluted by the groundwater flow and its decreasing concentration is measured over time by using a scintillation detector housed-in the measuring volume. A Rheometer probe equipped with multiple accessories such as control unit, data logger, computer, tracer injection system,

homogenization system and a radiation detection system was employed to determine the filtration velocity at specified location.

The filtration velocity depends on two variables; the temporal response of the detector and the extent of distortion of the groundwater flow field caused by the presence of the well.

The concentration of the tracer injected in the measurement volume decreases exponentially with time. The filtration velocity 'V_f' of groundwater (2) has been derived from simple differential equation (1) as given below:

$$\frac{dC}{dt} = -\frac{CQ}{V}, \quad (1)$$

$$V_f = \frac{V}{\alpha F t} ln\left(\frac{C_0}{C}\right), \quad (2)$$

Where Q is discharge through the well, V is the measurement volume, F is cross-section of measurement volume, C_0 is tracer concentration at t=0, C is tracer concentration at time t, α is the convergence factor for water flow lines due to construction of borehole.

For a well screen of inner radius "R_1" and the measurement volume with a height of "h", the values of $V = \pi(R_1)^2h$ and $F = 2R_1h$ substituted as:

$$ln\left(\frac{C}{C_0}\right) = -\frac{2\alpha . V_f}{\pi R_1} \times t \quad (3)$$

Tracer concentration versus time field data are analyzed by plotting the natural logarithm of the ratio of tracer concentration (C) at any time to the initial concentration (C_0) versus time. The tracer dilution is caused by water flowing through the test section and the logarithm of this ratio (C/C_0) exhibits a linear trend, and its slope (m) is equal to the factor "". Therefore, the filtration velocity "V_f" can be calculated using equation

$$V_f = -\frac{m \times \pi \times R_1}{2\alpha} \quad (4)$$

The value of "α" generally varies between 0 to 8 (Gaspar E., 1987) and it mainly depends on two key factors; firstly, construction design of the well and secondly, the nature of the porous medium. Mathematically "α" may be calculated using the equation of Klotz (Klotz D., 1978). Finally, V_f was calculated by incorporating various design parameters of the experimental wells and the field data in equation 4.

Porosity, ρ of a porous medium is mathematically defined as

$$\rho = \left(\frac{V_v}{V_0}\right) \times 100 \ \%$$

In an isotropic system the flow rate is equal to the product of flow velocity and cross-sectional area of the flow pipe. The equation Q=A×V is commonly known as the discharge equation, where, Q is discharge rate, A represent area and V is velocity. By comparison of filtration and real velocity, the relationship among these two parameters can be written in term of porosity as following

$$Q = A \times V_f = A_v \times V_r \quad , V_f = V_r\left(\frac{A_v}{A}\right)$$

$$V_f = V_r\left(\frac{A_v L}{AL}\right) \rightarrow V_r\left(\frac{Vol_{void}}{Vol_{total}}\right)$$

$$V_f = V_r \times Porosity$$

The experimental setup constructed for groundwater flow direction and point dilution experiment was also employed to estimate a vital hydrogeological parameter known as effective porosity. To calculate the effective porosity, experiments of real velocity and filtration velocity were conducted side by side and their results were subsequently incorporated in a simple mathematical correlation (Freeze R. A. and Cherry J. A., 1979)

$$Vr = \frac{V_f}{p_{eff}}.$$

9.4.9. Hydraulic Conductivity of Aquifer

Soil samples from each borehole were also collected for grain size analysis. Various approaches exist to relate saturated hydraulic conductivity (K s) to grain-size data. Most methods use a single grain-size parameter $K_s = c(d_{10})^2 \frac{cm}{\sec}$ (Hazen. A., 1982) and hence omit the information encompassed by the entire grain-size distribution. The formula, which is based only on the single particle size, is less accurate than the formula, which is based on the entire particle size distribution and particle shape [Ahuja, L. R. 1989. & Udong, J. 2007]. For estimation of hydraulic conductivity approach of Salarashayeri and Siosemarde was adopted which incorporate entire particle distribution $K_s = 10.06 + 118.54(d_{10}) - 12.5(d_{50}) - 7.32(d_{60})$ (Salarashayeri A. F. and Siosemarde M., 2012).

Hydraulic conductivity or coefficient of permeability was also calculated using simple Darcy's law for comparison purposes. Two boreholes on either sides of the experimental setup for filtration velocity in the direction of groundwater flow were constructed for determination of hydraulic gradient and hydraulic conductivity was estimated using well known Darcy formula

$$K = \frac{v_f}{I}.$$

9.4.10. Compilation of data from Previous studies

Until this time IAD PINSTECH has concluded two major hydrological investigations during 1991–1993 and 2005–2007. The data generated in these investigations and several small scale studies is used as a baseline for the present investigation.

The samples collected during 1991–1993 show different ranges for stable isotope fractions. $\delta^{18}O$ & $\delta^{2}H$ values for surface water varies from –13.03 to –11.2‰ and –90.95 to –88.1‰, Shallow groundwater from –12.42 to –4.11 ‰ and –85.57 to –23.27‰, Deep groundwater from –11.82 to –6.2‰ and –79.8 to –35.5‰, respectively. The $\delta^{18}O$ & $\delta^{2}H$ plot reflects that both shallow and deep groundwater are mainly recharged mostly from river indus and local surface water bodies, while a minor population shows mixed recharge either from rain or mixing of evaporated rain with surface water (Fig. 9.4). Furthermore, tritium data suggested that most shallow groundwater samples were in the range of 4–40 TU with the average tritium concentration of 23.7 TU indicating relatively shorter residence time and fresh recharge, while deep groundwater shows mixed trends for tritium levels with some having relatively lower tritium values as compared to shallow, while the other exhibits higher tritium values indicating contribution of mixing with post 1950 water and snowmelt from the glaciers developed during high tritium period respectively.

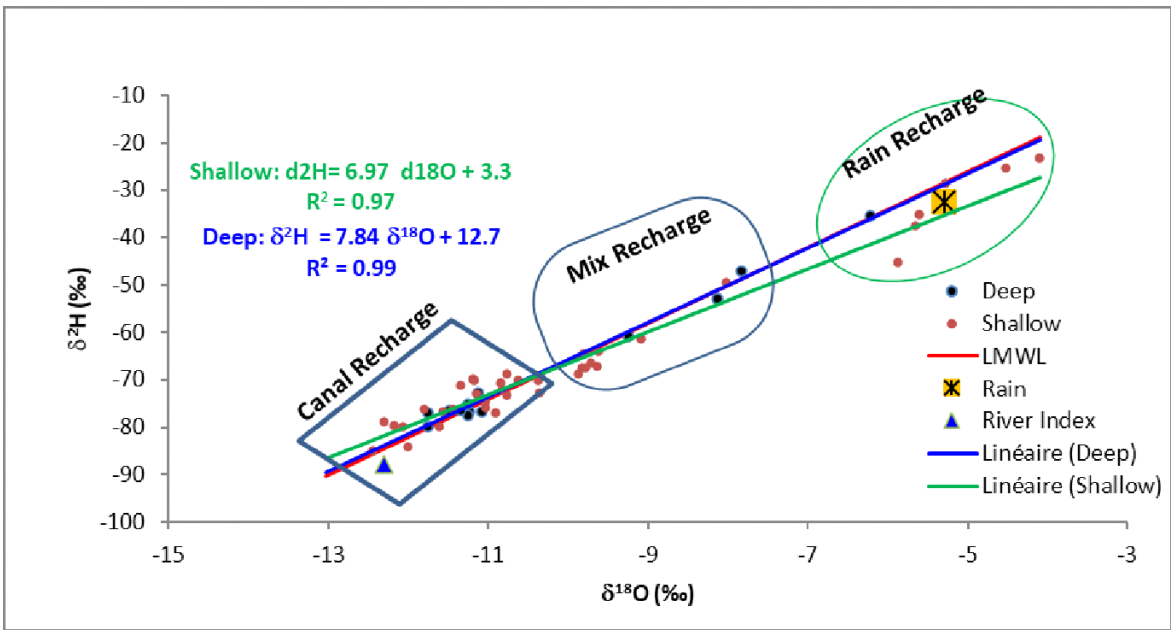

Fig. 9.4. Plot of $\delta^{18}O$ vs $\delta^{2}H$ of water samples in the vicinity of Chasma Site (1992)

Similar trends were observed from isotopic data of water samples ($\delta^{18}O$ & $\delta^{2}H$) collected during 2005–2007 study except some minor diversities.These minor diversities could be attributed to the temporal variations in isotopic and hydrochemical parameters caused by local agriculture activities, weather conditions and atmospheric changes.$\delta^{18}O$ & $\delta^{2}H$ values for rain water varies from –7.37 to –3.10‰ and –54.41 to –29.71‰, River water from –12.99 to –10.48‰ and –91.36 to –65.86, Shallow groundwater from –12.42 to –3.26 ‰ and –90.57 to –21.27‰, Deep groundwater from –11.85 to –8.16‰ and –87.52 to 57.98‰, respectively. Tritium values for rain water ranging from 12.3-13.2 TU, for river water 10-19 TU, for shallow groundwater 0.60-20TU and for deep groundwater 0.80–10.60 TU, respectively. The observed isotopic data ($\delta^{18}O$ &$\delta^{2}H$ and ^{3}H) interpreted that the predominant recharge source for the study area is river and canals. Moreover, tritium data interpretation also indicates similar trends as for the previous study (1991–1993).

Water level contours of study area for 1977 and 1990 (NESPAK, 1992) are also included for model input as initial conditions and calibration purpose respectively. The water level contours of both periods show a similar trend of groundwater direction towards river in the direction of west with slight lowering of water table.

Following conclusions were drawn from the isotopic data:

✓ There are two sources of groundwater recharge i.e. Indus River System and rain. The deep groundwater in the study area is mainly recharged by the Indus River System having contribution 70–90%.

✓ Major source of recharge for shallow groundwater is the river system having contribution more than 60%.

✓ Heavy exploitation of ground water would change the relative contributions of the two sources of recharge and induced infiltration from the river and canal system will increase.

✓ Tritium data show that the mean residence time of most of the groundwater varies from few years to 40 years except some locations having tritium values less than 1 TU, which indicate mean residence time more than 50 years (IAD-84/CFR/2008).

9.5. Results and Discussion

9.5.1. Groundwater Recharge Mechanism

The control points to interpret the isotopic data of any area in terms of recharge mechanism are meteoric water line, rain index and river system index in the area under investigation. Extensive samplings over a long period of time are required to establish these control points or indices. The weighted average "$\delta^{18}O$: –3.62 ‰, $\delta^{2}H$: –19.14‰" of Chasma rain data (2005–2007) was taken as rain index while average "$\delta^{18}O$: –11.38 ‰, $\delta^{2}H$: –75.31‰" monthly isotopic data of same period of river system in the study area was taken as isotopic river index. For Local meteoric water line (LMWL) shown in Fig. 9.5, it was established during 2005-2007 using actual slope and intercept of all rain samples (non-weighted), slopes 7.58 and 6.97 were taken respectively as reference. The average isotopic signatures "$\delta^{18}O$: –11.9‰, $\delta^{2}H$: –83.4‰" of River Indus at Basham, 300 km upstream at altitude of 625 m were also included for reference to compare the isotopic values with some higher altitude location.

The isotopic data for the collected groundwater samples revealed the relative contribution of recharge sources such as rain, river and canal. During pre-monsoon season isotopic values for $\delta^{18}O$ & $\delta^{2}H$ in surface water samples varies from –11.07 to –11.31 ‰ and –71.9 to –72.93 ‰, in the shallow groundwater –6.84 to –12.03 ‰ and –42.66 to –79.9 ‰ and in the deep groundwater –10.91 to –11.73 ‰ and –73.93 to –77.29‰, respectively. During post-monsoon season, isotopic values of $\delta^{18}O$ and $\delta^{2}H$ in surface water samples range from –11.52 to –12.62 ‰ and –79.95 to –84.79 ‰, shallow groundwater varies –8.17 to –11.97 ‰ and –51.71 to –81.07 ‰ and in the deep groundwater –8.9 to –11.13 ‰ and –59.31 to –75.98 ‰, respectively. Whereas, transition period with relatively enriched isotopic values for $\delta^{18}O$ and $\delta^{2}H$ is characterized with surface water samples varies from –11.11 to –11.37 ‰ and –74.6 to –78.34 ‰, shallow groundwater ranges from –5.52 to –12.64 ‰ and –32.28 to –82.97 ‰ and the deep ground water extends from –10.53 to –11.49 ‰ and –69.66 to –75.58 ‰, respectively.

The $\delta^{18}O$ *vs* $\delta^{2}H$ plots of three sampling campaigns are shown in (Fig. 9.5). The isotopic data indicates that most of the groundwater samples are situated marginally above the LMWL and closer to the river index, which indicates shallow groundwater is mainly recharged by the river and surface water resources. On the other hand, mixed recharge is associated with the samples located among river and rain index. Whereas, samples with depleted isotopic values are aligned nearer to the LMWL, indicating major contribution of river and canal water. A few deep groundwater samples show mixing of evaporated rains but most of them are predominantly recharged by surface water.

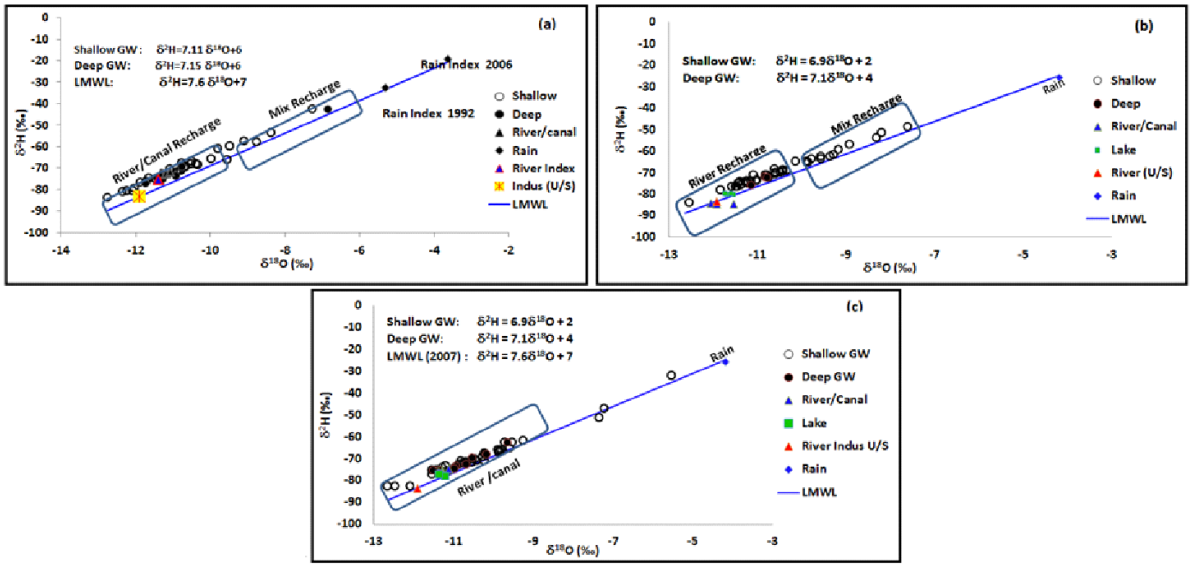

Fig. 9.5. $\delta^{2}H$ vs. $\delta^{18}O$ plot of water sample: (a) pre-monsoon, (b) post-monsoon, (c) transition period

Seasonal effect reveals that during pre-monsoon, the isotopes are relatively enriched in comparison to the post-monsoon. This could be attributed to the enrichment of heavy isotope in the pre-monsoon season (Fig. 9.5, a) by two key factors; temperature effect and the amount effect. Firstly, Temperature effect derives its roots as lower the atmospheric temperature higher will be the isotope fractionation, which may lead to the enrichment of surface water with respect to heavier isotopes ($\delta^{18}O$ & δ^{2} H) during pre-monsoon season. Secondly, the amount effect which does not contribute considerably for modification of isotopic values, owing to few rain events in pre-monsoon season. Conversely, depletion of isotopes ($\delta^{18}O$ and $\delta^{2}H$) during the post-monsoon season (Fig. 9.5, b) is primarily due to heavy rains and high tides condition in river Indus.

Additionally, depletion of isotopic values could be credited to isotopically depleted snow/glacier melt coming from high mountains of Himalayas contributing to river Indus, which is the major recharge source for the study area. Similar trends for transition period (Fig. 9.5, c) were observed as temperature is substantially low in winter season, which results in enrichment of surface water and subsequent enrichment of shallow and deep groundwater in terms of heavy isotopes. Therefore, it is concluded that river and canal water is the main recharge source for the study area.

9.5.1.1. Spatial variation of $\delta^{18}O$

The spatial distribution of Oxygen-18 (Fig. 9.6) shows exactly similar trends as revealed in previous studies. The $\delta^{18}O$ varies with the distance between the sampling station and river/canal system indicating considerable effect of the canal water to the groundwater. Furthermore, samples located near to river and canals exhibiting depleted isotopes also signify that the possible source of groundwater replenishment is river/canals water.

During the dry period river Indus in the vicinity of the study area behaves like a gaining stream. Only for a short period when the river flows at full swing, it contributes to nearby groundwater. $\delta^{18}O$ *vs* $\delta^{2}H$ Plot (see Fig. 9.5) and spatial distribution of $\delta^{18}O$ (see Fig. 9.6) clearly indicates this phenomenon during different seasons.

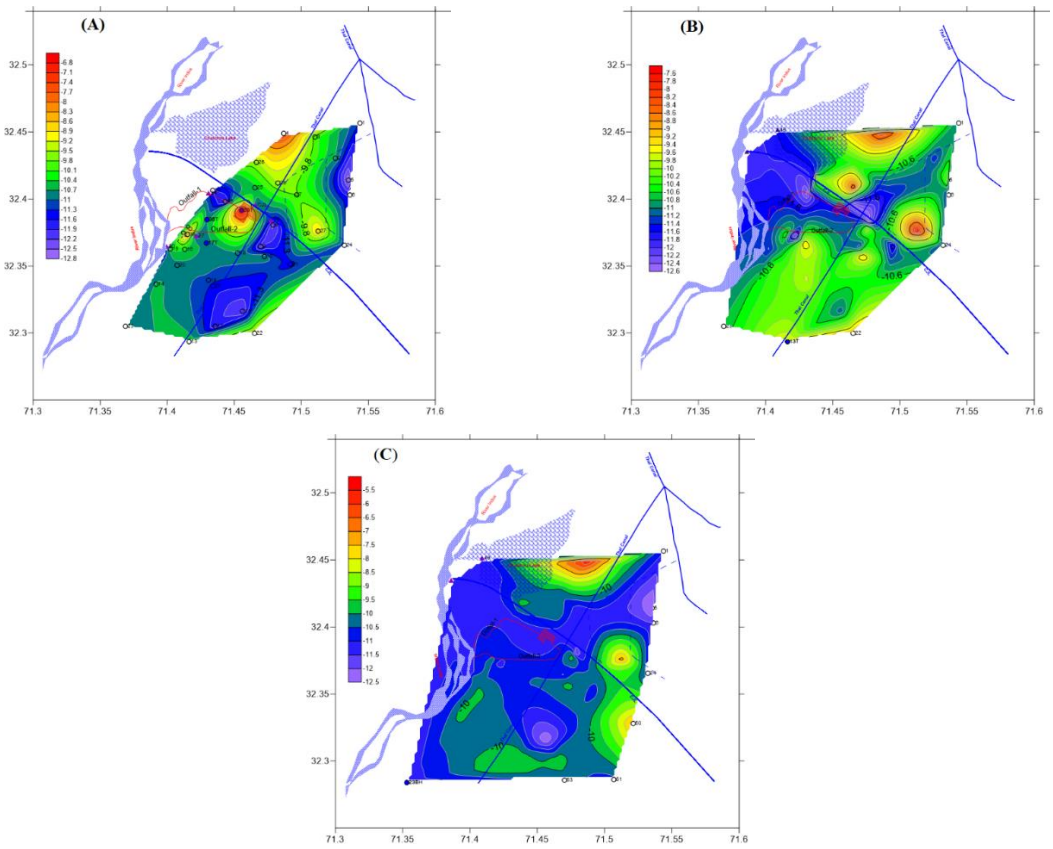

Fig. 9.6. Spatial Distribution of $\delta^{18}O$: (A) March, (B) September, (C) December, 2017

Overall, spatial distribution of $\delta^{18}O$ and EC unveiled analogous findings as inferred from the distribution of both pre and post monsoon season.

9.5.1.2. Emerging Organic Compounds

The signature of organic compounds of water samples 28, 34, 35, 36, 37 and 39 (Table 9.1) had more than 80% matching of organic compounds with reference sample CJL canal. Location of 28 canal is near the Thal canal but EOC signature indicates CJL canal as its recharge source. CJL canal is the potential recharge source for these points as organic compounds of each sample have extreme matching with organic compounds of the canal which also support the finding of stable isotopic data.

The most prevalent organic compounds in the water samples of 1, 2, 5, 7, 12, 13, 18 and 19 suggested the thal canal is the possible recharge source of these sites as maximum matching of organic signatures were observed between these samples and Thal canal (Table 9.2).

Apart from it some of these samples 21, 24, 27 indicate mixed recharge source of CJL and Thal canal. Additionally, a large number of significant peaks were obtained in these samples as compared to the rest of the other samples. This could be credited to the great number of anthropogenic activities that might be associated with these sites. The EOC signatures of Sample 6 look like the signatures of Thal canal but have some different peaks that may be due to some anthropogenic activities due to its location inside a small village.

The samples 35, 36 and 37 are near the river but data suggested here a CJL canal recharge. It showed that river water may not be following that path. However organic signatures of sample No. 4 and 26 are matching with organic signatures of Chashma lake that shows the lake is recharging this area.

Organic data validates that rain is not the major recharge source of these locations, rather these areas are either canal recharged or river recharged. Results showed that 4 sites 20, 23, 30 and 32have close resemblance with the river (Table 9.3). Organic signatures of sample 23 had close matching with the river that clearly mirrors off that water here was recharged through the river besides its location on predicted flow pattern.

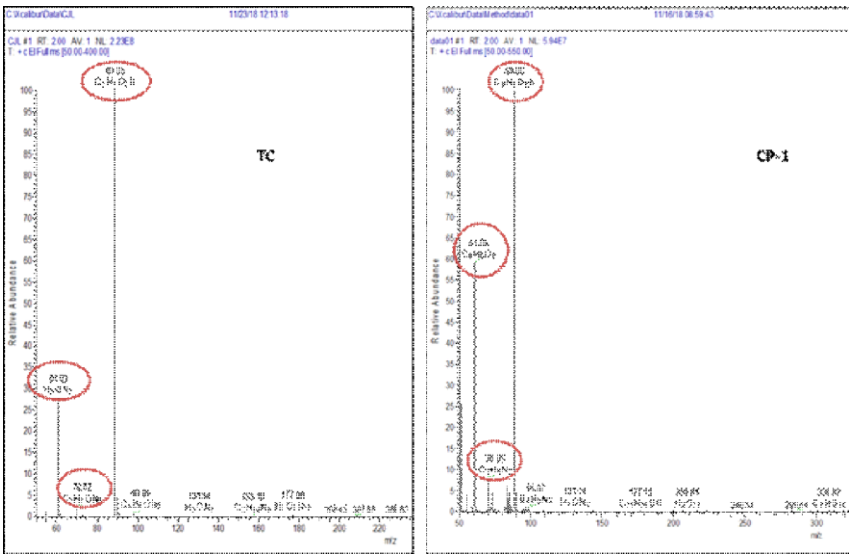

Fig. 9.7. Part of full scan total ion chromatogram of Thal canal and sample No. 1

A portion of full scan total ion chromatogram by GC-MS of Thal canal and sample No. 1 is given in Fig. 9.7 as an example of organic compound comparison between two samples and the recharge pattern as predicted by EOCs are given in Fig. 9.8.

9.5.2. Groundwater Residence Time

The mean residence time (MRT) of groundwater is a critical hydrological parameter required for the groundwater dynamics studies. Tritium, CFCs and Noble gas isotope technique was applied for determination of MRT.

9.5.2.1. Tritium

Frequency histograms of tritium concentration in surface and groundwater samples collected during March, September and December 2017 are shown in Fig. 9.9.

The Fig. 9.9 shows frequency histogram of tritium content in water samples of different seasons over the year. The histogram from Fig. 9.9 (A) to (C) represents the tritium variation during the pre-monsoon, post-monsoon and transition period in various categories of waters comprising shallow groundwater, deep groundwater, surface water and rainwater.

In shallow groundwater tritium concentration during various seasons exhibits diverse range, extending from 2-20 TU. During pre-monsoon, post-monsoon and transition periods, 72% (n=29), 69% (n=25) and 75% (n=30) of the shallow groundwater samples range from 8–14 TU, respectively. Likewise, 17% (n=05), 25% (n=09) and 20% (n=08) of pre-monsoon, post-monsoon, and transition period, respectively, exhibit tritium concentration ranges from 2–6 TU. Whereas, only a few shallow groundwaters lie in the range of 16–20 TU, with 10% (n=03) of pre-monsoon, 8% (n=03) of post-monsoon and 5% (n=02) of transition period. Comparing histograms with the spatial distribution diagrams (Fig. 9.10) it is observable that most of the samples having similarity of tritium concentration with the surface waters lie near the water channels indicate quick recharge while a smaller population having lower tritium concentration are relatively farther from surface water resources have higher residence time. The stable isotope values and the groundwater direction depicted by water table contours (Fig. 9.16) also supports this finding. Few samples having extraordinary higher tritium concentration may be attributed to some glaciers-melt in Northern Areas of Pakistan still having higher tritium and contributing to river Indus.

A few deep groundwater samples were available during each sampling. The temporal trend of tritium in deep samples depicts almost similar ranges as shallow groundwater samples. During pre-monsoon, samples generally have low tritium values varying from 2–7 TU (n=03) indicate higher residence time. One location in post-monsoon and transition period having 14 TU and one location having 12 TU are medium depth (about 200 ft) boreholes developed by local farmers for irrigation purposes suggest a few years of residence time and quick recharge.

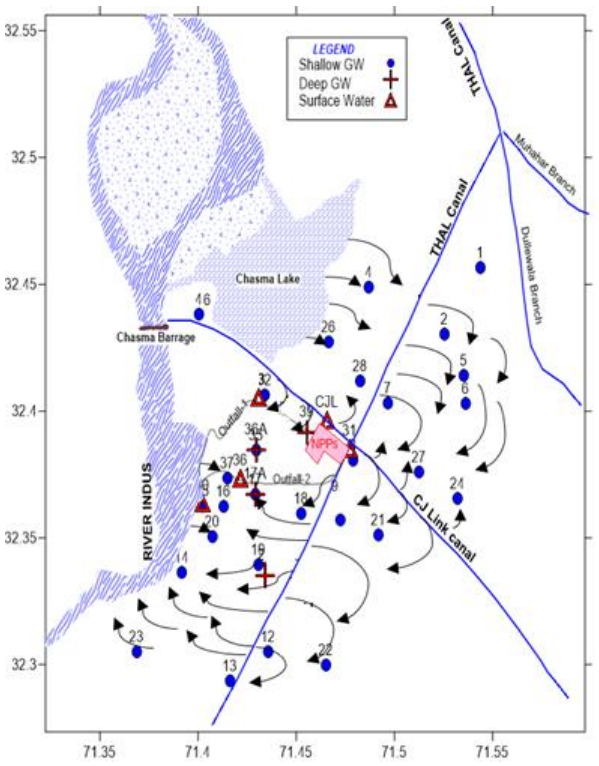

Fig. 9.8. Recharge patterns depicted by EOC signatures in study area

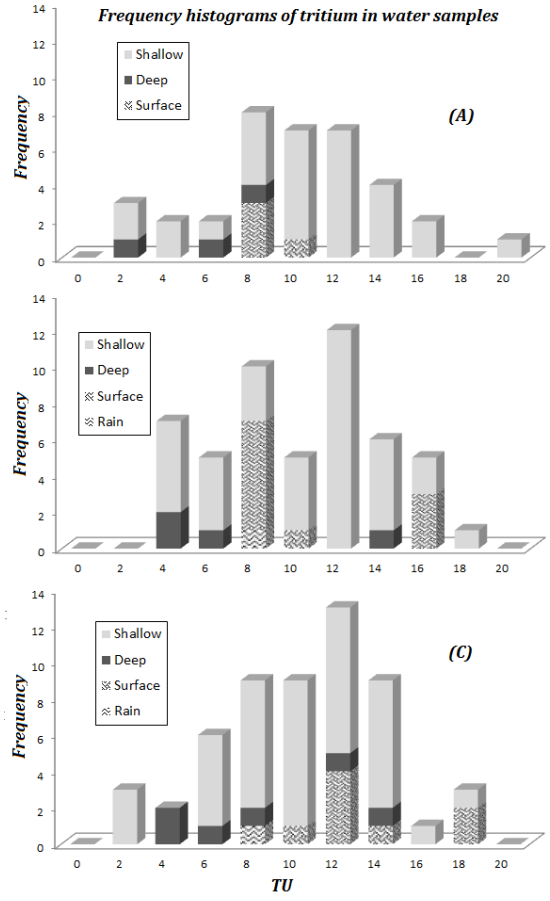

Fig. 9.9. Frequency histograms of Tritium in water samples:
(A) March, (B) September, (C) December, 2017

Tritium concentration in surface ranges from 8–10 TU (n=04), 8–16 TU (n=10) and 10–18 TU (n=08) for pre-monsoon, post-monsoon and transition period, respectively, whereas, tritium in rain samples collected during post-monsoon and transition period shows a value of 8 TU.

The spatial distribution (Fig. 9.10) suggests that some of the deep groundwater samples (16, 36) showing high tritium values (13–18 TU) are located in the southwest of the NPPs and near the river Indus, which indicate mixing of groundwater with river base flow water. On the other hand, the majority of the samples located near the CJL and Thal canals exhibit tritium values range from 7–12 TU, illustrate their shorter mean residence time and also suggest their predominant recharge source is surface water. While, a few samples (1, 9, 17, 18, 21, 23) having tritium concentration from 1–6 TU, delineate mixed water, designating presence of some fraction of old groundwater with surface water.

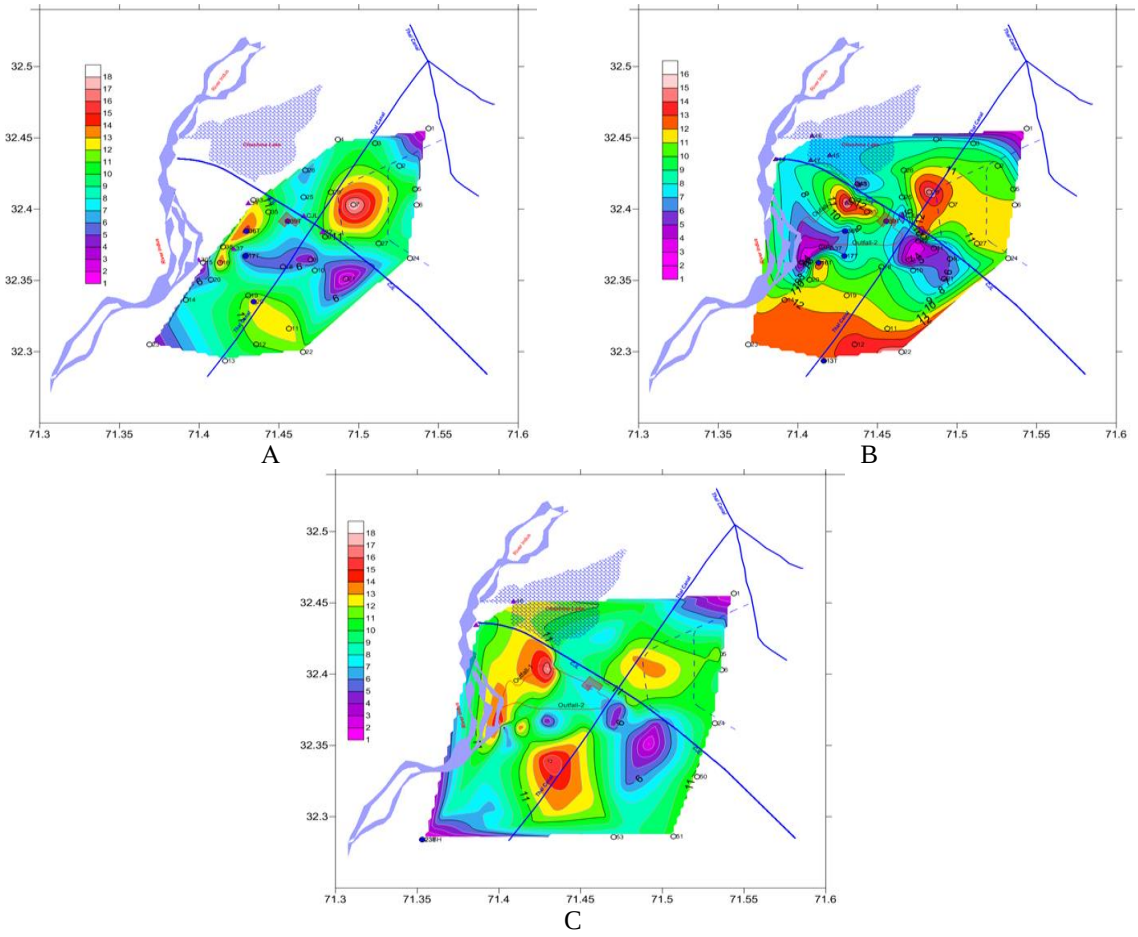

Fig. 9.10. Spatial distribution of Tritium:
(A) March, (B) September, (C) December, 2017

9.5.2.2. CFCs

Chlorofluorocarbons (CFCs) offer exquisite capability to use them as tracer for dating young water (≤50 Years). The mechanism of groundwater age dating with CFCs is based on Henry's law of solubility by measuring concentration of the gas dissolved in water in equilibrium with air. The age dating using CFCs is subjective to numerous parameters such as recharge temperature, Salinity, excess air in the water sample and altitude at location of recharge (Cox, S. E., 2003). Transformation of groundwater age or mean residence time (MRT) to 'Modeled age' needs a mathematical model. Thus, simple lumped parameter model (Tracer LPM) was used to describe distributions of age in a more precise manner (Fig. 9.11). Tracer LPM approach is very useful because it integrates CFCs data over large temporal and spatial scales.

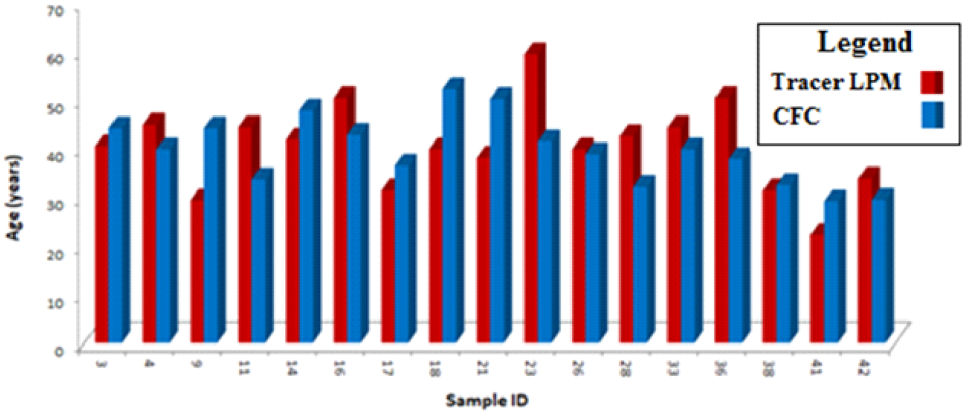

	Tracer LPM (years)	CFC (years)
Maximum age	59	52
Minimum Age	22	29

Fig. 9.11. Groundwater mean residence time determined by CFCs and Tracer LPM model

CFCs analysis of collected groundwater samples reveals that CFC-ll ranges from 0.02 to 12.96 pmol/kg, CFC-12 varies from 0.13 to 2.63 pmol/kg, and CFC-113 concentrations span from 0.02 to 6.35 pmol/kg.

The groundwater ages predicted by incorporating the experimental data of CFCs (CFC-11, CFC-12 and CFC-113) range from 29 to 52 years and by Tracer LPM range from 22 to 59 years (see Fig. 9.11). Overall, the results demonstrated comparable age ranges calculated by both CFCs and Tracer LPM, which confirms the application of Tracer LPM in groundwater age dating.

9.5.2.3. Noble Gases Isotopes (NG)

UA and CE, NGT models yield average temperatures (Fig. 9.12) range from 9° to 39° C, which are significant according to mean annual air temperature (MAAT). Wide range of recharge temperature (9-39) suggested that recharge sources are of mixed nature comprising of surface water (river & canals) to rainwater. Mean Residence time (age) in years calculated by applying total dissolution model considering the recharge temperature and excess air parameters is from 14 to 53 years which suggested a young groundwater as concluded by Tritium and CFCs data.

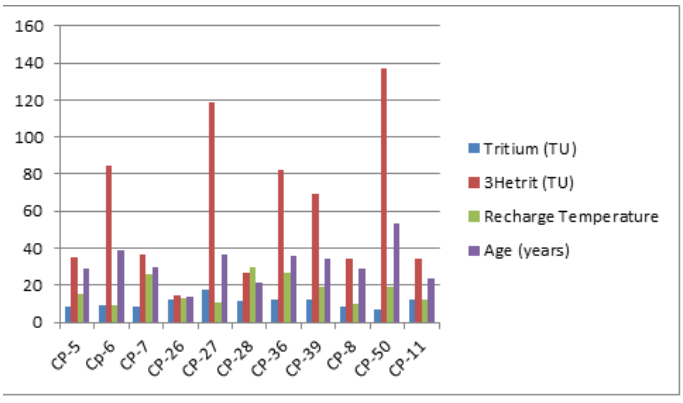

	Recharge Temp	Age:
Minimum:	9 °C	14 years
Maximum:	39 °C	53 years

Fig. 9.12. Recharge temperature and groundwater age using NGT models

Both the CE and UA models suggested that the amount of ^{3}He and ^{4}He in samples is a result from air saturated water (ASW) and dissolved excess air and all He present in the water had an atmospheric origin (Fig. 9.13) (Saar et al., 2005).

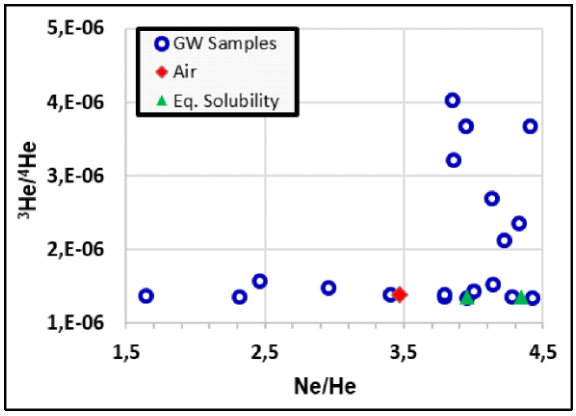

Fig. 9.13. $^{3}He/^{4}He$ vs Ne/He plot for origin of groundwater

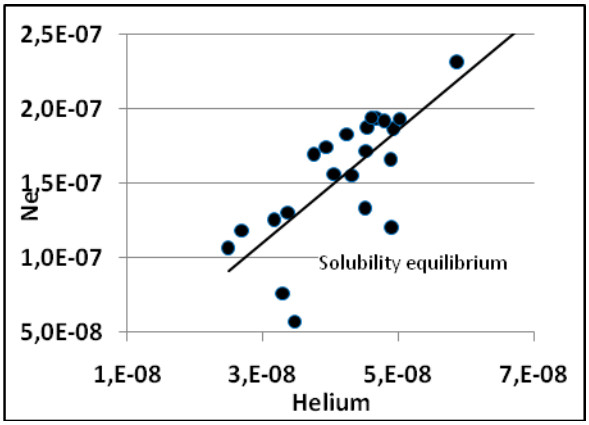

Fig. 9.14. Solubility equilibrium with infiltration temperature

Almost all samples have high equilibrium gas solubility (Fig. 9.14) which is indicative of no degassing or gas stripping. Noble gas data suggested absence of denitrifying activities or anoxic conditions, these findings were supported by chemical data as well.

9.5.3. Assessment of Radon Concentration

The activities of the radon gas by using RAD7 radon detector ranged from 20 pCi/l to 310 pCi/l with a mean value of 160 pCi/l 9 (Fig. 9.15). Variations in levels of radon concentration appear due to the locations of the individual sampling sights. Which shows that all values are within the safe limits (300–10,000 pCi/l) [ICRP 1990] as proposed by the ICRP recommended action limits. thus pose no threat to the people of the locality.

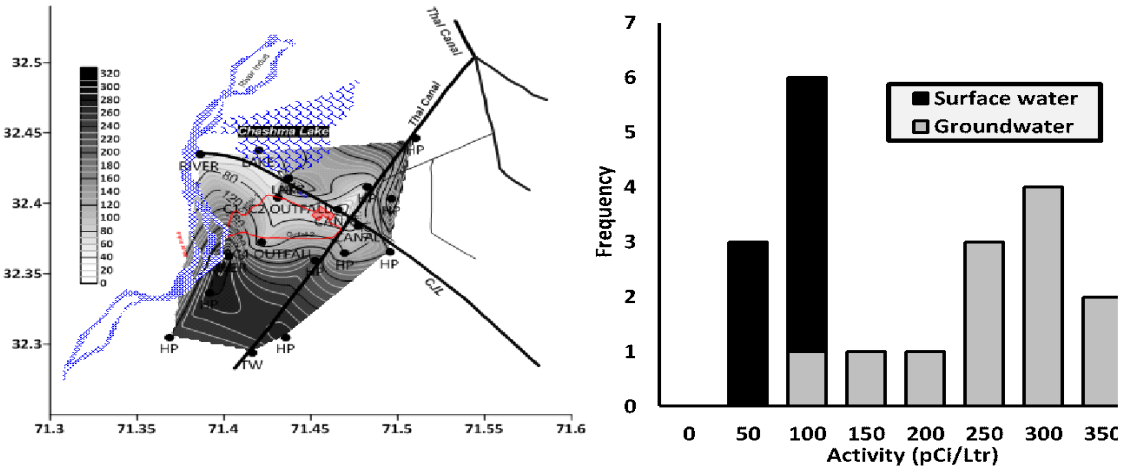

Fig. 9.15. Spatial distribution and frequency histogram of Radon concentration around NPPs

Various environmental tracers are commonly used to understand the interconnectivity of surface water and groundwater. Rivers and canals are key hydrological features nurturing the groundwater of an area. The response of these surface water sources varied over the period of time, depending on precipitation pattern and seasonal variation. To identify the recharge and discharge pattern in a

hydrological system, among various hydrochemical tracer, radon is extensively used because it offers an inexpensive and time efficient way to understand and estimate the surface water – groundwater interaction in varied hydrogeological settings.

The radon data of measured surface and groundwater samples was plotted in the form of spatial plot and frequency histogram (see Fig. 9.15). Frequency histogram shows that radon concentration in surface water samples ranges from 50 to 100 pCi/L, while a broad range exists in groundwater samples, extends from 100 to 350 pCi/L.

The spatial plot of radon activity reveals that surface water in the form of canals and lakes has an influential impact on groundwater recharge of the study area, which is manifested by low radon concentrations in groundwater samples located near the surface water sources and in the vicinity of Chashma NPPs. However, samples located in the south-west quadrant of the spatial map indicate groundwater discharge to the river Indus, which is characterized by relatively high radon values near the river.

9.5.4. Groundwater Flow Parameters

Based on the described methodology, the general direction of groundwater was guesstimated towards the river in the south-west direction.

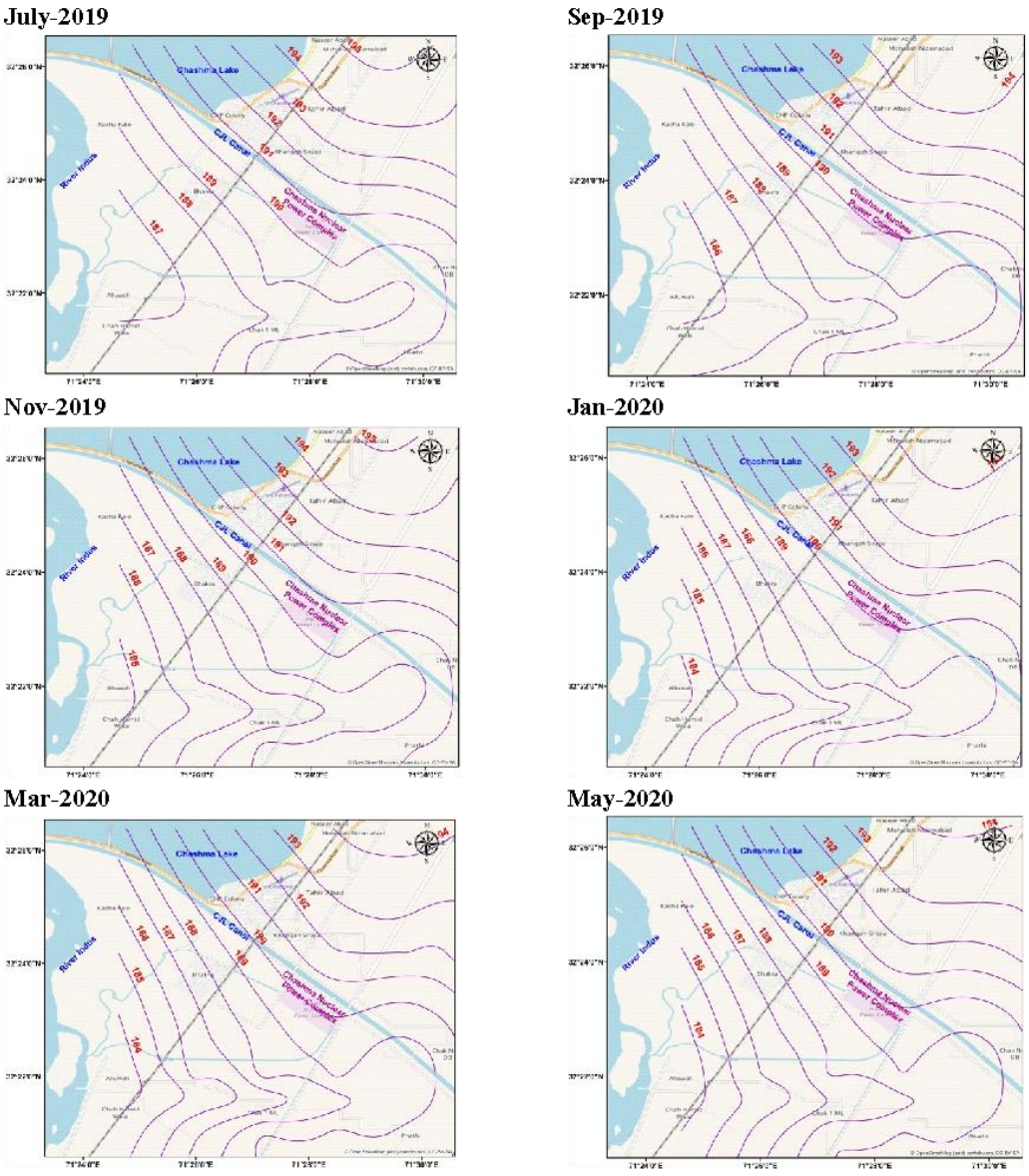

Fig. 9.16. Groundwater contours showing temporal fluctuation in water table and flow direction

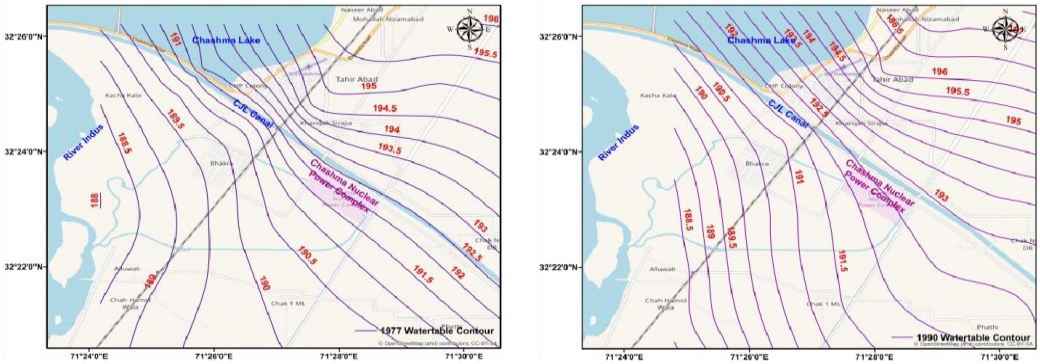

Fig. 9.17. Water table contours of study area during 1977 and 1992

The water table contour maps (Fig. 9.16) show that groundwater flow direction is predominantly towards the river in the direction of south-west with minor fluctuation throughout the year. The flow pattern in the aquifer system therefore suggests that the southern region of the study area is susceptible to groundwater contamination that may release from NPPs in case of any leakage.

Comparing the present water table contours maps with the maps of 1977 and 1990 (Fig. 9.17.), similar trends are observed with slight lowering of water table in the area. This lowering may be due to general scarcity of water or due to heavy abstraction of groundwater for agriculture and domestic use.

9.5.4.1. Groundwater real velocity

The tracer was first appeared in detection well T_4 (see Fig. 9.3) located in the southwest of the injection well on November 12th 2019 at 1630 hours. The breakthrough time was calculated as 223.8 hours (9.32 days). The monitoring of radiotracer was continued in T_4 and all other detection wells in the inner semicircle. The peak value was observed in T_4 on November 19th 2019 at 2230 hours indicating transit time for maximum activity of 395.8 hours (16.5 days). The groundwater velocity for water front was calculated as 21.65 cm/day. After the breakthrough in T_4 all the wells in the second semicircle were also continuously monitored for tracer presence. Finally, the tracer appeared in detection well T_{12} in the outer circle after 527.8 (21.99 days) hours of injection on November 25th 2019 at 1030 hours, indicating breakthrough velocity of 22.74 cm/day in the same direction as determined by appearance of tracer in T_4. The appearance of tracer in any other boreholes in second semicircle was not detected as the count rate remained within $(\pm 3\sigma)$ and three times the background count rate. Table 9.4 summarizes the key events of the described multi-well experiment.

Table. 9.4. Summary of key events during real velocity experiment by multi-well technique (Injection: November 3rd, 2019 at 16:45)

Detection BH	Distance (cm)	Break Through	Transit time		Velocity
			Hours	Days	(cm/day)
T-4	200	11/12/2019 16:30 hrs	223.8	9.32	21.65
T-12	500	11/25/2019 1030 hrs	527.8	21.99	22.74
				Average Real Velocity	22.2

9.5.4.2. Groundwater Filtration Velocity

The value of "α" convergence factor was mathematically estimated on two key factors, the construction type of the well and the nature of the porous medium using the equation of Klotz (Klotz D., 1978). The estimated value of "α" was 2.75.

From the field results of tracer tests carried out in PDT well, $ln\left(\frac{C}{C_0}\right)$ was determined and plotted against time 't' (Fig. 9.18). The Slope of the best-fit lines (dilution lines) having groundwater flow velocity term, which is represented by equation (3) was determined. Groundwater filtration velocity was then calculated as 0.0076 cm/min (10.94 cm/day) using the parameters (i.e. α and R_1) of wells in equation (4).

Using filtration velocity and real velocity in-situ effective porosity is calculated as

$$Porosity = \rho = \frac{V_f}{V_r} = \frac{10.94}{22.2} = 49.3\%$$

which is in good agreement with the porosity of medium to fine sand.

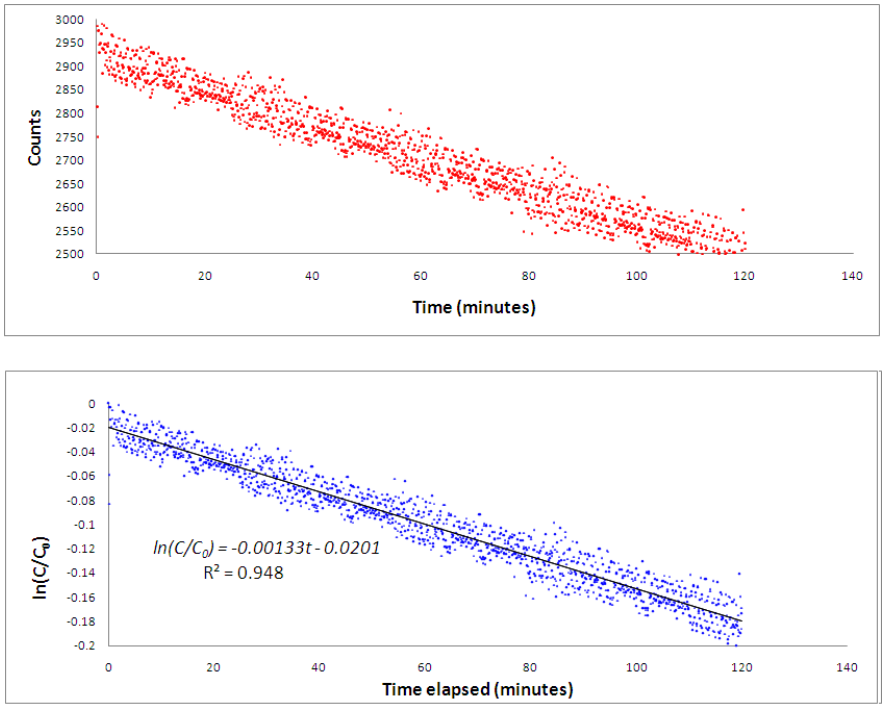

Fig. 9.18. Plot of detector response and $\ln(C/C_o)$ vs time showing dilution rate in PDT well

9.5.4.3. Hydraulic Conductivity of the Aquifer

Hydraulic conductivity of aquifer was estimated by grain size analysis adopting Salarashayeri and Siosemarde formula [Salarashayeri A. F. and Siosemarde M., 2012] which incorporate entire range of grain size i.e., d^{10}, d^{50} and d^{60}. Spatial distribution of Hydraulic conductivity is presented in the form of contours (Fig. 9.19). Hydraulic conductivity of the aquifer around the NPPs ranges from 48 to 278 m/day, indicating an increasing trend from Noth-East to South-West direction.

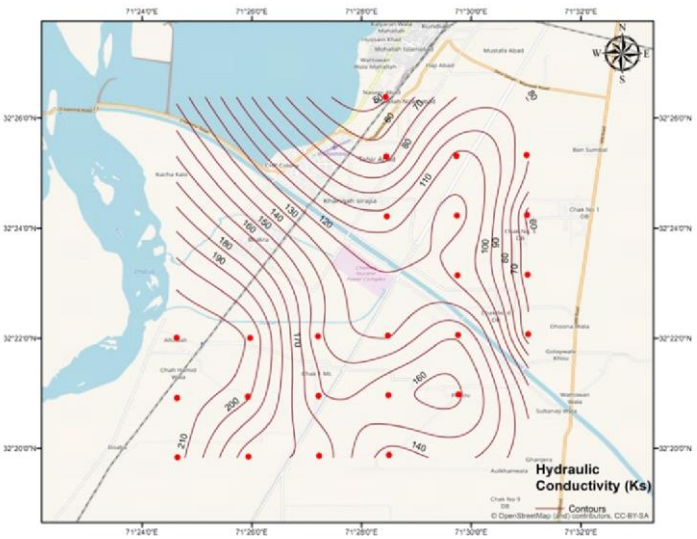

Fig. 9.19. Spatial distribution of Hydraulic conductivity around NPPs site

Hydraulic conductivity or coefficient of permeability was also calculated using simple Darcy's law for comparison using Darcy formula

$$K = \frac{v_f}{I}$$

where:

I = hydraulic gradient = (h1-h2)/d = 1.01/1506 = 0.000761,
h1 = water table in BH-1 = 190.12 m,
h2 = water table in BH-2 = 189.11 m,
d =distance (BH-1 and BH-2) = 1506 m.

Filtration velocity = 10.94 cm/day = 0.1094 m/day.
Hydraulic Conductivity = K = 0.1094 / 0.000761 = **163 m/day.**
Thickness of alluvium = > 300 m (NESPAK, 1992).
Transmissivity (T) = K x Thickness of aquifer = 163 x 300 = **48,900 m^2/day.**
The hydraulic conductivity estimated by both approaches is in good agreement.

9.6. Geo-Hydrochemistry

9.6.1. Physico-chemical characteristics of groundwater

Groundwater of the study area has relatively low TDS as indicated by the EC values of the collected samples.

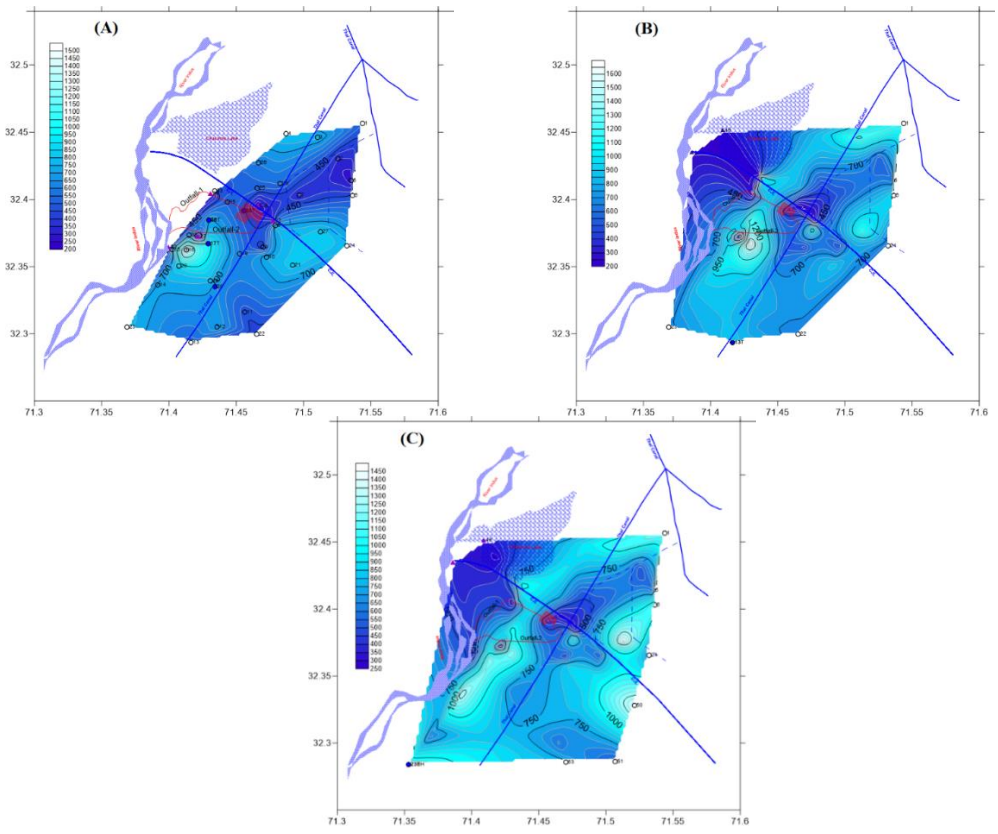

Fig. 9.20. Spatial Distribution of EC

Most of the pre-monsoon samples have electrical conductivity in the range of 220 – 1515 $\frac{\mu S}{cm}$ with an average of 599 µS/cm, whereas during the transition period it ranges from 213 – 1688 $\frac{\mu S}{cm}$ with a mean value of 692 $\frac{\mu S}{cm}$ and then post monsoon, with EC values ranges of 287 – 1543 $\frac{\mu S}{cm}$ with an average value of 783 $\frac{\mu S}{cm}$.

The EC data established that there is no considerable difference in TDS contents of shallow and deep groundwater among three seasons. Moreover, spatial variation of EC (Fig. 9.20) indicates that most of the shallow and deep groundwater samples fall in fresh water zone with minor seasonal variation that may be attributed to the transients occurring in water level of river Indus and the associated canal system. Likewise, pH values of shallow and deep groundwater are similar ranging from 7.5–8.6 with an average of 8.02, which shows no substantial differences with seasonal variation and this suggests that groundwater have neutral to slightly alkaline character owing to abundance of HCO_3^{-1} ion in the groundwater system.

On the other hand, spatial distribution pattern of EC (see Fig. 9.20) illustrates that low EC values are generally found near a watercourse, indicating a major contribution of surface water to the groundwater recharge. However, a few sampling locations (4, 25, 27 and 37) located along the CJL canal and between CJL canal and Thal canal possess relatively high EC values. This might be ascribed to the local waste water originating from household and nearby commercial areas and infiltration of this waste water to a shallower depth saturated zone could be a potential source of moderately high EC values.

9.6.2. Hydro-Geo-Chemical facies of groundwater

Hydro-geochemical processes usually have no sharp boundaries in respect of a single source, as it usually occurs simultaneously depending upon the availability of minerals and equilibrium conditions required for the specific reaction proceeding. Sustainable water resource management required information regarding types of water and their underlying phenomena changing the hydro-geochemistry. For determination of geochemical facies of groundwater, percentage of equivalent concentration of each cation and anion (milli equivalent/liter) as a function of total cation and anion concentration respectively was calculated. Piper diagram (Fig. 9.21) is generally used for the categorization of different types of water constituting an aquifer.

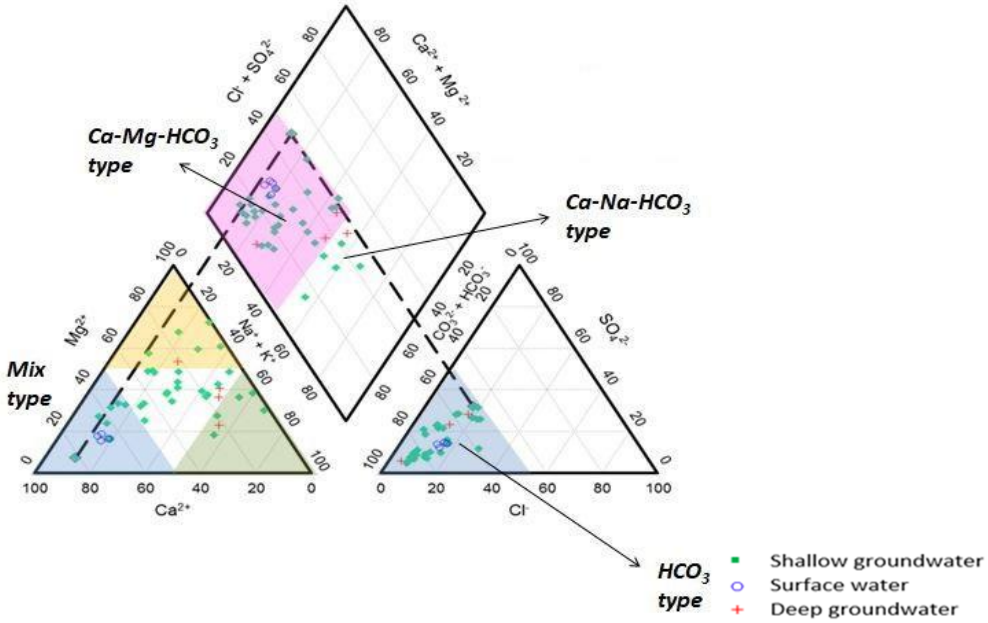

Fig. 9.21. Hydrogeochemical facies of groundwater

In the present study Piper diagram successfully explains categorization on the basis of type of water. It clearly explains the variations or domination of cation and anion concentrations during pre-monsoon and post-monsoon periods. It is depicted from the piper diagram for each of the season that almost all the surface water samples and most of shallow groundwater belongs to $Ca - Mg - HCO_3$ type, which is an indicator of surface water as a predominantly recharge source for shallow groundwater. However, the deep GW samples exhibits mixed behavior as most of them are mixed $Ca - Na - HCO_3$ type, with a few are $Ca - Mg - HCO_3$ type water. From temporal variation of

groundwater types, there is no significant change observed in hydro-chemical facies during the study period, which specifies that most of the major ions are natural by origin.

9.6.3. Geochemical evolution of groundwater

Groundwater chemistry does not change abruptly during the movement of groundwater until and unless its interaction occurs with rocks having entirely dynamic chemical characteristics. Temporal and spatial variation in groundwater chemistry at a specific site is the result of continued action of evaporation, dissolution, ion exchange and precipitation processes. During the movement of groundwater, electrical conductivity usually increases results from the multiple processes occurring simultaneously caused by dissolution, ion exchange and precipitation.

Gibbs plot (Fig. 9.22) is used to determine and discriminate major processes controlling the groundwater chemistry. The data points on the Gibbs diagram suggests that groundwater chemistry is principally controlled by rock water interaction and to some extent precipitation is the dominant factor leading towards shaping the groundwater chemistry.

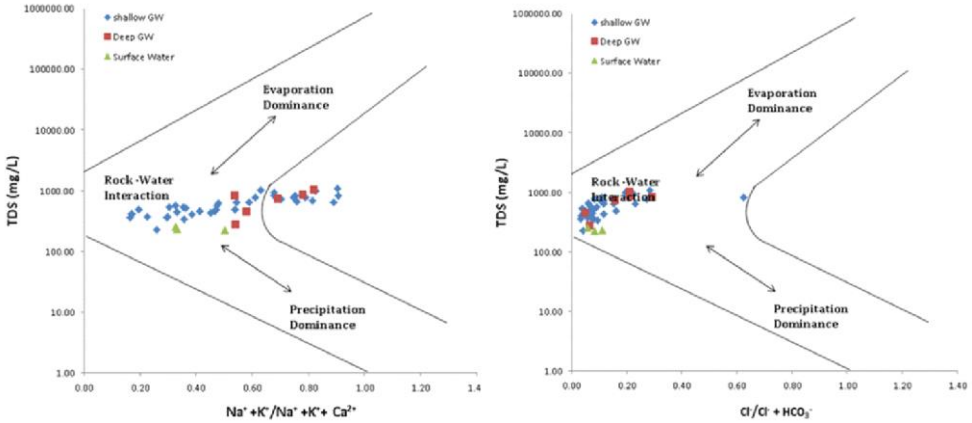

Fig. 9.22. Identification of various hydrogeochemical processes using Gibbs diagram

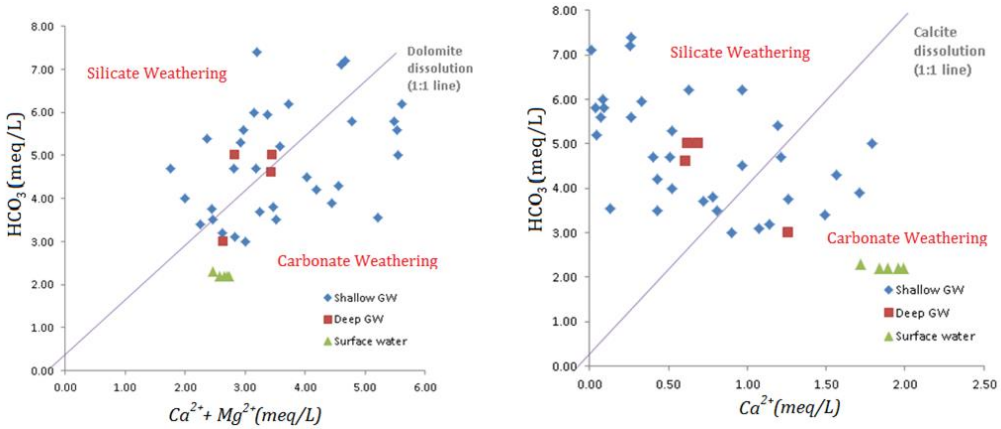

Fig. 9.23. Binary diagram to identify the weathering phenomena

To identify the dominant mineral in the rock weathering process, bivariate plots of $Ca\ vs\ HCO_3$ and $Ca + Mg\ vs\ HCO_3$ (Fig. 9.23) reveals two main groups. First group indicates Calcite dissolution with slope equal to unity where majority of the samples are situated above the 1:1 line, which shows an excess of HCO_3 that can be explained by the dolomite dissolution. The $Ca + Mg\ vs\ HCO_3$ plot indicates that samples lie below the 1:1 line indicating mixed weathering of carbonates (Calcite) and Silicates minerals (dolomite). Therefore, it can be concluded that most of the surface water, shallow and deep groundwater is predominantly originated by silicate weathering and dolomite is the key source of mineral dissolution, whereas calcite dissolution is the secondary source of ions in the study area.

9.7. Conceptual Hydrological Model

Due to the importance of groundwater in every field of life, the rational and efficient use of water resources has become very important. In this context, the use of numerical models as a tool for the diagnosis, management, and prediction of water behavior in the ground has been gaining considerable importance in recent years. Mathematical modeling is a dynamic tool that must constantly be reviewed and updated in a continuous improvement process during the search for accurate representations of natural phenomena.

A conceptual model should be developed before building the numerical model. A conceptual model is a hydrogeologist's mental representation of the groundwater flow system. It is essential to have field data characterization to support our conceptual model and allow calibration of the numerical model.

The conceptual model based on findings of present study will help to develop a numerical model which may facilitate the prediction of water table response and groundwater flow patterns in future, considering the anticipated groundwater withdrawal in different development options. As indicated in the modeling scheme (Fig. 9.24), three main components are involved in defining a conceptual model, i.e. structure, properties and boundary conditions.

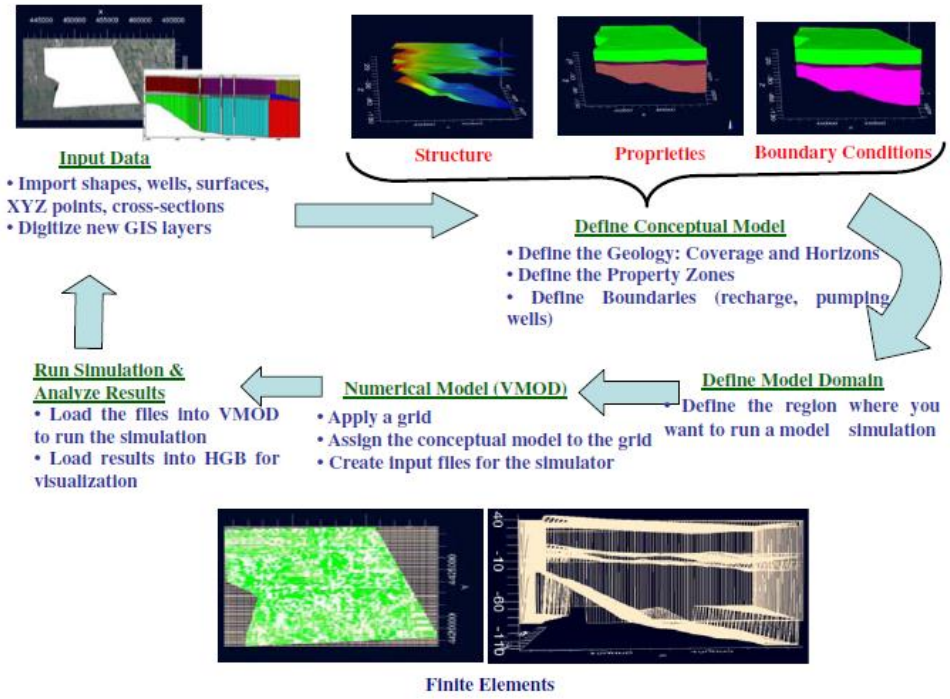

Fig. 9.24. Scheme of hydrological modeling (After Seyf-Laye A. M. et al., 2012)

9.7.1. General Approach for development of Conceptual model

For the development of the conceptual model of NPPs site in consonance with the hydrogeologic conditions, following parameters are used as follows.

9.7.1.1. Type of aquifer and number of layers

The Study Area is underlain by alluvial sands with lenses of clay. These clay lenses are of small areal and vertical extent and hence, do not impede the movement of groundwater on a regional basis. Accordingly, the alluvial aquifer behaves as a single groundwater reservoir overlying the older rocks (Pleistocene to Permian as exposed in Sheikh Badin Hills across the river and in Namal Lake Area, north-east of Mianwali).

During the course of investigation boreholes drilled upto 183 m (600 feet) depth bottomed in the alluvium. The exact depth to the impervious layer/bedrock is not known around the NPPs. Although

bore holes drilled by WAPDA in the south eg. At Kallur Kot encountered alluvial sands up to 1,202 feet (366 m) such specific information is not available for the study area. The depth to bedrock may be comparatively less under the study area due to the proximity to Sheikh Badin Hills exposed along the right bank of Indus river. Keeping in view the above factors the aquifer has been treated as a single layer and under water table conditions. The bottom of the aquifer has been considered as varying between 4.10 m to 12.83 m above sea level with a constant thickness and sloping in accordance with the water table gradient.

9.7.1.2. Aquifer Parameters

On the basis of present study and review of the existing data values of some vital aquifer parameters may be employed as input of the model adopted as below:

- ✓ Saturated Hydraulic Conductivity (K) = 48-278 (Average: 130.56) m/day
- ✓ The model area may be divided into three zone with low, medium and high value of K
- ✓ Effective In-situ Porosity (ρ) = 49.3 %
- ✓ Specific Yield (S) = 0.25 [NESPAK, 1992]
- ✓ Average gradient towards South to South-west = 3.23 E-4 (approximately 1 : 3100)

9.7.1.3. Components of Recharge and Discharge

The major components of inflows and out-flows (recharge and discharge) has been considered as below:

- **Recharge**
  - i) Infiltration from rainfall
  - ii) Groundwater flow from adjacent areas particularly from north-east;
  - iii) Seepage from Chashma reservoir, river and canals; and
  - iv) Percolation from irrigated fields including return flow from groundwater abstraction.
- **Discharge**
  - i) Abstraction through wells; and
  - ii) Groundwater out-flow towards rivers/other areas.

Infiltration from rainfall has been considered as 10 percent of the annual rainfall over the area.

The groundwater inflows and outflows are handled by the model from the input data on hydraulic heads estimated from the water level observation data and aquifer parameters, seepage from irrigation fields through surface supplies is estimated as 30 percent. Groundwater abstraction may be splitted into Rabi and Kharif seasons from 1977 to 1990 (NESPAK, 1992). Groundwater abstraction of Rabi and Kharif seasons for onward periods may be gathered from the irrigation department.

All these components have varying degrees of seasonality which must be incorporated into the model. The above components may be converted into daily rates for each node and for each stress period. Within the model area stress period is defined as a period over which all the inflow and outflow components remain constant.

9.7.1.4. Calibration period

Water level observation data and information on groundwater abstraction are important factors for the calibration of the model. These data are available to a reasonable extent for 1977, 1990, 2005 and 2020. Hence, for the simulation of groundwater conditions under comparatively observed conditions and known response of the aquifer to various recharge and discharge components, the model may be calibrated for the period 1977–1990 and 1990–2005–2020.

Choosing a short stress period such as one month or even more preferable a day would mean that seasonality could be handled very accurately but model data requirements would be enormous and the available data may not be suitable, as there is no satisfactory record available on abstractions and water levels. A stress period of about six months, based on the pumping pattern for Rabi and kharif may be selected i.e:

Length	=	m (metre)
Time	=	day

Discharge	=	Cu m/day
Permeability	=	m/day
Conductance	=	sq m/day.

9.7.1.5. Boundary Conditions

Hydrogeologic boundary conditions around NPPs are highly complicated due to the interaction of the groundwater regimen with various sources of recharge and discharge viz; River Indus, Chashma reservoir, C-J link, Thal canal etc. it is very difficult to fit all the natural boundary conditions into a model hence, some simplifications have to be made for simulation of groundwater conditions within reasonable margin of error.

The boundary conditions for the model area are shown in Fig. 9.25. Fig. shows two sets of cell/nodes viz. variable head cells and fixed head cells (Chashma reservoir and Indus river). Fixed head boundary cells are denoted with blue color.

9.7.1.6. Model Domains

The project site is located in the vicinity of Chasma complex which covers an area of about 40 km^2 which may be taken as area of interest. Initially a rectangular strip of approximately 260 km^2 area around the complex situated between geographical coordinates from Latitude $32°17' N$ to $32°28' N$ and Longitude $71°21' E$ to $71°33' E$ may be defined as the "Project Area/Study Area" or model area.

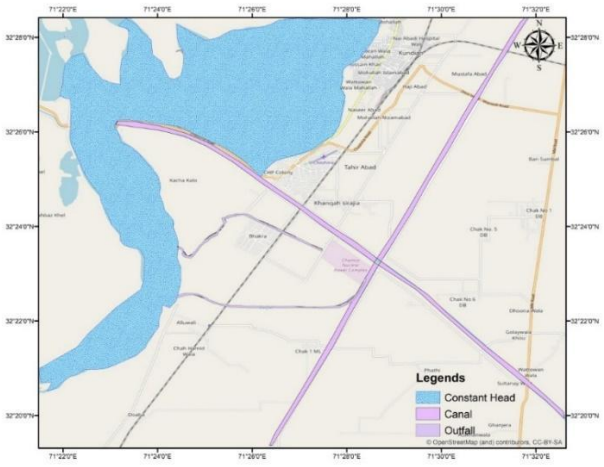

Fig. 9.25. Boundary conditions for model inputs

9.8. Conclusions

The study was conducted for hydrological re-assessment and changes in different parameters like quality, recharge and discharge patterns, flow paths, surface water-groundwater interaction and dynamics using conventional, common isotopic techniques and emerging techniques as a result of several year operation of NPPs.

- The physico-chemical parameters and major ion chemistry suggested that the general quality of both shallow and deep groundwater is suitable for domestic and drinking purposes. Hydro-geochemical analysis identifies $Ca - Mg - HCO_3$ type as the predominant water type in the study area, which specifies fresh water recharge to the aquifer system. Stable isotopes of Hydrogen and Oxygen concluded that canals, river and Chashma lake are the main recharge source for the study area except a few locations with enriched $\delta^{18}O$ values, indicating either contribution of irrigation return flow or mixed with evaporated rain water. EOCs signatures in groundwater not only validated the findings of the stable isotope but also pinpointed the most probable recharge sources for individual locations.

- Gibbs plot suggested water-rock interaction and silicate weathering as controlling phenomena of groundwater chemistry and principal weathering phenomenon of rock weathering respectively. The two key factors, evaporative enrichment and contribution of high-altitude rain, were identified as the governing phenomena for seasonal variation in isotopic signatures of both shallow and deep groundwater.
- Groundwater age predicted by the Tracer LPM, CFCs and NGT was in good agreement, which determined groundwater age in the range of 14–59 years. Tritium concentration in the majority of samples range from 5 to 13 TU, revealing that most of the groundwater samples have fresh recharge and are classified as young water. Although, a few samples located near the river Indus exhibits relatively high tritium (15–19 TU), suggest a major contribution of glacier melt with high tritium from Himalayas.
- UA and CE, NGT models yield recharge temperatures ranges from $9^{o}C\ to\ 30^{o}C$, which suggested that recharge sources are of mixed nature. Noble gases isotope data also suggested that there are no de-nitrifying activities or anoxic conditions and the findings were defended by chemical data as well.
- The water table contours indicated that the groundwater generally flows towards the river in south-west direction which is also verified by multiwall trace experiment. The flow pattern in the aquifer system therefore suggested that the south-western region of the study area is susceptible to groundwater contamination that may release from NPPs in case of any leakage.
- A combination of very common point dilution and multiwall radioactive tracer technique was also introduced to estimate in-situ effective porosity. The findings of experiment revealed that the real and filtration velocity were 22.2 cm/day and 10.94 cm/day, respectively, whereas the estimated in-situ effective porosity of the aquifer is 49.3 %, which is in good agreement with the porosity of fine to medium sand.
- The hydraulic conductivity of the aquifer varies from 48 to 278 m/day with increasing trend from Noth-East to South-West direction in the study area. The average hydraulic conductivity was found to be 139 m/day
- Organic compounds data suggested that main river, lake and canals water coming through different geological conditions have different organic signatures. EOCs signatures also segregated the sampling points recharged through lake, passing by canals, river water, interlinked and having mixed recharge. The overall flow direction in the area as indicated by EOCs was from Chasma Lake and crossing Thal and CJL canals and ultimately curved towards Indus River. Organic signatures of groundwater samples supported the finding of isotopic and chemical data and provided additional information in terms of groundwater recharge and direction.
- The NPPs operation did not impose any destructive impact on groundwater regime as there is no significant change in groundwater quality and flow patterns in the vicinity of study site except a slight lowering of water table which may due decline in river flow, rainfall patterns and/or increased water abstraction for regional agriculture activities.

References

Aeschbach-Hertig, W., Peeters, F., Beyerle, U., Kipfer, R., 1999. Interpretation of dissolved atmospheric noble gases in natural waters. Water Resour. Res. 35, 2779–2792.

Ahuja, L.R., D.K. Cassel, R.R. Bruce, and B.B. Barnes.1989, Evaluation of spatial distribution of hydraulic conductivity using effective porosity data, Soil Science 148, no. 6: 404-411.

Andrews and Lee, 1979]; John N. Andrews, David J. Lee, “Inert gases in groundwater from the Bunter Sandstone of England as indicators of age and palaeoclimatic trends” Journal of Hydrology”, Volume 41, Issues 3–4, May 1979, Pages 233-252

Bethke C. M., Torgersen T. Park J. “The 'age' of very old groundwater: Insights from reactive transport models”, Journal of Geochemical Exploration 69:1-4, June 2000, DOI: 10.1016/S0375-6742(00)00115-1

Bottomley D.J, Dross J. and Clarke W. B. “Helium and neon isotope geochemistry of some ground waters from the Canadian Precambrian Shield”, Geochimica et CosmochimicaActa, Volume 48, Issue 10, October 1984, Pages 1973-1985.

Cox, S. E, “Estimates of Residence Time and Related Variations in Quality of Ground Water Beneath Submarine Base Bangor and Vicinity, Kitsap County, Washington”. US Department of the Interior, US Geological Survey, 2003.

C. W. Fetter (1980), Applied Hydrogeology, 4th edn., USA: Waveland Press, Inc.

Freez, R. A. and Cherry, J. A., (1979). Ground Water, published by Prentice-Hall, Inc. Englewood Cliffs, New Jersey.

Gaspar E. (1987), Modern trends in tracer hydrology. CRC Press, Florida.

Glassmeyer, S.T., Furlong, E.T., Kolpin, D.W., Cahill, J.D., Zaugg, S.D., Werner, S.L., Meyer, M.T., Kryak, D.D., 2005. Transport of chemical and microbial compounds from known wastewater discharges: potential for use as indicators of human fecal contamination. Environ. Sci. Technol. 39 (14), 5157-5169.

Hazen, A. 1892. Some physical properties of sands and gravels. Massachusetts State Board of Health, Annual Report, 539-556

IAD, “SURFACE WATER / GROUNDWATER STUDIES AT AND AROUND C-2 SITE”, Consolidated Final Report, IAD-84/CFR/2008

ICRP 1990, “Recommendations of the International Commission on Radiological Protection”, ICRP Publication 60 Ann. ICRP (Oxford: Pergamon)

Kipfer R., Aeschbach W., Peeters F. and Stute M., “Noble Gases in Lakes and Ground Waters”, Reviews in Mineralogy and Geochemistry, January 2002, DOI: 10.2138/rmg.2002.47.14

Klotz D. (1978), a-werteausgebauterbohrungen. GSF-Bericht R 176, Inst. fur Radiohydrometrie, Munich.

NESPAK (1992), Report on Groundwater Studies, Chashma Nuclear Power Project, NESPAK Pvt. Ltd., 417 WAPDA House, Lahore.

Saar, M. O., M. C. Castro, C. M. Hall, M. Manga, and T. P. Rose (2005), “Quantifying magmatic, crustal, and atmospheric helium contributions to volcanic aquifers using all stable noble gases: Implications for magmatism and groundwater flow”, Geochem. Geophys. Geosyst., 6, Q03008, doi:10.1029/2004GC000828

Sadia Sami, 2019, “Emerging organic contaminants and stable isotopes in groundwater as tracer of groundwater recharge in Mianwali district, Punjab”, MS thesis 648-FBAS-MSES-S17, 2019 Inernational Islamic University Islamabad, Pakistan

Salarashayeri A.F. and Siosemarde M., “Prediction of Soil Hydraulic Conductivity from Particle-Size Distribution”, World Academy of Science, Engineering and Technology International Journal of Geological and Environmental Engineering Vol:6, No:1, 2012

Seyf-Laye, A.M., Mingzhu, L., Djanéyé-Bouindjou, G. et al. Groundwater flow and contaminant transport modeling applications in urban area: scopes and limitations. Environ SciPollut Res 19, 1981–1993 (2012). https://doi.org/10.1007/s11356-012-0744-0

Shepherd, R.G. 1989. Correlations of Permeability and Grain Size. Ground Water 27, no. 5: 633-638

Stuart, M.E., Lapworth, D.J., Thomas, J., Edwards, L., 2014. Fingerprinting groundwater pollution in catchments with contrasting contaminant sources using microorganic compounds. Sci. Total Environ. 468, 564-577.

Stute, M., Schlosser, P., Clark, J.F. and Broecker, W.S. (1992). Paleotemperatures in southwestern United States derived from noble gases in Groundwater. Science, 256, 1000–1003.

Stute, M., Schlosser, P., 2000. Atmospheric noble gases. In: Cook, P.G., Herczeg, A.L. (Eds.), Environmental Tracers in Subsurface Hydrology. Kluwer Academic Publisher, Boston, pp. 298–348.

Tazioli G.S. (1973), Metodologie e tecnicheradioisotopiche in idrogeologia. Geol. Appl. e Idrogeol., 8, 2, 209-229, Bari

Torgersen and Ivey (1985), Helium accumulation in groundwater. II: A model for the accumulation of the crustal 4He degassing flux, Geochimica et CosmochimicaActa, Volume 49, Issue 11, November 1985, Pages 2445-2452

Udong, J. 2007. Evaluation of Empirical Formulae for Determination of Hydraulic Conductivity based on Grain-Size Analysis. Journal of American Science, 3(3), 54-60.

Annexure A

Table 9. 1. Mass to charge ratio (m/z) of organic compound recharged by CJL canal

CJL Canal	CP-28	CP-34	CP-35	CP-36	CP-37	CP-39
55.03	55.03	55.03	55.05	55.03	55.04	55.02
57.06	57.06	57.05	57.08	57.05	57.06	57.05
59.05	59.06	59.05	59.07	59.06	59.06	59.06
61.03	61.03	61.03	61.05	61.03	61.04	61.02
62.07	62.08	62.08	62.09	62.07	62.08	62.07
63.06	63.06	63.06	63.08	63.07	63.07	63.05
70.02	70.02	70.01	70.03	70.02	70.03	70.01
71.07	71.07	71.07	71.08	71.07	71.08	71.07
73.04	73.04	73.04	73.05	73.04	73.04	73.02
75.05	75.04	75.05	75.06	75.04	75.05	75.03
83.06	83.08	83.05	83.04	83.04	83.06	83.06
86.96	86.95	87.23	86.98	87.00	86.96	87.02
89.05	89.06	89.06	89.07	89.05	89.06	89.05
90.09	90.09	90.10	90.10	90.10	90.10	90.09
91.08	91.08	91.08	91.10	91.08	91.09	91.07
98.05	98.05	98.06	98.07	98.06	98.06	98.04
114.04	114.07	114.04	114.07	114.06	114.07	114.05
116.07	116.08		116.09	116.08	116.09	116.08
131.04	131.04	131.04	131.03	131.05	131.04	131.03
177.06	177.06	177.06	177.06		177.05	177.04

Table 9.2. Mass to charge ratio (m/z) of organic compound recharged by Thal canal

Thal Canal	CP-1	CP-2	CP-5	CP-7	CP-9	CP-12	CP-13	CP-18	CP-19
61.04	61.02	61.02	61.05	61.04	61.03	61.07	61	61.08	61.07
70.02	70.05	73.07	73.07	73.07	73.06	73.09	73.06	73.09	73.09
83.05	83.05	83.05	83.05	83.05	83.05	83.07	83.05	83.07	83.23
89.05	89.05	88.99	89.07	89.05	89.09	88.97	89.01	89.04	
98.07	98.07	98.09	98.01	98.04	98.06	98.11	98.08	98.06	98.13
101.04	101.03	101.03	101.05	101.04	101.04	101.06	101.06	101.07	101.11
122.07	122.06	122.07	123.62	122.07	124.36	121.33	122.23	122.88	122.08
131.04	131.04	131.05	130.98	130.96	131.16	130.99	130.93	131.1	131.18
149.02	149.o7	149.01	149.03	149.02	149.05	149.02	148.88	149.18	148.96
177.12	177.06	177.07	177.07	177.07	177.05	177.07	177.05	177.03	177.04
198.45		197.34	198.23	197.95	198.03	198.24		198.27	218.96
207.69	209.91	209.85	209.69	209.88	209.67	209.18	209.22	209.34	266.06
228.60	248.54	316.02	228.46	228.39	228.56	228.72		228.38	315.08

Table 9.3. Mass to charge ratio (m/z) of organic compound recharged by Indus River

River	CP-20	CP-23	CP-30	CP-32
55.03	55.05	55.05	55.03	55.04
57.06	57.06	57.08	57.06	57.06
59.06	59.06	59.07	59.06	59.06
61.03	61.04	61.05	61.03	61.02

62.08	62.08	62.09	62.07	62.08
63.06	63.07	63.08	63.06	63.06
70.02	70.03	70.04	70.02	70.02
71.07	71.07	71.09	71.07	71.07
73.03	73.04	73.06	73.04	73.04
75.03	75.06	75.07	75.05	75.04
83.07	83.06	83.08	83.07	83.07
87.05	87.05	87.08		87.09
89.06	89.06	89.07	89.05	89.06
90.09	90.10	90.11	90.10	90.10
91.08	91.08	91.10	91.08	91.08
98.06	98.06	98.08	98.06	98.06
114.06	114.05	114.06	114.05	114.06
116.07	116.08	116.10	116.07	116.09
131.04	131.03	131.06	131.04	131.04
177.05	177.07	177.07	177.05	177.07

UKRAINE

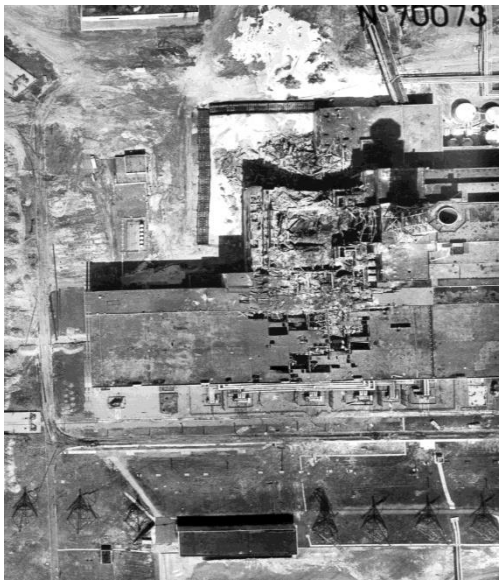

The accident at Unit 4, which occurred in April 1986

The containment over Unit 4. Shelter Object (SO). November 1986

New Safe Confinement (NSC or Arch) was moved over the Shelter Object in November 2016. Complex NSC-SO

10. METHODS FOR ANALYZING THE HYDROGEOLOGICAL CHARACTERISTICS OF THE AQUIFERS IN THE VICINITY OF THE CHORNOBYL NUCLEAR POWER PLANT USING INDICATORS

M. I. PANASIUK[1], I. O. KOVALENKO[1], N. V. SOSONNA[1], M. G. BUZYNNYI[2]

[1] Institute for Safety Problems of Nuclear Power Plants of the NAS of Ukraine, 36-a, Kirova st., Chornobyl, Kyiv. reg., 07270, Ukraine
[2] The Marzeev Institute of Public Health, 50, Popudrenko st., Kyiv, Ukraine

Abstract

An analysis of the radioactive contamination of groundwater (^{3}H, ^{90}Sr) at the industrial site of the Chornobyl Nuclear Power Plant was carried out. As a result of monitoring of the tritium volumetric activities and analysis of its distribution halos, the direction of groundwater movement near the 3rd and 4th units of the Chornobyl Nuclear Power Plant was estimated. To assess the filtration parameters, an indicator bromide-ion in the form of NaBr was introduced into the aquifer.

The mathematical modeling of migration of the unsorbed indication on the way of filtration flow of the first from the surface alluvial aquifer underground waters was completed. The imitation modeling was performed to justify the use of isotope or indicator methods to obtain reliable data on aquifer parameters, in particular, the permeability coefficient. Three-dimensional geo-filtration model was used and the verification of received predictive results with the results of the field observations was completed.

The Visual Modflow 2011.1 software package was used as a tool to determine the filtration parameters of the aquifer.

Keywords: ^{3}H, ^{90}Sr, mathematical model, groundwater, mass transfer indicator, bromide-ion, permeability coefficient, Shelter object.

10.1. Introduction

Determination of levels and formation mechanisms for groundwater contamination by ^{3}H, ^{90}Sr, uranium and transuranium element (TUE) at the industrial site of the Chornobyl nuclear power plant (ChNPP) was being conducted since 1996. In 2018–2020, this work was financed by the IAEA grant under the Coordinated Research Project CRP F33.0.22.

New Safe Confinement (NSC or Arch) (Figs. 10.1 and 10.2) was moved over the Shelter object in November 2016. Observation research of wells is still carried out, despite the fact that some of them got inside the Arch (see Fig. 10.1). Also, within the framework of monitoring of radioactive and chemical contamination sources of the environment are studied: water accumulations (block waters or unit – derived) inside the Shelter object, 4th Unit of the ChNPP, and into the aquiferous communications (see Fig. 10.2).

The objective of this work is to analyze the distribution of radioactive isotopes in groundwater and develop methods for assessing hydrogeological parameters. The assessment of hydrogeological parameters was carried out comparing the conditions of migration of isotopes and indicators in the aquifer and the results of mathematical modeling.

The complex methodology for assessing the parameters of aquifers consisted in mathematical modeling of the groundwater movement in such a way that the predicted results (concentrations, trajectories and propagation rates of indicators or radioactive isotopes) coincide with the data of actual field observations of propagation (Br^{-} or 3H) in the aquifer.

10.2. Site description

Industrial site of the ChNPP has a developed aquifer relevant to alluvial sands of the first above the floodplain terrace of the Pripyat river (see Fig. 10.2). The aquifer thickness ranges from 26 to 28 m.

The alluvial aquifer is underlain by a layer of impermeable marks, with a thickness of 6–8 m. The pressure flow underground water of Buchak aquifer is spread underneath.

After decommissioning of the cooling pond (2014–2015), the direction of groundwater movement changed from the North to the North-East. Discharge of radioactively contaminated groundwater occurs in the riverbed of the Pripyat river and in the residual lakes on the site of the former cooling pond (Fig. 10.3).

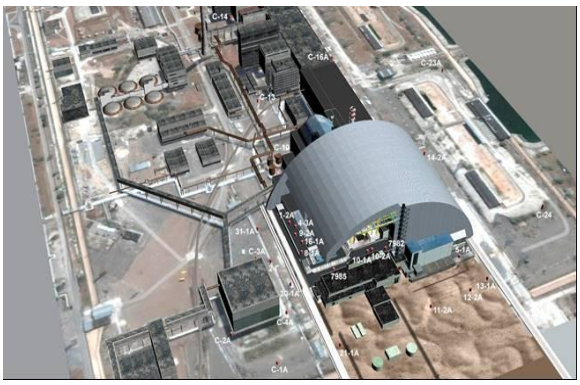

Fig. 10.1. Scheme of observation wells location and a view of the NSC

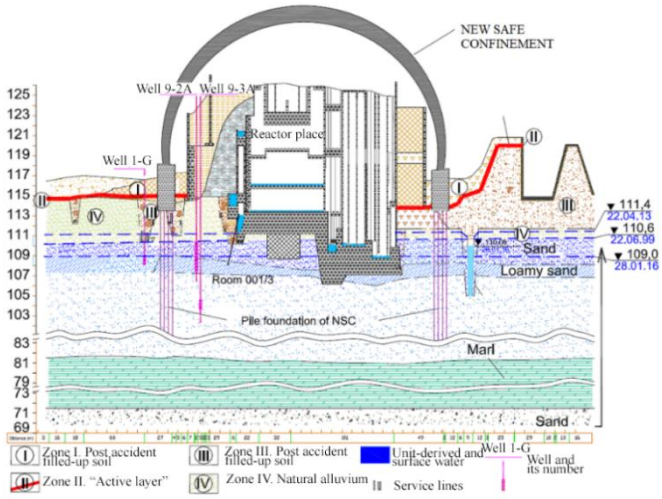

Fig. 10.2. Hydrogeological section of the Arch complex base – the Shelter Object

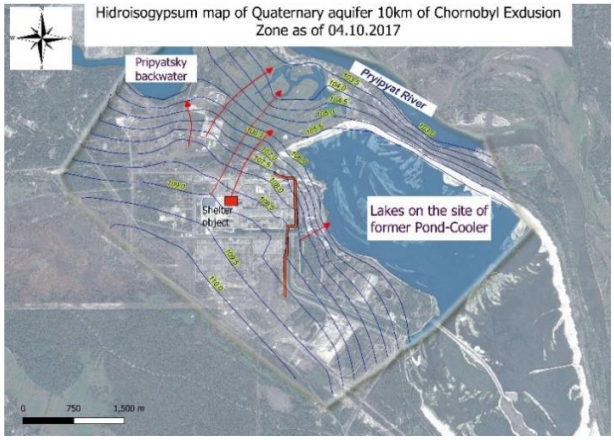

Fig. 10.3. Direction of groundwater flow (shown by arrows) after decommissioning of the cooling pond

A peculiarity of the anthropogenic and hydrogeological conditions for the SO site location is arrangement of 424 concrete piles of the Arch foundation, which overlap the aquifer by half of its power, and could have probable impact on change in the chemical composition of groundwater (see Fig. 10.2).

In Fig. 10.2, the accumulations of highly active water masses inside the premises of the destroyed fourth unit of the ChNPP so-called “block waters”, which are sources of radioactive contamination of groundwater are mapped with cyan color. In particular, block waters are a source of tritium entering the aquifer.

10.3. Materials and methods

The analysis of the distribution of radioactive isotopes in groundwater was carried out by taking water samples from observation wells. The activity of ^{3}H, ^{90}Sr, ^{137}Cs, U, $^{238,\ 239+240}Pu$, ^{241}Am and the concentration of the main ions are determined in groundwater samples in the laboratory.

The permeability coefficient of aquifers is one of the main parameters of soils, which significantly affects the accuracy of forecasts of changes in radio-hydrogeological conditions of the territory and the radiation situation in the environment. High accuracy of forecasts is the key to the effectiveness of management decisions on the non-proliferation or minimization of groundwater radionuclides spreading in the environment and protection of groundwater from pollution. A permeability coefficient, which is equal to 30 m/day for the entire thickness of the alluvial aquifer, at the territory of ChNPP, was determined in 2014, according to two pumping water from wells (Panasiuk M. I., 2014). However, the first unconfined aquifer consists of sandy layers, ranging from dusty to medium sized, from medium-sized to large ones with gravel and pebble inclusions and thus possibly having varying filtration properties.

Therefore, the determination of the permeability coefficients of individual sandy layers was proposed to be carried out using input of artificial tracer (bromide-ion as NaBr) or isotope (tritium) with the involvement of mathematical modeling of migration processes (Kovalenko I., 2020).

The essence of the method includes:

1) Preliminary mathematical modeling of the launch and propagation of an indicator (for example, sodium bromide) or an isotope (for example, tritium);
2) Preliminary modeling is performed for different values of the permeability coefficient;
3) Introduction of the indicator into the aquifer;
4) Observing the movement of the indicator with groundwater;
5) Mathematical modeling of the movement of the indicator with groundwater for different variants of the permeability coefficient;
6) The coefficient of permeability of sediments will correspond to the coefficient of permeability adopted in the model in variant, when the results of mathematical modeling coincided with observations of the movement of the indicator with groundwater.

A 3D geofiltration model created with Visual Modflow 2011.1 was used for modeling.

Thus, it is possible to determine the filtration parameters in individual intervals of the aquifer, in which the indicator migrates (Kovalenko I., 2020; Panasiuk M. I., Lytvyn I. A., 2017).

Sodium bromide is used as an indicator.

10.4. Results and discussion

10.4.1. Analysis of the distribution of radioactive isotopes in groundwater

10.4.1.1. Strontium-90

In recent years, in several observation wells located downstream the groundwater flow from the SO, there has been a significant increase in the content of ^{90}Sr by 200–500 times, as well as uranium and TUE by 2–12 times (Panasyuk M. I., Litvin I. A., 2017). In this, for individual wells, the concentration of ^{90}Sr increases to values 700–2,100 Bq/l. (Fig. 10.4).

According to our research, the mechanism for the formation of high volumetric activity of ^{90}Sr is associated with the formation of a highly alkaline medium in groundwater (Matrosov D., Shevchenko A., Nosovskyi A., Panasiuk M., 2018). Also, high volumetric activity of ^{90}Sr in groundwater is associated with high concentration of calcium–ion.

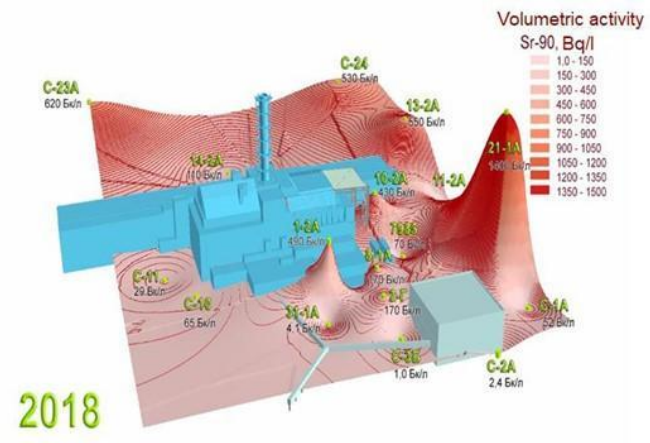

Fig. 10.4. Visualization of 3D model halo of distribution of ^{90}Sr volumetric activities in groundwater near the Shelter object complex

It is known from literary research that the degree of ^{90}Sr sorption from alkaline medium can reach 60–100%. But, according to our data it appears opposite. In the Fig. 10.5, the dynamics of the values of the pH (top graph) and the ^{90}Sr volumetric activity (bottom histogram) during the observation period of 1996–2017 is represented. On the graph, depending on the pH values, three periods marked with Roman numerals and different colors are identified. As can be seen from the Fig. 10.5 with pH values of the groundwaters mainly in the range of 7.5–8.5 (period I), ^{90}Sr volumetric activities in the underground waters are generally in the range of 6–8 Bq/l.

pH values of groundwater, mainly in the range of 8.5–9.5 (period II), the maximum plot of the distribution of ^{90}Sr volumetric activity is reduced to an interval of 2–4 Bq/l. However, at pH higher, basically, 9.5 (period III), the most frequent values of ^{90}Sr volumetric activity increases sharply to 40–60 Bq/l, with a maximum of 160–340 Bq/l.

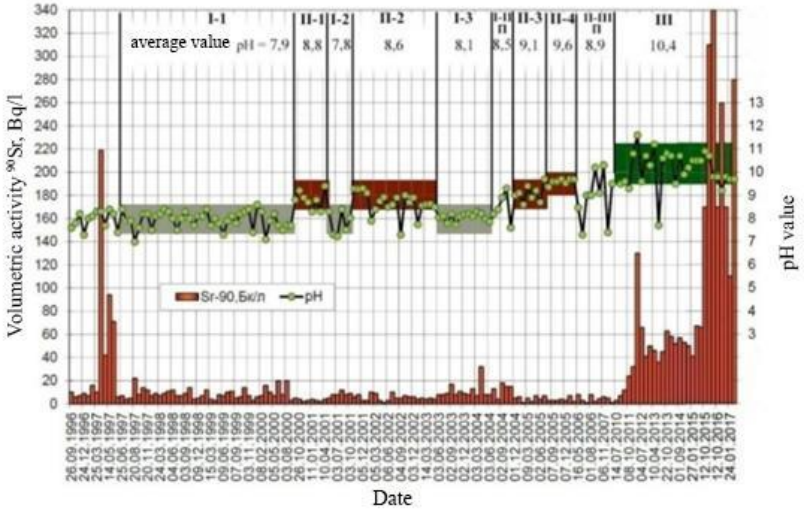

Fig. 10.5. Dynamics of pH values and ^{90}Sr volumetric activity in the samples of water obtained from 2-Г well. At the top are numbers of periods and subperiods and the average pH for each selected subperiod

The reason for reducing of ^{90}Sr concentrations at pH in the range of 8.5–9.5 (period II) is that, at pH 8.3–8.5 the hydrocarbonate ions in part turn into carbonate ions, which, in turn, form with the calcium and strontium ions insoluble compounds, that could fall out from the solution of groundwater into the precipitations.

A similar pattern is traced through wells 4-Г (Fig. 10.6), 1-2A, 1-1A, and others.

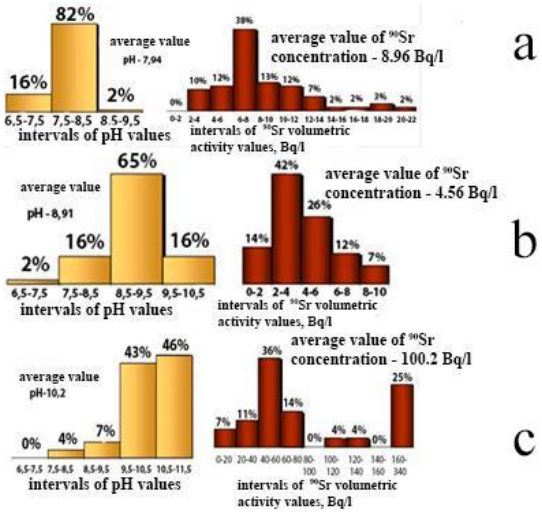

Fig. 10.6. Distribution of pH values and ^{90}Sr volumetric activity for selected 3 periods:
a – period I; b – period II; c – period III

As can be seen from Fig. 10.7, in well 4-Г, at pH values in the range of 7.5–8.5 (period I), volumetric activity of ^{90}Sr in groundwater mainly is in the range of 20–35 Bq/l. At pH in the range of 8.5–9.5 (period II) ^{90}Sr volumetric activity decreases to an interval of 1–2 Bq/l. When pH values reach values higher than 9.5, values of volumetric activity ^{90}Sr increases to 300–400 Bq/l, with a maximum of 650–680 Bq/l (Kovalenko I. O., Panasiuk M. I., Skorbun A. D. et al.).

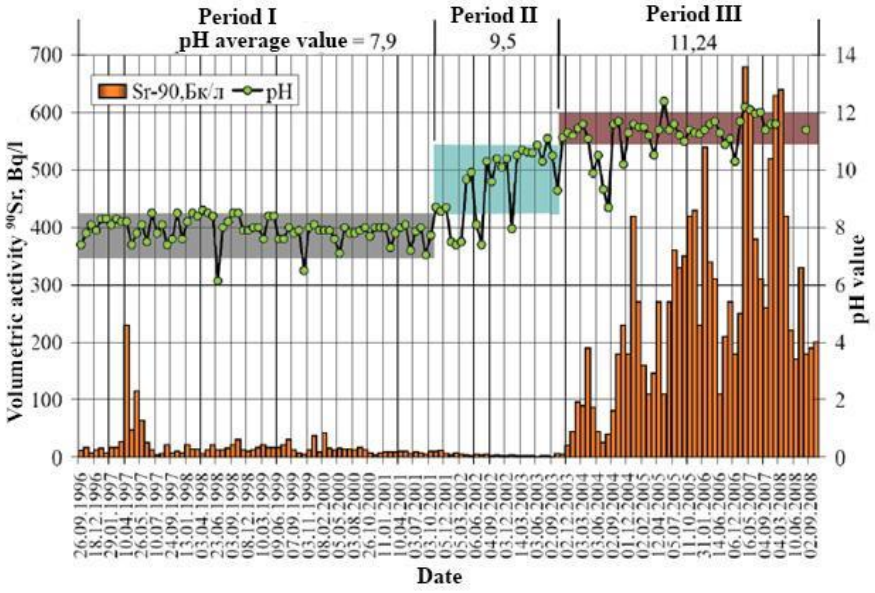

Fig. 10.7. Dynamics of pH values and volumetric activity ^{90}Sr in the samples of water from 4-Г well.
Numbers of periods are at the top

As shown in (Panasiuk M. I., 2014 ; Kovalenko I., 2020; Panasiuk M. I. et al., 2017; Matrosov D. et al., 2018), according to the research of the phase differentiation of ^{90}Sr in samples of groundwater from the well 4-Г (Fig. 10.8) for the period III in comparison with the periods I and II, growth of ^{90}Sr volumetric activity is characteristic in the ion-dispersed (soluble) form from 53–54 to 91–98% of the total volumetric activity of ^{90}Sr in the sample.

Decrease portions of ^{90}Sr in coarse-dispersed phase from 38–41% (periods I-II) to 1–8% and colloidal phase from 9.5% (periods I-II) to 0.6–0.7% (period III) unambiguously points to process of desorption of radioactive strontium from the surface of particles of sandy soils of the alluvial aquifer.

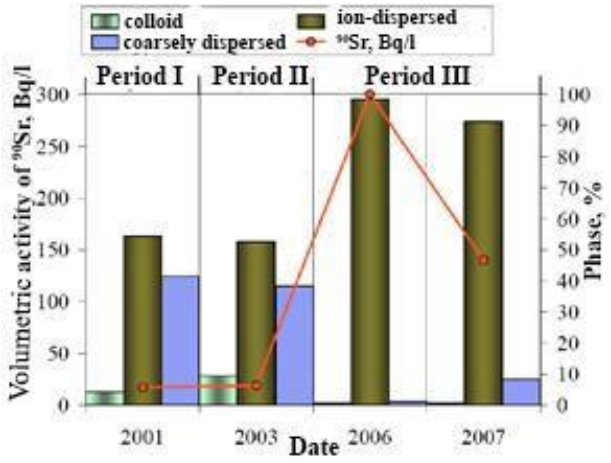

Fig. 10.8. Phase distribution of ^{90}Sr in samples of groundwater from a well 4-Г

Thus, obviously, with the high pH-value (9.5–12.5) ^{90}Sr forms complex compounds, which are poorly absorbed by sandy soil of the alluvial aquifer.

High pH-values are formed because of a contact between the groundwater and concrete bases of constructions. In case of pH-value increase up to 9.5–10 through concrete corrosion of the piles foundation of the NSC (see Fig. 2), that blocks a part of the aquifer, it is possible to register considerable growth in volumetric activity of ^{90}Sr, U and TUE.

Nevertheless, the fact of ^{90}Sr volumetric activity decreases with pH-value of the groundwater in the range of 8.5–9.5 (II period) seems to suggest that artificial sustaining in the aquifer of these pH-values can slow the spread of ^{90}Sr by flow of the groundwater beyond the industrial site of the ChNPP.

10.4.1.2. Tritium

Tritium as a "natural" indicator was used to estimate conditions for entering "unit-derived waters" into groundwater (Fig. 10.9 and 10.10). It is also used within this research. Tritium is detected in considerable amount only in "unit-derived waters". The content of high concentrations of tritium downstream from the Shelter object indicates for sure the locations of radioactive contamination of groundwater resulted by entering of contaminated waters and the leakage of the Shelter object.

After the moving of the Arch in November 2016, the access of precipitation to the destroyed ChNPP 4th unit was stopped. This led to the fact that the flow of water containing high concentrations of radionuclides from the destroyed unit to the environment was stopped. That's why tritium concentrations in groundwater samples decreased from 900–1,100 to 30–50 Bq/l (Fig. 10.11 – 10.14). Also, in full accordance with the change in the direction of movement of groundwater from north to northeast, the direction of the halation of tritium distribution has changed. In the C-10 well, which is located in the northeast direction from the destroyed 4th unit, at the end of 2018, an increase in the volumetric activity of tritium from 2 to 30 Bq/l was recorded (see Fig. 10.12, Table 10.1).

Fig. 10.13 shows that well 9-3A recorded an increase in the volumetric activity of tritium from 17.1 Bq/l in 2018 to 235.7 Bq/l in 2020 (Table 10.1). Groundwater flow direction of the halation of tritium distribution did not change in 2020 as compared to 2018.

Thus, the use of the isotope method made it possible to determine the conditions (sources) of radioactive contamination of groundwater, the direction and speed of groundwater movement.

The change in the direction of movement of groundwater led to a change in the direction of impact of the Shelter object on radioactive and chemical contamination of groundwater. To control new ways of spreading pollutants, it was necessary to change the system of observation boreholes.

The locations of the new boreholes were selected taking into account the results of the analysis of changes in the halo of tritium migration, and mathematical modeling of the spread of radioactive contamination under unit 4. Observation boreholes location installed along the path of the proposed new pathways for pollutants. New clusters C-10K, C-11K, and C-19K (Figs. 10.15) consist of three wells, the filter intervals in which are installed in the upper, middle, and lower parts of the aquifer.

Table 10.1. Volumetric activity of tritium in samples from observation wells in the vicinity of the ChNPPUnit 4

Well No.	Sampling Dates/Concentration ^{3}H, Bq/l			
	24-25.04.2018, 09.06.2018	08-11.10.2018	05-25.06.2019	14-16.07.2020
1-2A	3,1	3,1	10	-
1-3A	38,7	2,3	12, 7	12,5
1-4A	5,8	4	6	5,2
16-1A	4,4	0.8	-	-
16-2A	36,5	22.6	-	21
31-1A	5,4	4	2	3,1
4-2Г	10,4	2.8	10	-
4-3A	54,2	53.2	20	21,7
8-1A	2,7	-	3,9	-
9-2A	2	2.7	5.4	-
9-3A	32,6	17.1	-	235,7
C-10	2,1	30,6	1,4	9,2

In the upper part of the aquifer in 2020–2021 in samples from new wells C-11A and C-19A increased concentrations of ^{3}H (9.9–83.3 Bq/l) were observed (see Fig. 10.14). This indicates that the change in the direction of groundwater movement in 2014–2015 led to a change in the direction of movement of radionuclides with groundwater. However, the existing network of wells did not control the spread of radionuclides under the SO due to the lack of observation points in the area between wells C-10 and 31-1A (see Fig. 10.1). Therefore, new well clusters were drilled in this area.

The relatively high concentrations of ^{3}H (see Fig. 10.14) in water samples from new wells indicate the correct choice of location and design of new observation wells.

10.4.2. Hydrochemical conditions

Hydrochemical investigations are carried out to determine the levels and conditions of aquifer pollution, to determine the areas of influence of chemical pollutants sources into groundwater as well as formation mechanisms of high radionuclide concentrations. As it is known and as mentioned above, the chemical composition of groundwater can have a significant impact on the migration capacity of radionuclides.

10.4.2.1. Impact of the Shelter object on groundwater chemistry

The SO is a significant source of nitrates (NO_3^-) (Fig. 10.16), nitrites (NO_2^-), ions Na^+ and K^+ in groundwater, and as a result, there is an increase of mineralization in the process of groundwater flowing under the complex NSC–SO. If we take into account that the composition of saw suppressing solution, which is fed into the middle of the SO, includes nitroxide hydolinium, then there is nothing remarkable in such distribution of nitrates. According to the data of mass-spectrometric analyses, the underground waters also contain gadolinium.

The study of the effect of the SO is performed by comparing the chemical composition of groundwater samples from wells (13-3A, 5-1A, 14-2A, C-24) that are located upstream (before the SO) and downstream (behind the SO) of the groundwater flow.

Observation well blocks (1-2A and 1-3A, 4-2G and 4-3A, 8-1A and 1-4A, 9-2A and 9-3A 16-1A and 16-2A) are located downstream of groundwater, i.e., north and northeast of the SO (see Fig. 10.1). According to these wells observe changes in the chemical composition of water that flows out of the Unit 4 (SO) and compare with the results of chemical analyses of water samples from wells, which are located in front of the SO.

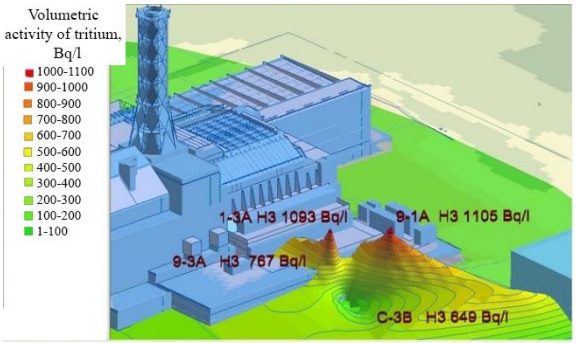

Fig. 10.9. Area of tritium distribution into the groundwater in the vicinity of the ChNPP Unit 4 in 2008

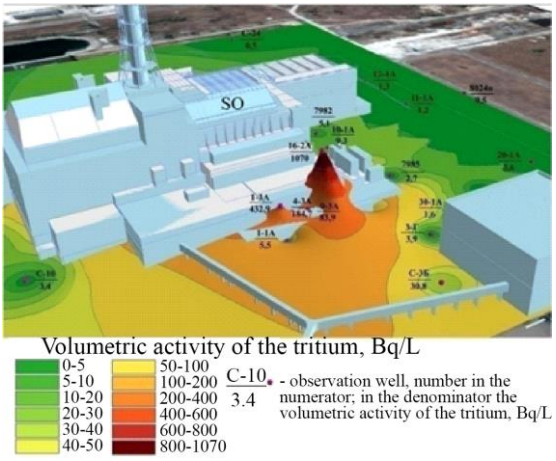

Fig. 10.10. Area of tritium distribution into the groundwater in the vicinity of the ChNPP Unit 4 in 2013

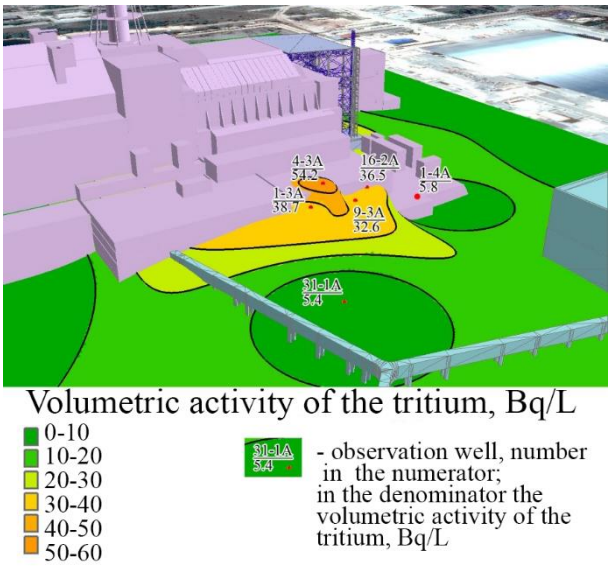

Fig. 10.11. Area of tritium distribution into the groundwater in the vicinity of the ChNPP Unit 4 in the first half of 2018

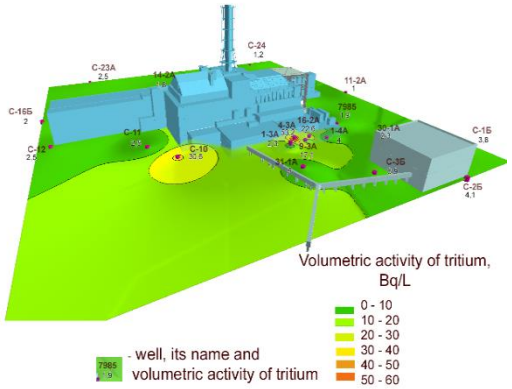

Fig. 10.12. Area of tritium distribution into the groundwater in the vicinity of the ChNPP Unit 4 in the second half of 2018

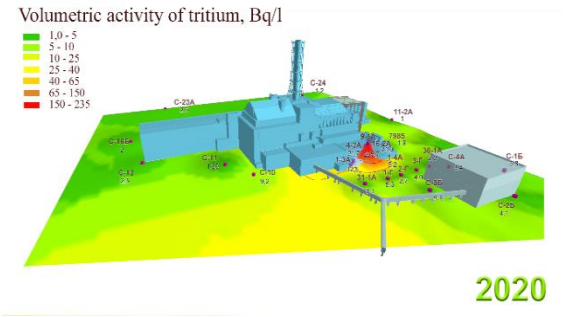

Fig. 10.13. Area of tritium distribution into the groundwater in the vicinity of the ChNPP Unit 4 in the second half of 2020

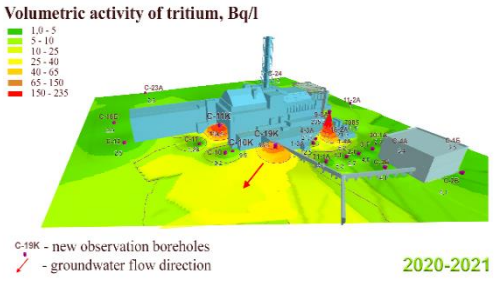

Fig. 10.14. The area of distribution of tritium to groundwater in the area of the ChNPP Unit 4 in 2020–2021, taking into account the results obtained for the new wells C-10K, C-11K, and C-19K

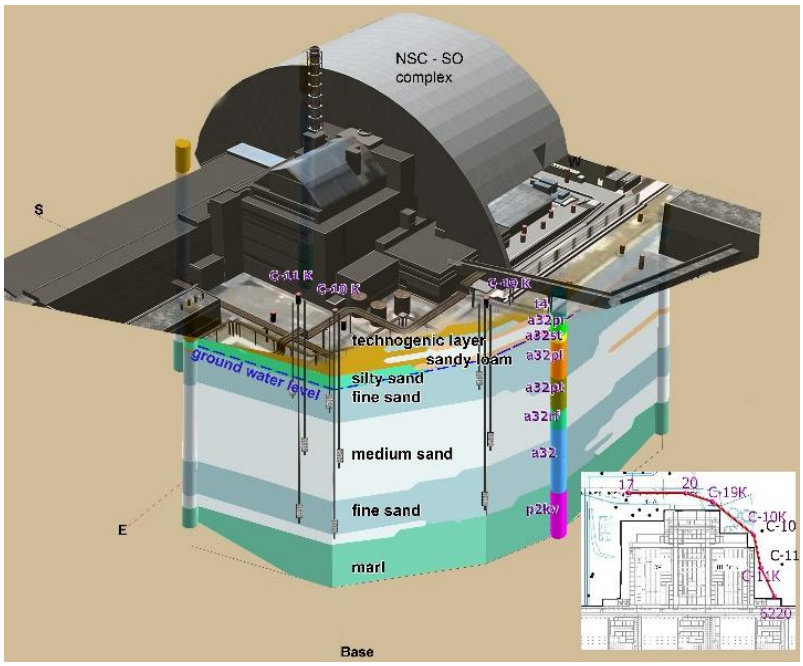

Fig. 10.15. Section and mutual placement of new observation wells, structures of the NSC – SO complex and Unit 3 of the ChNPP

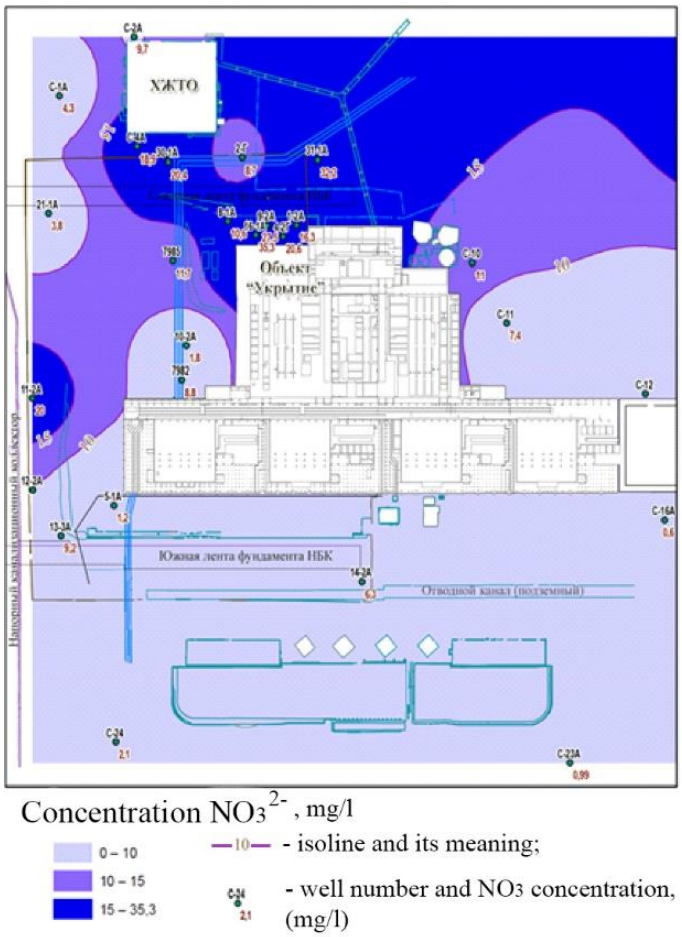

Fig. 10.16. Distribution of nitrate-ion (NO_3^-) concentrations in groundwater

10.4.2.2. Analysis of changes in the chemical composition of groundwater by means of Piper and Durov diagrams

The analysis of Piper and Durov diagrams (Fig. 10.17) shows that in the chemical composition of underground water that passed the filtration process under the NSC-SO the concentration of sodium and potassium ions increases and the volume of calcium ions decreases. Also, the impact of the NSC-SO complex is manifested in the increase of pH value to the strongly alkaline medium too.

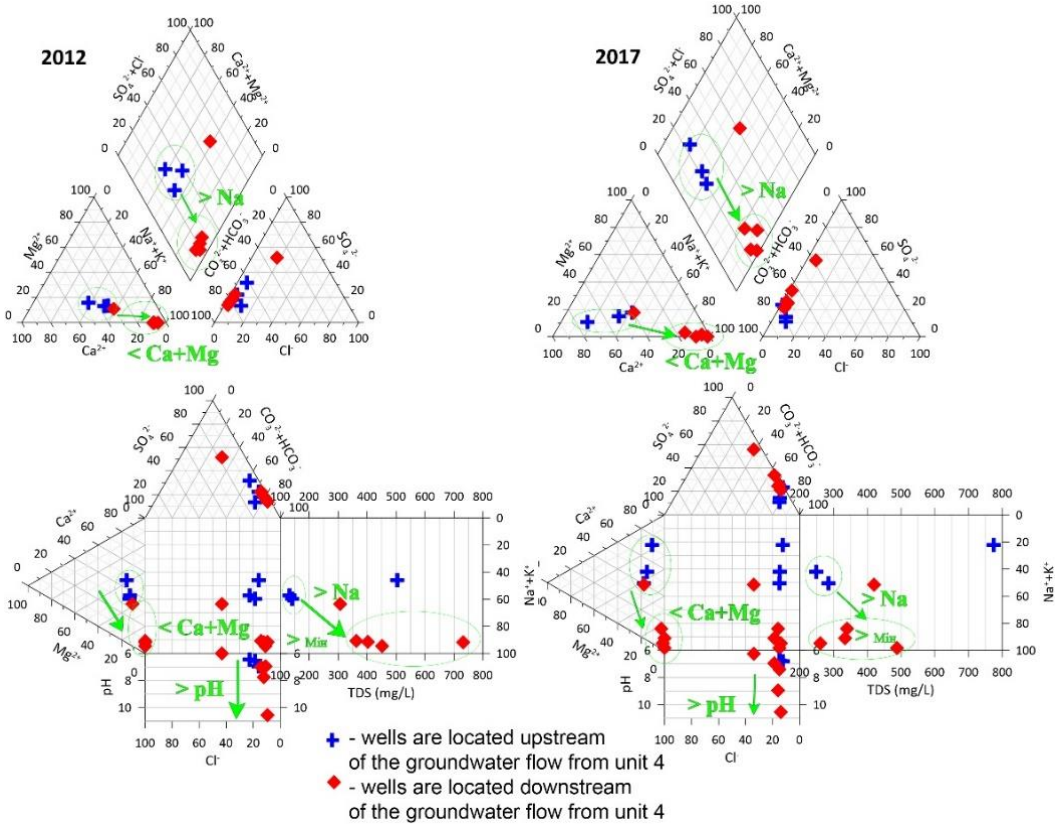

Fig. 10.17. Chemical composition of groundwater in the observation wells located upstream of the groundwater flow from the NSC-SO complex and downstream of it

10.5. Developing methods for assessing hydrogeological parameters

10.5.1. Conditions for introducing the indicator into groundwater to determine the parameters of aquifers

Within the framework of this project, activities for determination of input places and kinds of tracer were carried out as following: conducting measurements of groundwater levels on observation wells; water table contour mapping for determination of general groundwater movement direction; analysis of observation wells location**;** analysis of depths and structures of observation wells; sampling of groundwater and determining the background concentrations content of various supposed tracers (tritium, bromide ions, chlorine ions) in it; selection of indicator material; sampling of groundwater and determining in it the background concentration of tracer; selection of observation wells located in the same line of stream of groundwater flow for tracer input and for monitoring of its spreading.

As a result of the preparatory work, a bromide ion was chosen and used as a tracer. For the injection and observation of its spreading there were selected wells 16-1A and 9-3A located in the same line of stream of groundwater flow.

On May 24, 2018 the bromine-ion indicator was injected into the well 16-1A (Fig. 10.18).

A sharp increase in the concentration of bromide-ion in observation well 9-3A occurred 20 months after its introduction into well 16-1A (Fig. 10.19).

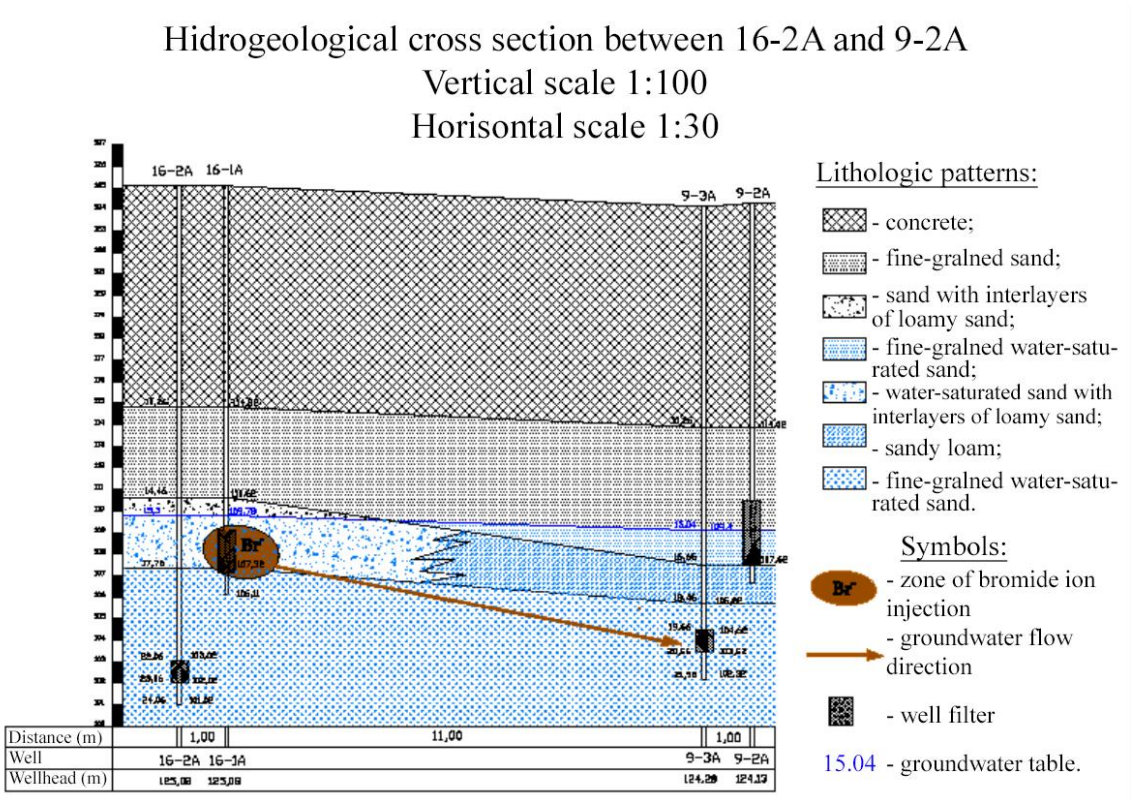

Fig. 10.18. Hydrogeological cross section between 16-2A and 9-2A. Input of sodium bromide (NaBr) tracer into the well 16-1A

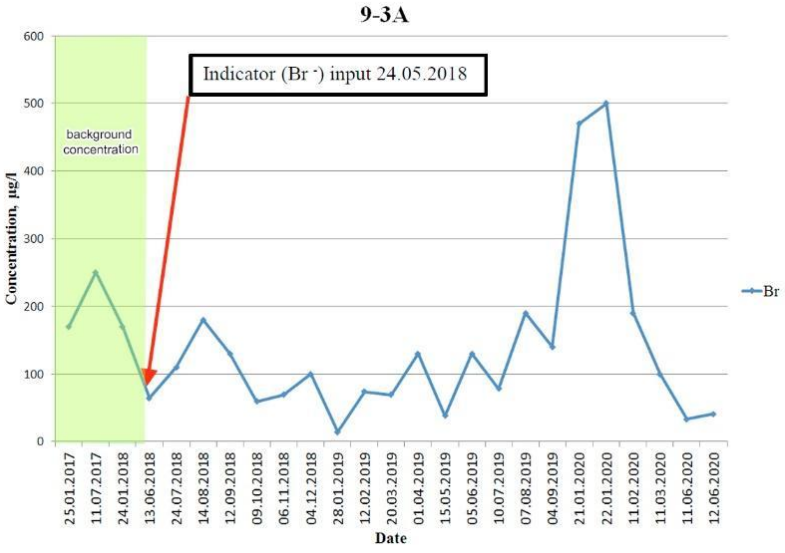

Fig. 10.19. The dynamics of the indicator concentration (Br-) in samples from the observation well 9-3A

Thus, the indicator experiment was successfully completed. And the next step is mathematical modeling of this indicator experiment.

10.5.2. Mathematical modeling

The filtration and capacity parameters of the aquifers were selected after mathematical modeling of the indicator spread so that the predicted results (concentrations, trajectories and propagation rates of indicators) coincide with the data of actual observations.

For the simulation, a three-dimensional geofiltration model was created using Visual Modflow 2011.1 and used (Panasiuk M. I., 2014; Kovalenko I., 2020).

Simulation mathematical modeling in Visual Modflow 2011.1 is aimed at obtaining the prognosed trajectory of bromide ion movement in groundwater on slice between wells 16-1A and 9-3A. These wells are located near the walls of the Shelter object on the first ledge of the cascade wall. Now they are located under the Arch.

We used to create earlier three-dimentional finite-difference model of the ChNPP site and 30 km territory around it and supllemented with a new data.

To develop the model, the investigated area is divided by the system of planes into elementary, interconnected, blocks and all filtration hydrodynamic parameters belong to the center of such a block, called the computational node.

This model covers a rectangular territory approximately 8 km long and 13 km wide (Figs. 10.20 and 10.21). In total, the model consists of three layers, which are divided into 412 columns and 301 rows. It includes data of aquifers, aquitards, permeability coefficients, etc.

Model reproduces a three-layer filtration region, which consists of two aquifers - the upper unconfined and the lower confined, separated by a weakly permeable layer in the filtration plan.

Visual Modflow 2011.1 lets you simulate, among other things, the movement of indicators in groundwater, and what has been used (N. I. Panasyuk et al., 2012; N. I. Panasyuk et al., 2011).

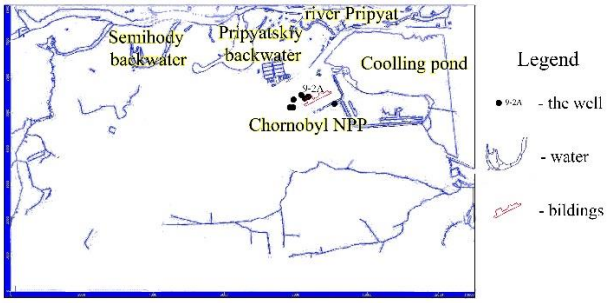

Fig. 10.20. General view of the mathematical model of the 30 km territory adjacent to the ChNPP

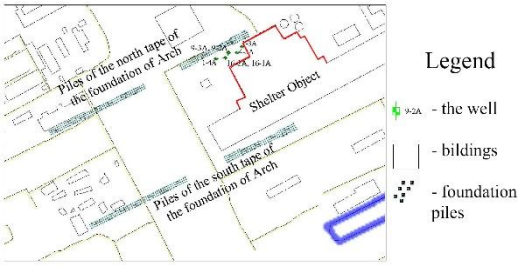

Fig. 10.21. Fragment of a mathematical model, used in experiment with tracking of bromide-ion moving

Sodium bromide was chosen as an indicator for the experiment. We selected 16-1A and 9-3A wells, located in a single line of groundwater flow, for modeling distribution of the bromide-ion.

According to the results of real observation time for indicator, passing from wells 16-1A to wells 9-3A is 20 months.

As a comparison, we simulated the movement of indicators with a filtration coefficient of 30 m/day and simulated situations, in which the results more closely match the actual data obtained from our indicator experiment.

The model contains the permeability coefficient of the entire thickness of the alluvial aquifer - 30 m/day. Figs. 10.22 and 10.23 show the simulated trajectory of the tracer from well 16-1A towards well 9-3A. The arrows indicate the direction of travel, and the steps between the arrows are 30 days. Considering the possible modeling error, we can say that the indicator will reach well 9-3A in 2–2.5 months with a filtration coefficient of 30 m/day.

The next step in modeling was the option, in which the indicator will reach well 9-3A in 20 months.

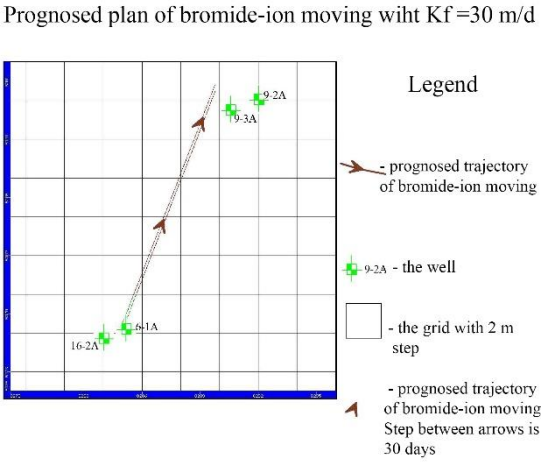

Fig. 10.22. Estimated trajectory of sodium bromide (NaBr) movement, injected into the well 16-1A with K_f = 30 m/day

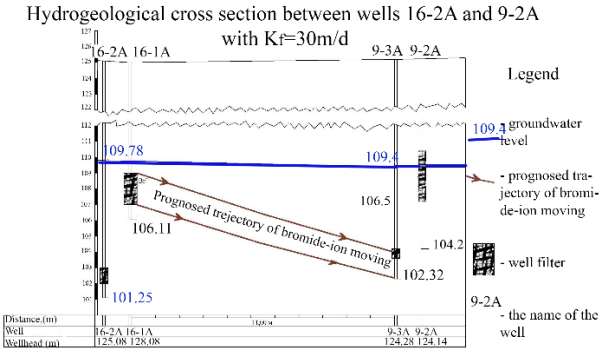

Fig. 10.23. Estimated motion trajectory profile of sodium bromide (NaBr), injected into the well 16-1A at K_f = 30 m/day

The results of the indicator experiment modeling (Figs. 10.24 and 10.25) showed that the permeability coefficient in the upper layer of the aquifer is 1.8 m/day. Difference between the filtration coefficient of the whole layer is 30 m/day, and 1.8 m/day for the upper layer of the aquifer indicates the filtration heterogeneity of soil layers that are part of the aquifer. The heterogeneity of the layers is manifested in different filtration rates. The actual velocity of groundwater movement throughout the entire thickness (K_f = 30 m/day) is 55 m/year. And in the upper part of the aquifer (K_f = 1.8 m/day), the actual flow rate of groundwater is about 6 m/year.

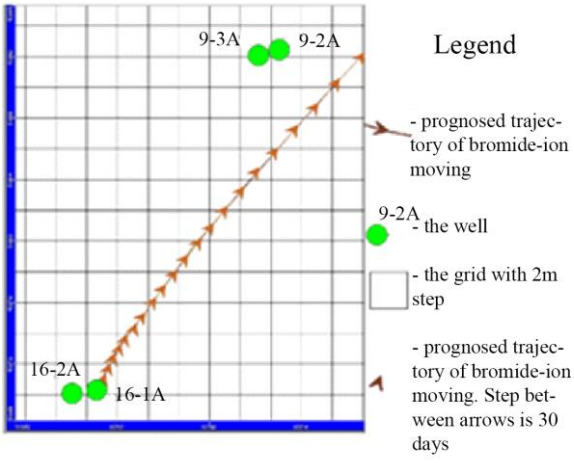

Fig. 10.24. Estimated trajectory of sodium bromide (NaBr) movement, injected into the well 16-1A with K_f = 1.8 m/day

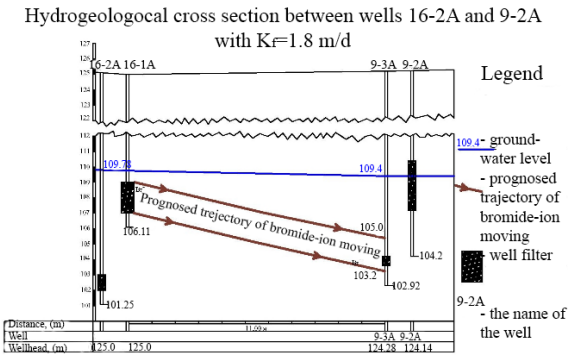

Fig. 10.25. Estimated motion trajectory profile of sodium bromide (NaBr), injected into the well 16-1A with K_f = 1.8 m/day

10.6. Conclusion

Analysis of the distributions of the volumetric activities of ^{90}Sr in groundwater samples from observation wells confirmed the previously identified new mechanism for the formation of its high migration capacity in a highly alkaline environment at pH above 9.5. At pH above 9.5, the volumetric activity of ^{90}Sr in samples from observation wells increases 200–500 times to values of 400–700 Bq/l due to a decrease in the sorption capacity of soils and the entry of ^{90}Sr into groundwater during its desorption from the surface of particles composing the aquifer.

Studies of the distribution of tritium in groundwater made it possible to apply the isotope method to clarify the hydrogeological parameters near the 4th Unit of the ChNPP. These parameters include the conditions for the entry of radioactive contamination from sources into the aquifer, the direction and speed of groundwater movement, and hence the further spread of radionuclides in the environment. After the withdrawal of the cooling pond from operation in 2014–2015. The halo of tritium distribution in groundwater changed from north to north-east in full accordance with the predicted change in the direction of groundwater movement. The sliding of the Arch over the Shelter object in November 2016 led to the fact that atmospheric water stopped flowing into the 4th unit of the ChNPP. As a result, the flow of water containing high concentrations of radionuclides from the destroyed unit to the aquifer stopped. At the same time, the concentration of tritium in groundwater samples decreased from 900–1,100 to 30–50 Bq/l.

To assess the impact of the Arch – SO complex on the chemical pollution of groundwater, samples were taken and the concentration of the main ions (Na^+, K^+, Mg^{2+}, $Ca^{2+,}$ Cl^-, SO_4^{2-}, HCO_3^-, CO_3^{2-}) in them was determined. An analysis of the Pfeiffer and Durov diagrams shows that in the chemical composition of groundwater that has passed the filtration process under the NSC – SO complex, the concentration of sodium and potassium ions significantly increases and the amount of calcium ions decreases. Also, the influence of the NSC-SO complex is manifested in an increase of the groundwater pH to 11–12, which corresponds to a strongly alkaline environment.

To assess the filtration parameters of individual layers of the aquifer, an indicator method is proposed using mathematical modeling of the conditions of its distribution with groundwater. The possibility of its application in real field conditions has been demonstrated. As a result of applying the above mentioned methodology, the filtration coefficient of the upper part of the aquifer was determined to be 1.8 m/day. Whereas, the filtration coefficient of the entire stratum of the aquifer was 30 m/day.

Due to the new data obtained on the hydrogeological conditions of the aquifer, the location of some observation wells was moved to make the observation system and the goals and objectives of radiohydroecological monitoring coinciding.

References

Panasyuk M. I., Definition of the filtration coefficient in the alluvial sands area of the industrial Chornobyl NPP//Problems of Nuclear Power Plants' Safety and of Chornobyl. – 2014. - Iss. 23. - P. 124 – 130.

Michael Buzinny, Nikolay Panasjuk, Nikolay Tsygankov. LSC-based approach for water analyses around the Chornobyl NPP. In Liquid Scintillation Spectrometry 2005, Proc. of the Int. Conf. on Advances in LSC 2005, Katovice, Poland, October 9-13, 2005. Eds. S. Chalupnik and J.E. Noakes, Radiocarbon. Tucson 2006, pp. 297 - 303.

Kovalenko I., Methods for Analyzing the Hydrogeological Characteristics of the Aquifers in the Vicinity of Nuclear Power Plants using Indicators/ I. Kovalenko, N. Sosonna, M. Panasiuk, Saravana KUMAR U.//Nuclear power and environment.-№2(17). -2020.-C.95 -101.

Kovalenko I. O., Panasiuk M. I., Skorbun A. D et all., Correlation between chemical composition and ^{90}Sr concentrations in groundwater of the Chornobyl NPP industrial site/ Kovalenko I. O., Panasiuk M. I., Skorbun A. D., Sosonna N. V., Ojovan M. I., Shevchenko O. L., Onyshchenko I. P.// Journal of Environmental Radioactivity. - 2021. URL: https://doi.org/10.1016/j.jenvrad.2021.106756

Panasyuk M. I., Lytvyn I. A. Laws of distribution of uranium in groundwater of CHNPP industrial site // Nuclear physics and atomic energy. – 2017. - Vol. 18, № 1. - C. 56 - 62.

Matrosov D., Shevchenko A., Nosovskyi A., Panasiuk M.. "Data analysis of radiation and hydroecological monitoring of ground waters located at the industrial site of Chornobyl NPP."// XII International Scientific Conference "Monitoring of Geological Processes and Ecological Condition of the Environment"13–16 November 2018, Kyiv, Ukraine. https://www2.scopus.com/record/display.uri?eid=2-s2.0-85060440628&origin=AuthorNamesList&txGid=78430a61651c59d63d0e6441861fd632

Matrosov D., Shevchenko A., Nosovskyi A., Panasiuk M. "Data analysis of radiation and hydroecological monitoring of ground waters located at the industrial site of Chornobyl NPP."// XII International Scientific Conference "Monitoring of Geological Processes and

Ecological Condition of the Environment”13–16 November 2018, Kyiv, Ukraine. https://www2.scopus.com/record/display.uri?eid=2-s2.0-85060440628&origin=AuthorNamesList&txGid=78430a61651c59d63d0e6441861fd632

Belitsky A.S., Orlova E.I. Protection of underground waters from radioactive contamination. - Moscow: Medicine, 1968 (in Russian)

Lytvyn I. A., Panasyuk M. I., G. V. Levin, I. P. Onyshchenko. Groundwater contamination by ^{90}Sr on the territory of the “UKRYTTYA” OBJECT of the Chornobyl nuclear power plant//Problemy bezpeky atomnyh electrostantsiy i Chornobylya (Problems of Nuclear Power Plants' Safety and of Chornobyl). – 2016. - Iss. 26. - P. 122 - 127. (Rus);

Rudenko L. I., Khan V. E.-I., Panasyuk M. I. Physico-chemical justification for radionuclides migration from the "Shelter" object and its industrial site to the ground waters // Radiochimiya. – 2003. – Vol. 45, № 3. - P. 268 - 272. (Rus);

Rudenko L.I., Khan V. E.-I., Microparticles contribution in the mechanism of radionuclide migration from the "Shelter" object and its industrial site to the ground waters // Radiochimiya. – 2005. – Vol. 47, № 1. - P. 89 - 90. (Rus);

Rudenko L., Khan V., Kukhar V. Migrations of radioactive nuclides from «Shelter» object. Scientific fundamentals of liquid radioactive waste products purification from organic substances and transuranium elements // Bulletin of NAS of Ukraine. – 2008. - № 4. – P. 10 – 22. (Ukr);

Panasyuk N. I, Alfyorov A. M., Starikov M. B., Litvin I. A., Liushnya E. P. Results of detailed modeling of influence pile foundations in hydrogeological conditions in the New Safety Confinment district construction // Problems of Nuclear Power Plants’ Safety and of Chornobyl, 2011a. - Iss. 16. - P. 124 – 129.

Panasyuk N. I., Alfyorov A. M., Levin G. V., Starikov M. B. Mathematical modeling of geomigratory processes in water-saturated soil in area of object “Ukryttya”// Problems of Nuclear Power Plants’ Safety and of Chornobyl, 2011b. - Iss. 17. - P. 124 – 130.

VIETNAM

Ninh Thuan 1 the nuclear power plant

11. USE OF ISOTOPE TECHNIQUES TO CHARACTERIZE GROUNDWATER SYSTEM IN THE VICINITY OF THE FIRST NUCLEAR POWER PLANT IN NINH THUAN PROVINCE, VIETNAM (VIE 20481)

NGUYEN KIEN CHINH, HUYNH LONG, TRAN THI BICH LIEN, NGUYEN VAN PHUC

Center for Nuclear Techniques, 217 Nguyen Trai Str., 1st District, Hochiminh City, Vietnam

Abstract

As a part of the Coordinated Research Project F33022 entitled "Use of Isotope Hydrology to Characterize Groundwater Systems in the Vicinity of Nuclear Power Plants", this study focuses on characterizing hydrogeological conditions in the Ninh Thuan province where the first NPP of Vietnam planned to set up using isotope hydrology tools as the first step to elucidate how radioactive contaminants would be released by NPP coming into groundwater.

To study, the groundwater samples, surface water, rainwater, air, aquatic plants and tree leaves were collected and studied for stable and radioactive isotopes to determine their status around the NPP. In addition, the tracer injection experiment was conducted to determine the infiltration velocity in the aquifers.

As the study results, groundwater in the study area is of rainwater origin based on its stable isotopic composition and is modern water due to its high content of tritium and 14C. By using tracer techniques, the movement velocity of groundwater that ranges from 0.59 cm/day to 1.22 cm/day and the average infiltration (recharge) rate of precipitation in an unsaturated zone of 0.25cm/day have been determined. At the same time, tritium and radiocarbon concentration and nuclides, which could escape from an operating NPP, was surveyed to define their background level in the environment. The reported average values of tritium and 14C in air, aquatic plants, tree leaf and seawater can be used as their natural background level.

Keywords: Stable isotope (^{2}H, ^{18}O), tritium (^{3}H), radiocarbon (^{14}C), groundwater, tracer technique, isotope technique, infiltration rate.

11.1. Introduction

In Vietnam, electricity is supplied mainly from hydroelectricity and thermal sources. Although wind and solar power are being strongly invested, they meet only a small part of total demand. While hydropower has been fully exploited, thermal power as a major source of environmental pollution is still an additional source to meet electricity demand. Therefore, meeting the power demand and aiming at improving the environment projection of nuclear power is a priority.

The national nuclear power plan had been approved by the Vietnamese parliament since 2009, but it was halted in 2016 for more preparation of infrastructures for the NPP exploitation. Hence nuclear power is still in the country's plan to develop its energy resources.

Before halting the nuclear power program in 2016 the first nuclear power plant (NPP) in Vietnam had been planned to be built in Ninh Thuan, a coastal province in the south of the Central region of Vietnam. Although the NPPs design and operation had followed very strict safety guidelines there would be possibilities of unforeseen accidents, which would cause the release of radioactive materials into the environment contaminating groundwater. Even in normal operating conditions there is always a certain amount of radioactive material released into the environment around the NPPs. These materials, depending on their fate accumulate over time would cause problems for the environment and water resources. This study focuses on characterizing hydrogeological conditions in the Ninh Thuan province where a NPP will be set up using isotope hydrology tools and radioactive tracer isotopes. This is the first step to elucidate how radioactive contaminants released by NPP coming into groundwater.

With that goal, as the first study, isotope techniques and tracer injection experiment will be used to define the origin, recharge source and the interaction with surface water of groundwater, to evaluate the infiltration rate of rain water in unsaturated zone (groundwater recharge rate) and flow rate of groundwater in the study area. At the same time, a survey on radiocarbon and tritium content in seawater, plants, and the air water vapor in the same area will be conducted.

11.2. Site description

Ninh Thuan is a coastal province in the middle part of Vietnam. Lying from 11°18'14" to 12°09'15" N latitude and 108°09'08" to 109°14'25" E longitude, Ninh Thuan borders on Khanh Hoa province in the north, Binh Thuan province in the south, Lam Dong province in the west and the East Sea in the east. With an area of about 3,400 km^2 and 590 thousand people, it is a province with high potential for aquaculture, forestry and tourism (Fig. 11.1).

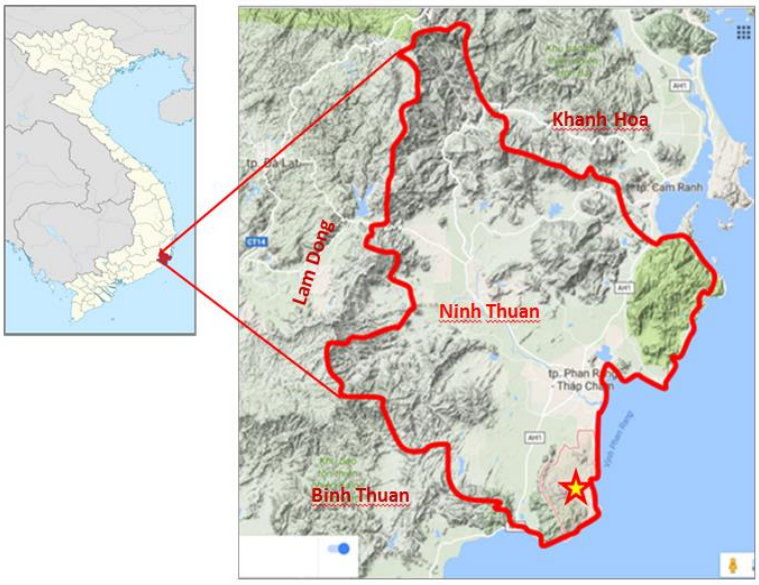

Fig. 11.1. Study area

In term of topography, the terrain in Ninh Thuan province is lower from the northwest to the southeast with three terrain types: mountains accounting for 63.2% in the northwest and north, hilly areas with semi-mountain terrain accounting for 14.4% in the north and southwest, and coastal plain accounting for 22.4% in the province's center where almost people concentrated.

Dominated by the tropical monsoon regime, there are two distinguished seasons in the study area. Normally the wet season is short beginning in September and ending in November. The dry season is long, ranging from December to August. The average rainfall in this area is lower than the other ones of Vietnam (ranging from 700–800 mm/year in Phan Rang and gradually increasing with altitude to about 1100 mm/year in the mountains) while the evaporation is high, from 670 to 1,827 mm per year. With low rainfall, strong wind and high evaporation Ninh Thuan is the driest area in Vietnam. The area has an average annual temperature of 27 °C, large energy radiation (about 160 Kcal/cm^2 per year) and low average air humidity (about 70–75%).

The study area has low river mesh density (0.1–0.15 km/km^2). Total river length is about 200 km and Cai River is the main river in this area. Consequently, the surface water, a main source for water supply in the region, is limited.

In Ninh Thuan, a part of groundwater exists in porous formations which are distributed in the plain area. Groundwater in the study area can be divided into three aquifers: Holocene, Pleistocene and Upper Pliocene aquifer. In the existing aquifers, only Holocene and Pleistocene aquifers are water-rich and Pliocene aquifer is very poor in water and has no exploitation value.

Outcropping on the surface, Holocene aquifer has a distribution area of about 236 km^2, and concentrates mainly in the Cai River Delta area of Phan Rang. The thickness of the aquifer varies from 0.0m to 24.5 m, with an average of 5.2 m. Static water level in the aquifer varies by regions. The highest is 0.12 m and the lowest is 7.5 m below soil surface, the average value of static water level is 2.20 m.

The Pleistocene layer is widely distributed in the study area throughout the delta of the study area. The surface part of the aquifer has an area of about 542 km^2; the rest is covered by Holocene sediments. The thickness of the aquifer varies from 0 m to 43.5 m typically 10 m to 15 m. Water level in this aquifer varies by region too. The highest and lowest values of water level are 0.70 and 10.0 m, respectively. The mean water level of this aquifer is about 2.1 m below soil surface.

The lithological composition of the Holocene and Pleistocene aquifers is mainly sand from coarse to fine, while the Upper Pliocene aquifer is formed mainly by powder and very fine sand. As being unconfined or partly unconfined aquifer, the source of water in aquifers could be rainwater which infiltrates into aquifers through aquifer's outcrop and/or from shallower aquifer.

Figs. 11.2 and 11.3 (Nguyen M. K., 2015) describe the area's hydrogeological map and two main cross sections of the study area.

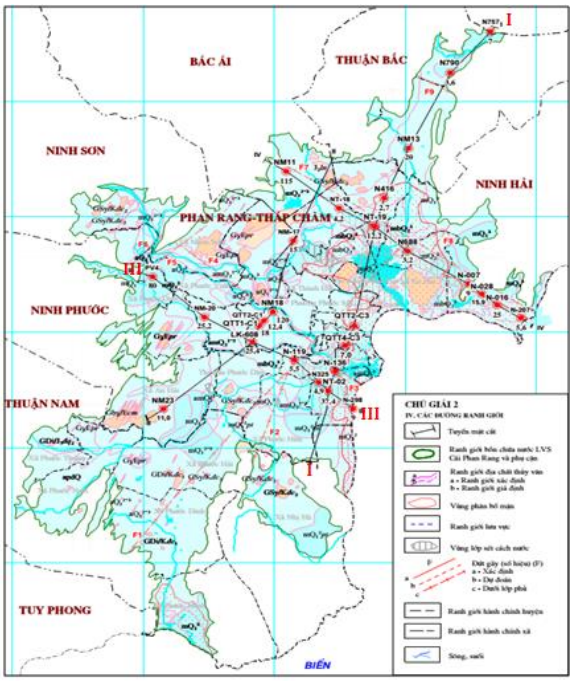

Fig. 11.2. Hydrogeological map of the Ninh Thuan province.
The blue area bounded by the green line is the distribution of water bearing porous formations in the study area.
The red and yellow line is cross section I and III

According to cross section III–III, all aquifers are high in the northwest and low in the southeast, so the main movement direction of water in the aquifers will be from the northwest to the southeast. On the other hand, after the cross section I–I, all existing aquifers are higher in the northeast and southwest and lower towards the center of the study area. Hence the water in the aquifers tends to flow towards the center, and then flows in the northwest-southeast direction and out into the sea.

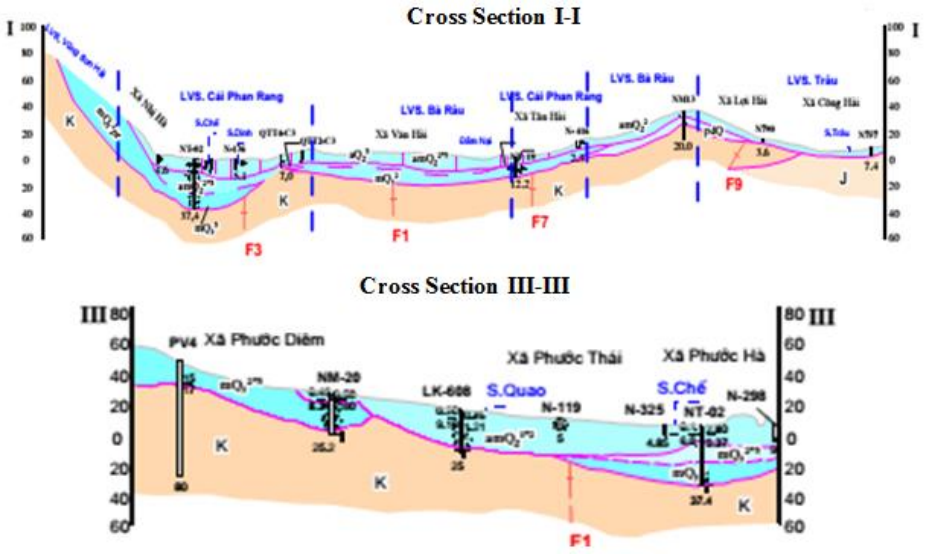

Fig. 11.3. Hydro-geological cross section I-I and cross section III-III

Up to now there are some studies on the effects of NPPs to groundwater but not enough to provide basic information that can be used for predicting the fate of radioactive contaminants released into groundwater in case of radiological accident and/or during normal operations. Actually, in almost all countries around the world groundwater is the most important source of water for supplying.

This study focuses on characterizing hydrogeological conditions in a region where a NPP will be set up using isotope hydrological tools as well as tracer technique using radioactive isotope. Water stable isotopes are used for finding out the source of water in existing porous aquifers, tritium and C-14 are used to date groundwater and tracer techniques are used to determine the infiltration rate of rainwater as well as to define groundwater movement velocity in the aquifer. At the same time, tritium and C-14 isotope (which release from NPP) content are also estimated in the air, surface water, sea water and types of plants to establish tritium and C-14 background for further monitoring and investigation using isotope techniques.

11.3. Method and sampling

To understand the source of water in existing aquifers, groundwater was sampled in wells that have almost necessary technical information (coordination, depth...) for stable isotope, tritium and C-14 analysis. Local precipitation and river water were also collected for stable isotopes and tritium analysis. Stable isotopic composition of water samples has been used to interpret the source of groundwater while tritium and C-14 data of groundwater used to assess water age for defining direction and movement rate of groundwater.

A total of 31 groundwater samples, 44 rainwater samples (monthly and daily) and 14 river water samples were collected in this study. The collection of water samples was performed in 2016, 2017, 2018 and 2019. Groundwater sampling points are mapped in Fig. 11.4. All collected water samples were analyzed at the CNT's laboratory.

To define the background of tritium and C-14 isotopes in the study area, some samples of air, seawater and plants were collected. Water vapor in the air was condensed for tritium analysis while CO2 in the air was precipitated into Na_2CO_3 by aeration through sodium hydroxide (NaOH) solution for C-14 analysis. Water in plants was extracted by distillation under vacuum conditions for tritium analysis. Organic carbon in tree leaf, aquatic plants was also synthesized into C6H6. Tritium and 14C in seawater were determined in a similar way as groundwater samples.

In this study, 16 plant samples including 11 tree leaf and 5 aquatic plant samples, 5 samples of seawater and 15 samples of air were taken. All taken samples were analyzed at the CNT's laboratory too.

The obtained survey data are used as tritium and 14C environmental background data before operating the first NPP.

Fig. 11.4. Groundwater sampling points

Stable isotope ratios ($\delta^{18}O$, $\delta^{2}H$) of water samples were analysed by laser absorption technique using Liquid Water Isotope Ratio (LWIR) analyser LGR DLT 100 (Penna et al., 2010) with measurement precision was ±0.15‰ for the $\delta^{18}O$ and ±1‰ for the $\delta^{2}H$. Analyses are reported in ‰ versus VSMOW.

Carbon 14 content of collected samples was determined by liquid scintillation technique. Organic carbon in plants and inorganic carbon ($BaCO_3/Na_2CO_3$ which was precipitated from groundwater/air) was synthesized into C_6H_6 before counting by the Liquid Scintillation Analyze (LSA) Packard 3170 TR/SL to determine C-14 activities. Results of ^{14}C abundances are reported as percent of modern Carbon, pmC (Stuiver and Polach, 1977).

For analysing tritium, collected water must firstly be electrolyzed to reduce sample volume (tritium enrichment) and was measured by the LSA Packard 3170 TR/SL which has detection limit of 0.3 TU (Taylor, 1976). ^{3}H content is expressed in Tritium Units (TU) with 1 TU is defined as the isotope ratio $^{3}H/^{1}H=10^{-18}$.

In this study, the point-dilution method using only one well (Bedmar, 1983) is applied to determine flow rate of groundwater. According to the method when flowing through a well the horizontal (filtration) flow component of groundwater will bring tracer substance away, in consequence, the concentration of tracer will decrease gradually and this decrease depends on this flow component, structure of well and the stratigraphy of aquifer. Based on that the tracer is initially injected into the total water column inside the screen part of the well and let it mix well in the water column. Tracer concentration in this water column is measured time by time then to get the distribution of tracer concentration in depth. These distributions show the decrease of tracer concentration by time as mentioned above. Based on the decrease of tracer concentration and time we can calculate the horizontal velocity of water along the screen stretch. By using this method, the vertical flow in the well can also be determined if it exists.

The filtration velocity of groundwater can be calculated as follow: The tracer concentration C in a segment of well with volume V will decrease after time by a horizontal flow rate Q of groundwater following below differential equation:

$$\frac{dC}{dt} = -\frac{C}{V}\frac{dV}{dt} = Q\frac{C}{V}$$

Make integral above equation, we have:

$$C_t = C_0 e^{\frac{Q}{V}t},$$

where C_0 is initial tracer concentration and C_t is tracer concentration at time t in volume V. Then the flow rate:

$$Q = \frac{V}{t}\ln\frac{C_0}{C_t}.$$

Velocity of water through the well will be:

$$V_s = \frac{\pi r}{2t}\ln\frac{C_0}{C_t}$$ (r is radius of the well)

$$V_f = \frac{V_s}{\alpha} = \frac{\pi r}{2\alpha t}\ln\left(\frac{C_0}{C_t}\right)$$

Due to the existence of the well distorts pattern of ground water natural flow so that velocity through the well V_s is higher than real velocity flow in the aquifer V_f (Darcy velocity) by one factor of hydraulic dynamic distortion α which is calculated using below formulae (Halevy et al., 1967):

$$\alpha = \frac{8K_1K_2}{K_2A + KB}$$

with $$A = (K_1 + K_2)\left[1 + (\frac{r_1}{r_3})^2\right] + (K_1 - K_2)\left[(\frac{r_1}{r_2})^2 + (\frac{r_2}{r_3})^2\right]$$

$$B = (K_1 + K_2)\left[1 - (\frac{r_1}{r_3})^2\right] + (K_1 - K_2)\left[(\frac{r_1}{r_2})^2 - (\frac{r_2}{r_3})^2\right]$$

In which: K - hydraulic conductivity of the aquifer

K_1 - hydraulic conductivity of the well

K_2 - hydraulic conductivity of gravel pack

r_1 - inner radius of the well

r_2 - outer radius of the well

r_3 - radius of gravel pack

To evaluate the seepage and infiltration rate of water in an unsaturated zone, tracer technique was used. After being injected into soil, the tracer dissolves into soil water and a radioactive water layer (marked water layer) is formed at the depth where tracer was injected. That marked water layer will move down with soil water according to piston principle because the soil continuously receives irrigating and/or rain water. By tracking the position of the marked water layer (the center of radioactivity distribution at a moment as definition) we can determine the seepage depth and so the infiltration rate of soil water is calculated based on the displacement depth and time of tracer.

11.4. Results and discussion

11.4.1. Source of groundwater in the area

Isotopic analysis results of groundwater, river water and rain water samples collected in the study area are listed in Tables 11.1–3.

As listed in Table 11.3, deuterium (^{2}H) content in monthly rainwater samples ranges from -60.8 to -1.7 ‰ with an average value of -36.3 ‰ and their oxygen-18 (^{18}O) content varies from -8.70 to -1.01 ‰ with the average value of -5.91 ‰. The equation of the local meteoric water line (LMWL) that built based on 44 isotopic composition data of daily and monthly local rainwater samples is $\delta^2H = 7.47*\delta^{18}O + 7.56$ with $R^2 = 0.97$. The mean tritium content of rainwater in the study area is 1.08 TU.

Stable isotopic composition of groundwater ranges from -50.4 ‰ to -17.5 ‰ for ^{2}H and from -7.41 ‰ to -2.55 ‰ for ^{18}O (Table 11.1). The mean value of deuterium content in groundwater is -37.7 ‰ and that of ^{18}O is -5.73 ‰.

As plotted in Fig. 11.5, the change of ^{2}H and ^{18}O content in groundwater is entirely within the content variation of these isotopes in collected rainwater and the fresh groundwater samples distributed along the LMWL. These show that the groundwater in the study area originated from the rainwater.

In the other hand, all collected groundwater samples have tritium with minimum content of 0.62 ± 0.26 TU that is higher enough than detection limit (0.3 TU) and have high C-14 concentration with the minimum value of 80.8 ± 3.7 pmC and the maximum value of 102.0 ± 3.4 pmC. This means groundwater is modern (Table 11.1).

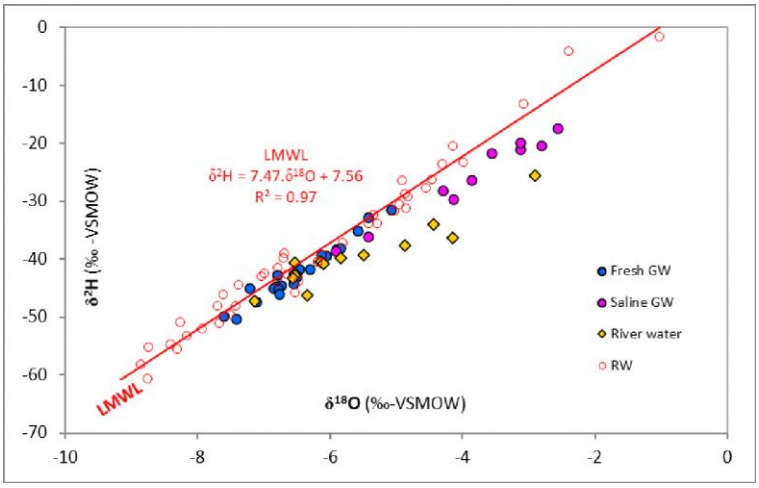

Fig. 11.5. Stable isotope composition of water samples in Ninh Thuan area

In the other hand, all collected groundwater samples have tritium with minimum content of 0.62 ± 0.26 TU that is higher enough than detection limit (0.3 TU) and have high C-14 concentration with the minimum value of 80.8 ± 3.7 pmC and the maximum value of 102.0 ± 3.4 pmC. This means groundwater is modern (Table 11.1). Stable isotopic composition of groundwater and river water and mean isotopic value of rainwater is described in the Fig. 11.6.

As seen in the Fig. 11.6, saline groundwater in the area is the consequence of the mixing between fresh groundwater and seawater. Indeed, the saline groundwater samples are all located along the pink line starting from the fresh groundwater cluster and tending to pass through the seawater group (brown square empty points).

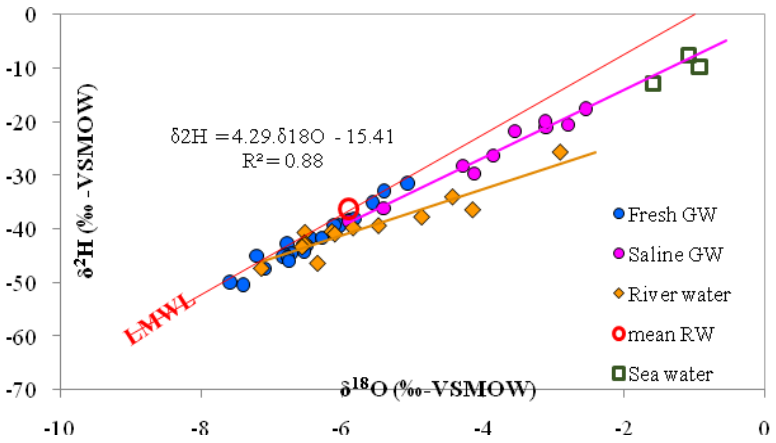

Fig. 11.6. Stable isotope composition of rain water, groundwater, river and sea water samples

Surface water (river water) in the area has evaporated. In the Fig. 11.6, surface water samples (diamond orange symbols) distribute along the line $\delta^2H = 4.3*\delta^{18}O - 15.4$ ($R^2 = 0.88$) that starts from meteoric water (groundwater) and has a slope of 4.3 showing the evaporation. This means river water is discharged groundwater and evaporates in a high temperature and low humidity environment, after. The relationship between groundwater and river water level according to the observation data obtained from November 2016 to October 2017 at the Cai Phan Rang River and groundwater close to the river is shown in the Fig. 11.7. This good relation suggests that river water originated mainly from groundwater too.

The relationship between groundwater and river water level according to the observation data obtained from November 2016 to October 2017 at the Cai Phan Rang River and groundwater close to the river is shown in the Fig. 11.7. This good relation suggests that river water originated mainly from groundwater too.

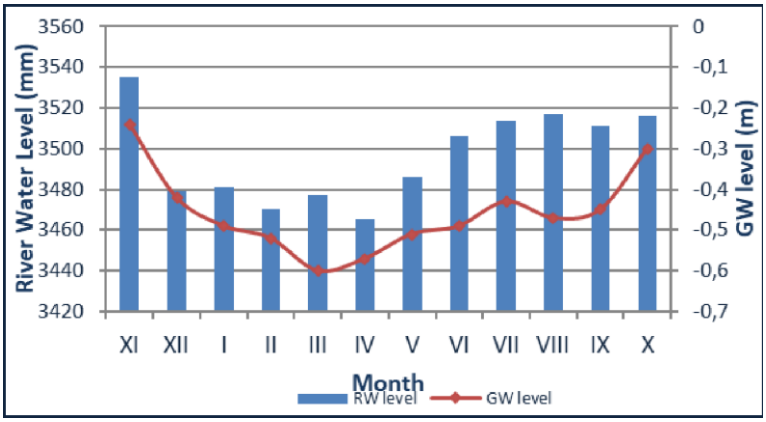

Fig. 11.7. Relationship between groundwater and river water level in the study area

11.4.2. Groundwater movement direction

All ^{14}C content of groundwater samples collected in the study area is reported in Table 11.1. The ^{14}C content of fresh groundwater samples at the study area were plotted as the Fig. 11.8.

In this map, three samples collected water from fracture rock at 80 to more than 100 m deep that have lower ^{14}C content (G21, 81.8pmC; G22, 76.5pmC; and G24, 80.8pmC, see Table 11.1) and eight saline groundwater samples were not plotted. According to the distribution of fresh groundwater's ^{14}C content, although not so clear, a groundwater flow direction drawn as yellow arrows from northwest to southeast was defined.

Fig. 11.8. Distribution of ^{14}C content in fresh groundwater at the study area

In a previous study, based on the water level contour lines built on monitoring data (Fig. 11.9) three flow directions including northwest-southeast, northeast-southwest and southwest-northeast were determined (Nguyen M. K., 2015).

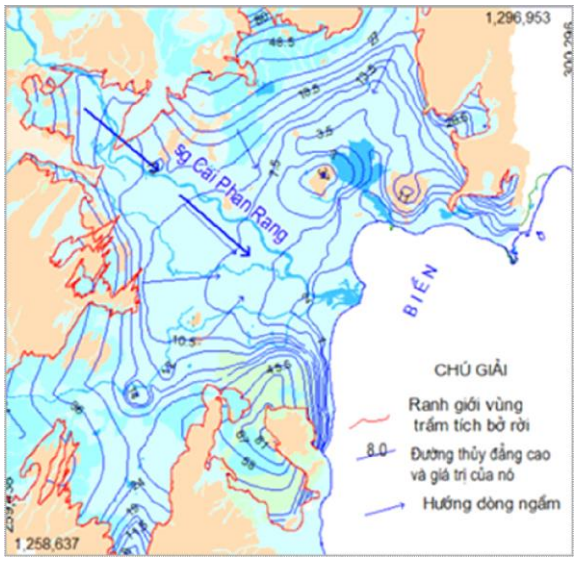

Fig. 11.9. Map of groundwater level contours (blue lines) and groundwater flow directions (blue arrows)

Based on the obtained isotopic data and monitoring data on groundwater level in this area we can conclude that water in the porous aquifer moves in three directions that are northwest-southeast, northeast-southwest and southwest-northeast with the main flow direction is northwest-southeast.

Table 11.1. Isotopic data of groundwater samples

No.	Sample Code	Sampling Date	Coordinate		Well depth (m)	Cond. (µs/cm)	$\delta^{18}O$ (‰)	$\delta^{2}H$ (‰)	^{3}H (TU)	C-14 (pmC)
			X	Y						
1	G1	Nov-16	11.8392	108.9071	12.5	94.1	-6.52	-43.1	1.09	97.21
2	G2	Nov-16	11.8225	108.8712	14.0	319.0	-6.73	-44.6	1.11	97.94
3	G3	Nov-16	11.7600	108.7915	20.5	116.5	-6.81	-44.8	1.03	98.51
4	G4	Nov-16	11.7392	108.8404	16.0	137.0	-5.83	-38.1	0.97	101.92
5	G5	Nov-16	11.7149	108.8317	15.0	336.0	-6.84	-46.8	1.12	101.54
6	G6	Nov-16	11.7092	108.8165	17.0	1639.8	-6.45	-41.7	1.12	99.72
7	G7	Nov-16	11.7011	108.8704	25.0	337.0	-6.12	-41.2	0.82	95.14
8	G8	Mar-17	11.6099	108.7849	13.0	231.1	-5.57	-35.1	1.16	99.33
9	G9	Mar-17	11.7850	109.0730	18.0	116.6	-6.50	-43.1	0.88	99.65
10	G10	Mar-17	11.6736	109.0200	23.0	537.3	-6.54	-44.2	0.92	99.77
11	G11	Jul-18	11.6245	108.9288	20.5	319.1	-6.78	-45.3	0.96	93.89
12	G12	Jul-18	11.5065	108.8786	15.0	158.4	-6.29	-41.7	1.02	98.96
13	G13	Jul-18	11.4676	108.8723	27.5	684.8	-6.76	-46.0	0.85	96.48
14	G14	Jul-18	11.5566	108.9751	16.0	5049.8	-5.91	-38.6	1.21	100.14
15	G15	Jul-18	11.5286	108.9895	24.0	7690.4	-5.42	-36.2	0.82	99.37
16	G16	Oct-18	11.4942	109.0056	19.0	26600.0	-4.30	-28.2	1.03	99.08
17	G17	Oct-18	11.4180	109.0094	18.0	33610.0	-3.11	-21.1	1.18	99.92
18	G18	Oct-18	11.3826	108.9863	24.5	31600.0	-3.12	-20.0	0.88	97.47
19	G19	Jun-19	11.6587	108.6882	18.5	215.0	-5.90	-38.3	0.85	91.53
20	G20	Jun-19	11.7025	108.7610	25.0	491.9	-6.60	-41.8	0.69	91.13
21	G21	Jun-19	11.8585	108.8178	96.0	257.4	-7.41	-50.4	0.70	81.77
22	G22	Jun-19	11.8597	108.7724	101.0	214.6	-7.60	-49.9	0.62	76.52
23	G23	Jun-19	11.6255	108.8544	35.5	1839.7	-6.05	-39.4	1.08	94.69
24	G24	Jun-19	11.7134	108.9412	80.0	416.6	-7.21	-45.0	0.80	80.82
25	G25	Jun-19	11.7489	109.0290	7.0	197.1	-5.41	-32.9	1.21	95.26
26	G26	Jun-19	11.8310	109.0470	33.5	920.9	-5.08	-31.5	1.13	92.83
27	G27	Jun-19	11.4812	108.8268	38.0	1325.5	-6.13	-42.7	1.00	92.62
28	G28	Jun-19	11.7186	109.0480	41.5	787.3	-6.79	-42.8	0.85	87.12
29	G29	Jun-19	11.3635	108.8778	30.0	35100.0	-2.70	-21.5	0.82	91.12
30	G30	Jun-19	11.4623	108.9654	57.5	26300.0	-3.86	-26.3	0.71	85.66
31	G31	Jun-19	11.5835	109.1120	36.5	29610.0	-3.36	-25.5	0.90	88.03

Table 11.2. Stable isotopic composition in river water samples

No.	Sample Name	$\delta^{18}O$ (‰)	$\delta^{2}H$ (‰)	^{3}H (TU)	No.	Sample Name	$\delta^{18}O$ (‰)	$\delta^{2}H$ (‰)	^{3}H (TU)	No.	Sample Name	$\delta^{18}O$ (‰)	$\delta^{2}H$ (‰)	^{3}H (TU)
1	S1	-5.84	-39.74	1.30	6	S7	-6.15	-40.43	1.20	11	SQ2	-6.10	-40.87	1.02
2	S2	-7.14	-47.26	1.02	7	SL1	-4.43	-33.98	1.05	12	N1	-6.35	-46.32	1.19
3	S3	-6.52	-40.60	1.13	8	SL2	-2.91	-25.65	0.90	13	N2	-6.53	-42.86	1.33
4	S4	-5.48	-39.32	0.88	9	SL3	-4.87	-37.70	1.15	14	N3	-6.57	-43.26	1.48
5	S6	-6.53	-42.49	1.00	10	SQ1	-4.15	-36.37	1.26					

Table 11.3. Isotopic composition of Ninh Thuan rainwater

No.	Sample name	$\delta^{18}O$ (‰)	$\delta^{2}H$ (‰)	Precipitation (mm)	^{3}H (TU)	No.	Sample name	$\delta^{18}O$ (‰)	$\delta^{2}H$ (‰)	Precipitation (mm)	^{3}H (TU)
1	May-16	-4.14	-20.6	60.1		23	25-Oct-17	-4.46	-26.3	28.9	
2	Jul-16	-4.82	-29.3	40.2		24	28-Oct-17	-4.30	-23.8	8.4	
3	Aug-16	-6.18	-40.5	107.5	1.40	25	Aug-18	-6.78	-41.5	135.7	1,25
4	Sep-16	-6.70	-39.9	175.6	1.29	26	Sep-18	-7.66	-51.1	153.6	1.15
5	Oct-16	-7.42	-48.2	361.2	0.72	27	Oct-16	-8.16	-53.3	207.6	1.01
6	Nov-16	-4.55	-27.8	75.1	1,52	28	Nov-18	-5.80	-37.2	167.1	1.30
7	Dec-16	-1.01	-1.7	3.4		29	4-Aug-18	-4.84	-31.4	8.4	
8	19-Aug-16	-6.11	-39.3	17.1		30	17-Aug-18	-5.28	-33.9	5.6	
9	20-Sep-16	-6.52	-45.8	1.5		31	11-Sep-18	-8.25	-51.0	18.2	
10	16-Oct-16	-6.78	-44.0	9.7		32	14-Oct-18	-8.40	-54.8	46.1	
11	17-Oct-16	-6.47	-43.9	23.9		33	22-Oct-18	-6.98	-42.5	38.6	
12	22-Oct-16	-7.38	-44.6	7.8		34	26-Oct-18	-7.92	-52.1	34.9	
13	23-Oct-16	-8.73	-55.3	68.8		35	May-19	-2.39	-4.2	7.2	
14	28-Nov-16	-5.01	-31.9	4.48		36	Jun-19	-3.08	-13.3	18.0	
15	Jul-17	-4.91	-26.5	92.40	1,82	37	Aug-19	-6.18	-40.5	71.5	
16	Aug-17	-6.64	-42.7	84.53		38	Sep-19	-6.68	-39.1	165.6	1.06
17	Sep-17	-8.30	-55.7	173.0	1.31	39	Oct-19	-7.02	-43.1	221.2	1.35
18	Oct-17	-7.51	-49.7	218.0	0.94	40	Nov-19	-8.75	-60.8	428.1	0.59
19	Nov-17	-5.34	-32.4	139.6	1.03	41	15-Jun-19	-3.98	-23.3		
20	24-Jul-17	-4.87	-28.9	5.0		42	25-Oct-19	-7.61	-46.1		
21	25-Jul-17	-5.41	-33.9	2.5		43	7-Nov-19	-8.85	-58.3		
22	17-Sep-17	-4.94	-30.7	2.6		44	26-Nov-19	-7.69	-48.1		

11.4.3. Groundwater horizontal filtration velocity

Moving velocity of groundwater is defined by single well techniques using a suitable tracer. To measure tracer concentration, the gamma rate meter with a scintillation detector (Miniken, Australia) was used.

Two wells named QT and QS1 located at two sides of the Cai Phan Rang River were chosen for determining water's horizontal filtration velocity in the aquifer. These wells were set up for tracer experiment with clear technical parameters (determined experimentally by technician).

A small amount of ^{131}I solution was introduced into the filter part of the experiment wells. Let the tracer mix and move together with aquifer water. By monitoring tracer concentration (^{131}I activity) we can define the groundwater horizontal filtration velocity as listed in the Table 11.4 below.

Table 11.4. Well name, tracer type, tracer amount, well technical parameters, traced water depth (screen part) and the groundwater horizontal filtration velocity defined in field experiments

Exp. well	Tracer type	Tracer amount (mCi)	Traced water depth (m)	Parameters	α factor	Horizon velocity (cm/day)	Vertical flow
QT	I-131	1.0	From 25m to 35m below ground surface	K= 0.01 cm/s K_1= 3.00 cm/s K_2= 0.10 cm/s r_1= 4.50 cm r_2= 4.75 cm r_3= 8.40 cm	3.035	1.22 ± 0.24	No
QS1	I-131	1.0	From 25m to 30m below ground surface	K= 0.01 cm/s K_1= 3.00 cm/s K_2= 0.10 cm/s r_1= 3.00 cm r_2= 3.25 cm r_3= 6.50 cm	3.254	0.59 ± 0.17	No

11.4.4. Seepage depth and penetration rate of water in the soil

The selected tracer experiment site was a plot of about 30 m^2 in a regularly watered vegetable farm at the outskirts of Phan Rang town. In this experiment, ^{131}I in the form of Na ^{131}I solution was used as tracer and carrier was non-radioactive NaI solution. To detect positions of the marked water layer by the soil depth, a well of 60 mm diameter, PVC casing and 180 cm deep was established. Tracer's concentration (radioactivity) was measured by the same device as used in the experiment on groundwater flow rate.

Table 11.5. Positions and displacement of water marked layer over experiment time

Measurement date	Elapsed time (day)	Position of marked water layer (cm)	Displacement [b] (cm)	Infiltration rate (cm/day)
12/05/2019	0	-33.55 [a]	0	
12/06/2019	30	-37.49	3.94	0.131
02/07/2019	49	-40.40	2.91	0.153
20/07/2019	66	-41.35	0.95	0.056
14/08/2019	90	-54.27	12.92	0.538
11/09/2019	116	-56.84 [a]	2.57	0.095
26/09/2019	130	-59.88	3.04	0.217
18/10/2019	151	-72.97	13.09	0.623
29/10/2019	162	-82.47	9.50	0.950
13/11/2019	177	-84.76	2.29	0.153
02/12/2019	195	-86.72	1.96	0.109
20/12/2019	212	-87.19	0.47	0.028

[a] Position of marked water layer at the ^{131}I injection dates.

[b] The displacement is calculated as the difference of the center depth of the two radioactivity distributions at two consecutive times.

Firstly tracer and carrying matter were injected into soil. In this experiment, the injection depth was of 28.0 cm below soil surface and evenly 20 cm from the measuring well center and the first position of marked water layer at 33.55 cm deep below soil surface was determined.

The seepage experiment lasted 7 months, from May to December. During experiment time, tracer (with carrier) was added in September when tracer concentration was lower than the detection limit of the used gamma detection device. 12 radioactive measurements were conducted and the obtained experiment results are represented in Table 11.5.

The obtained data show that the infiltration rate of water is uneven. That is mainly due to the difference in the properties and structure of the soil layers. Below the depth of 80 cm, the infiltration rate is reduced. This may be caused by the water pressure in the saturation zone, but the water still seeps down.

Thus, with an infiltration depth of 53.64 cm and a seepage time of 212 days, the average infiltration rate of water in the unsaturated zone is 0.25 cm per day.

11.4.5. Tritium and radiocarbon concentration in environment

To survey the environmental level of nuclides which could be released in NPP operation or by accident, we collected environmental samples such as sea water, tree leaf and aquatic plants for tritium and radiocarbon analysis. Some air moisture was collected also for tritium analysis to survey tritium level in the air.

For sea water, due to high sulphate problem, we use a simple tool designed by the IAEA (Fig. 11.10, right) to collect dissolved inorganic carbon for radiocarbon analysis.

By that tool, ortho-phosphoric acid is firstly added into sea water sample container, acid reacts with carbonate and bicarbonate and liberate CO_2 then, generated CO_2, supported by peristaltic pump goes through the descant and is precipitated into Na_2CO_3 in a glass bottle containing NaOH solution.

To collect carbon in the air for analysis, we precipitate CO_2 in the air with the support of an air compressor (see Fig. 11.10, left). CO_2 gas at the outlet of the air compressor goes through plastic tubes to bottles containing NaOH solution and is precipitated to Na_2CO_3.

The obtained carbon is synthesized into benzene before determining the content (activity) of radiocarbon by liquid scintillation technique.

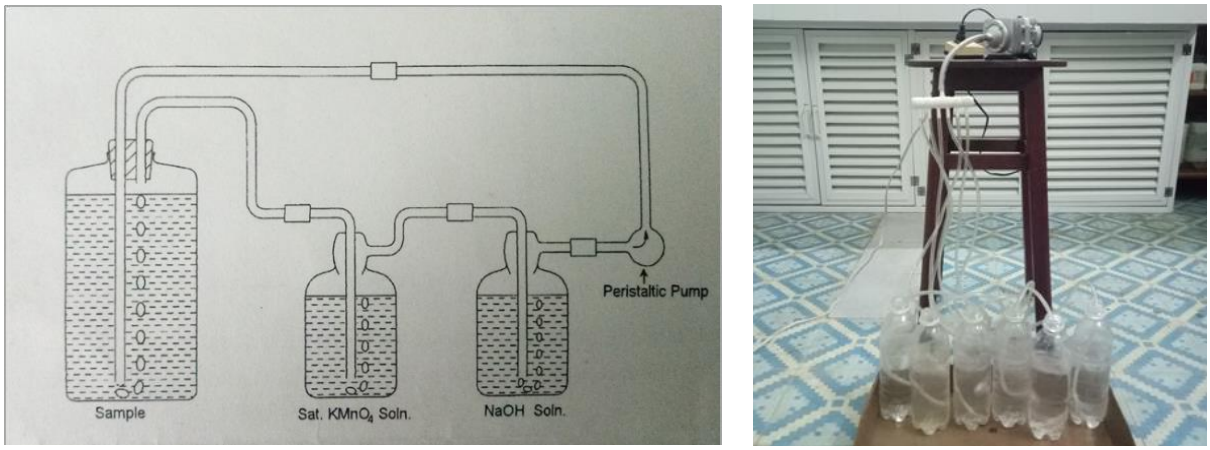

Fig. 11.10. Inorganic carbon sampler in sea water (left) and in the air (right)

To collect water in tree leaf, aquatic plants we extract water in tree leaf and aquatic samples using a distillation tool (Fig. 11.11, right). Collected samples are heated up to 105^{o}C in the spherical glass vase, escaped water vapor is condensed by cooling and sample water flows to the triangular glass bottle. This system needs to be a closed system.

For analyzing tritium in the air, we use an air dehumidifier to collect needed water amount. In dehumidifier the air is blown through its chilled system and the water vapor in the air is condensed as liquid water and is taken for analysis.

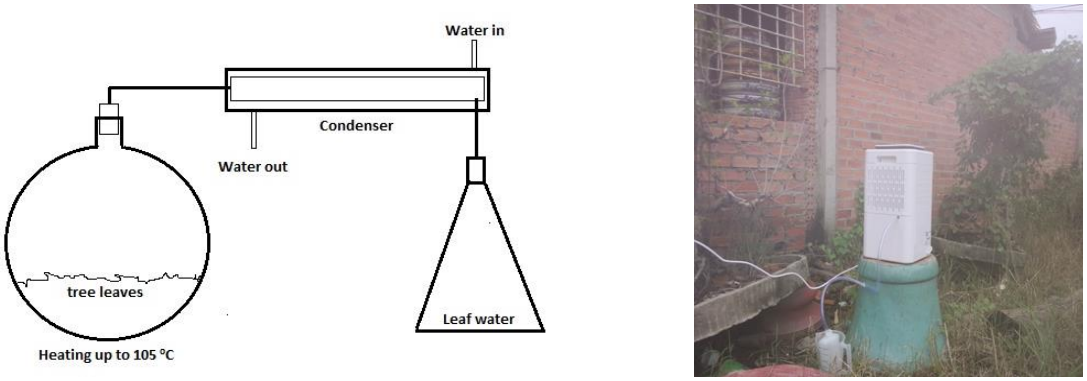

Fig. 11.11. Water extraction system (right) and air water vapor sampler (left)

In this study we collected seawater, air moisture samples, tree leaf (tamarind, neem, cashew, jujube and vine tree) and aquatic plant (shichito, beach morning glory, duckweed, sea chive and sargassum-gulf weed) samples for radiocarbon and tritium analysis. Number of samples and their radiocarbon, tritium content (min., max, average and standard deviation) are listed in the below Table 11.6. These data can be used as pre-NPP environmental data on tritium and radiocarbon.

Table 11.6. Radiocarbon and tritium content in plants, air and sea

Sample type	No. of samples	C-14 (pmC)				H-3 (TU)			
		Min.	Max.	Average	Stdev.	Min.	Max.	Average	Stdev.
Air moisture	15	97.9	103.7	101.5	1.8	0.72	1.62	1.16	0.27
Sea water	5	90.6	93.0	92.3	1.0	0.37	0.58	0.46	0.10
Tree leaf	11	97.3	102.0	99.9	1.4	0.75	1.72	1.12	0.27
Aquatic plants	5	94.6	102.8	100.1	3.2	0.81	1.37	1.18	0.22

11.5. Conclusion

Research is executed with financial support of the International Atomic Energy Agency, which forms a part of the Coordinated Research Project F33022 entitled “Use of Isotope Hydrology to Characterize Groundwater Systems in the Vicinity of Nuclear Power Plants”.

In this study, the regional groundwater system has been characterized:

- The obtained isotopic data (^{2}H, ^{18}O, H-3 and C-14) in groundwater and local rainwater show that groundwater in unconsolidated sediments in the study area is young and recharged directly by rainwater. The analysis data of stable isotope composition in groundwater and river water in this area also shows that there is an interactive relationship between groundwater and river water, whereby river water is mainly discharged groundwater.

- In the aquifer, the water moves in a northwest-southeast direction and drains into the East sea. In addition, along two banks of the Cai Phan Rang River, groundwater also moves in both directions northeast-southwest and southwest-northeast, drains into the river and then flows into the sea. The velocity of water in the aquifer is determined by the single well technique using artificial radioisotope I-131 as an indicator from 0.59 cm/day to 1.22 cm/day. By tracer technique using I-131, this study also determined the average infiltration (recharge) rate of rainwater in the soil (unsaturated zone) was 0.25cm/day.

- At the same time this study also determined the natural radioactivity of tritium and radiocarbon in the air, sea water and plants. This obtained data are used as their background.

The information obtained is the basis for monitoring and predicting the impact of the NPP's activities on groundwater and for studying area environment.

References

Bedmar, A. P. (1983) Single well techniques using radioactive tracers. In: Tracer Methods in Isotope Hydrology, 17-46. IAEA-TECD0C-291, International Atomic Energy Agency, Vienna, Austria.

Drost, W. (1983) Single well techniques. In: Tracer Methods in Isotope Hydrology, 7-16. IAEA-TECDOC-291, International Atomic Energy Agency, Vienna, Austria.

Drost, W. & Klotz, D. (1983) Aquifer characteristics. In: Guidebook on Nuclear Techniques in Hydrology, 223-256. Tech. report no. 210. International Atomic Energy Agency, Vienna, Austria.
International Atomic Energy Agency, Stable isotope Hydrology: Deuterium and Oxygen-18 in the Water Cycle, Tech. Reports Series No. 210, IAEA, Vienna, 1981
Mazor E, (1997). Chemical and Isotopic Groundwater Hydrology. The Applied Approach. Marcel Dekker, Inc.
Penna, D., et al., 2010. On the reproducibility and repeatability of laser absorption spectroscopy measurements for d2H and d18O isotopic analysis. Hydrological Earth Systems Science 7, 2975-3014.
Rozanski K. (2005) Isotopes in Atmospheric Moisture. In: Isotopes in Water Cycle. Past, Present and Future of a Developing Science, 291-303, Springer.
Stuiver, M., Polach, H., 1977. Reporting of 14C data. Radiocarbon 19 (3), 355-363.
Taylor, C.B., 1976. IAEA Isotope Hydrology Laboratory. Technical Procedure Note No. 19. International Atomic Energy Agency, Vienna.
Walker J.F &Krabbenhoft D.P. Groundwater and Surface-Water Interaction in Riparian and Lake-Dominated. In: Isotope Tracers in Catchment Hydrology. Elsevier, 1998.

LIST OF PARTICIPANTS

ARGENTINA	Ms. Paula Verónica Sánchez PROAÑO Centro Atómico Constituyentes Comisión Nacional de Energía Atómica (CNEA) Buenos Aires
BRAZIL	Mr. Virgílio Lopardi BOMTEMPO Centro de Desenvolvimento da Tecnologia Nuclear (CDTN) Belo Horizonte, Minas Gerais
CHINA	Ms. Yihui DONG East China University of Technology (ECUT) Nanchang
ITALY	Ms. Luisa STELLATO Centre for Isotopic Research on Cultural and Environmental heritage (CIRCE). Dip. di Matematica e Fisica, Seconda Università degli Studi di Napoli
JAPAN	Mr. Atsunao MARUI National Institute of Advanced Industrial Science and Technology Tsukuba City
LITHUANIA	Mr. Robert MOKRIK Department of Hydrogeology and Engineering Geology, Vilnius University, Vilnius
MOROCCO	Mr. Mohamed QURTOBI Centre National de l'Énergie, des Sciences et des Techniques Nucléaires (CNESTEN) 10001 Rabat
PAKISTAN	Mr. Naveed IQBAL Pakistan Institute of Nuclear Science and Technology (PINSTECH) Islamabad
UKRAINE	Mr. Mykola PANASIUK Institute for Safety Problems of Nuclear Power Plants of Ukrainian National Academy of Sciences (NASU) Kyiv
VIETNAM	Mr. Kien Chinh NGUYEN Centre for Nuclear Techniques Hochiminh City

Credit: IAEA

Visit of TRIGA Mark I Research Reactor, Remote Control, Nuclear Technology Development Center/Brazilian Nuclear Energy Commission (CDTN/CNEN) Belo Horizonte, Minas Gerais, Brazil

Visit of TRIGA Mark I Research Reactor, Central hall, Nuclear Technology Development Center/Brazilian Nuclear Energy Commission (CDTN/CNEN) Belo Horizonte, Minas Gerais, Brazil

Visit to Environmental Tritium Lab and to IRMS Lab, Nuclear Technology Development Center/Brazilian Nuclear Energy Commission (CDTN/CNEN) Belo Horizonte, Minas Gerais, Brazil

Монографія містить результати скоординованого дослідницького проекту (СДП), проведеного Міжнародним агентством з атомної енергії з метою вивчення використання нових ізотопних методів разом із звичайними для кращої оцінки гідрогеологічних умов в геологічних умовах майданчиків атомних електростанцій та надання основної інформації, яка може бути використана для прогнозування частки радіоактивних забруднювачів, таких як тритій, що викидаються в підземні води в разі радіологічної аварії та/або під час нормальної експлуатації. З цією метою в десяти країнах було проведено дослідницькі проекти щодо характеристики системи підземних вод поблизу атомних електростанцій, які знаходяться на різних стадіях розвитку. Монографія містить звіти цих десяти дослідницьких проектів та підсумок досягнень окремих проектів. Використано результати визначення ізотопів ^{18}O, ^{2}H, ^{13}C, ^{14}C, ^{3}H, ^{3}He, ^{4}He та благородних газів у воді. Було також використано результати традиційних гідрохімічних аналізів та розподілів ^{90}Sr, урану та трансуранових елементів у підземних водах. Цей СДП має на меті розробку керівних принципів для вивчення гідрогеологічних характеристик підземних вод у місцевих та регіональних системах підземних вод поблизу атомних електростанцій з використанням ізотопів навколишнього середовища та традиційних методів.

Для вчених та інженерів, які працюють у галузі гідрогеології, радіоекології та безпеки в атомній енергетиці, а також для студентів та аспірантів геолого-фізичних факультетів університетів.

Наукове видання

ВИКОРИСТАННЯ ІЗОТОПНОЇ ГІДРОЛОГІЇ ДЛЯ ХАРАКТЕРИСТИКИ СИСТЕМ ПІДЗЕМНИХ ВОД БІЛЯ АТОМНИХ СТАНЦІЙ

Результати скоординованого дослідницького проекту (СДП) F33022, 2016–2020

Монографія

(Англійською мовою)

Формат 60 × 84/8. Ум. друк. арк. 23,25.
Наклад 150 пр. Зам. №.

Інститут проблем безпеки АЕС НАН України
Київська обл., 07270, м. Чорнобиль, вул. Кірова, 36а
Свідоцтво суб'єкта видавничої справи ДК № 2114 від 25.02.2005 р.

Віддруковано в друкарні ПП «Видавництво «Фенікс»
Свідоцтво суб'єкта видавничої справи ДК № 271 від 07.12.2000 р.
03067, м. Київ, вул. Шутова, 13б